Developments in Applied Chemometrics:
AMT, acoustic chemometrics and N-way image analysis

Dr.ing. (Ph. D) thesis by

Jun Huang

Supervisor: Prof.Dr. Kim H. Esbensen

Applied Chemometrics Research Group
Telemark University College
Kjølnes Ring 56, N-3914, Porsgrunn
Norway

Thesis submitted to the
Norwegian University of Science and Technology (NTNU)
for the degree of Dr.ing.

March, 2001

Data without generalization is just gossip.

----- *Robert Pirsig*

PREFACE

It's been nearly four years since I came to Norway and fired up the engine for a Ph.D study (Dr.ing in Norwegian) in the fall of 1997 (see the scenario depicted below in the box). I have been delighted and excited to condense my work word by word in this dissertation throughout the process, and I strive to provide maximum value. I am pleased to see that I persevered to the very end of study, writing, refining and forging ahead with good spirits (not all the time though).

Most of the work has been carried out at Telemark University College, Porsgrunn, Norway during the period of 1997 to 2001; some courses were taken at the Norwegian University of Science and Technology (autumn semester, 1999), Trondheim, Norway. Part of thesis work was accomplished during my stay as a visiting Ph.D student at the group of Prof. Lars Munck, Royal Veterinary and Agricultural University, Copenhagen, Denmark.

This dissertation, I do hope, delivers some new developments and useful applications in multivariate data analysis/applied chemometrics. The motive of this work has been my curiosity and fascination, for the problems surrounding the core idea, the combination of multivariate data analytical techniques with imaging, acoustics and feature extraction tools. The proposed methodologies/approaches have proven themselves successful in a wide range of applications.

More understanding of multivariate data analysis/chemometrics has been achieved as I went through those courses, books, discussions and conferences. From " PCA", "PCR" and "PLS "to " unfold-PCA/PLS", PARAFAC" and "Tucker3", and from " FFT", "WT" to "AMT", and then from "MIA/MIR/MIX", "MAR" to "N-way Image analysis", "PPV" and "Acoustic Chemometrics", I have been confused, impressed, surprised, amazed and finally I learned many things. (Don't worry if you don't understand what all these abbreviations stand for) I realize that I have been keeping my knowledge/understanding evolving and somewhat unwittingly created this Ph.D thesis with six articles. I'm excited and proud of this achievement in my life.

Cheers to all of you involved with my study for your kind help as this thesis was honed and re-honed.

I especially wish to thank the Norwegian State Department, who originally "found me" through an agreement with China, called "kvotestipendier". I wish to thank Prof. Sunil de Silva for winning such stipends for HIT/TF, and Prof. Kefa Cen for his strong recommendation. When the dust had settled, and I found myself as one of the chosen few (and had found my way to an originally very obscure town called Porsgrunn - it was indeed a very long way from Hangzhou in China!), I was soon taken under the very competent wings of Mrs. Unni S. Solvi and Mrs. Trine Ellefsen, who have guided me through all of the necessary bureaucratic intricacies for which I am most grateful. Additionally I highly appreciate the management of HIT/TF, who early in my stay here decided to add some much needed extra support to my stipend. Finally I wish to recognize the NFR-project: "PARFLU" (operated through Tel-Tek, Telemark Technological R&D Center), which has also carried an important part of the costs involved in my four years at HIT/TF in Porsgrunn.

ACKNOWLEDGEMENTS

At this moment, it is definitely time to say thank-you to those who helped me as I struggled. I'd like to thank everyone involved with this thesis work.

First of all, I'm greatly indebted to a versatile and kind man, Prof. Kim H. Esbensen, who has been not only my guiding light on my way towards this goal, but also my good friend. The dissertation you are holding at hand would not be possible at all were it not for his ebullient, enjoyable, and inspiring instructions throughout my Ph.D work. I have fun working with him, so I have fun learning from him. What I've learned from him will always be appreciated, cherished, and treasured for the rest of my life. Some "spicy" stuff added to the less funny parts of the Ph.D study, is also unforgettable: dining out in fancy restaurants, imbibing in many multivariate "establishments", partying on the island of Løvøy ("Kroken"), or appreciating art in the museums etc…My heartfelt thanks to you, Kim!

I have been blessed with wonderful colleagues, including: Kim, Thorbjørn Lied, Maths Halstensen, Maria Lundhaug, (and myself) who formed Applied Chemometrics Research Group (ACRG). Many thanks to them for their technical help and constructive discussion! And to the "honorary member", Inger H. Matveyev (Ai Lin), a Norwegian M.Sc student who, among very many other accomplishments, also speaks amazingly good Chinese!

To Prof. Sunil de Silva, at POSTEC, Porsgrunn, who brought me to the field of powder technology, for the constructive discussion with him and his support.

To all the staff at Telemark College who kindly helped me during my stay here, in particular: Trine, Annita, Unni, May-Britt, Finn, Rune, David.

To Prof. Saba Mylvaganam at Telemark College, for his assistance with fascinating process sensor technology.

To Prof. Lars Munck, at Royal Veterinary and Agricultural University, Copenhagen, Denmark, for giving opportunity to work at his group for four months as a visiting Ph.D student. Also to all other folks at this famous chemometrics group, in particular: Rasmus, Birthe, Elizabeth, Claus, Allan, Gilda.

To Prof. Kefa Cen, at Institute of Thermal Eng., Zhejiang University, China, for his long-time support!

To the folks whom I had a lot of fun with: Steve, Afshin, Elizabeth, Rune, My, Maria, Heidi, Yngve, John, Stine…

To my Chinese friends who helped me in many ways, Anna, Zhuang, Qianpu, Jin, Mao, Baoan in Norway and Ruan Wei, Yu Liang, Wenjie in China.

Finally and as always, I'd like to extend my deepest gratitude to my parents and sister, for their love and long-standing encouragement along my way.

May this thesis pay for itself many times over.

Jun Huang

Porsgrunn, Norway
Mar 18, 2000

ABSTRACT

This Ph.D dissertation is concerned with selected developments within applied chemometrics, focusing on AMT (Angle Measure Technique), N-way image analysis and acoustic chemometrics.

The core of this dissertation consists of 6 papers, mostly dedicated to combining multivariate chemometric methods with AMT, acoustic sensor technology and image analysis to provide new, simple and robust solutions to various technical and industrial problems. A range of multivariate models are employed in conjunction with multivariate feature extraction techniques. Multivariate models concerned include: Principal Component Analysis (PCA), Partial Least Square (PLS), Unfold-PCA/PCA, Parallel Factor Analysis (PARAFAC), and Tucker3 modeling etc. Transformation techniques such as AMT, FFT and WT are used as powerful preprocessing facilities for subsequent multivariate data modeling.

Paper I-IV presents a new, unified image AMT approach for characterization/discrimination and quantitative predictions, based on image analysis, AMT and multivariate data modeling.

Paper V gives an overview of relationships and applications of multi-way methods in image analysis. The primary objective in this paper is to investigate alternative multivariate approaches, to clarify some confusing concepts and to investigate the relationships and suitability of the various methods applied in N-way image analysis. It is elaborated that data configuration and problem formulation has direct impacts on the choice of the pertinent multi-way methods.

Paper VI presents a contribution to acoustic chemometrics, a non-invasive quantitative measurement technique for monitoring powder breakage during pneumatic transportation.

The significance of these contributions to the continued development of chemometrics will hopefully find good use in the applied technological and industrial sectors.

KEYWORDS: Chemometrics; Multivariate data analysis; AMT (Angle Measure Technique); N-way image analysis; Acoustic chemometrics; Multi-way

LIST OF PAPERS

I. J. Huang and K.H. Esbensen, Applications of AMT (Angle Measure Technique) in Image Analysis Part I. A New Methodology for *in-situ* Powder Characterization. *Chemometrics and Intelligent Laboratory Systems*. *54/1*. (2000) 1-19

II. J. Huang and K.H. Esbensen, Applications of AMT (Angle Measure Technique) in Image Analysis Part II. Prediction of Powder Functional Properties and Mixing Components using Multivariate AMT Regression (MAR). *Chemometrics and Intelligent Laboratory Systems, In print*, 2001

III. J. Huang, B. Møller, L. Munck and K.H. Esbensen, Development of a new method for characterization of barley germination by automated image analysis and AMT (Angle Measure Technique). Submitted for publication in *Journal of the Science of Food and Agriculture*, 2001

IV. K.H. Esbensen and J. Huang, Applications of AMT (Angle Measure Technique) in Image Analysis Part III. High sensitivity particulate impurity detection and quality control. Submitted for publication in *Chemometrics and Intelligent Laboratory Systems*, 2001

V. J. Huang and K.H. Esbensen, Multi-way methods in Image Analysis: Relationships and Applications. Submitted for publication in *Journal of Chemometrics*, 2001

VI. J. Huang, S. Ose, S. de Silva and K.H. Esbensen, Non-invasive Monitoring of Powder Breakage during Pneumatic Transportation using Acoustic Chemometrics. Submitted for publication in *Powder Technology*, 2001

CONTRIBUTIONS:

Jun Huang has contributed to each of the above six papers in the following proportions:

1. ***75%*** 2. ***75%*** 3. ***50%*** 4. ***50%*** 5. ***90%*** 6. ***75%***

Kim H. Esbensen, Supervisor
(Sign)

CONTENTS

1. INTRODUCTION AND DEFINITIONS

We live in a multivariate world where "data" come from every field constantly, and in more varied forms than ever. The proliferation of sophisticated instruments, coupled with new development in modern sensor and computer technology, has caused vast amounts of complex data that often contain many inter-correlated measurements simultaneously. Chemometrics is a powerful tool to extract information from such complex data in order to obtain knowledge and understanding of the systems under investigation. Chemometrics has several useful definitions, of which the following is from *Chemometrics: a textbook Elsevier, NY, 1998*, by D.L. Massart et al.

Chemometrics is the chemical discipline that uses mathematical, statistical and other methods employing formal logic
1) to design or select optimal measurement procedures and experiments, and
2) to provide maximum relevant chemical information by analyzing chemical data.

Chemometrics has evolved rapidly over the past three decades, supported by the availability of ever more powerful computers and advanced analytical instruments. Chemometrics is widely used in analytical chemistry, but it has been adopted in many other fields as well. Its power is broadening as it becomes more interdisciplinary, combined with other important areas such as information technology, electronics, sensor technology etc.

In fact, many methods in chemometrics are also found in different fields such as economics, psychology and biology, and the similar definitions such as econometrics, psychometrics and biometrics characterize handling these types of data.

Therefore, multivariate data analysis would today seem to be a general term as it is comprised of a set of mathematical and statistical tools that can be applied to very many fields. It is concerned with data which consist of multiple measurements on a number of individuals, objects or data samples. The measurement and analysis of dependence between variables is fundamental to multivariate analysis. Multivariate data analysis offers a wide range of mathematical tools in conjunction with exploratory approaches, and thus provides plenty of new possibilities in extracting hidden information from vast amounts of covariate data and facilitates solving multivariate problems to gain knowledge and achieve a deeper understanding of the problems under investigation. It can also be used for e.g. decision making. In this sense, multivariate data analysis is a technology rather than a discipline, since it is a set of techniques/tools that can be adopted in very many areas and thereby do useful work for all these disciplines [Munck, personal communication].

A significant part of multivariate data analysis can be covered by the following three types of problem formulations or data analysis objectives [Esbensen, Wold & Geladi, 1989]:

- Data description (Explorative Data Structure Modeling);
- Discrimination and Classification;
- Regression and Prediction.

The purpose of data description can be manifold: determination of simple means and variations, correlations, underlying structures etc. Principal Component Analysis (PCA) is one of frequently used methods for multivariate data description.

Discrimination deals with separation of groups of data. Classification has a similar purpose, but typically a set of relevant groupings in the data are known beforehand. The aim of classification analysis is to assign, or to classify new samples to different established groups. These definitions lead to unsupervised and supervised pattern recognition, respectively.

Regression aims to relate two sets of variables to each other. In the chemometric practice, regression models will e.g. often be established between indirect observations obtained from e.g. instruments (X-block) and properties (Y-block) that may be too expensive, difficult, or time-consuming to measure. Multiple Linear Regression (MLR), Principal Component Regression (PCR) and Partial Least Squares (PLS) are some commonly used regression methods. Prediction means determining Y values from new X measurements, based on previously calibrated X-Y models. *Multivariate calibration*, Martens & Næs (1987), is a term that covers both regression modeling and prediction. Proper validation should receive more attention in this process since it is imperative in evaluating how well the calibrated model can be used for the future working situations of the prediction models.

The applications of multivariate data analysis have increased enormously in a wide range of academia and industrial sectors in the past two decades. These include process monitoring, fault detection, classification, data mining, quality control, relations between chemical compositions and structures and chemical properties, and determination of concentrations of constituents of samples from a multitude of measurement series, etc. Industrial sectors range from chemical, pharmaceutical, biotechnology, food and beverages to semiconductors, telecommunication, and marketing data analysis etc.

This dissertation is mainly focused on the development of some interesting novel techniques, methodology and applications using multivariate data analysis, covering areas such as image analysis and acoustic monitoring. In particular, it aims to combine multivariate techniques with e.g. classical image analysis, acoustic sensor technology to achieve a better understanding of system/products under observation, and to provide simpler and more pragmatic approaches to achieve the desired technological and industrial goals, from multiple images/acoustic signals acquired by various imaging instruments/sensors.

2. MULTIVARIATE TECHNIQUES

In the following only the models that are covered in the research work related to this thesis will be briefly described, though there is already a plethora of literature on multivariate modeling. The purpose is to review these models in general as well as to keep this thesis systematic.

2.1. Principle Component Analysis (PCA)

PCA in many ways forms the most fundamental basis for multivariate data analysis [S. Wold, et al. 1987]. The essence of PCA is to represent the original multi-dimensional data with (significantly) fewer descriptive parameters (principal components, or latent factors) which capture the main variation residing in the data through orthogonal decomposition. Assume that the data matrix **X** is composed of I objects (rows) and K variables (columns). Objects can be samples taken to the lab, time points of a process, batches from batch process, etc. Variables can be absorbance at different wavelengths, frequency, scales, pressure, temperature, flow, etc.

Mathematically, PCA can be written

$$X = \sum_{f=1}^{F} t_f p_f' + E$$

F denotes the number of components, indicative of the complexity of the observed variations in data. The principal components represented by $\mathbf{t}_f \mathbf{p}_f$ pairs are ordered by amount of variance captured. Orthogonal scores, $\mathbf{t}_f$, describe sample relationships, and orthonormal loadings, $\mathbf{p}_f$, variable relationships. Residuals are contained in **E**.

PCA is a versatile exploratory tool, which has a wide range of application areas. It can be used from initial screening to discrimination and classification, etc. with visualized graphical representations. Visual tools such as score and loading plots, plots of Hotelling T^2 statistics and lack of model fit statistics Q, residual plots give a very convenient way to understand data. PCA has been used throughout the following papers for studying data structure, discrimination, classification and interpretation etc.

2.2. Partial Least Squares (PLS)

The PLS approach was originated around 1975 by Herman Wold who developed a simple but efficient way, NIPALS (Nonlinear Iterative Partial Least Squares), to estimate the parameters in the modeling of complicated data sets in terms of chains of matrices (blocks), which led to the acronym PLS for these models.

PLS is a method for relating two multivariate data matrices, **X** and **Y**, to each other by finding projections into lower dimensional subspaces of **X** and **Y** which maximize the covariance between them. See Figure 1.

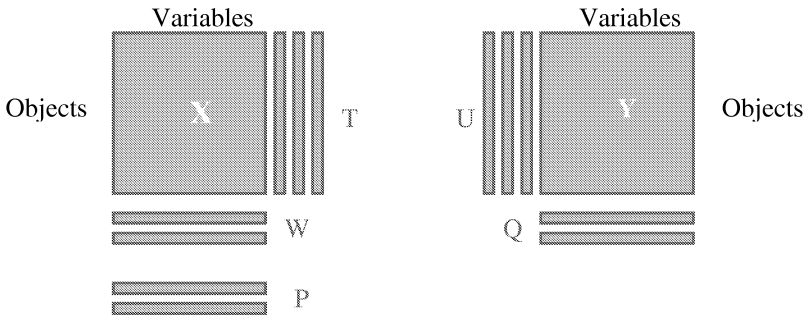

Figure 1. A schematic overview of PLS modeling

X and **Y** are modeled as:

$$X = \sum_{f=1}^{F} t_f p_f' + E$$

$$Y = \sum_{f=1}^{F} u_f q_f' + F$$

These are known as outer relationships. The relationship, the regression link, between **X** and **Y** is established with the inner relationship $\mathbf{u}_f = b_f \mathbf{t}_f$, i.e. the scores in **Y** are modeled as a linear combination of the scores in **X**.

PLS does not perform two independent PCA on the two matrices independently. PLS aims to improve the predictive efficiency of the regression model by finding score vectors for X that are maximally correlated to the scores for Y. Unlike Principal Component Regression (PCR), PLS allows the Y-structure to intervene directly in the X-decomposition [Esbensen, 2000].

The PLS2 NIPALS Algorithm is given below [Wold, et al, 1984, Höskuldsson, 1996]:

0. Initialization of **X** and **Y** matrices appropriately (centering, scaling, etc.).
   f=1; $\mathbf{X}_f$=**X**; $\mathbf{Y}_f$ =**Y**
1. Choose the column in **Y** with highest sum of squares for initial $\mathbf{u}_f$
2. $\mathbf{w}_f = \mathbf{X}_f^T \mathbf{u}_f / | \mathbf{X}_f^T \mathbf{u}_f |$ (**w** is normalized)

3. $\mathbf{t}_f = \mathbf{X}_f \mathbf{w}_f$
4. $\mathbf{q}_f = \mathbf{Y}_f^T \mathbf{t}_f / | \mathbf{Y}_f^T \mathbf{t}_f |$ (**q** is normalized)
5. $\mathbf{u}_f = \mathbf{Y}_f \mathbf{q}_f$
6. Go to step 1 until convergence of e.g. $|\mathbf{t}_{f,new} - \mathbf{t}_{f,old}| < \mathbf{limit}$, $\mathbf{u}_f$ may be used alternatively
7. $\mathbf{p}_f = \mathbf{X}_f^T \mathbf{t}_f / \mathbf{t}_f^T \mathbf{t}_f$
8. $b_f = \mathbf{u}_f^T \mathbf{t}_f / \mathbf{t}_f^T \mathbf{t}_f$
9. $\mathbf{X}_{f+1} = \mathbf{X}_f - \mathbf{t}_f \mathbf{p}_f^T$ **and** $\mathbf{Y}_{f+1} = \mathbf{Y}_f - b \mathbf{t}_f \mathbf{q}_f^T$
10. $f = f+1$
11. Save the current intermediate factors and go to step 1.

This algorithm can be simplified when there is only one column in **Y**, namely PLS1. In this case, **y** vector becomes **u**, and algorithm is much simpler as follows (in fact it is not even iterative any more):

1. Initialization of **X** and **y** appropriately (centering, scaling, etc.)
   $f = 1$; $\mathbf{X}_f = \mathbf{X}$; $\mathbf{y}_f = \mathbf{y}$
2. $\mathbf{w}_f = \mathbf{X}_f^T \mathbf{y}_f / | \mathbf{X}_f^T \mathbf{y}_f |$ (**w** is normalized)
3. $\mathbf{t}_f = \mathbf{X}_f \mathbf{w}_f$
4. $q_f = \mathbf{y}^T \mathbf{t}_f / \mathbf{t}_f^T \mathbf{t}_f$
5. $\mathbf{p}_f = \mathbf{X}_f^T \mathbf{t}_f / \mathbf{t}_f^T \mathbf{t}_f$
6. $\mathbf{X}_{f+1} = \mathbf{X}_f - \mathbf{t}_f \mathbf{p}_f^T$ **and** $\mathbf{y}_{f+1} = \mathbf{y}_f - \mathbf{t}_f q_f$
7. $f = f+1$
8. Save the current intermediate factors and go to step 1.

PLS has seen unparalleled application success in both chemometrics and many other fields. It plays a key role in calibration and prediction in very many modern fields within science and technology, e.g. perform indirect measurements of Y, which may be expensive, difficult, laborious, time consuming, dangerous, etc, from an already established PLS model based on the manifest X-variables instead, in the multivariate calibration context [Martens & Næs, 1987]. PLS has been used for regression and prediction in combination with some other techniques in this thesis work.

2.3. Multi-way methods

Multi-way methods are concerned with multi-way data measured as a function of three or more "ways". Nowadays multi-way data come massively as many highly sophisticated instruments are developed, e.g. hyphenated instrument that give a physical separation followed by spectroscopy. Typical application areas cover image analysis, sensory analysis, process analysis, spectroscopy, chromatography etc.

One traditional approach to multi-way analysis is to perform *unfolding*, followed by ordinary two-way analysis, e.g. unfold-PCA/PLS. These are then called "weak" multi-way methods as they do not fully utilize the multi-way structure. By contrast, "strong" multi-way methods refer to those using a complete multi-way structure in the modeling, e.g. PARAFAC, Tucker3 etc. The reason for using multi-way methods is not necessarily to obtain better fit, but rather more adequate, robust and interpretable models. Furthermore, true multi-way models explicitly establish relationships between factors in all modes spanned by the data array under investigation.

2.3.1 Unfold-PCA/PLS

Unfold-PCA/PLS is simply unfolding a multi-way array to a matrix along one of the modes, and then performing standard two-way methods like PCA. Conceptually, this is much simpler than strong multi-way methods, but it is not so in a multi-mode sense since unfolding may bring some loss of information and difficulty of interpreting the loadings mixed by the unfolded modes. It also tends to overfit the model with more noise included in the model. However, this is problem-dependent. In Multivariate Image Analysis (MIA), unfolding images along object (pixel) modes will cause nothing to lose for e.g. classification purpose. Unfold-PLS works in the same way as unfold-PCA with respect to unfolding. If there is quality variable (s) associated with each sample, the data can be unfolded (across the sample/object mode) and a regression can be performed. In Paper V, unfold-PLS is used to predict rheological properties of cheeses from microscopic images corresponding to each cheese.

For three-way data array, there are two model representations in terms of data configuration. For OOV and OVV data arrays (O denotes object mode, and V variable mode), they can be written as follows [Paper V]:

$$\underline{X} = \sum_{f=1}^{F} T_f p_f + \underline{E}$$

$$\underline{X} = \sum_{f=1}^{F} t_f P_f + \underline{E}$$

where T_f denotes back-folded score matrix (score image), p_f loading vector, t_f score vector, and P_f back-folded loading matrix (loading image).

The difference is caused by the fact that unfolding is carried out along two object modes (sample) for OOV data array, while two variable modes are unfolded for OVV data array. See details in Paper V.

2.3.2. PARAFAC

PARAFAC is a true multi-way decomposition method. The PARAFAC algorithm is not sequential, and hence refitting is necessary, while PCA is a least squares model, fitted sequentially (NIPALS). PARAFAC algorithm can be based on Alternating Least Squares (ALS), GRAM/DTLD, PMF3 etc. A detailed tutorial on PARAFAC is given by Bro [Bro, 1997]. A PARAFAC model of a three-way array is expressed by three loading matrices, **A**, **B** and **C** with elements a_{if}, b_{jf}, c_{kf}, and the corresponding residuals. It can be written

$$x_{ijk} = \sum_{f=1}^{F} a_{ij} b_{jf} c_{kf} + e_{ijk}$$

where ***F*** is the number of components, e_{ijk} denotes the residual elements.

It can also be written

$$\underline{X} = \sum_{f=1}^{F} a_f \otimes b_f \otimes c_f$$

where a_f, b_f, c_f are the *f*th column of the loading matrices **A**, **B** and **C** respectively, and the symbol $\otimes$ denotes Kronecker multiplication.

2.3.3. Tucker3 model

Tucker3 model is another basic multi-way method. As compared to PARAFAC, it allows more flexible solutions, e.g. the number of components can vary in **A**, **B** and **C** through $\underline{\mathbf{G}}$. By leaving one or two modes uncompressed, Tucker3 model becomes Tucker2 and Tucker1 model respectively. Tucker1 is actually identical to unfold-PCA. Tucker2 may sometimes be beneficial, e.g when one of modes contains very few observations. Tucker1 (unfold-PCA) is adopted in MIA.

A tucker3 model is a weighted sum of all possible outer products between the factors stored as columns in **A**, **B** and **C** with the weight of outer product determined by a core array $\underline{\mathbf{G}}$ (w_1, w_2, w_3). It can be written in a same manner to PARAFAC

$$x_{ijk} = \sum_{d=1}^{D} \sum_{e=1}^{E} \sum_{f=1}^{F} a_{id} b_{je} c_{kf} g_{def} + e_{ijk}$$

where the index ***D, E, F*** denotes the number of components in each mode, and g_{def} the elements of core array **G**.

2.3.4. Multi-way Calibration

There are many possible multi-way calibration methods, among which unfold-PLS and N-PLS associated with a trilinear (PARAFAC-like) model are introduced here. Unfold-PLS is characterized by performing ordinary PLS on a two-way array unfolded from a three-way array and y variable(s), while keeping the object mode of **X** in common with dependent y intact. N-PLS based on PARAFAC model can be represented graphically in Figure 2 (with one y variable illustrated). As described earlier, the Y-block can be a vector, a two-way matrix, or a three-way (N-way) matrix.

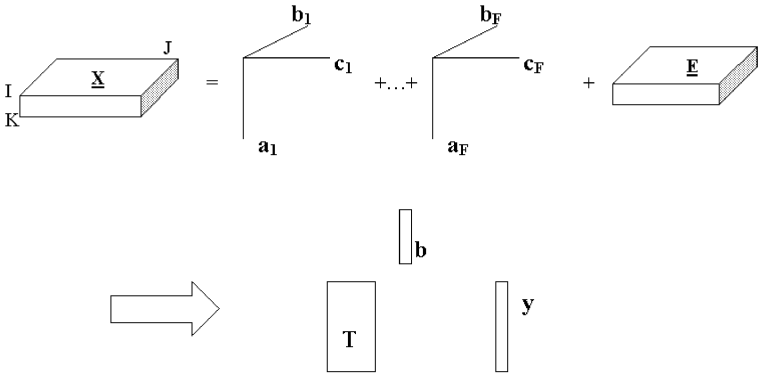

Figure 2. N-PLS model based on two steps: PARAFAC decomposition of X, followed by PLS on scores from X and y.

Details on multi-linear calibration are given by [Bro, 1996, Smilde, 1997]. Bro pointed out that the advantages of N-PLS (including tri-PLS) over unfold-PLS can be highlighted by the following two points: 1) The trilinear model is more parsimonious, simpler and thus easier to interpret; 2) Less prone to noise due to decomposition across all modes.

N-PLS is used to relate Y—rheological properties of cheeses to X—microscopic images in Paper V. The results show that N-PLS models are apparently superior to unfold-PLS models in this case.

However, there is no general rule in choosing which method to use. The knowledge of data sets under investigation and a priori knowledge of calibration methods, namely proper problem formulation, is always a must. For instance, we have found unfold-PLS works very well in

multivariate image regression (MIR). There might also be a possibility of applying N-PLS in multivariate image regression, i.e. finding regions of interest.

2.4. Validation

Validation, a controversial topic within chemometrics, has provoked a wide range of discussions in recent years. Validation is now gaining more attention from reflected chemometricians. Validation is an important aspect of any multivariate data analysis, prediction, classification, and other data modeling. Validation, in a data analytical context, means assessing the performance of a data analytical modeling or a prediction validation. The purpose of validation is to substantiate that a particular model will work according to its purpose, not only in the calibration/modelling situation, but also in the future for new, similar data, as well as to avoid either overfitting or underfitting of data models. Validation may thus typically be used both for optimizing model complexity, e.g. the determination of the optimal number of PLS-components ("internal validation"), and for prediction validation by assessing e.g. the RMSEP of future prediction ("external" validation). Already when we select training objects for calibration, for instance, we must also think of how the model should be validated. A prediction model that is not properly validated is useless.

An introductory overview of Principles of Proper Validation (PPV) may be outlined by a set of characterizing distinctions [Esbensen, 2001]:

1. *There is no single universal method of validation (- contrary to many myths)*
2. *Validation cannot be fully understood by focusing on the methods of validation only*
3. *Validation can only be understood in terms of the underlying principles behind proper validation*
4. *PPV is always a reflection of the specific data structure present in any given problem or data set*
5. *The objective of PPV is to establish a proper correspondence between method and the empirical data structure*
6. *PPV is general and applies to all situations in which assessment of performance is desired, be this prediction-, classification-, time series forecasting-, modeling validation a.o.*

In chemometrics, validation is perhaps most well known regarding prediction validation, of which there are (at least) three types, namely test set validation, cross validation and leverage correction validation. The concept of "sampling variance difference" is intimately connected with proper understanding of the different validation methods offered in the data analysis communities. Figure 3 shows an overview of external and internal validation, describing the relationships of sampling, test validation, cross validation, leverage correction to one another.

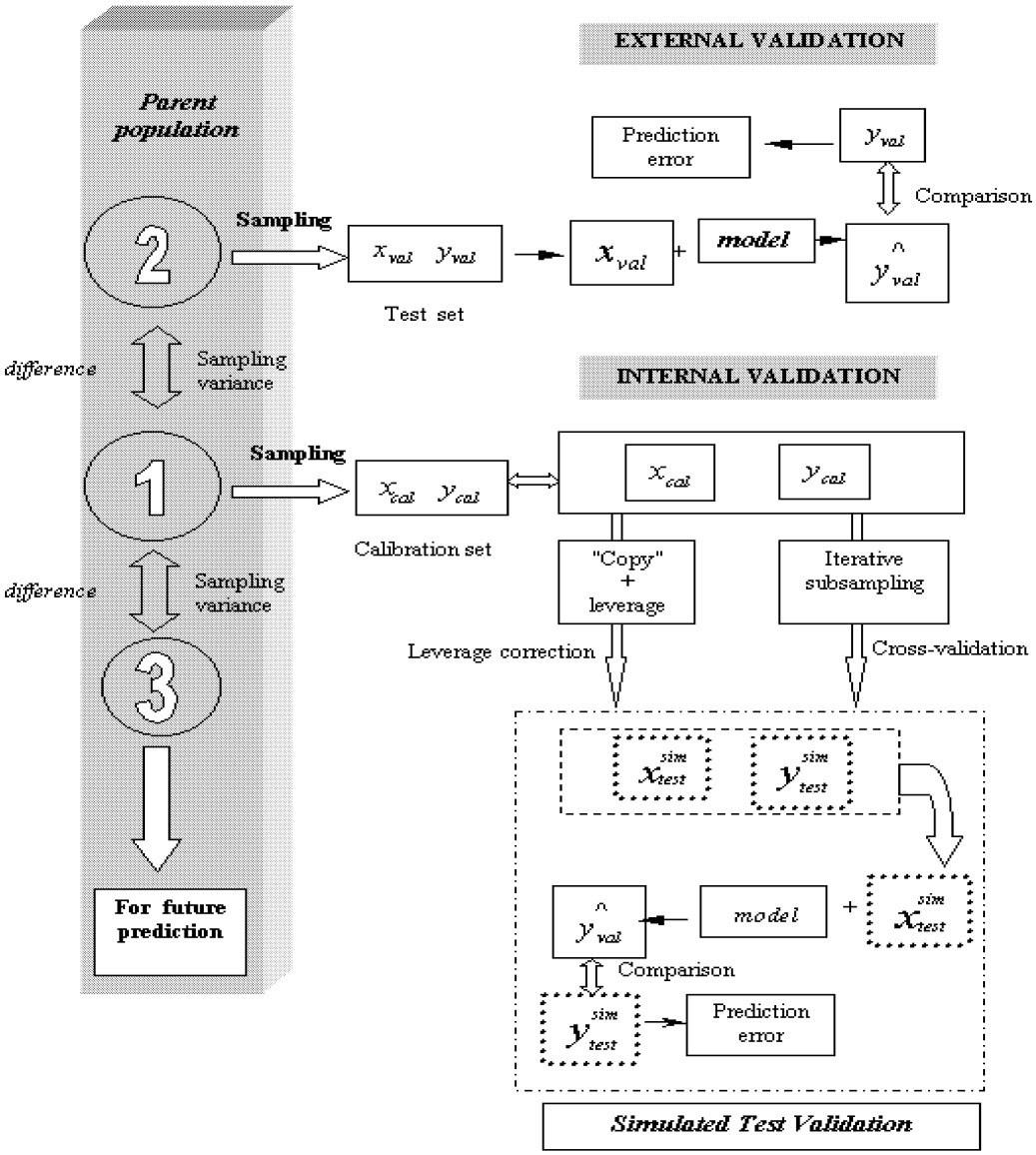

Figure 3. Schematic overview of internal and external validation. Cross-validation segments only functions as virtual, temporary small test sets. With cross-validation there is no second sampling from the target population: Cross-validation is a simulation of the test set validation only. With leverage-corrected validation a direct copy of the training set serves as the virtual test set, suitably "modified" by leverage corrections to the prediction residuals; leverage-corrected validation can also be viewed as a weighted, one-segment cross-validation. Both cross-validation as well as leverage-corrected validation are internal validations only. Only test set validation approach incorporates the essential sampling variance difference.

2.4.1 Sampling variance difference

If/when one has secured two (or more) optimally sampled, "representative" data sets, there can effectively be only one variance component that will differ between them: the *sampling variance difference*. There will principally be an inherent sampling variance difference between any set(s) of independent correct samplings from one parent population. It is unacceptable, both from a philosophical as well as from a practical scientific point of view, a priori to discard the very possibility to assess the contribution from this sampling variance difference. But this is exactly what all validation schemes do, which do not include the critical sampling variance difference component.

It is also this sampling variance difference that will help us quantify fully the data model performance in future situations (predictions, classifications...) – provided only that the test set is representative and structurally correct in the above sense. For these reasons it is only a test set validated model that will ever be able to render a fair and valid estimate of both the number of optimal components to be used in, say, a particular prediction model as well as the error to be expected in future predictions (RMSEP). There is one fundamental bonus associated with this insight [Esbensen, 2001] – it is only necessary to perform one proper test set validation in order both to estimate the inherent model dimensionality (internal objective) as well as the RMSEP (external), all in one, optimal, valid procedure.

2.4.2 Test set validation

A proper test set should preferentially be as large as the training set, and cover the same ranges and covariance features – drawn under the same sampling conditions. In other words, both test set and training set must be as similarly drawn as at all possible, albeit with the critical difference that the test set necessarily must represent a second, "future" sampling from the parent population. Drawing such a test set will represent a similar situation to that which a calibrated model is to be used for future prediction.

2.4.3 Cross validation

Certainly one often cannot always get access to "as many objects as fully desirable". Realistically, there are often limits so that test set validation is *de facto* out of the question. Naturally the validation issue does not stop here - in fact, it just becomes more challenging. Suffice here to mention just some of the more often encountered reasons for this:

- not enough resources (money, equipment, sample containers, operators, ...)
- not enough time before the opportunity to acquire a second/third relevant data set is gone.

- not enough experience/knowledge (that indeed a second/third data set was necessary)
- wrong information/myths ("all that's needed is a good cross-validation procedure")

If so, we plainly have to resort to another method. Obviously cross-validation comes to the fore:

In this situation it is optimal that one tries to make the calibration set as big - and thus as statistically representative - as possible. With cross-validation a series of sub-model calibrations will be run with different, non-overlapping subsets of calibration objects, all from the training data set, used as temporary virtual validation objects. Their formal usage is only in a similar fashion as for real test set objects. In reality with cross-validation there is no second sampling from the target population: Cross-validation is but a simulation of the proper test set validation, without taking into account the essential sampling variance difference.

With cross-validation one in fact only assesses the *internal robustness* of any covariance data structure by selecting different sizes of segments for cross-validation and/or by using several repeated cross-validation sub-samples.

There are two major types of cross validation:

- *"Full" cross validation (or Leave-One-Out validation, LOO)*
  Often used if the training data set is "small". For the larger and more well-balanced data sets, full cross validation will eventually tend to lead to more-and-more over-optimistic validation results, because one left-out sample on average will give a significantly smaller simulated sampling variance contribution. For larger data sets one would eventually rather choose *segmented cross validation*, which will then be a more realistic validation configuration.

- *Segmented cross validation*
  This approach is often used if there is a relatively large number of samples in the training data set, but we nevertheless don't know exactly how to pick out a representative subset. The number of segments will always depend on the size and structure of the data set and on its covariance complexity. The choice of the proper number of cross-validation segments from the calibration data set is in fact very much related to the actual model structure, and it is the responsibility of the data analyst always to observe the specific data structure of a given training data set and to determine the proper number of segments accordingly [Esbensen, 2001]. The pertinent information source is the *t-u plot* (or similar graphic plots for other types of data analysis). A plot of t-scores against u-scores is the specific PL-regression reflection of the pertinent X-Y relation (correlation) for one particular component of a PLS model, e.g. t1-u1, t2-u2 etc.

- *Leverage correction*
  Leverage correction is a "quick-and-dirty" validation method. It is quick because it only requires us to make one model, dirty because the prediction error will always be an over-optimistic estimate. This is because all objects are used for both modeling and validation. We only use leverage correction in the first runs to get the initial impression. Like cross validation, we also never use a separate test set but use the correction approach to simulate the test set validation.

The entire validation dilemma can be summarized by the following *distinctions* [Esbensen, 2000] :

- Cross-validation endeavors to simulate test set validation, in that small, test set segments are apparently used, but they are not independently sampled (as they were de facto sampled simultaneously with all other training set objects), and they are invariably replaced into the training set.
- With any type of cross-validation the training data set size - the model support - is invariably reduced by a factor ranging from N/(N-1) to 0.5, so that the very purpose of modeling is in fact always partially impaired. This leads to a refocusing on:
- The importance of the second (third…) test set - the test set imperative.
- This also leads to a re-focusing on the "problem" of how to choose the "optimal" number of segments, S, in segmented cross validation - Which guidelines for this choice exists?
- The t-u plot comes to the fore for all of these endeavors

Full exposition of these validation issues can be found in the recent tutorial: "Principles of Proper Validation (PPV)" [Esbensen, 2001].

3. MULTIVARIATE FEATURE EXTRACTION TECHNIQUES

There are many multivariate feature extraction techniques that have been used in extracting information from raw data, such as FFT, WT, Single Value Decomposition (SVD), autocorrelation and autocovariance functions (ACF), histogram, AMT etc [Kvaal, 1998, Wold, 1999, Huang & Esbensen, 2000]. They all have something in common when working on images: image feature extractors. Different features extracted from images can be categorized into three types: spectral, textural, and contextual features [Haralick et al, 1973]. Spectral features is concerned with multi-spectral images since it gives information about characteristics of spectrum as a function of wavelengths. Textural feature analysis has been one of primary tasks in computer vision applications. Textural features contain information about spatial variation distribution within one single image channel, while contextural features are extracted from blocks of pictorial data surrounding the region of interest. These three types of features are bound to contain useful information from images, and hence can be utilized in combination with multivariate data analysis. When it comes to multivariate characterization, these transform techniques operate on images as powerful preprocessing facilities for subsequent multivariate modeling (PCA, PCR, PLS etc.). In Paper I-V, attempts have been made to characterize samples/images and establish links between images and properties of samples.

The following domain transform techniques have been touched upon in this thesis work:

- Fourier transform (FFT)
- Wavelets Transform (WT)
- AMT (Angle Measure Technique)
- Single Value Decomposition (SVD)
- Autocovariance (ACOV) and autocorrelation (ACOR) spectra

It is noteworthy, that all these transform techniques are global feature extractors which view individual images as a whole, instead of working locally on part of an image within one band. FFT, WT and AMT have also been used to extract features from the acoustic time series in connection with chemometric modeling in this thesis work.

3.1. Fourier transform

This classical domain transformation has been introduced to the field of chemometrics in recent years. FFT frequency domain representation of original time domain provide FFT power spectra, a new optimal type of X-spectra for multivariate data modeling. When it is used for multivariate calibration, this approach is called Fourier regression. In Fourier regression, a

regression model is formed between the FFT-transformed frequency components and a dependent variable(s), e.g. in acoustic chemometrics, where Fourier regression was used to relate the acoustic signals to process monitoring, see Paper VII.

In Paper V, 2-D FFT transform of an image is used as a preprocessing step before regression. Frequency components of images will form a three-way data subject to three-way modeling. FFT transform is also used in acoustic chemometrics to extract information from acoustic signal in combination with multivariate calibration, see Paper VII.

3.2. Wavelet transform (WT)

Wavelet transform has been applied successfully for signal processing and image analysis in chemistry in the past decade. WT was mainly employed for de-noising and data compression in analytical chemistry, including chromatography, IR spectrometry, mass spectrometry, NMR spectrometry, etc[A.K. Leung, 1998, B.K. Alsberg,1997, S.G.Nikolov, 1996] One of main features of WT is that both time and frequency information of signal are retained. An other advantage is that a lot of basis functions can be chosen, while only the sine and cosine function can be basis in FFT. In analogy to Fourier regression, wavelet transform has been introduced as a preprocessing step before the regression, leading to the concept of Wavelet regression. Wavelet transform can also be regarded as a feature extraction tool for use in multivariate calibration in this context. The wavelet transform of signal(s) is coded as wavelet coefficients which act as regression vectors for the dependent variable(s) in the regression model.

In the work for Paper V, 2-D wavelet transform of an image was also tried out. A three-way data array composed of 2-D wavelet coefficients matrices from a set of images was subjected to multivariate data modeling. But the results were not as good as those for the 2-D FFT transform. In Paper VII, FFT worked better than WT in extracting information from acoustic signals in conjunction with chemometric modeling.

3.3. Angle Measure Technique (AMT)

The theory and applications of Angle Measure Technique (AMT) comprise a significant part of this thesis work. AMT is a new domain transform technique, which transforms the original signal into complexity spectra in a completely new scale domain. AMT was originally proposed by Robert Andrle [1994] as a novel substitute for fractal analysis to explain the complexity of geomorphic lines. This technique was later introduced into chemometrics and further to as a generic approach for all measurement series [Esbensen et al, 1996, Huang &

Esbensen, 2000]. The AMT in this thesis works mainly in image analysis as an image feature extractor. The most useful aspect of this new AMT transform is that the compound spectra (Mean Angle, Mean Difference Y, etc.) can be used as 1-D object vectors in multivariate data modelling (e.g. PCA, PCR or PLS). For 2-D image objects it is the both global and local texture of the field-of-view which is transformed into a corresponding 1-D linear complexity spectrum. These complexity spectra implicitly carry a truly remarkable information richness related to all scale(s). This is the principal feature of AMT which performs as a useful texture-characterizing pre-processing tool in very many of applications.

Some major characteristics of AMT in image analysis are:

- Digital image arrays are often (very) large 3-way data. AMT transforms a 2-D image into a 1-D complexity spectrum, without losing textural information.
- AMT can thus also (partly) be considered as a data compression method.
- AMT has a high sensitivity w.r.t. even (very) small complexity-scale changes, see Huang et al. [2001], Esbensen & Huang [2001].

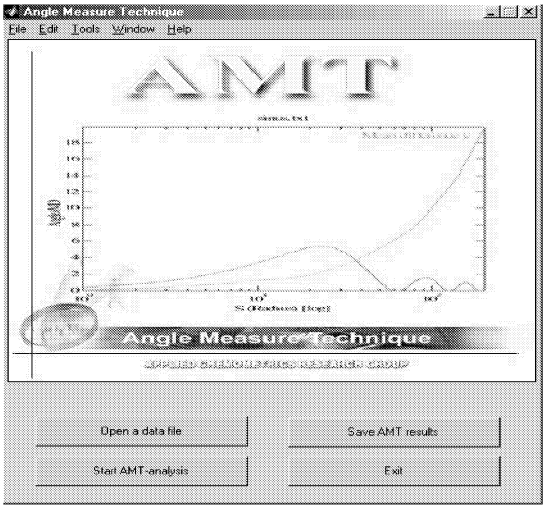

Figure 4. Graphical User Interface (GUI) of the AMT toolbox for Matlab 5.x

The author has been developing the AMT software package during this Ph.D study. Figure 4 shows a GUI of AMT toolbox for image AMT transform, which allows for selecting images, different channels, AMT calculations etc. It is designed for general purposes, so it is an easy-to-use toolbox. The core calculation part is written in Mex C (Matlab EXcutable C) and compiled to DLL in advance for much higher speed. For an image of size 512*512, it only takes a second or so to acquire AMT complexity spectra in a Pentium III computer. This toolbox is, therefore, quite promising for on-line industrial applications.

The AMT transform calculates "Mean Angle (MA)", as well as the other indices e.g. "Mean Difference Y (MDY)", by averaging all individual measures over a set of randomly chosen points along entire measurement series, Figure 6. By incrementing the scale, "S", the AMT produces the MA complexity spectra as function of scales.

Figures 5-8 illustrate the derivation process of AMT complexity spectra from a microscopic image of yogurt.

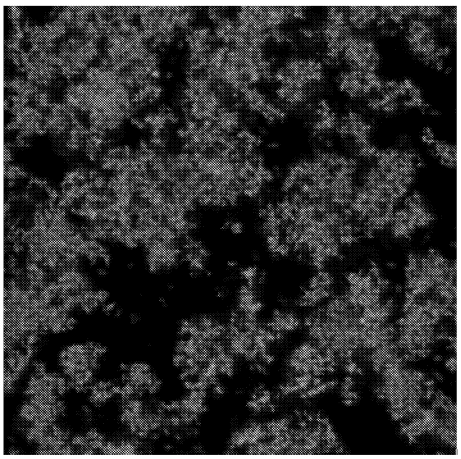

Figure 5. Microscopic image of yogurt. (*Courtesy of Arla Foods, Denmark*). Note the background is water (black).

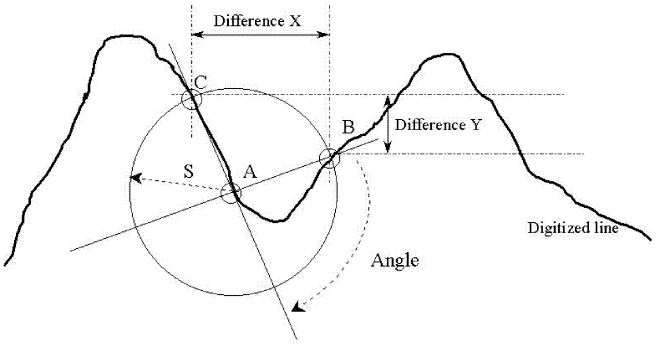

Figure 6. Explanation of the AMT derivation. The solid line represents the 1-D measurement series unfolded from a 2-D gray-level image in this case. The individual "Angle" is measured as the supplement to angle CAB. Difference X and Y is the horizontal and vertical distance between point C and B, respectively. [Huang & Esbensen, 2000]

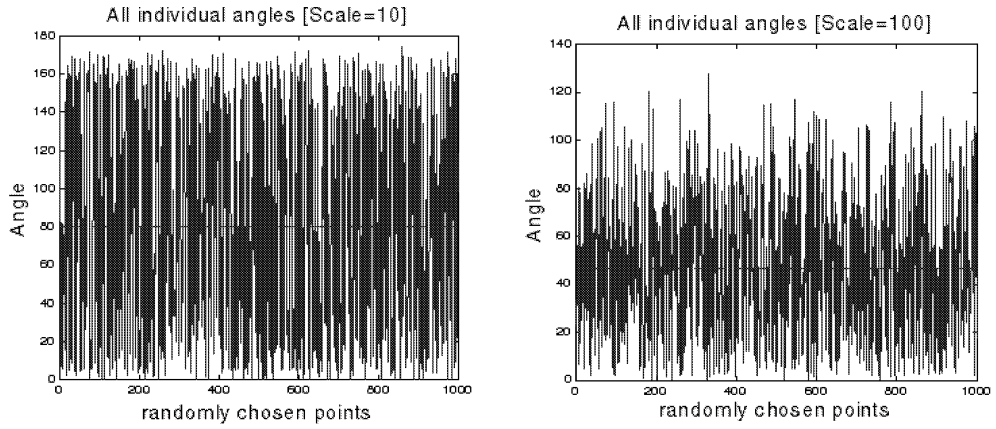

Figure 7. All individual angles measured along a number of randomly chosen 1000 points when scale =10 (left panel) and 100 (right panel).

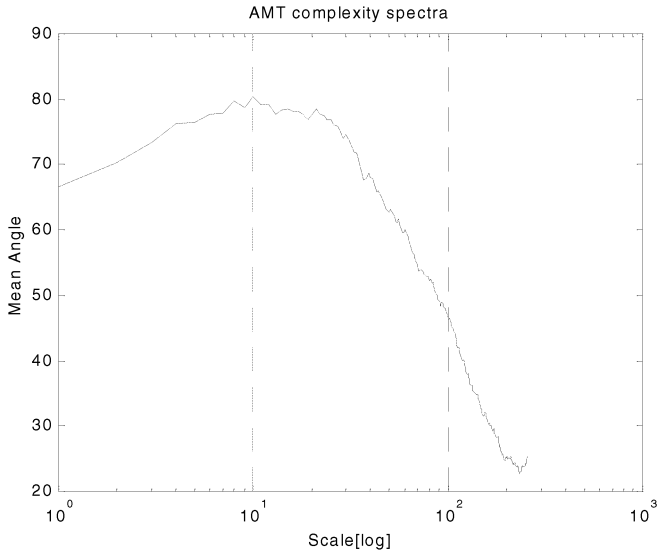

Figure 8. AMT complexity spectrum (Mean Angle) derived from the illustration above, with scale ranging from 1 to 256 (pixels). Note that Mean angles measured at scale=10, 100 from Figure 7 are marked by the two dashed lines.

This AMT toolbox also allows for preprocessing of images. For instance, images under study may contain "useless" background, or conversely, this background percentage needs to be determined. In such a case, the freedom is given to users to remove background by choosing a certain cut-off gray level, as shown in Figure 9. The AMT transform can then be performed on

a new measurement series where the "background" pixels have been removed, while the "above-cutoff" parts of the image are dynamically juxtaposed. Figure 5 is a good illustration of this type of image, where an inherent background is always present.

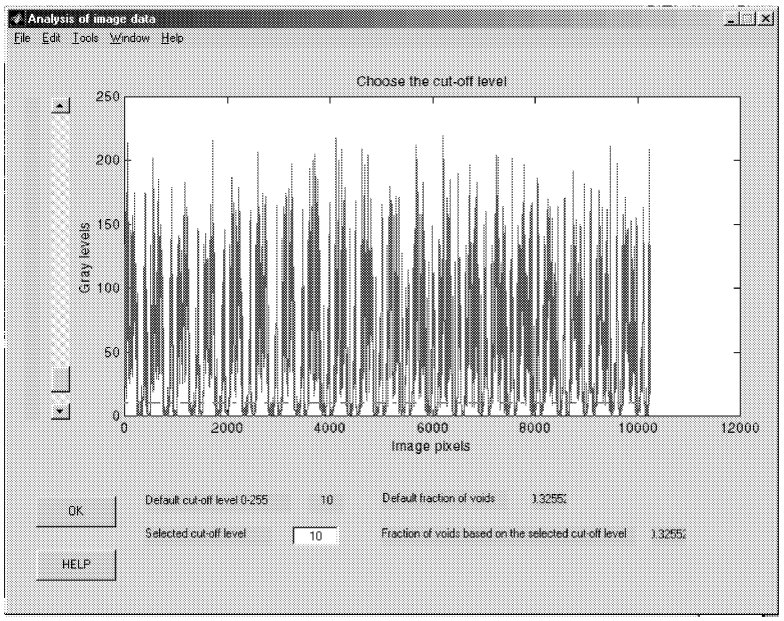

Figure 9. A dialog box for choosing cut-off level of an image for subsequent AMT calculation

The AMT complexity spectrum (MA) is calculated based on the same image, but without this background. Comparison of two relevant spectra is shown in Figure 10. The spectrum with background removed, gives higher complexity in general than the original spectrum, as can be seen from apparently more local peaks-and-valleys and higher MA-values at most of the scales. It is also indicated that some smooth information are eliminated from original signal. For detailed interpretation, see Paper I-IV.

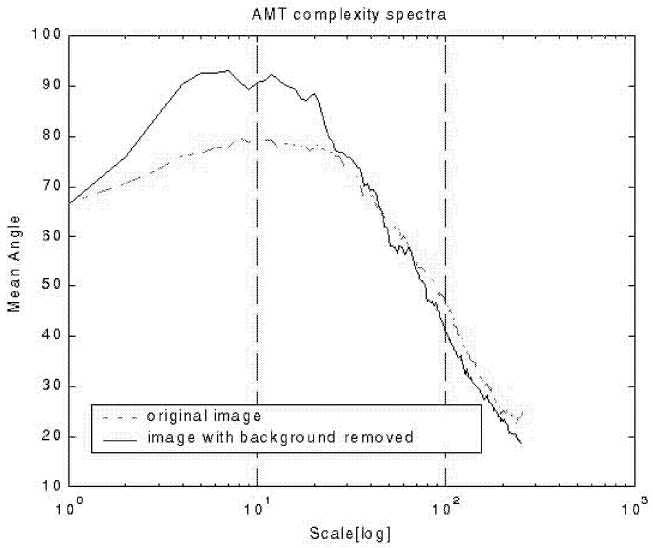

Figure 10. Comparison of AMT spectra derived from original image and "background removed" image.

Recently a new development in AMT was proposed by Kvaal & Bro [personal communication, 2000]. The basic idea is to calculate a histogram of all angles for each scale instead of mean angle. Figure 11 shows the histograms of angle measures at scale=10, 100. The argument is that some information may reside in histograms of all angles which possibly are also much related to inhomogeneous feature in the signal/image. Subsequently, a 3-way AMT landscape can be used for multivariate modeling, with the aid of 3-way methods such as Tucker3, PARAFAC, N-PLS etc. See Figure 12.

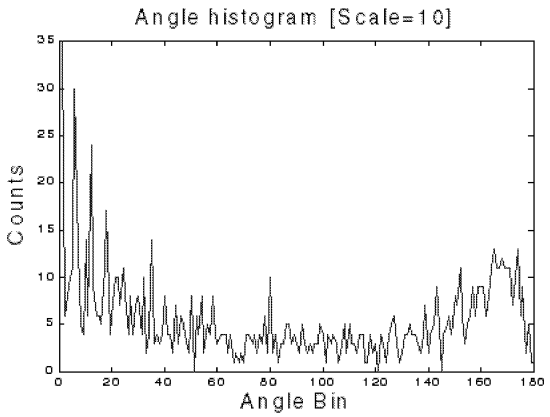

(a)

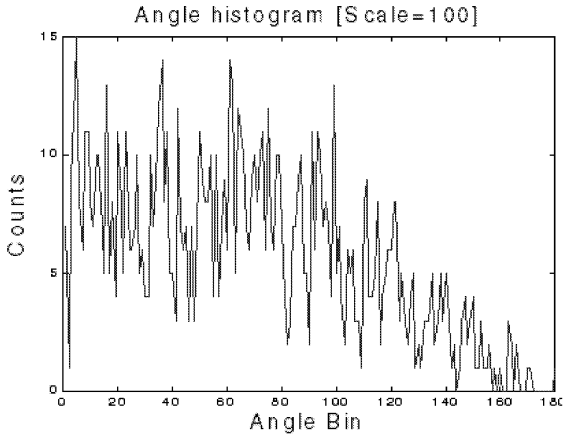

(b)

Figure 11. Angle histogram with 180 bins corresponding to a specific scale. (a) Scale=10; (b) Scale=100

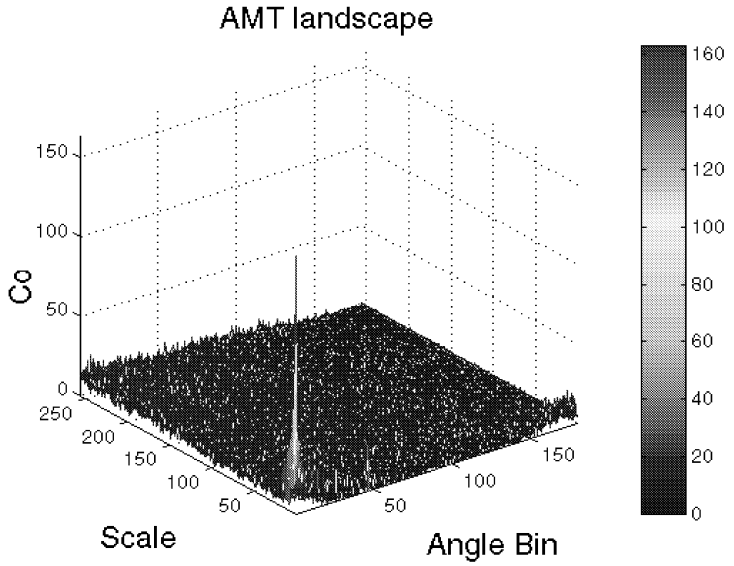

Figure 12. Two-way AMT landscape

In analogy with the above, AMT regression makes use of the AMT spectra, such as MA, MDY etc., which carry potential regression information at each corresponding scale. An AMT regression model is established between the AMT complexity spectra and a dependent variable (s).

More details are given in Paper I-IV.

3.4. Singlular Value Decomposition (SVD)

Singlular Value Decomposition(SVD) is related to principal component analysis [Geladi,1996, Kvaal 1998, Wise, 1999]. Consider an image, **X** of size ($i \times j$). The SVD of this image matrix **X** is given below:

$$\mathbf{X}=\mathbf{USV}'$$

where **U** and **V** are orthogonal matrices of size $i \times r$ and $j \times r$, respectively, and **S** is a diagonal matrix of size $r \times r$. r is the rank of **X**.

The singular values are sorted in descending order on the diagonal of **S**. The SVD spectrum λ of an image is defined as the vector of diagonal elements from **S**:

$$\lambda = \text{diag}(\mathbf{S})$$

Usually a truncated version of the SVD spectrum will be used :

$$\lambda_{tr} = diag(S_{tr})(tr \leq \min(i, j))$$

The SVD spectra containing information from a set of images can now be arranged as object vectors for subsequent multivariate data modeling. This technique has been used e.g. to predict the sensory porosity from bread images [Kvaal, 1998].

3.5. Autocovariance (ACOV) and autocorrelation (ACOR) spectra

The Autocovariance (ACOV) and autocorrelation (ACOR) spectra are also used for multivariate feature extraction due to their statistical interpretations and potential of reflecting characteristic information of different textures. Like AMT and SVD spectra, they also give decaying spectra containing information from images. How fast the spectra decay gives indication of different textural characteristics, e.g. texture images with large amounts of local variation generate slowly decaying spectra. The 1-D ACOV and ACOR spectra can also be estimated from images, and then facilitated for multivariate characterization [Kvaal, 1998].

There are certainly many more feature extraction tools for images. But only those techniques in relation to this research work are discussed here.

In conclusion, image feature extraction techniques in conjunction with multivariate methods provide a powerful approach for a variety of promising applications, e.g. discrimination and classification of samples, prediction of properties of samples from images etc. On-line applications e.g. monitoring image features can be made possible by using rapid imaging and multivariate modeling. It is, however, important to realize that the choice of multivariate feature extraction techniques depends much upon *a priori* knowledge of data/images under investigation, e.g. the structures of images. Experience from Paper I-V indicates that FFT works better than WT for prediction of rheological properties from microscopic cheese images, for example, and AMT seems superior for capturing information from irregular texture images, *ibid*.

4. MULTI-WAY METHODS IN IMAGE ANALYSIS

Spontaneously, the question " why multi-way methods in image analysis" would arise at first sight of this title. Images, coming in various forms, from microscopic via digital camera to satellite images, provide a set of low-cost tools, with rich information, to characterize complex samples and hence are receiving more and more attention nowadays. Image data, such as in chemistry and chemical engineering, are inherently multivariate due to the fact that they can be up to three spatial dimensions and many spectral dimensions. Time, temperature, or environmental studies can add more dimensionalities to the image data. Tackling these image data begs for multi-way models from chemometrics. MIA is a typical example of using the unfold-PCA model. The extended concept, N-way image analysis, is concerned with applying both "weak" and "strong" multi-way methods to image analysis. Paper V is dedicated to this issue and hopes to be inspiring for more contributions to this area. In this paper, both weak and strong multi-way methods are applied in order to decompose and characterize image data (macro satellite images, virtual fluorescence images and microscopic images), and obtain systematic insight into their abilities to capture data structure. Attempts are also made to investigate the relationships between serial images and their corresponding properties. Comparisons of the efficiencies of these methods are also given. However, the goal of comparison is not to verify one method over another, but rather to explore some new, alternative approaches to N-way image analysis and furthermore to investigate the differential suitability of the methods applied.

4.1. Relations of image analysis, processing and data analysis

The concepts of image analysis, image, data analysis and image processing are used widely but with little consistent terminology discipline. As described in the book *Digital Image Processing* by Gonzalez & Woods (1992), image analysis is composed of three areas, low-level, intermediate-level, and high –level processing. In the low-level processing, image acquisition and preprocessing are treated. Intermediate-level processing extracts and characterizes the components in an image resulting from a low-level processing. This encompasses segmentation and representation. Finally, high-level processing involves recognition and interpretation, which is usually the principal point of image analysis. Image analysis distinguishes itself from image processing in that the ultimate output of image analysis is numerical data and knowledge rather than a direct image(s). Geladi & Grahn (1996) generalized the relation of image analysis and data analysis as shown in Figure 13.

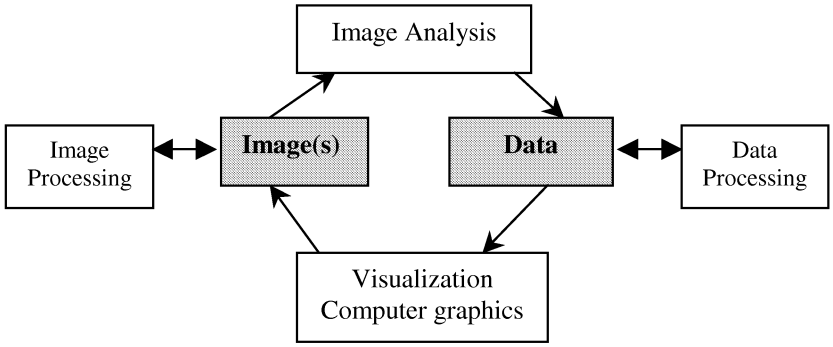

Figure 13. Relationships between images, data, analysis and processing. [Geladi & Grahn, 1996].

A huge literature can also be found on color imaging/univariate digitized image analysis [Gonzalez & Woods, 1992, Bernd, 1997, Geladi & Grahn, 1996]. Many numerical, mathematical, or statistical techniques have been applied to image data in the vast area of image analysis. Common methods for recognition are decision-theoretic methods that represent patterns in vector form, and structural methods based on symbolic form (such as strings and trees). Correlators, Bayes classifiers and neural networks are typical approaches to decision-theoretic recognition, while symbolic matching and syntactic methods form the structural approaches. Techniques for image interpretation are based on predicate logic, semantic networks, and production systems.

Present techniques for recognition and interpretation are based on multivariate data analysis, e.g. Multivariate Image Analysis, N-way image analysis which will be described in Paper V.

4.2. Terminology and history in N-way image analysis

In recent years, multivariate techniques have also be introduced to image analysis, dealing with data modeling of complex images. The introduction of multivariate data analysis to image analysis has opened up new approaches to analyze image, e.g. segmentation, representation, recognition and interpretation etc. Multivariate Image Analysis (MIA) including Multivariate Image Regression (MIR)/Multivariate teXture analysis (MIX) are typical methods [Esbensen & Geladi, 1989, Geladi & Grahn, 1996, Windig, 1998, Esbensen & Lied, 1999]. MIA is not separate from the three levels of processing mentioned above. It focuses more on intermediate and especially high-level processing, with its own unique approach. Based on multivariate techniques like PCA and PLS, MIA offers a completely different new way to image analysis (segmentation, recognition and interpretation). A MIA model uses a bilinear decomposition of image data (soft modeling) to segment, recognize and interpret image with the aid of visual

graphical plots, which allows for a great deal of flexibility. Applications have been found in many fields such as microscopy, satellite remote sensing, medical imaging, radiology, process technology, chemistry, spectroscopy and astronomy, etc [Esbensen & Geladi, 1989, Macgregor et al, 1997, Windig et al, 2000, Lied & Esbensen, 1999, Huang & Esbensen, 2000, etc.].

A new, more general term for multivariate data analysis on images, N-way image analysis, is proposed in this work for the application of all multi-way methods to image analysis [Paper V]. The unique aspect of N-way image analysis is a.o. also the possibility of modeling of *multiple* images simultaneously, not just of *one single* image. Here multiple images can refer to multivariate images (congruent), as well as more easily obtainable images (incongruent) which possess common properties and interrelationships. Different multi-way models are applied to different types of multivariate images. It is underlined that *a priori* knowledge of image data and appropriate problem formulation is imperative in choosing pertinent multi-way models for properly configured image data.

Some interesting work has been done in food technology, in which multivariate techniques made it possible to carry out a combinatorial study of data from different measurement systems e.g. fluorescence, NIR, image features etc. Models were established to determine complex quality characteristics in food [J.P. Wold etc. 2000].

However, the huge potential of multivariate data analysis on images has not been explored widely, which can be seen from the still rather limited number of literature in this area.

4.3. Data configuration in multivariate data analysis on images

Many multivariate models are available for N-way image modeling. However, one can not just apply different models directly on “image data”, but one must have a clear overview of data configuration and scientific objectives as mentioned earlier.
It has been pointed out in Paper I and Paper V that proper data configuration is important in multivariate data analysis on images. It is essential that choosing an optimal data analytical methodology require an appropriate data configuration pertaining to the salient problem formulations in N-way image analysis. Arrangement of the often huge amount of image data is intimately connected with a scientific goal or pertinent problem formulation. One of the fundamental prerequisite of multi-way modeling is that data array be trilinear (for three-way). Arrays of three-way data can be characterized by a categorical object/variable (**O/V**) convention. Four different three-way configurations are represented by codes (**OOO**), (**OOV**), (**OVV**) and (**VVV**), of which the two extremes are usually of no practical consequence for multivariate data analysis. A three-way data array composed of a multivariate image, for instance, may be organized as **OOV**, which is perhaps most familiar three-way data array in N-way image analysis. Data configuration may become more complicated when a third categorical

direction (mode) is introduced, *Time*. It is argued that Time should be treated as a **V**-direction or its own direction, as *Time* would appear to be equivalent to V-direction in process chemometrics. Multi-temporal multivariate images are a stack of images of the same object characterized at different time intervals. This type of image data array can be represented as **OOT**.

In a simpler case, two-way data arrays can be constructed with the aid of multivariate feature extraction techniques, such as AMT, SVD, ACOR/ACOV etc. Any of these techniques can transform 2-D images into 1-D object vectors, in a new domain which helps form a new variable mode (s) for subsequent 2-way modeling [Paper I-IV].

It is noteworthy that advanced imaging and spectroscopic technology today allows for rapid collection of both spectral data and images. Spectroscopy could be considered a special case of imaging, a 1-D image. Both spectral data and images can be combined by means of multivariate chemometric modeling to provide a powerful approach to extract maximum information from the system(s) under investigation.

5. ACOUSTIC CHEMOMETRICS

Acoustic chemometrics is a non-invasive quantitative measurement technique, characterized by easy "clamp-on" deployment of acoustic sensors, followed by an essential and integrated signal analysis/multivariate calibration data modeling. Acoustic chemometrics is an emerging discipline, encompassing diverse fields such as electronics, applied engineering and chemometrics and combines acoustic sensor technology with multivariate data analysis [Esbensen et al, 1998, 1999].

The generic data flow path in acoustic chemometrics is shown in Figure 14 below.

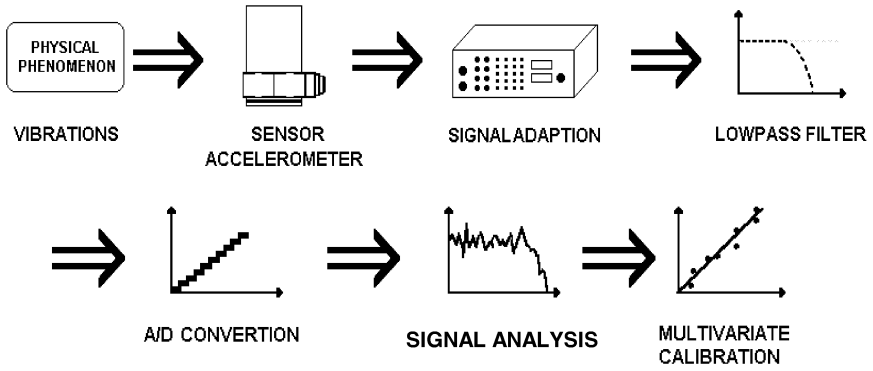

Figure 14. Schematic data flow path in acoustic chemometrics (*Courtesy of M. Halstensen*).

The working of acoustic chemometrics principally consists of four main elements:

Sensor technology: Selection of types/number of sensors, positioning, mounting etc;
Data acquisition: cabling, signal conditioning (amplification, filtering), signal processing (A/D conversion etc.);
Signal analysis: Transformations including FFT, Wavelets, AMT (Angle Measure Technique) [5], autocorrelation, etc;
Multivariate modeling/calibration: PLS regression for multivariate calibration and prediction of quality parameters of interest from acoustic data.

Acoustic chemometrics aims to be able to measure directly from the outside of a pipeline/container wall, at a valve, on suitable flanges or similar constructions by "listening" to the acoustics from inside the conduit etc. The basis of this approach is due largely to the fact that emission of "noise" is an inherent characteristic of many production, manufacturing and transportation processes. "Noise" here means acoustic energy output not only in the audible range (5-20KHz), but also denotes the forms of vibrational energy in contiguous frequencies outside audible range, i.e.0-5, 20-250KHz. Acoustic signals generated from process e.g.

pneumatic transport lines must contain abundant information about the process. The establishment of links between the acoustics and the parameters of process/products demands the use of chemometrics. It plays a major role in searching for the correlations between acoustics and process/products under investigation. It is indispensable as an integral part of many new measurement techniques. In sum, acoustic chemometrics makes use of domain transformations of acoustic signals characterizing vibration spectra developed in the process, as X-input for multivariate calibration of parameters Y.

The phenomenological master equation (associated with FFT) for acoustic chemometrics can be written as

FFT X-spectra =F (intrinsic physical/chemical properties, *i.e. concentration, velocity, flow-rate, temperature, particle size distribution, etc….*)

This is to be related to a multivariate regression modeling (associated with PLS)

Y parameter(s)= PLS-R (FFT X-spectra)

Acoustic chemometrics is used to monitor powder breakage during pneumatic transport in Paper VI.

6. APPLICATIONS OF AMT, MULTI-WAY METHODS IN IMAGE ANALYSIS AND ACOUSTIC CHEMOMETRICS

The development and applications of multivariate chemometric tools within the realm of this thesis has been largely driven by the need for efficient methods in extracting information and exploring data structures from raw data such as images and acoustics, and establishing models that can relate sample properties to easily obtainable raw data.

Figures 15-18 generalize the unified multivariate approaches developed for multivariate characterization and prediction, and applications detailed in Paper I-VI.

6.1. AMT applications

In powder industry, traditional image analysis for powder characterization focuses on the *individual particles* typically using e.g. microscopic imaging and individual morphology description etc. There is very often a long and troublesome procedure before even trying to translate this piecemeal information to characteristics of powders. Traditional image analysis also necessarily involves a difficult and time-consuming *sample-preparation* process, such as *dispersion* of the powders before microscopic imaging etc. This makes it extremely difficult to carry out a on-line, or at-line measurements in practical situations. Completely discharging any specific dealings with the individual particles, the present alternative multivariate AMT chemometric approach, acquires images directly from *in-situ* powders with *an absolute minimum sampling preparation* necessary, followed by the AMT transforms, multivariate image analysis and/or chemometric modeling. This type of imagery, recordings of the entire field-of-view of powders, also contain some information relating to the individual particles, but mainly about the *bulk powder*, which is a reflection of the complex bulk, *interacting* properties of the powder, for example “stickiness”, flowability, fluidization velocity etc. The advantage of using AMT is that AMT characterizes the complexity of both local individual particles and global bulk powders simultaneously. For example, some local properties like individual particle size, shape, roughness, smoothness, regularity etc. can be represented, from which the related global properties like flowability, fluidization velocity, wall friction angle can also be described by multivariate AMT regression. These important powder functional properties usually have to be measured by running large-scale experiments, which requires much time and money. The AMT approach derives *predictions* of the relevant powder properties under one roof, however. The AMT image features—spectra---contain information necessary to predict a great many of these properties. This work explores to what extent this is possible. The image analytical global field-of-view approach based on simple and direct powder image analysis, coupled with chemometric data analysis, appears very practical and well suited for industrial use, and especially for at-line or in-line characterizations, see Figure 15. Details are given in Paper I and II.

Further applications of Multivariate AMT approach are given in Paper III and IV.

This unified approach has also been used to conduct fast and automated monitoring of a germination process. Germination frequency and speed of germination plays a key role for yield assessment in agriculture and for estimating malting quality in the brewing industry. It is crucial for the malting industry to obtain a fast and homogeneous germination in the malt house. Therefore it is of great importance to have a fast and objective germination test to investigate the malting barley before malting it. High percent germination and vigorous growth means a good malting barley variety. Selecting a variety is the first step in successful production and marketing of malting barley. Currently, there is a lack of efficient methods available to measure germination percentage of barley. The number of germinated barley kernels is usually counted manually in the laboratory. This is very laborious, time-consuming and subjective. There is a strong need from industry calling for fast, automatic methods in measurements of germination percentage. The present new compound method, multivariate AMT approach in combination with image analysis appears promising for industrial use due to its simple imaging and fast modeling as shown in Figure 15. This approach is able to characterize germination process and conduct indirect measurement of percentage of germination varying with time. [Paper III]

The existence of non-neglectable quantities of *impurities* (pollutants) in virtually any mass produced product is unavoidable in many industry sectors because of competitive economic and production technology pressures a. o. Sectors like food, feed and beverage production are prime examples, but the problem of a non-zero impurity level is almost universal in the *particulate industries*. The purity of final products is one of the critical criteria for many quality evaluations. Sugar manufacturers, for instance, need strict control and very high-sensitivity detection of the impurity levels in their process and products. Wheat/rice producing companies have to check very thoroughly for impurities of foreign grains, e.g. sand and small stones in their products. The currently used techniques used for impurity detection are typically either too laborious, too expensive, or too slow to be applied for effective on-line, precise manufacturing control. In fact current processes often badly demand fast, cheap and time-saving methods for higher profits. The new AMT chemometric approach is comprised by a novel image feature extraction technique and multivariate calibration (PLS), allowing for very accurate and precise impurity detection by image analysis. Fast digital imaging of *in-situ* powders with a calibration range of trace amounts of various pollutants, coupled with fast multivariate AMT regression provide a unified approach for quick quantitative impurity detection as shown in Figure 15. [Paper IV]

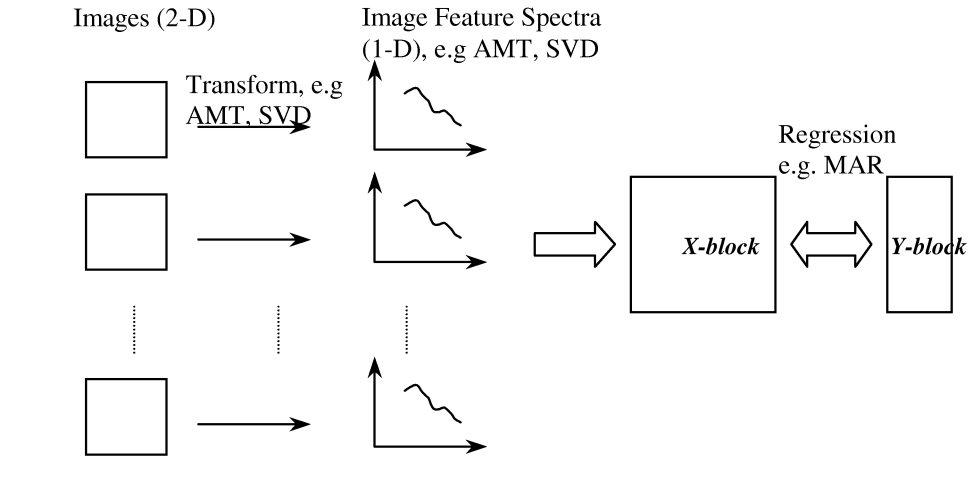

Applications of this approach and multivariate models touched upon in this thesis

- Powder characterization and discrimination.(PCA) [Paper I]
  Problem: Difficult sampling, microscopic imaging, individual particles, morphology descriptions…
  Solution: imaging of an assembly of particles, easy sample preparation, AMT transforms, multivariate image analysis and/or chemometric modeling

- Prediction of Powder Functional Properties (PLS-based Multivariate AMT Regression (MAR)) [Paper II]
  Problem: No efficient and accurate methods to measure or predict powder functional properties…
  Solution: Multivariate AMT Regression + simple imaging

- Characterization of barley germination process (PLS-based Multivariate AMT Regression (MAR)) [Paper III]
  Problem: Germination test is laborious, and fast, automated methods are in demand …
  Solution: High sensitivity of AMT to image change, Multivariate AMT Regression + simple imaging

- High-sensitivity particulate impurity detection and quality control. (PLS-based Multivariate AMT Regression (MAR)) [Paper IV]
  Problem: Efficient methods for impurity detection in industry…
  Solution: High sensitivity of AMT to image change, Multivariate AMT Regression + simple imaging

Figure 15. A schematic overview of multivariate chemometric approaches combined with multivariate feature extraction techniques and applications discussed in the text.

6.2. Applications of Multi-way methods in image analysis

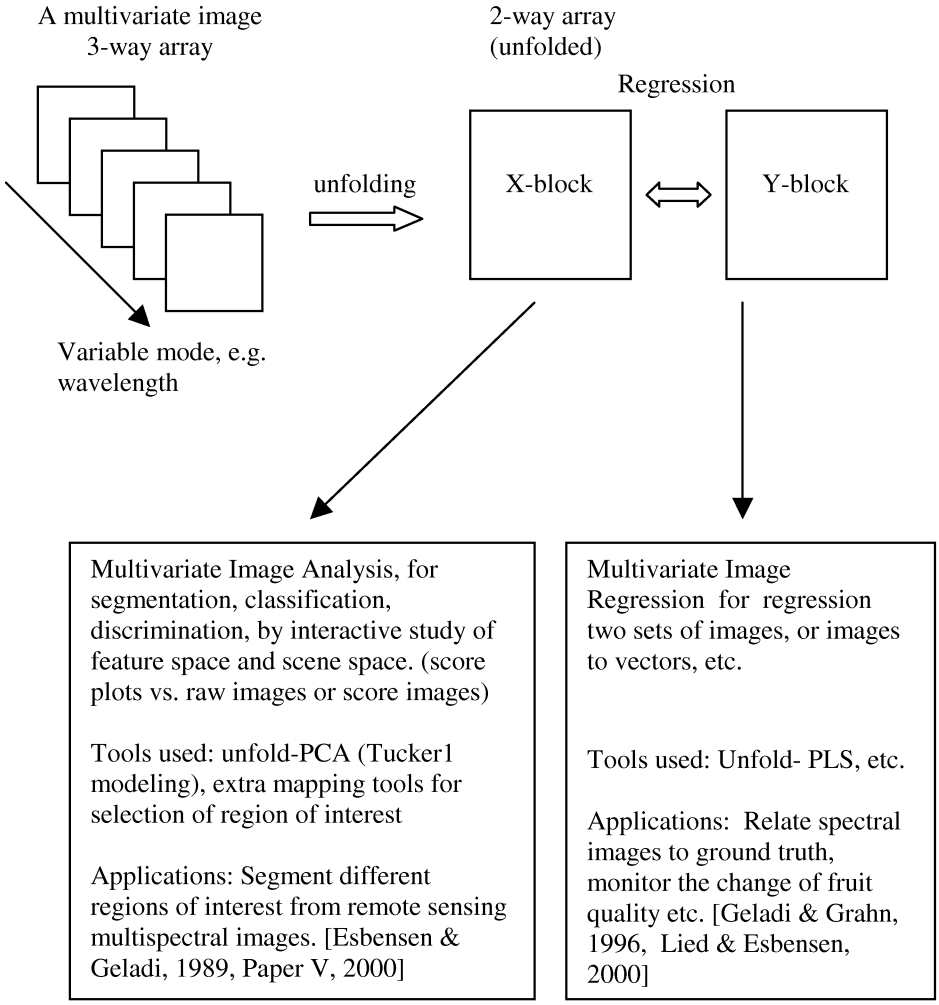

Figure 16. An overview of the MIA approach and its applications discussed in the text

Paper V gives an overview of multi-way methods in image analysis, elaborating the proper relationships between strong and weak multi-way data decompositions, their pro's and con's and their relative merits. The paper presents a fairly complete catalogue of representative usages of the many multi-way methods by displaying three application examples on multi-spectral images, virtual fluorescence images and microscopic functional property images using both weak and strong multi-way methods.

Application I shows the possibility for application of strong multi-way methods on multi-spectral images, otherwise conventionally analyzed by MIA approach shown in Figure 16. By

contrast, application II attempts to investigate the feasibility of applying MIA models on typical three-way data, normally handled by strong multi-way methods and provides a new perspective of dealing with fluorescence spectra as images. In application III, microscopic images were taken on a set of different cheeses, which were made from a factorial experiment by varying coagulation temperature and the amount of rennet enzyme at a number of levels. The objective here ultimately is to derive functional properties prediction models. Reference rheological properties for these cheeses were tested by uniaxial compression techniques. Attempts have been made to discriminate different cheeses and predict rheological parameters from these cheese images by multi-way methods.

The objective of Paper V is to review the multi-way methods from the perspective of proper (i.e. problem-dependent) data array organization and the many multi-way methodological methods presented in the literature.

Figure 17 shows the general approach of 3-way (N-way) image analysis in relation to typical problem formulations.

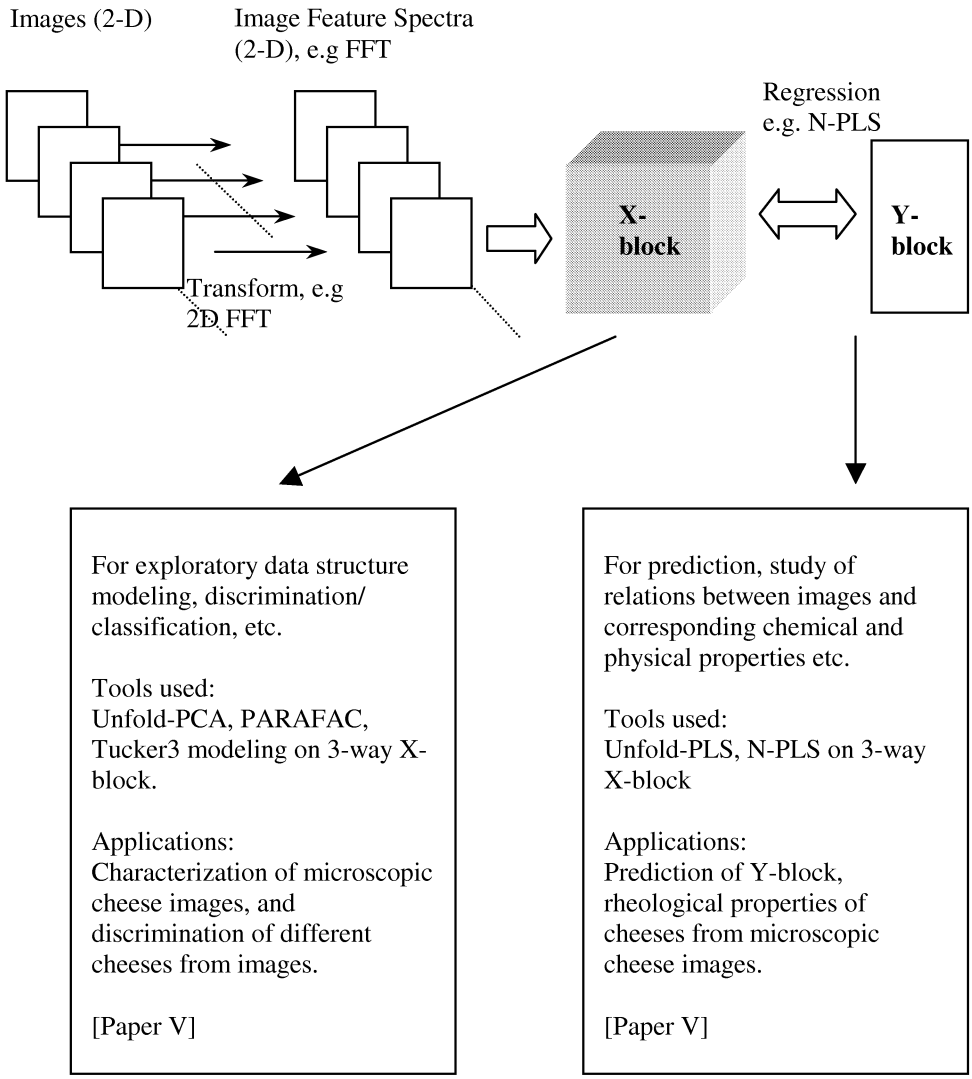

Figure 17. The development and generalization of 3-way (N-way) image analysis and its applications discussed in the text.

6.3. Applications of acoustic chemometrics

The objectives of acoustic chemometrics are manifold, such as quantitative measurements and process monitoring. This approach has been used for quantitative measurement of volume flow rate, multi-component mixture concentrations, density, particle size distribution, and other physical/chemical parameters in multi-phase flow. Figure 18 generalizes this acoustic chemometric approach and industrial and technological applications.

In the present application, acoustic chemometrics is used for non-invasive monitoring of powder breakage during pneumatic transport. Six types of alumina with different particle size distributions have been tested for breakage in a plant-scale transport rig. We have investigated the correlation between acoustic signals and the breakage of particles during pneumatic transport, and the applicability of acoustic chemometrics as a tool for discovering quality variations (i.e. varying particle size). By relating the acoustic information to dust fractions from the process, we assess the possibility of predicting powder breakage during transport, based on acoustic sensor technology and multivariate data modeling.

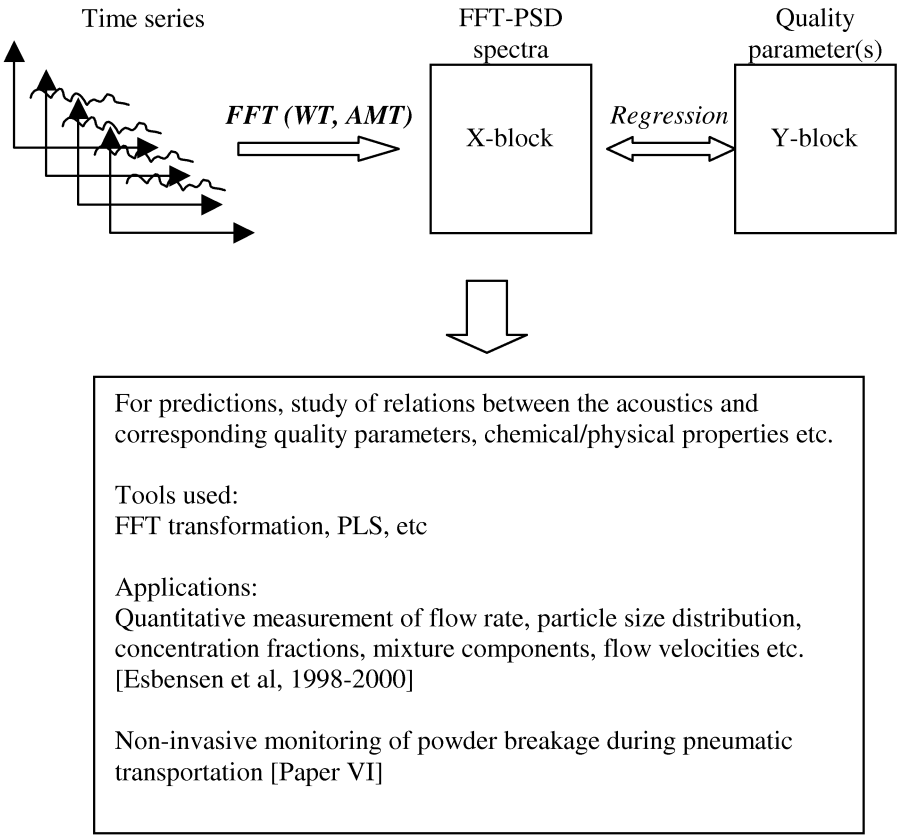

Figure 18. Acoustic chemometric approach and applications, see details in the text.

7. DISCUSSION AND CONCLUSIONS

7.1. DISCUSSION AND CONCLUSIONS

The main topics in this thesis resulted in selected developments in applied chemometrics: AMT, N-way image analysis and acoustic chemometrics.

In Paper I, a new, compound approach for powder characterization/discrimination, based on image analysis, AMT and PCA modeling is presented, where the theory of AMT is described in detail. A companion Paper II proposes a unified methodology for this type of data analysis, Multivariate AMT Regression (MAR), opening up for a wide range of application areas. These AMT approaches are able to extract and characterize multivariate features stemming from digital video images, as well as to discriminate/classify different powder types and predict powder functional properties and mixing components from images.

Further applications of this image AMT chemometric approach are given in Paper III and IV. Paper III describes the characterization of barley germination process from images using combined image AMT, while Paper IV demonstrates the use of this approach for high-sensitivity particulate impurity detection and quality control

In the above multivariate AMT approaches, the AMT functions as a versatile feature extraction tool to obtain information from complex systems. It also helps to facilitate image data arrays for chemometric modeling in terms of new data configuration(s). Other domain transform techniques can perhaps also analogously be used to extract features and configure data for modeling in a similar way.

Paper V gives a systematic overview of relationships and applications of multi-way methods in image analysis, N-way image analysis. The primary objective in this paper is to review multi-way methods from the perspective of proper data array organization and problem formulation, and to investigate the relative suitability of the models applied. It should be underlined that data configuration and problem formulation has direct impacts on the choice of pertinent multi-way methods. In chemometrics, there are many rather bewildering issues concerning how to organize the object-, variable-, time-way etc, and which particular method to use in terms of the stated scientific goal(s). We have in particular applied strong and weak multi-way methods on both conventional OOV and OVV image arrays. The suitability of the models varies from example to example. For instance, MIA based on unfold-PCA is very well suited for multi-spectral image (OOV) classification, while PARARFAC is suited for recovering pure spectra from three-way fluorescence data (OVV). N-PLS works better than unfold-PLS in predicting functional properties from a 3-way image array (OVV). A fairly representative set of multi-way methods were applied in this survey, including deliberate “cross-over” experiments, in order to

show that how exploitation of multi-way methods is logically restricted by the problem and data array prerequisites.

In Paper VI, acoustic chemometrics is used to monitor powder breakage during pneumatic transport. This non-invasive method is generally successful in relating the acoustics to the particle size distributions of aluminum powders transported. There are still many remaining issues concerning the details of the physics behind acoustic vibrations which are decomposed, how precise this approach can be in the real-world applications, and more signal domain transform techniques to be tried out etc.

7.2. FUTURE WORK

The AMT methodology and applications have been a prominent part of this thesis work. There are still some remaining issues in AMT study concerning the following:

- How to exactly interpret the AMT spectra. More quantitative and qualitative information might be extracted by further and deeper understanding of the mechanisms behind the successful predictions.
- The AMT work here has been largely focused on image analysis. We have also tried to apply AMT on NIR spectra and acoustics. The difficulty we had is how to choose the optimal AMT parameter settings in terms of specific signals.
- Instead of Mean Angle, a histogram of all angles for each scale may be calculated to obtain a 2-way AMT spectra. This makes it possible to apply 3-way modeling on 3-way AMT data. Some extra information may perhaps be obtained especially for e.g. inhomogeneous images in this way.

Further work on AMT can be continued towards the above problems.

In this thesis there is also an important emphasis on multi-way methods in image analysis. Further study of the relationships between multi-way models and data configuration needs to be carried on. New types of image data may need to be investigated and properly configured, and require suitable multi-way methods. There is definitely a huge potential of applications in image analysis, e.g. to combine spectroscopy and digital imaging for chemical analysis.

It will be another focus in the near future to carry out a systematic comparison study of different preprocessing techniques (WT, FFT, AMT…) in acoustic chemometrics as well as in other applications.

Much fascinating and challenging work remains in the above areas.

7.3. SUMMARY OF ACHIEVEMENTS

The following summary lists the most important achievements in this thesis:

Methodology developments:

- Multivariate AMT approach
  --AMT image analysis (Paper I-IV)
  --Multivariate AMT Regression (Paper II-IV)
- Preprocessing facilities to multivariate chemometric modeling
  --Systematic approach of using feature extraction techniques with multivariate modeling (Paper I-VI)
  --FFT, WT transformations on images and acoustic signals combined with PLS, N-PLS (Paper V, VI)
- Systematics of multi-way methods in image analysis (Paper V)
  --Relationships of multi-way models in N-way image analysis
  --Guidelines in choosing pertinent multi-way models for properly configured image data

Applications:

- Powder science and technology examples (Paper I-II, IV, VI)
- Food science and technology examples (Paper III, V)
- Industrial application examples (Paper I, II, VI)

Software developments:

- The AMT toolbox for Matlab™ (see details in appendix)

Collaborations:

- POSTEC (Powder Science and Technology), Tel-Tek, Porsgrunn
- Chemometrics group, Royal Veterinary and Agricultural University, Copenhagen
- *Arla Foods*, Denmark
- *Danisco,* Denmark
- *CAMO ASA,* Oslo

8. EPILOGUE

Some interesting discussions and debate on image/signal analysis are going on via the ICS-L chemometrics web forum at the time I'm finishing this thesis. The central issue is related to whether or not some terms such as image analysis, signal processing should be categorized into the field of chemometrics, as well as awareness of the need to create new terms in chemometrics or not [Wold, Chang, 2000]. The chemometrics history has seen more and more image analysis combined with chemometric techniques in the past decade. Some pioneering work, e.g. Multivariate Image Analysis, has been carried out by Geladi & Esbensen since 1989. S. Wold pointed out that image analysis is at least part of the new chemometric wave [ICS-L web forum, 2000]. The reason is very simple and obvious. Images, from microscopic via digital camera to satellite images, provide a vast set of tools, with low cost and rich information, to characterize complex samples and hence will be used everywhere very soon. It is certainly reasonable to state that image analysis is now a part of chemometrics in a sense that new simple and robust chemometric approaches can be developed to make use of image information. Furthermore, chemical data come in more varied fashions than ever, and images containing chemical information can certainly be called chemical data. The chemometric analysis of such images with the purpose to obtain chemical information/knowledge is then within the field of chemometrics as well as image analysis.

This is the same case with signal analysis such as Fourier and Wavelet analysis. When they are introduced to chemometrics, they can be used with classical and modern chemometric techniques, and then become part of new chemometric approaches or techniques, i.e. Fourier regression and Wavelet regression. Analogously, the term "multivariate AMT regression (MAR)" arises when AMT is used in conjunction with regression modeling. Acoustic chemometrics is another typical example, which combines acoustic sensor technology with chemometric modeling. Some other terms in relation to image analysis developed in this thesis work include MIA/MIR, 3-way (N-way) image analysis etc, as well as some new approaches/techniques for multivariate image feature extraction, discrimination/classification, prediction etc.

All in all, those terms/methods can be collected under the label of chemometrics when they are used in a typical chemometric context. It is, therefore, not illegal and sometimes necessary to create new, proper terminology which may differ from the same thing used elsewhere, but this should always be done with care and with the proper respect for the pertinent origins.

I'm proud and happy to be a part of this continued chemometics movement. Chemometrics is very exciting!

9. FULL PUBLICATION LIST

1. J. Huang and K.H. Esbensen, Applications of AMT (Angle Measure Technique) in Image Analysis Part I. A New Methodology for *in-situ* Powder Characterization. *Chemometrics and Intelligent Laboratory Systems. 54/1*. (2000) pp 1-19

2. J. Huang and K.H. Esbensen, Applications of AMT (Angle Measure Technique) in Image Analysis Part II. Prediction of Powder Functional Properties and Mixing Components using Multivariate AMT Regression (MAR). *Chemometrics and Intelligent Laboratory Systems*, *In print*. 2001

3. J. Huang, B. Møller, L. Munck and K.H. Esbensen, Development of a new method for characterization of barley germination by automated image analysis and AMT (Angle Measure Technique), Submitted for publication in *Journal of the Science of Food and Agriculture*, 2001

4. K.H. Esbensen and J. Huang, Applications of AMT (Angle Measure Technique) in Image Analysis Part III: High sensitivity particulate impurity detection and quality control. Submitted for publication in *Chemometrics and Intelligent Laboratory Systems*, 2001

5. J. Huang and K.H. Esbensen, Multi-way methods in Image Analysis: Relationships and Applications. Submitted for publication in *Journal of Chemometrics*, 2001

6. J. Huang, S. Ose, S. de Silva and K.H. Esbensen, Non-invasive Monitoring of Powder Breakage during Pneumatic Transportation using Acoustic Chemometrics. Submitted for publication in *Powder Technology*, 2001

7. K. H.Esbensen and J. Huang, Functional parameter prediction using the new, powerful Angle Measure Technique (AMT). *POSTEC Newsletter No. 19*, Porsgrunn, Norway

8. K. H.Esbensen and J. Huang, The Angle Measure Technique (AMT) for textural pre-processing in Multivariate Image Analysis (MIA). *NAmICS Newsletter No. 21*, NAmICS, 2000.

9. T. T. Lied, I. H. Matveyev, D.F. Karlsrud, J. Huang and K.H. Esbensen, Image-Analytical Quantitative Monitoring of Heterogeneous Mixture Processes: Comparing and Combining Angle Measure Technique (AMT) and Multivariate Image Regression (MIR). Submitted for publication in *Chemometrics and Intelligent Laboratory Systems*.2000

REFERENCE

(This compilation lists all references used in the present thesis work, either referenced in the introduction above, or in the individual papers; or as used in the examination courses required for the degree of Dr.ing.)

1. A. Höskuldsson, Prediction Methods in Science and Technology. Thor Publishing. 1996. ISBN 87-985941-0-9
2. A. K. Leung, F. Chau, J. Gao, A review on applications of wavelet transform techniques in chemical analysis: 1989-1997. Chemometrics and Intelligent Laboratory Systems, 43 (1998) pp 165-184.
3. A.K. Smilde, Comments on multilinear PLS. Journal of Chemometrics, vol 11, 367-377 (1997)
4. B. Antalek, J.P. Hornak, and W. Windig, Multivariate Image Analysis of Magnetic Resonance Images with the Direct Exponential Curve Resolution Algorithm (DECRA), Part 2: Application to Human Brain Images, Journal of Magnetic Resonance, 132, 307-315, 1998
5. B. Wise et.al., A comparison of principal component analysis, multiway principal component analysis, trilinear decomposition and parallel factor analysis for fault detection in a semiconductor etch process, Journal of Chemometrics, **13**, 379-396 (1999)
6. B.G.M.Vandeginste,et.al, Handbook of Chemometrics and Qualimetrics: Part B. Data Handling in Science and Technology, Elsevier Science 1998. ISBN 0-444-82853-0
7. B.K. Alsberg, A. M. Woodward, D.B. Kell, An introduction to wavelet transforms for chemometricians: A time-frequency approach. Chemometrics and Intelligent Laboratory Systems, 37 (1997) pp 215-239
8. B.K. Alsberg, et.al, Wavelet denoising of infrared spectra, Analyst, 1997, Vol.122 pp 645-652
9. C. E. Miller, Chemometrics for on-line spectroscopy applications - theory and practice. Journal of Chemometrics, 14 (2000) 513-528.
10. C. Lu, P.C. Chung, C.F. Chen, Unsupervised texture segmentation via wavelet transform. Pattern Recognition. Vol.30, No.5. pp. 729-742. 1997.
11. C.A. Andersson and R. Bro, Improving the speed of multi-way algorithms. Part I:Tucker3, Chemom. Intell. Lab. Syst.42, 93-103 (1998)
12. C.A. Andersson and R. Bro, Interactive course for N-way analysis, Royal Veterinary and Agricultural University, Denmark. URL: http://www.models.kvl.dk/
13. C.A. Andersson and R. Bro, The N-way toolbox for Matlab, Royal Veterinary and Agricultural University, Denmark. URL: http://www.models.kvl.dk/source/
14. C.A. Andersson, Exploratory Multivariate Data Analysis with Applications in Food Technology. Royal Veterinary and Agricultural University, Denmark. (2000)
15. D. Hanselman and B. Littlefield, Mastering Matlab 5 – A comprehensive Tutorial and Reference, Prentice Hall, Upper Saddle River, New Jersey, 1998.
16. D.A. Skoog, F.J. Holler, T.A. Nieman, Principles of Instrumental Analysis. Saunders College Publishing. 1998
17. D.L.Massart, et.al, Chemometrics: a textbook. Data Handling in Science and Technology, Elsevier Science 1998. ISBN 0-444-42660-4
18. D.L.Massart, et.al, Handbook of Chemometrics and Qualimetrics: Part A. Data Handling in Science and Technology, Elsevier Science 1997. ISBN 0-444-89724-0
19. Eigenvector Research, Inc & R. Bro, Lecturing notes on course 'applied multi-way analysis', SSC6, Porsgrunn, Norway, 1999
20. H. A.L. Kiers, Towards a standardized notation and terminology in multiway analysis. Journal of Chemometrics, 14 (2000) 105-122.
21. H.Martens and T. Næs, Multivariate Calibration. John Wiley& Sons. 1989. ISBN 0-471-90979-3
22. J. A. Westerhuis, T. Kourti and J.F. Macgregor, Comparing alternative approaches for multivariate statistical analysis of batch process data. Journal of Chemometrics, **13**, 397-413 (1999)
23. J. Bernd, Digital image processing: concepts, algorithms, and scientific applications - 4th. Berlin , Springer, 1997.

24. J. Buckheit et al., Wavelab Reference Manual. Stanford University. URL: http://www-stat.stanford.edu/~wavelab. 1999
25. J. Guilment, S. Markel, and W. Windig, Infrared Chemical Micro-Imaging Assisted by Interactive Self-Modeling Multivariate Analysis, Applied Spectroscopy, 48/3, (1994) 320-326
26. J. Hilland, On-line Quality Determination of Petroleum Fluids by means of Dielectric Spectroscopy and Chemometric Modelling . Ph.D thesis. University of Bergen. 1997. Norway. ISBN 82-992715-2-5.
27. J. Huang and K.H. Esbensen, Applications of AMT (Angle Measure Technique) in Image Analysis Part I. A New Methodology for *in-situ* Powder Characterization. Chemometrics and Intelligent Laboratory Systems. *54/1*. (2000) pp 1-19
28. J. Huang and K.H. Esbensen, Applications of AMT (Angle Measure Technique) in Image Analysis Part II. Prediction of Powder Functional Properties and Mixing Components using Multivariate AMT Regression (MAR). Chemometrics and Intelligent Laboratory Systems. *In print*. 2000
29. J. Huang and K.H. Esbensen, Multi-way methods in Image Analysis—Relationships and Applications. Submitted. 2000
30. J. Huang and K.H.Esbensen, Comparison study of domain transforms (FFT, Wavelet, AMT) in multivariate analysis of images. *(In prep.)* 2001
31. J. Huang, B.Møller, L.Munck, K.H.Esbensen, Development of a new method for characterization of barley germination by automated image analysis and AMT (Angle Measure Technique), Submitted. 2001
32. J. Huang, S. Ose, S. de Silva and K.H. Esbensen, Non-invasive Monitoring of Powder Breakage during Pneumatic Transportation using Acoustic Chemometrics. Submitted for publication in Powder Technology, 2001
33. J. Tryggard and S. Wold, PLS regression on wavelet compressed NIR spectra. Chemometrics and Intelligent Laboratory Systems, 42 (1998) pp 209-220
34. J.D. Barrow, Pi in the Sky, counting, thinking and being. Penguin Books. 1992.
35. J.D. Barrow, The World within the World. Oxford University Press. 1992.
36. J.P. Bentley, Principles of Measurement Systems. Longman Goup Ltd. 1995. ISBN 0-582-23779-3.
37. J.P. Wold, K. Kvaal and B. Egelandsdal, Quantification of intramuscular fat content in beef by combining autofluorescence spectra and autofluorescence images, Applied spectroscopy, Vol.53, No.4, 1999
38. J.P. Wold, Rapid quality assessment of meat and fish by using near-infrared spectroscopy autofluorescence spectroscopy and image analysis. Ph.D thesis. Agricultural University of Norway. 2000.
39. K. H.Esbensen and J. Huang, Functional parameter prediction using the new, powerful Angle Measure Technique (AMT). POSTEC Newsletter No. 19, Porsgrunn, Norway
40. K. H.Esbensen and J. Huang, The Angle Measure Technique (AMT) for textural pre-processing in Multivariate Image Analysis (MIA). NAmICS Newsletter No. 21, NAmICS, 2000.
41. K. Kvaal et.al, Multivariate feature extraction from textural images of bread. Chemometrics and Intelligent Laboratory Systems, 42 (1998) pp 141-158
42. K.H. Esbensen and J. Huang, Applications of Angle Measure Technique (AMT) in image analysis - III: High-sensitivity particulate impurity detection and quality control. *Submitted.* 2000
43. K.H. Esbensen and J. Huang, Chemometric AMT analysis of microscopic yogurt images. Project report for Arla Foods, Denmark. 2000
44. K.H. Esbensen and J. Huang, Proper Principle of Validation. Submitted. 2000
45. K.H. Esbensen and P. Geladi, Strategy of Multivariate Image Analysis (MIA), Chemometrics and Intelligent Laboratory Systems, 1989, 7 pp 67-86
46. K.H. Esbensen and P. Geladi, The start and early history of chemometrics: selected interviews. Part II. Journal of Chemometrics, 1990, 4, pp 389-399
47. K.H. Esbensen, et.al, Image analysis in chemistry I. Properties of images, gray-level operation, the multivariate image. TrAc, Trends in Analytical Chemistry, 1992.11(1) 41-53
48. K.H. Esbensen, K. Kvaal and K.H. Hjelmen, The AMT Approach in Chemometrics—First Forays. Journal of Chemometrics, 10, 569-590. 1996.
49. K.H. Esbensen, Multivariate Data Analysis—in practice 4th , CAMO ASA, Oslo, 2000
50. K.H. Esbensen, P. Geladi and H. Grahn, Strategies for multivariate image regression, Chemometrics and Intelligent Laboratory Systems, 14 (1992) 357-374

51. K.H. Esbensen, S. Wold, and P. Geladi, Relationships between higher-order data array configurations and problem formulations in multivariate data analysis. Journal of Chemometrics, Vol. 3, pp.33-48. 1988
52. K.H. Esbensen,et.al., Acoustic Cheomoetrics for fluid flow quantifications---II: a small constriction will go a long way. Journal of Chemometrics, 13 (1999) 209-236.
53. K.H. Esbensen,et.al., Acoustic Cheomoetrics—from noise to information, Chemometrics and Intelligent Laboratory Systems, 44 (1998) 61-76.
54. K.H. Hjelmen, 'AMT (Angle Measure Technique) – implementation at Telemark Institute of Technology and applications on time series and similar measurement series', M.Sc.(Eng.) thesis, Telemark Institute of Technology, Porsgrunn, Norway, 1995 (in Norwegian)
55. L. Eriksson, et.al, Introduction to Multi- and Megavariate Data Analysis using Projection Methods (PCA &PLS). Umetrics AB. 1999
56. L. Munck et al, Chemometrics in food science – a demonstration of the feasibility of a highly exploratory, inductive evaluation strategy of fundamental scientific significance. Chemometrics and Intelligent Laboratory Systems, 44 (1998) 31-60.
57. L. Munck, Exploring research options across physical and cognitive borders – Possibilities and limits. A proposal for a new international center for human cognition through science. Invited opening lecture at the " Øresundssymposium 98" at SLU, Alnarp, Sweden. 1998
58. M. Andersson, Process analytical methods for monitoring of the film coating on pharmaceutical pellets and tablets using NIR spectrometry and image analysis. Lund University. Sweden. 1999.
59. M. Halstensen and K. Esbensen, New developments in acoustic chemometric prediction of particle size distribution - 'the problem is the solution'. Journal of Chemometrics, 14 (2000) 463-481.
60. M. Halstensen, S. de Silva, and K.H. Esbensen, Acoustic Monitoring of Pneumatic Transport Lines: From noise to information. KONA, Powder and Particles No.16 (1998)
61. P. Geladi and H. Grahn, Multivariate Image Analysis, John Wiley & Sons Ltd, 1996
62. P. Geladi and H. Martens et.al, A calibration tutorial for spectral data. Part II: Partial Least Squares regression using Matlab and some neural network results. J. Near Infrared Spectrsc. 4, 243-255 (1996).
63. P. Geladi and H. Martens, A calibration tutorial for spectral data. Part I: Data pretreatment and pretreatment and principal component regression using Matlab. J. Near Infrared Spectrsc. 4, 225-242 (1996).
64. P. Geladi and K H. Esbensen, Multivariate Image Analysis in chemistry: an overview, Applied Multivariate Analysis in SAR and Enviromental Studies, Kluwer, Dordrecht, pp.415-445
65. P. Geladi and K.H. Esbensen, The start and early history of chemometrics: selected interviews. Part I. Chemometrics and Intelligent Laboratory Systems, 1990, 4, pp 337-354
66. P. Geladi et.al, Principal Component Analysis of Multivariate Images, Chemometrics and Intelligent Laboratory Systems, 1989,5 pp 209-220
67. P. Geladi, Analysis of Multi-way (Multi-Mode) Data, Chemometrics and Intelligent Laboratory Systems, 7(1989) pp 11-30
68. P. Geladi, and K.H. Esbensen, Regression on multivariate images: Principal component regression for modeling, prediction and visual diagnostical tools. Journal of Chemometrics, Vol.5, 97-111 (1991)
69. P. Geladi, H. Bergner, L.Ringqvist, From experimental design to images to particle size histograms to multiway analyiss. An example of peat dewatering. Journal of Chemometrics, 14 (2000) 197-211.
70. P. Teppola and P. Minkkinen, Wavelet - PLS regression models for both exploratory data analysis and process monitoring. Journal of Chemometrics, 14 (2000) 383-399.
71. P.K. Hopke, Y.Xie and P.Paatero, Mixed multiway analysis of airborne particle composition data. Journal of Chemometrics, 13 (1999) 343-352.
72. R Bro and C.A. Andersson, Improving the speed of multi-way algorithms. Part II: Compression, Chemom. Intell. Lab. Syst.42, 105-113 (1998)
73. R. Andrle, The Angle Measure Technique: A New Method for Characterizing the Complexity of Geomorphic Lines. Mathematical Geology, 26, 83-97. 1994.
74. R. Bro, B.M.Wise and N.B. Gallagher, Applied multiway analysis, a short course. Eigenvector Research. Inc. CAC-2000. Belgium.

75. R. Bro, Multi-way analysis in the food industry. Doctoral thesis. Royal Veterinary and Agricultural University, Denmark. 1998
76. R. Bro, Multi-way calibration. Multilear PLS. Journal of Chemometrics, vol 10, 47-61 (1996)
77. R. Bro, PARAFAC. Tutorial and applications, Chemom. Intell. Lab. Syst.38, 149-171 (1997)
78. R. Ergon, Dynamic System Multivariate Calibration for Optimal Primary Output Estimation. Ph.D thesis. NTNU Trondheim. Norway. 1997. ISBN 82-471-0442-3
79. R. Henrion, N-way principal component analysis. Theory, algorithms and applications, Chem. Intell. Lab. Syst. 25, 1-23 (1994)
80. R. Karmer, Chemometrics Techniques for Quantitative Analysis. Marcel Dekker, Inc. 1998. ISBN 0-8247-0198-4
81. R.C. Gonzalez and R.E. Woods, Digital Image Processing, Addison-Wesley Publishing Company, 1993
82. S. Ose, ' Measuring Particle Size Distributions', Telemark Technological Center, POSTEC, Norway, 1995
83. S. Wold, chemometrics; what do we mean with it, and what do we want from it? Chemometrics and Intelligent Laboratory Systems, 30 (1995), pp 109-115
84. S.G.Nikolov, H.Hutter, M. Grasserbauer, De-noising of SIMS images via wavelet shrinkage. Chemometrics and Intelligent Laboratory Systems, 34 (1996) pp 263-273.
85. S.R.de Silva, ' Characterization of Particle Particulate Solids', Telemark Technological Center, POSTEC, Norway, 1995
86. SIMCA 7.0 – A new standard in Multivariate Data Analysis. Umetrics AB. 1998.
87. T. T. Lied, I. H. Matveyev, D.F. Karlsrud, J. Huang and K.H. Esbensen, Image-Analytical Quantitative Monitoring of Heterogeneous Mixture Processes: Comparing and Combining Angle Measure Technique (AMT) and Multivariate Image Regression(MIR). Submitted.2000
88. T. T. Lied, P. Geladi and K. H. Esbensen, Multivariate image regression (MIR): implementation of image PLSR – first forays. Journal of Chemometrics, 14 (2000) 585-598.
89. T.T. Lied and K.H. Esbensen, Principles of MIR, Multivariate Image Regression – I: regression typology and representative application studies. Chemometrics and Intelligent Laboratory Systems, 2001. In press.
90. W. Windig, B. Antalek, Resolving nuclear magnetic resonance data of complex mixtures by three-way methods: Examples of chemical solutions and the human brain, Chemometrics and Intelligent Laboratory Systems, 46 (1999). 207-219
91. W. Windig, J.P. Hornak, and B. Antalek, Multivariate Image Analysis of Magnetic Resonance Images with the Direct Exponential Curve Resolution Algorithm (DECRA) Part 1: algorithm and Model Study, Journal of Magnetic Resonance, 132, 298-306, 1998
92. W. Windig, Spectral data files for selt-modeling curve resolution with examples using the simplisma approach, Chemometrics and Intelligent Laboratory Systems, 36 (1997). 3-16

PAPER I

ELSEVIER

Chemometrics and Intelligent Laboratory Systems 54 (2000) 1–19

Chemometrics and intelligent laboratory systems

www.elsevier.com/locate/chemometrics

Applications of Angle Measure Technique (AMT) in image analysis Part I. A new methodology for in situ powder characterization

Jun Huang *, Kim H. Esbensen

Applied Chemometrics Research Group, Department of Technology (TF), Telemark University College (HiT), N-3914, Porsgrunn, Norway

Received 4 January 2000; received in revised form 4 May 2000; accepted 4 July 2000

Abstract

A new approach for powder characterization based on image analysis, "Angle Measure Technique" (AMT) and multivariate data modeling is presented. AMT is designed to describe signal complexity as a function of geometrical scale from local to global. In this application, powder images are first *unfolded* to produce 1-D measurement series, which AMT, subsequently, transforms into multivariate scale characterizations. This new compound approach is able to extract and characterize powder features, such as particle size(s), shape(s), smoothness, coarseness, graininess, mixing homogeneity, as well as to classify and discriminate between different powders and even predict bulk behavioral properties. Experimental work reported here involves digital imaging of several tens of different types of powders, using a problem-dependent, low-angle, asymmetric illumination. The unilateral illumination setup brings about a significant simplification of traditional image analysis in powder studies, which is usually orientated towards characterizing all individual particles before aggregating this information. The present new technique achieves the same objectives by a simple and direct imaging, followed by AMT chemometric analysis. Principal Component Analysis (PCA) on AMT spectra derived from this type of imagery is used here to illustrate the power of this new technique, specifically to discriminate between powder types.

Keywords: Angle Measure Technique (AMT); Image analysis; Powder characterization; Principal Component Analysis (PCA)

1. Introduction

1.1. AMT concept

The AMT concept was originally introduced by the American physical geographer Robert Andrle [1] for characterizing the complexity of geomorphic lines in a physical geography context only. A broader, *generic* AMT approach for technological applications was, subsequently, developed by us [2]. AMT is a technique for *simultaneous* description of the complexity of any measurement series. AMT is defined as a function of a scale-dimension "s" — from local to global, see Fig. 1. This creates a completely new *domain* with which to characterize all types of data series, e.g. time series, spatial series, as well as

* Corresponding author. Tel: +47-35-57-51-52; fax: +47-35-57-52-50.

E-mail address: jun.huang@hit.no (J. Huang).

0169-7439/00/$ - see front matter
PII: S0169-7439(00)00100-3

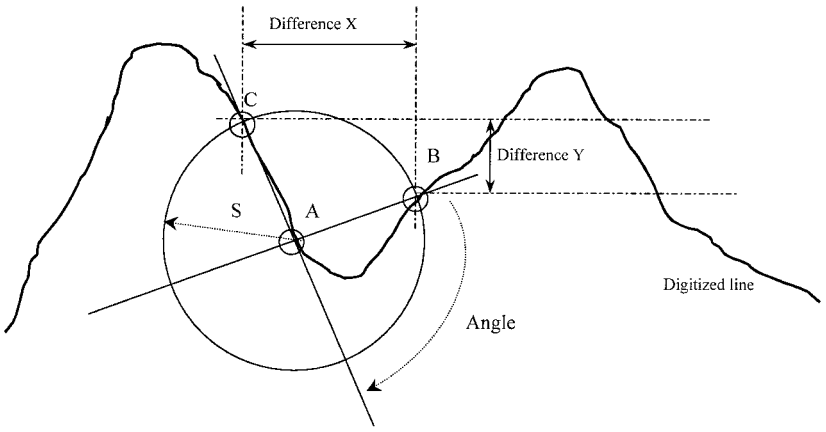

Fig. 1. Explanation of AMT. The individual "angle" is measured as the *supplement* to angle CAB. Difference of X and Y are the horizontal and vertical distances between points C and B, respectively.

any other *ordered* measurement series. AMT is neither an alternative to time-series analysis nor to the Fourier transform; the new scale domain represents a genuine novel *addition* to the time and frequency domains [2].

The AMT transform produces "complexity-spectra" by calculating a geometric angle, which characterizes the *directional change*, or the corresponding X/Y difference, when tracing the ordered series outward from a set of randomly chosen sample points along any 1-D or 2-D series for a set of increasing scales of measurement, see Fig. 1 below for details. Specifically, the individual angles of the AMT approach are measured along the measurement series by initial selection of a random point A as the center of a circle with radius "s", which may be termed the *contemporary scale*. The two fiducial points B and C are found as the intersections of the measurement series with this circle. The supplement to angle CAB is calculated and stored. Several calculation by-products (additional complexity indices, the mean difference between points C and B in the Y- and X-directions) are also obtained. This is carried out for a set of such points, "A", (say, 500), distributed randomly along the entire measurement series, after which AMT calculates a mean angle measure (MA), as well as the mean distance in the Y-direction (MDY), by averaging over all individual measurements; this also allows for an optional standard deviation measure (STD) for both MA and MDY.

By incrementing the scale, $s = s + 1$ (letting s start out from 1, corresponding to the digitization unit of the measurement series), AMT is now able to characterize the complete scale-complexity relationships of the measurement series, simultaneously for all scales. AMT, thus, transforms any 1-D measurement series from the pertinent signal-domain into the new scale-domain, resulting to *multivariate* complexity spectra MA and the MDY, (optional standard deviation, etc.). See Figs. 1 and 2, and Ref. [2,4] for further details.

MA and MDY, as used in the present applications, provide valuable *complementary information* on characterizing the complexity of a measurement series. MA has been found especially useful to characterize underlying scale modes (i.e. "characteristic scales") in the midst of significant noise fractions, while MDY has proved itself especially successful in delineating periodic or quasi-periodic phenomena. AMT-derived spectra can be used as any other standard multivariate preprocessing facility for further data analysis or modeling [2]. In the present application, isotropic 2-D powder images are unfolded to long 1-D vectors, which now form the measurement

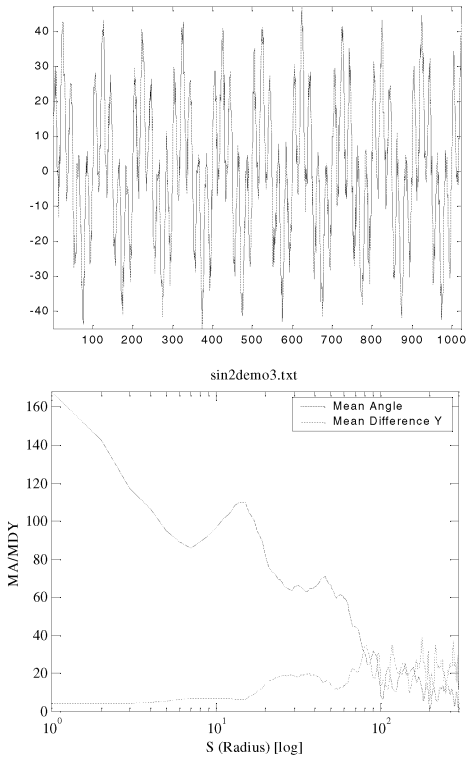

Fig. 2. Illustration of AMT transform from the measurement-space, in this case, the time domain (left panel) to the AMT scale-domain (right panel). The original measurement data were sampled at 1 Hz, from a signal containing 0.01 and 0.05 Hz periodicities, corrupted by zero-mean random noise. Both the MA and the MDY spectra are illustrated in the right panel.

series, subsequently, transformed into AMT spectra as illustrated above. These now contain information about the powders and their properties.

1.2. Why AMT and image analysis for powder characterization

There are many definitions of *powders* in the field of powder science and technology. The following is largely due to Ref. [9]. A powder is an assembly of particles surrounded by fluids, whose behavior is influenced by the nature and interaction of the individual particles and of the fluid that surrounds them, as well as by the interaction between these two phases. Traditional image analysis for powder characterization focuses on the *individual particles* typically using, e.g. microscopic imaging and individual morphology description, etc [10]. This approach involves a difficult and time-consuming *sample-preparation* process, such as *dispersion* of the powders before microscopic imaging, etc. Completely discharging any specific dealings with the individual particles, the present alternative approach acquires images directly from in situ powders with *an absolute minimum sampling preparation* necessary, followed by the AMT transforms, multivariate image analysis and/or chemometric modeling. This type of imagery, recordings of the entire field-of-view of powders, also contains some information relating to the individual particles, but mainly about the *bulk powder*, which is a reflection of the complex bulk, *interacting* properties of the powder, e.g. "stickiness", flowability, fluidization velocity, etc. AMT is particularly useful here to characterize both the local individual particle properties, as well as those pertaining to the global bulk powder simultaneously. The present image analytical global field-of-view approach would appear much more practical and promising for industrial use, and especially for at-line or in-line characterizations.

2. Basic methodology

2.1. Brief description of imaging camera with oblique illumination

The camera used in all present experiments goes by the name *Silvacam*, which originally is a standard three-channel JVC digital camera, type KA-20, intended for video recording in the visible spectrum (R/G/B). *Silvacam* was rebuilt by a Finnish, *Karelsilva OY*, for use in airborne remote-sensing multispectral image analysis. *Silvacam*'s frequency spectrum is translated toward the infrared part of the spectrum, the modified camera now using the red, green and near-infrared channels (R/G/NIR). The reason is that biological materials, as well as many other (inorganic) materials often has more diagnostic, selective information in the infrared region than in the blue. The camera lens is a FULINON-TV•Z, also modified to allow increased NIR transmittance.

Low-angle oblique illumination sources are used in our AMT applications [2]. The low-angle illumina-

tions result in critically detailed field-of-view imagery, such as shadows created by the individual particles (of which there are many in this type of imagery), or highlighted definitions of interstices and cavities *between* particles a.o. It is a distinct advantage by this particular illumination set-up that the individual particle surface roughness will contribute to the complex light-shadow pattern created.

Average optimal imaging settings for each series of powders to be characterised and compared need be obtained by experimental trial-and-error. We always run an initial *experimental design* for this purpose, taking into account such *factors* as: number of light sources, their (individual) angle of illumination, spatial resolution of camera, spectral characteristics of illumination sources a.o. It is critically important, however, that all powders to be compared be recorded under the *exact same conditions* of course. Clearly all this results in very complex light/shadow-enhanced imagery. On average there may be anything from, say a few hundred (large-grained) particles to several tens-of-thousand (very small-grained) particles in identically sized field-of-view frames. It may not be possible to *decompose*, to *analyze* this type of imagery by any traditional method operating in the image-plane with the objective of individual particle segmentation, etc.

2.2. Basic AMT image example illustrations

2.2.1. Interpretation of AMT spectra

The AMT transform can deal with a wide variety of types of measurement series. Some general illustrations on time series data and other typical measurement series were earlier presented in detail [1,2]. Below image analytical AMT applications will be in focus. It is advantageous to know how to interpret the image-information as judged from, or as described by, the AMT spectra. Below is a rough summary of typical interpretations of AMT spectra focusing on MA and MDY.

2.2.1.1. Mean Angle (MA).

- Characterizes both noise (irregularity)/stochastic signal parts, as well as periodicity.
- Low MA-values signify low local complexity (irregularity, sinuosity, roughness, etc.) at corresponding scales.
- High MA-values imply significant local complexity (irregularity, sinuosity, roughness, etc.) at the corresponding scales. High MA-values signify dramatically swift "peak-and-valley" swings at the contemporary scales, i.e. large directional angle changes in the original measurement series.
- Local maximum MA-values (peaks on the MA-spectrum), termed *characteristic scale(s)*, signify a complexity mode at a specific preferred scale.
- Characteristic scale(s), corresponding to characteristic angle(s), always indicate significant *changes* associated with this/these scale(s).
- Multiple MA-spectrum peaks each indicates a distinct complexity mode at these scales.
- Absolute local minima (valleys in the MA-spectrum) signify "simplicity" at these scales, e.g. often interpretable as, e.g. relative "smoothness" at this scale.
- The MA-spectrum is actually increasingly robust with respect to added noise [1].
- "Periodic peaks and valleys" on the MA-spectrum is a bona fide reflection of an intrinsic periodicity in the raw measurement series as well, but there is not an exact one-to-one relationship as, e.g. for the Fourier transform.
- The MA-spectrum always has relatively uncertain values for the small(est) scales.

2.2.1.2. Mean Difference Y (MDY).

- Excels in characterizing *periodicity* with a high degree of sensitivity. MDY is very robust with respect to added noise, largely noise-invariant for small and intermediate noise fractions
- Low MDY-values imply low local amplitude differences at corresponding scales
- High MDY-values imply large(r) local amplitude differences at corresponding scales
- MDY-spectrum "periodic peaks and valleys" indicates bona fide original signal periodicity
- Multiple MDY-modes indicative of super-positioned periodic signals
- Horizontal scale-distance between MDY-modes indicates signal period, or "frequency"
- Exponential increase with respect to logarithmic *s*-axis is an indication of signal trend(s)
- MDY absolute maximum values correspond to overall variance of measurement series

- MDY never interesting for "small *s*-values" in contrast to MA

The complementary MDX measure (Fig. 1) is only used for 2-D measurement series and will not be discussed further here. "STD" is an optional secondary AMT-measure. It is the standard deviation derived from the calculation(s) of MA and MDY. It is largely a damped counterpart to these two primary measures, which has rarely found any particular use in our experiences.

2.2.2. Optimal AMT spectra for isotropic images

The range of measurement scales for a series of comparative images is critically problem-dependent. There are a lot of initial comparative studies necessary when a new series of powders are to be AMT-characterized and compared. The "*s*-scales" used here range from 400–2000 pixel units.

Our AMT-transformation facility has recently been reprogrammed by the first author, and is now implemented as a MATLAB 5.3 program (core calculation part written in Mex C [7]). The program allows for problem-dependent changes of all critical parameters, such as scale range, scale length (increment), number of randomly chosen points "A", etc. It is imperative that all these parameters, as well as the scaling of the axes, always be held constant when the outputs are to be *compared* [2]. Images to be compared should of course also be kept in the same size and resolution.

AMT works on only one channel of a multispectral image, typically selected according to some problem-dependent criterion (alternatively, we sometimes use a particular score image [6]). Green channels of all images are used for AMT calculations in the present applications, since they are of optimal contrast. Subsequently, they are unfolded *row-wise* into 1-D vector measurement series. It is important that the direction of the unfolding of the recorded imagery be *aligned* with the horizontal trace of the axis of oblique illumination. This requirement was not properly emphasized in our earlier work, e.g. Ref. [2].

2.2.3. AMT-characterization of texture imagery

Traditional approaches quantifying the texture contents in an image are statistical, structural, and spectral [5]. Statistical approaches typically yield characterizations of textures based on a host of different "variability indices" a.o., resulting to quantitative measures for image textures that otherwise would only be described qualitatively as, e.g. smooth, coarse, grainy, etc. There are many such texture measures in the literature, and they keep growing in number. The defining characteristic for these techniques is that they all operate in the image-plane, by moving around "local" templates for local neighborhood characterization, thereafter the template(s) are translated to new positions, etc. — in short, they are *computationally very intensive*.

Structural techniques deal with detection, quantification and the spatial arrangement of so-called "image primitives", e.g. such as texture based on comparison with a template of regularly spaced parallel lines (a 1-D primitive) or other 2-D simple "units". Recently, this has developed into more refined use of specific "texture primitives", etc. But again there are a host of such approaches, and again these are also all computationally *very intensive*.

Spectral techniques are mainly based on the 2-D Fourier transform and are typically used to detect whatever "global periodicities" be present in an image. This technique differs principally from the above in that the FFT works in a *transformed domain*. This is very often a great advantage computationally. With our present foray into the possibilities for *real-time* powder characterizations, we are only interested in approaches, which are *fast*.

Texture image analysis is of significant interest in powder characterization because images of powders directly offer a presentation of the aggregate appearance of the powder, not of the dispersed individual particles. Intuitively, it is believed that powder characterization/discrimination is intimately related to the characterization of the complexity, roughness, periodicity, irregularity, etc., of this presentation of powders. Powders come in excruciatingly many forms, of very significantly different particle sizes, shapes, surface roughness, density, "stickiness", fluidizabilities and many other specific properties. Hitherto, it has been very difficult to get to the dynamic functional of these characterizations in any analytical way — except for direct experimental measurements in suitable scale-rigs, or even (for the most critical or difficult issues) in full-scale rigs. This has caused

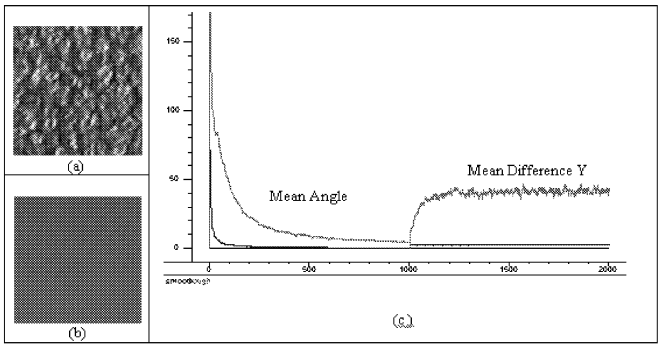

Fig. 3. (a) Image of a rough concrete surface. (b) Image of a smooth glass surface. (c) Comparison of spectra from both images. Note the spectra for rough surface lie far above those for the glass surface at all scales. The spectra for the rough surface are representative as a signature for "rough texture" (coarseness, intricacy, irregularity, etc.), as opposed to those for the smooth surface.

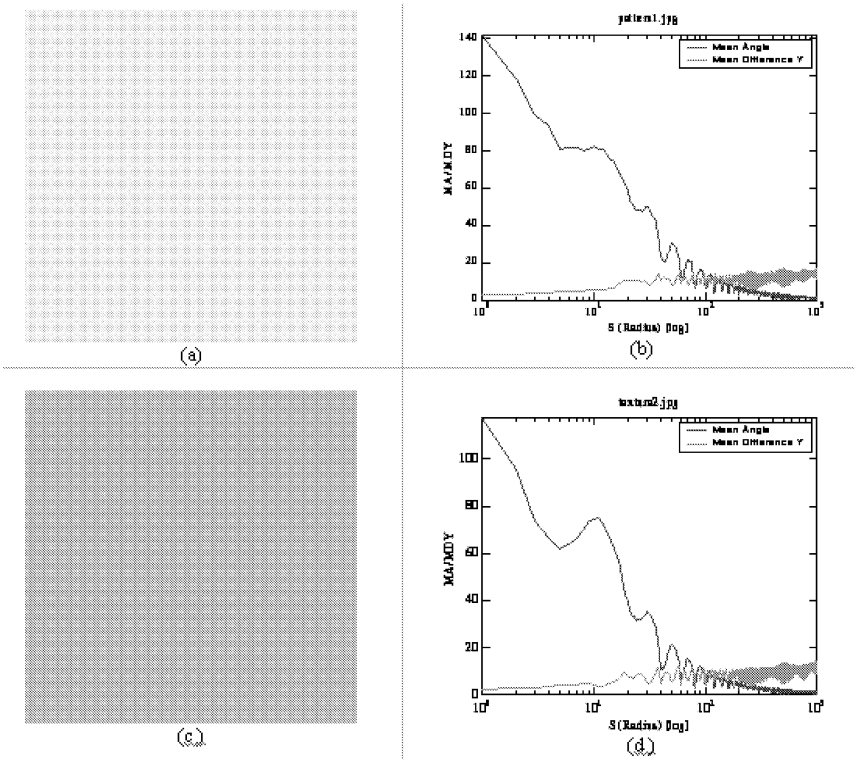

Fig. 4. Images showing different aspects of very regular periodic textures and their corresponding AMT spectra. Both MA and MDY reflect the periodicities in the scale domain (different from FT).

great difficulties to both academic research and industry. As a first introduction, below we show how AMT characterizes and discriminates between a typically (very) *smooth* and a correspondingly (very) *coarse* texture. There is also an example to give the reader a first feel for how the AMT description of periodic textures appears.

Fig. 3 shows an image of a smooth glass surface contrasted with an image with a rough concrete surface. The corresponding AMT spectra for both images are shown in the right panel. The marked differences between their AMT spectra are very promising. The MA-levels for the glass image are much *lower* at all scales than for the concrete image, as are the corresponding MDY relationships, which are even more different. This means that the concrete image has *much more* textural intricacy, roughness, etc., for all scales.

Fig. 4 shows two images with *periodic textures*. This type of texture image has traditionally been widely analyzed by the spectral approach based on Fourier transform. Fig. 4 illustrates how the AMT spectra characterize this type of textures. The distinguishing peaks in MA show clearly the periodic "characteristic angles", which reflect the periodicities. The sinusoidal MDY-spectra also show this strong periodicity.

As can be seen directly from the two periodic images (a and c), they actually have distinctly *similar patterns* with predominantly identical periodicities in both the horizontal and vertical directions, but their *texture primitives* are different. This is clearly reflected in their respective AMT spectra. MA shows that both have almost identical characteristic scales throughout but with clearly differentiating characteristic angles (Fig. 5). The MDY spectra likewise indicate the similar periodicities in the two images by giving the strong sinusoidal signals, but also here the distinction can be drawn between their MDY spectra (Fig. 6). Detailed appreciation reveals that there is almost no overlap between their (MA, MDY) spectra, regardless of the apparent similar shapes. The AMT spectra for image Fig. 4(a) are indicative of a higher degree of complexity than those for image Fig. 4(c). It is, therefore, straightforward to *discriminate* even between these two very similar texture patterns by analyzing their AMT spectra. These examples, while very simplistic, nevertheless, give a clear impression of the power of the AMT-description, especially for delineating more *intricate textures*.

We have shown that AMT is able to deliver very exact and discriminating characterizations of typical features as encountered in powder descriptions, e.g. local/global smoothness/roughness, as well as various forms of local/global periodicities. Real-world powders will of course show (much) more complex relationships than the above simple introductory examples, but also in these more realistic, and more

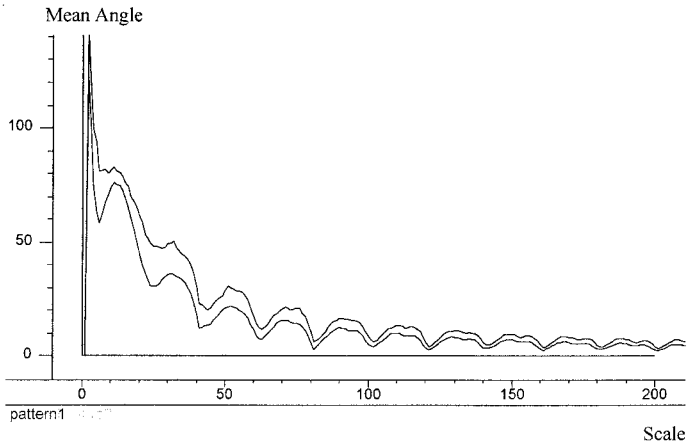

Fig. 5. Detailed comparison plot of MA relationships for the two images in Fig. 4.

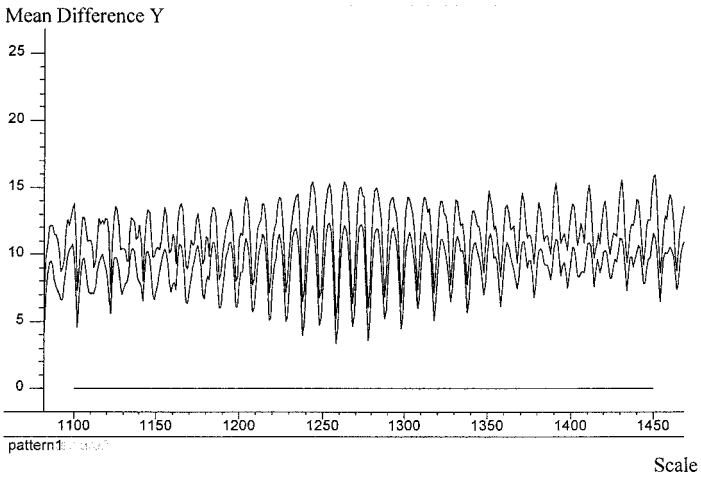

Fig. 6. Detailed comparison plot of MDY relationships for the two images in Fig. 4.

complex situations, which are always also characterized by an additional stochastic noise component.

3. Discriminability of AMT spectra of powder images

Here we illustrate on a set of real-world powders from POSTEC (a research institute in powder science and technology, Norway), which are *representative* among those widely used in industry. These seven *reference powders* in many ways span a useful experimental domain with respect to many of the intrinsic parameters of interest. An overview of their basic characteristics follows:

- *Microdol 100 (MD100)* is a limestone material with crystalline structure. It is often used in white paint mixed with water, e.g. in the auto industry and in road marking materials. MD 100 can also be utilized in cosmetics and in food production.

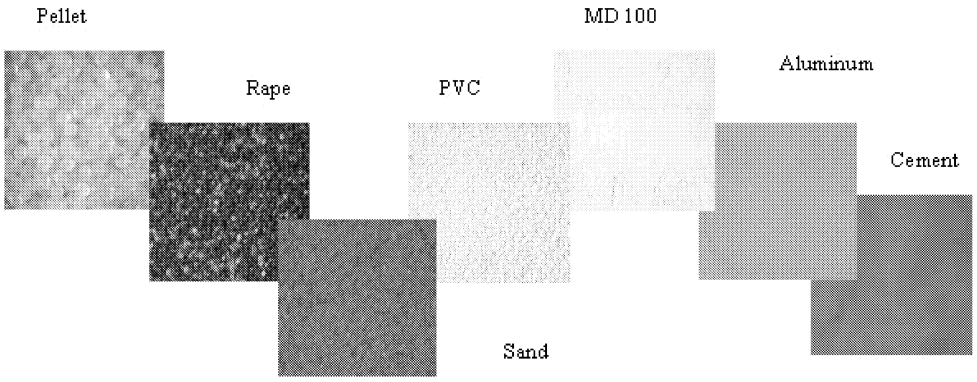

Fig. 7. Raw digital images for the seven POSTEC reference powders. Note the very varying appearances for selected parameters such as particle size, color, shape, roughness, etc.

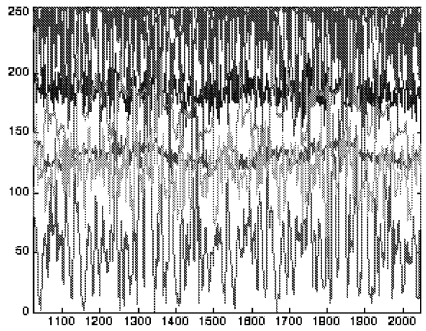

Fig. 8. Raw, *unfolded* 1-D series from the original reference powder images. Extensive overlap, signifying extremely *low discriminability* in this original 1-D spatial domain.

- *Polythene pellets* are quasi-spherical particles used as raw materials for plastic production. Compared to the other powders illustrated here, they have a relatively large particle size.
- *Rape seeds*. These biological seeds are spherical and used for synthetic oil production.
- *Sand* — "Leighton Buzzard sand", which appears yellowish with relatively sharp edges and narrow, oblong shapes.
- *PVC granules* are smaller PVC particles. This powder has special electrostatic properties and is used in PVC plastic production and elsewhere.
- *Alumina* come from bauxite and have high density. Alumina is used as raw material in the aluminum production. Fine-grained.
- *Cement*. Extremely fine-grained. Cement powders are especially cohesive, compared to others.

The raw images of these powders are shown in Fig. 7. Note that they differ greatly from each other in many aspects such as particle size, color, shape, roughness, etc. Fig. 8 shows the associated data series from the unfolded raw images.

The compound (MA, MDY) spectra give fully discriminating representations of the raw images, whose raw unfolded representations were hopelessly overlapped as shown in Fig. 8. Fig. 9 shows that cement, alumina and MD have particularly smooth curves, signifying much less complexity, when imaged directly as powders. By contrast, the four remaining powders display higher complexities and/or grain sizes, etc. The rape seeds (topmost) seem to have by far the most complex spectra. This is because the rape seeds have relatively larger, and more varied grain-sizes, as well as some *irregular impurities* (white petals, inorganic fragments, etc.). The PVC pellets have the largest overall grain-sizes but with more regular surfaces, almost uniform color and shape. The spectra for sand and PVC are somewhat similar but still with a clear difference. The two most similar spectra would be sand and PVC.

The above illustrates that it is *possible* to conduct quite detailed *interpretations* of the significance of the relative AMT spectra in relation to their original image appearance. But we shall not go into any details as to this issue here. We shall instead point out

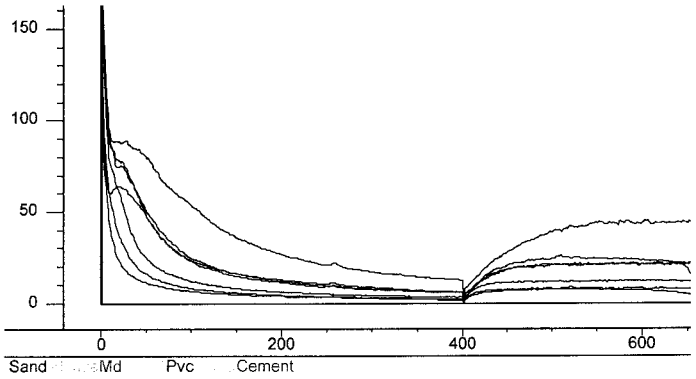

Fig. 9. AMT spectra for the seven POSTEC reference powders as above. No overlaps but *complete discriminability* in the AMT scale domain.

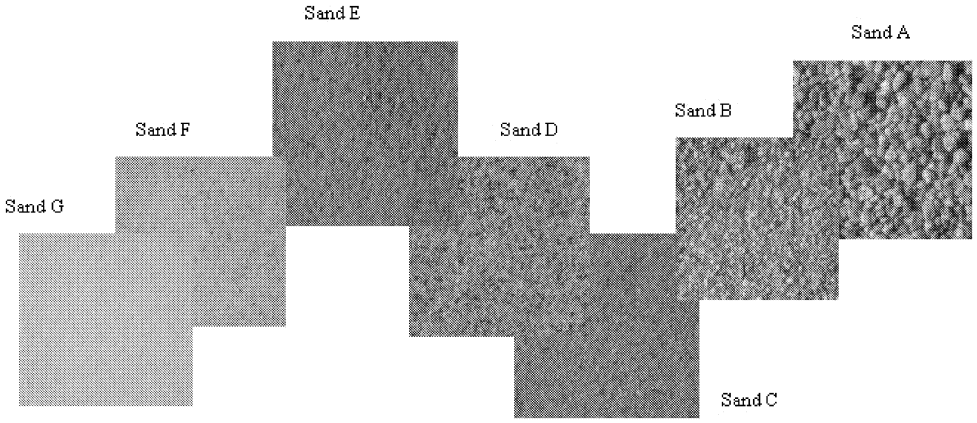

Fig. 10. Raw digital images of the different *sands*. This sand series differs mainly with respect to particle size, grain morphology, color and shape, etc.

that by using the entire compound (MA, MDY) spectra, there is now a potential *object vector* available for each powder, fully capable of complete distinction between these seven powders. This example furnishes a very clear demonstration of the power of AMT to facilitate *discrimination* between different powders, i.e. powders in which the gamut of all distinguishing features varies maximally between the powders. The second group of powders to be discriminated by the same AMT technique here is all of the *same type*; they are all *sands*. The AMT also shows here a powerful ability to *differentiate* between them. Their digital video appearance and the corresponding AMT spectra are shown in Figs. 10 and 11.

At opposite ends, sand A appears much more complex than sand G with respect to grain-size, grain-form, irregularities, etc. Sand G, in fact, has the smallest mean size, while sand A has the largest mean size. There is a very distinct systematic "development" from A to G, which is a reflection of the gradual differences between the sands as their corre-

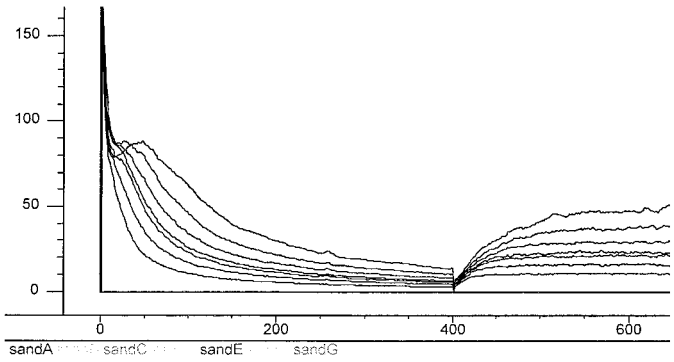

Fig. 11. AMT spectra for the sand data series. Unambiguous differences between all sands.

sponding powder images appear less and less complex. Such clear differences between the spectra can clearly be used for discrimination, e.g. in combination with PCA analysis and/or classification methods (SIMCA), etc [8].

The salient point made by the two illustrations above is that it is fully possible to use the AMT-derived spectra directly as is for various chemometric discrimination/classification purposes — even though one is not necessarily able to fully *interpret* all the intricacies of the relative appearances of the AMT-spectra.

4. PCA study for powder characterization and discrimination

4.1. Data configuration

Each image is unfolded/vectorized into a 1-D vector, followed by the AMT transform. AMT transforms each raw powder image into their corresponding complexity-spectrum, all with an *identical scale range* in the new scale-domain. This *common* scale-array, in fact, represent a new, *derived* variable-mode for the original images, which themselves make up the corresponding objects. Thus, AMT transforms a series of 2-D images (not a *stack* of multivariate images) into a series of 1-D complexity spectra with a common variable way. Subsequently, an X-matrix can be constructed from *aggregating* these AMT spectra for each powder. This ordinary two-way matrix can be used for any conventional matrix-based data modelling purpose, etc.

There exists some misunderstandings with respect to multivariate analysis on images regarding whether to use the *unfold-operator* or to use, e.g. three-way (N-way) analysis. The different images presented here do not have intrinsic variations or correlations between the pixels *at the same image positions*, unlike multispectral images, which are recorded at different wavelengths on the same field-of-view image basis. There is no variable mode, as in a three-way data array, precisely because there is only one channel, one variable, forming the image upon which AMT is applied. It is, therefore, not possible to arrange the raw images into a three-way array. An unfold PCA, or PLS, can only be applied on true multispectral images.

With the AMT transformation, the data density is reduced significantly. Analogously, FFT, wavelet also transforms raw images and create frequency- and

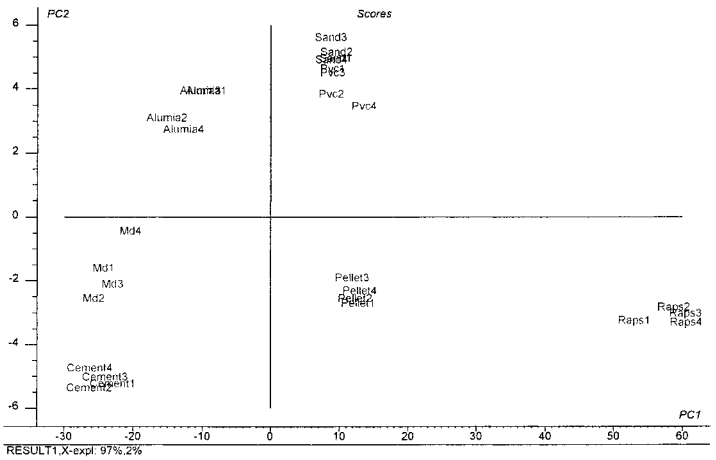

Fig. 12. PCA $t1 - t2$ score plot. All seven powders are clearly discriminated from each other. Note the individual sampling/measurement reproducibility as evidenced by the four replicates.

wavelet-scale domains, respectively. Subsequently, these frequency component vectors, or wavelet coefficients, can be used in the exact same way to construct a similar 2-D data matrix for multivariate modeling or calibration, etc. A comparative study on this issue will be presented in the sequel paper [11].

4.2. Discriminations

To compensate for unavoidable variances in sample preparation, illumination and image recordings, each powder is routinely replicated (imaged) four times for all measurements. The replicating takes

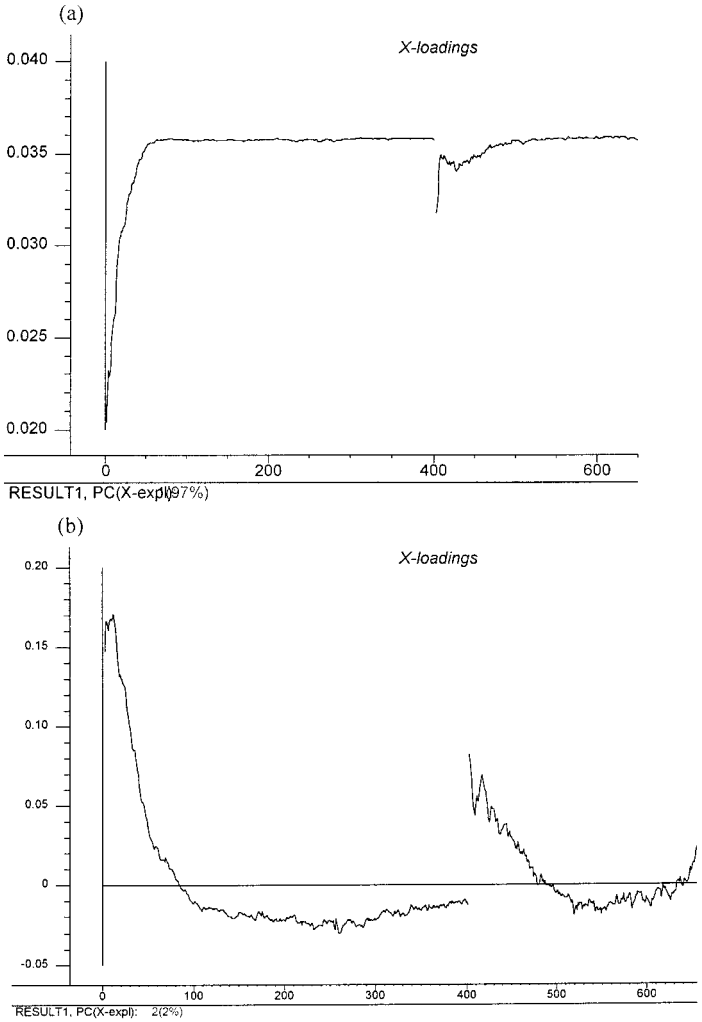

Fig. 13. Corresponding PCA loadings for PC1 and PC2. (a) PC1 loadings, note that variables are more important at larger scales. (b) PC2 loadings, note that variables at small scales are of major importance.

place by successive rotation of the sample container 90° clockwise. We often use both the individual recordings, as well as their averages in attempts to picture the sampling/measurement reproducibility. Examples to follow.

4.2.1. POSTEC powders

Fig. 12 shows PCA results from the seven reference POSTEC powders. The PCA model needs one component to explain over 97% of total X-variance, followed by 2% for PC2. The $t1 - t2$ score plot shows clearly all seven completely resolved powder types. PC1 signifies the "powder complexity", e.g. rape seeds rightmost while the leftmost is cement, which appear least complicated. Apart from this "macroscopic" PC1 discriminability, we see that the meager 2% variance accounted for by PC2, in fact, plays a highly significant role in the discrimination between four and five powders, along the PC2-direction.

Close inspection of the loadings for both PC1 and PC2 point to the remarkable discrimination sensitivities implicitly *hidden* in the raw AMT-spectra (Fig. 13). While the PC1-loadings are relatively simple and straightforward, there are much more detailed relationships revealed in PC2 and details, which relate to the tiny, but highly significant small(er) differences between the powders, which distinguish along the PC2-direction in the score plot. For PC2, the small(er) AMT-scales play a dominating role in contrast to the PC1-loading relationships. Clearly, using both PCs does the trick. This gets even better for AMT + PLS − DISCRIM a.o. to be further explored in the sequel paper [3].

4.2.2. Sand samples

Fig. 14 illustrates the same AMT + PCA approach for the discrimination between the homogenous sand series. Again, principal component PC1 is apparently dominating, as PC1 here accounts for 96% of the total X-variance in the data set, while PC2 takes care of only 3%. There is a very regular disposition of these seven sand types in the score plot. Their groupings are again clearly separated from each other, never to any degree affected by the sampling/measurement replicate errors. And again there are very important differences in the PC1 and PC2 loading relationships (see Fig. 15) which point to the entire scale-domain being important, as well as reiterating the significant difference between the parts of the

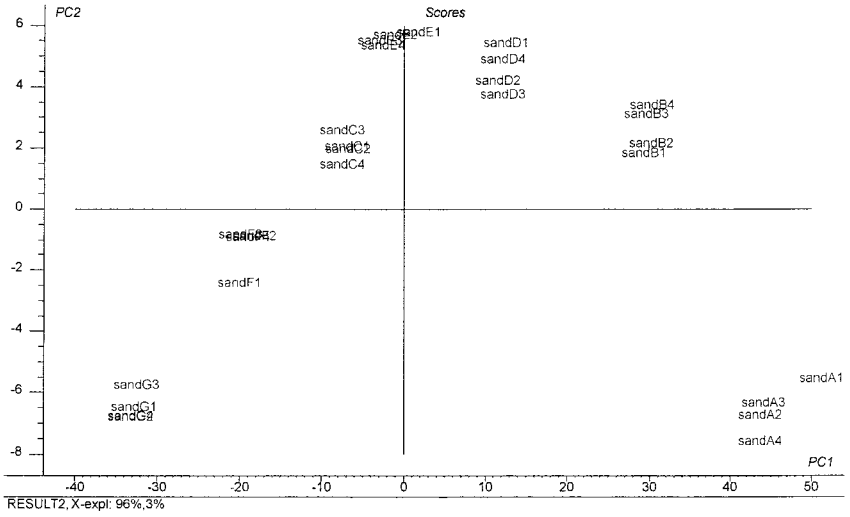

Fig. 14. Score plot ($t1 - t2$) for the more homogenous sand series.

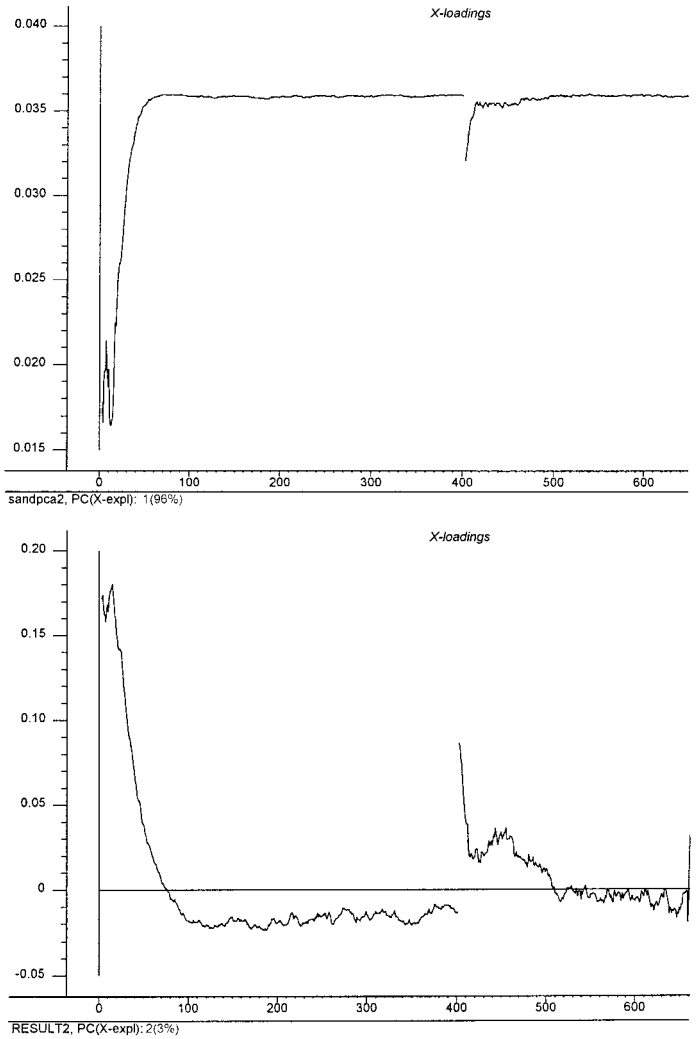

Fig. 15. PC1 loadings (left panel) and PC2 loadings (right panel) for the sand series. Note subtle differences in the differentiating capabilities of PC2 with respect to Fig. 13.

AMT-scales extricated along the *decomposed* PC1 and PC2 directions.

4.2.3. Master food powder example

As a final realistic testing of AMTs powder characterization potential we have put together a set of 17 widely varying powders, all related to food, food science or food production. The purpose of this master data set, which will also appear in the second paper in this series [3], is to furnish a "maximally difficult" real-world data set, with relevance for all industry sectors working with powders. Specifically, this data

set will allow several parallel studies with different, but interrelated objectives:

1. *Between-powder discrimination* (including *difficult*, *closely similar* powders, etc.)
2. Feasibility studies of *quantitative powder-mixture characterizations*
3. Feasibility studies of *quantitative impurity / pollutant detections*

Re. (1): As shown in the images below, some food powders display a great variety of intrinsic complexities, such as irregular shapes, roughness, sizes, color, surface structure, etc., while others, like salt and white sugar, appear relatively identical due to uniform color, size, shape.

Re. (2, 3): Quantitative mixture characterizations and quantitative impurity/pollutants detection, at the ultra-trace level, have never been attempted before

Fig. 16. Raw video images of the 16 different food powders, displaying a wide variety of most of the salient characterizing parameters, grain-size, form-aspect ratios, color, surface roughness (individual particles), *powder* surface characteristics a.o. A 17th powder is also included in this set, although not depicted here: *Cocoa*.

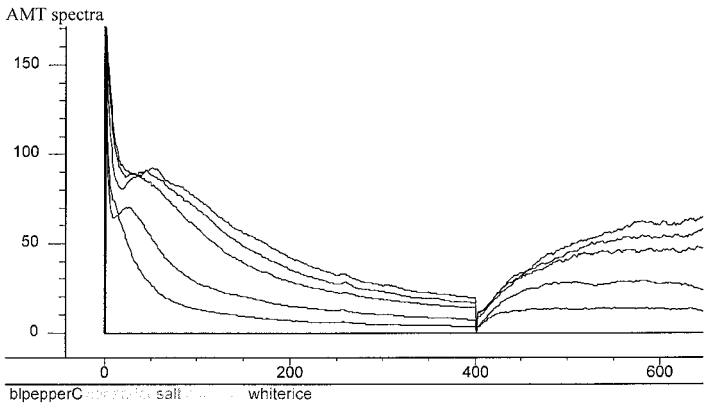

Fig. 17. AMT spectra from a *selected* subset of representative food powders. The spectra complexity generally increases from bottom to the top in the sequence: salt, white rice, black pepper (coarse), coriander and "Stranger".

based on direct video imaging. Clearly, there is a need for, e.g. pollutants detection in the food industry; likewise, for raw materials quality assurance, etc., when the raw material consists of a powder mixture. There would appear to be many obvious direct industrial applications for this new type of image analysis technology. We explore these features in our sequel paper.

Fig. 16 shows 16 different powders in their video appearances. The AMT spectra derived from these powder images are again capable of characterizing the complexities of all powders. Selected AMT spectra are shown below in Fig. 17. The topmost curve is the AMT spectrum from a "blind test" powder (termed "stranger"), courtesy of KVL/DTU, Denmark. This particular powder, as shown in the raw image, has a

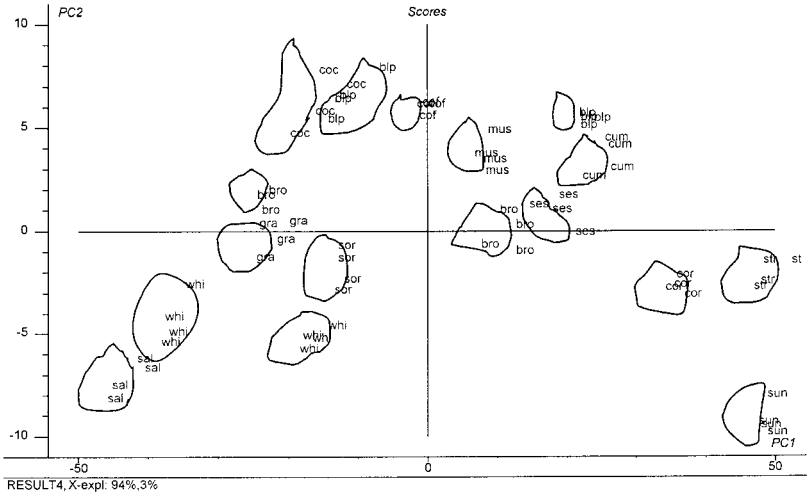

Fig. 18. PCA of all 17 food powder AMT spectra. Groups of quadruple replicates have been circled to show the capability of discrimination in the presence of *realistic* sample preparation/measurement error.

rather complicated structure, shape, size(s), surface appearance, etc. A closer look also shows specular reflectance from some individual particle surfaces. Appropriately, the "stranger" displays the *highest* MA- and MDY-values among all the selected powders, i.e. the most complex pattern.

The spectrum for salt appears smooth without any characteristic angles/scales, signifying the highest

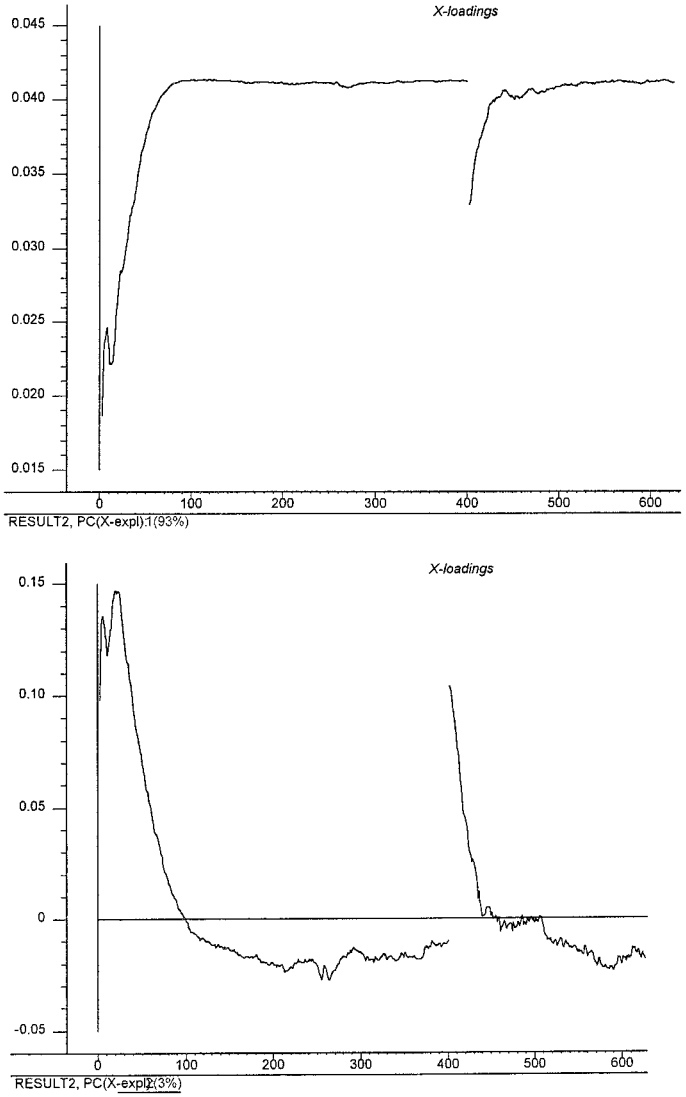

Fig. 19. PC1 loadings (left panel) and PC2 loadings (right panel) for the food powder series. Note the subtle differences in the differentiating capabilities of PC2 with respect to Figs. 13 and 15.

homogeneity. The white rice image likewise shows large relative uniformities, which also drag down the values of AMT spectra, to be positioned just above the salt spectra. However, a clear peak in the rice spectrum can be observed (approximately at scale 30–35), which is attributable to the very large *aspect ratio* (length/width) for this particular powder. The spectrum for coriander is positioned just below that of "stranger". As seen in the coriander image, the individual particles have very rough shells, some of which are broken, giving this high irregularity.

As shown from the discussions above, obtaining the basics for understanding "simple" and "complex" powder appearances is easy through the AMT characterizations. Thus, it should also be a relatively straightforward operation to characterize even the current complexities of these "difficult" powders and to discriminate between them by AMT plus PCA approach presented above.

The PCA results on the discrimination of these food powders are shown in Fig. 18, together with the appropriate PC1 and PC2 loadings in Fig. 19. The different groups are all successfully separated from each other, using these (94 + 03) 97% of the total variance. PC1 again mainly discriminates on the basis of the *overall complexity differences* between the powders. For example, the complex "stranger" is located on the extreme right along PC1, while the "simplest" salt occupies the extreme SW position in the plot.

But, in this analysis, the second PC now joins in a more complex fashion as, e.g. witnessed by the fact that both salt and the very distinct "sunflower" powder (boasting by far the largest grain-size) occupy *identicalght / shadow positions* on the negative PC2-axis. The overall discrimination is dependent on both the first two principal components; in fact, this feature is characteristic of all the above three AMT analyses, Figs. 13, 15 and 19). The overall PC1- and PC2-loading similarities are marked, while there are also subtle but significant differences with respect to the PC2-loadings. The PC2 relationships constitute subtle *morphological additions* to the dominating PC1-modelling, which mainly has to do with the general complexity/size differences between the powders.

Clearly, the powders displaying the highest PC2-scores at the positive end make for an interesting distinction: among these powders, we find cocoa, coffee, the fine-grained black pepper, mustard seed. On close inspection, the PC2 component in this example can perhaps be tentatively interpreted as a relative "appearance uniformity" axis, which would indeed be a feature, which is *orthogonal* to PC1. This is consistent with the fact that it is only the lower scales, which display high loadings on PC2.

5. Discussion and conclusions

As can be seen from all of the above examples, different powders can easily be quantitatively discriminated from each other, but similar powders are still likened very closely. In the overall description of powder appearances, there are many different aspects that need attention, among which would be *individual grain attributes*: size, aspect ratio, surface roughness, color, as well as bulk *powder attributes* color, shadow(s): particle–particle shadows and/or illumination artifacts, etc. It is, however, possible to characterize all these simultaneously with the AMT approach. It is emphasized that the use of unilateral low-angle illumination plays a decisive role in this endeavor; this resulting to very complex light/shadow pattern, which at first appears almost chaotic to the uninitiated eye, actually lends itself optimally to the AMT decomposing technique. This goes for porosity, as well [2]. The present AMT-implementation uses less than 2.0 s for a complete coverage of a 512×512 image for 400–600 AMT scale units (both MA and MDY) on a Pentium III computer. There would not appear to be any serious problems implementing a real-time on-line facility, which points to an obvious large industrial application potential.

This paper has shown, step-by-step, the basic concepts, typical interpretations and the first industrially relevant applications of AMT. The basic methodology has been developed for characterization and discrimination of powders. This new AMT approach has shown the capability of characterizing the complexities of unfolded 1-D measurement series, which stem from generally *isotropic 2-D imagery*. AMT spectra contain *abundant information* related to the raw data (2-D images, in the present case), which underline the need for multivariate data modeling as an integral part (e.g. PCA, SIMCA, etc.). The approach may, there-

fore, presumably also be used for prediction purposes in science and technology, say for prediction of, e.g. dynamic, *functional properties* in powder industry a.o. These aspects will be discussed in the sequel paper [3]. Multivariate AMT regression will be useful in many other areas for prediction of physical and other properties, e.g. for process analysis, monitoring and for quality control, etc. AMT opens up for a wide variety of potential application areas also outside the chosen powder science playground. Applications are legion. The remaining issue in the AMT study concerns how to exactly interpret the AMT spectra. It might be possible to extract even more qualitative, as well as quantitative information from the spectra, than what has been demonstrated here. Luckily, these are aspects which lend themselves eminently to further basic, as well as applied studies. More applications on the AMT will be given in our companion studies.

Acknowledgements

We thank the now disbanded "Applied Chemometrics" group at SINTEF, Oslo, for the long-standing collaboration regarding the "SilvaCam" camera. We thank Powder Science and TEChnology (POSTEC), Porsgruun, for supplying us with the valuable set of reference powders.

References

[1] R. Andrle, The Angle Measure Technique: a new method for characterizing the complexity of geomorphic lines, Math. Geol. 26 (1994) 83–97.
[2] K.H. Esbensen, K. Kvaal, K.H. Hjelmen, The AMT approach in chemometrics — first forays, J. Chemom. 10 (1996) 569–590.
[3] J. Huang, K.H. Esbensen, Applications of AMT (Angle Measure Technique) in image analysis: Part II. Prediction of powder functional properties and mixing components using multivariate AMT Regression (MAR), (2000) submitted.
[4] K.H. Hjelmen, AMT (Angle Measure Technique) — implementation at Telemark Institute of Technology and applications on time series and similar measurement series, MSc (Eng) thesis, Telemark Institute of Technology, Porsgrunn, Norway, 1995 (in Norwegian).
[5] R.C. Gonzalez, R.E. Woods, Digital Image Processing, Addison-Wesley, Reading, 1993.
[6] P. Geladi, H. Grahn, Multivariate Image Analysis, Wiley, 1996.
[7] D. Hanselman, B. Littlefield, Mastering MATLAB 5 — A Comprehensive Tutorial and Reference, Prentice-Hall, Upper Saddle River, NJ, 1998.
[8] K.H. Esbensen, Multivariate Data Analysis — In Practice, 4th edn., CAMO ASA, Oslo, 2000.
[9] S.R. de Silva, Characterization of Particle Particulate Solids, Telemark Technological Center, POSTEC, Norway, 1995.
[10] S. Ose, Measuring Particle Size Distributions, Telemark Technological Center, POSTEC, Norway, 1995.
[11] J. Huang, K.H. Esbensen, Comparison study of domain transforms (FFT, Wavelet, AMT) in multivariate analysis of images, (2000) in preparation.

PAPER II

PROOF VERSION

ELSEVIER

Chemometrics and Intelligent Laboratory Systems 1213 2001 xxx

Chemometrics and intelligent laboratory systems

www.elsevier.com/locate/chemometrics

Applications of AMT (Angle Measure Technique) in image analysis Part II: Predictions of powder functional properties and mixing components using Multivariate AMT Regression (MAR)

Jun Huang*, Kim H. Esbensen

Applied Chemometrics Research Group, Department of Technology, Telemark University College, N-3914 Porsgrunn, Norway

Received 4 September 2000; accepted 14 February 2001

Abstract

This paper presents a novel way to predict the bulk powder characteristics from unilaterally illuminated powders using Angle Measure Technique (AMT) image analysis in combination with multivariate calibration. It is demonstrated that the AMT transform can account for the complexity of images in the scale domain and be used as a strong preprocessing facility for multivariate regression modeling. The concept of multivariate AMT regression has been proposed for this purpose. A wide variety of types of powders was collected in order to study the reliability, reproducibility and representativity of the methods. PLS models have been established to quantitatively predict key physical and behavioral powder properties such as particle size, density, minimum fluidization velocity, wall friction angle, and angle of repose. Finally, a first attempt at prediction of mixing component fractions in powder mixtures has also been implemented, which can be used for on-line monitoring of many types of mixing process if fast digital imaging is available. © 2001 Published by Elsevier Science B.V.

Keywords: Angle Measure Technique (AMT); Partial Least Squares (PLS); Multivariate AMT Regression (MAR); Bulk powder properties; Image analysis; Mixing monitoring

1. Introduction

Bulk particle materials, with values of billions of dollars, are handled extensively in the industries around the world. They are characterized by their unpredictable behavior, which can range from liquid-like in an aerated state to near solid in a compacted state. Dealing with this situation in an acceptable manner requires development of reliable, reproducible and relevant methods of characterization. The current situation allows only little possibilities for building up of a body of knowledge regarding the interrelationships between characteristics and behavior. This systematic experimental work starts off with predictions of basic particle properties such as mean size and further investigate the interrelationships among bulk powder characteristics and predict the behavior such as in silos and pneumatic transport systems. The multivariate AMT regression technique, a new proposed concept to be described below, is put to use in constructing robust prediction models for these situations.

* Tel.: +47-35-57-51-52; fax: +47-35-57-52-50.
E-mail address: Jun.Huang@hit.no (J. Huang).

0169-7439/01/$ - see front matter © 2001 Published by Elsevier Science B.V.
PII: S0169-7439(01)00120-4

As presented in this paper, Angle Measure Technique (AMT) is applied on powder imagery in connection with multivariate calibration. The multivariate AMT regression is employed to establish a relationship between ordinary powder video imagery and functional powder properties. Images taken on in-situ powders are bound to contain information concerning irregularities, geometric shapes, sizes, roughness, smoothness, etc. of the individual particles. These basic characteristics can then be related to bulk powder functional properties and behavior, using proper multivariate calibration based on derived AMT-spectra.

The AMT transform, as a new signal description method, has shown potential in many areas of science and technology since its debut in 1994 [1]. It characterizes the scale-dependent complexity of data such as time series, spatial series, and any other measurement series, in a new domain—the scale domain. Possible applications now include image analysis, signal analysis, spectroscopy, analysis of drilling well log data, and measurement runs in quality control.

2. Theory

2.1. AMT concept

AMT is defined as a function from the local to global scale, s, which creates a new domain to characterize all data such as time series, spatial series, and any other *ordered* measurement series. AMT is neither an alternative to time-series analysis nor to the Fourier transform; the new scale domain represents a genuine novel *addition* to the time and frequency domains. See detailed descriptions in our companion paper [2], in which the AMT transform was applied to image analysis as an image feature extraction tool for powder characterization and discrimination with the aid of Principal Component Analysis. The basic interpretation of AMT spectra and some typical examples for image analysis have also been illustrated there. In this work, AMT-based image features are generalized and now used for predicting powder *functional properties* and *mixing components* in combination with multivariate calibration (PLS).

2.2. Multivariate AMT regression (MAR)

In recent years, some new regression techniques have sprung up in the field of chemometrics, such as Fourier regression, wavelet regression etc. In Fourier regression, a regression model is formed between the frequency components and a dependent variable(s), e.g. in acoustic chemometrics, where Fourier regression was used to relate the acoustic signals to process monitoring [3]. Similarly, wavelet transform has been introduced as a preprocessing step before the regression. In analogy to Fourier regression, Alsberg et al. proposed the concept of Wavelet regression [4]. Wavelet transform can also be regarded as a feature extraction tool for use in multivariate calibration in this context. The wavelet transform of signal(s) is coded as wavelet coefficients that act as regression vectors for the dependent variable(s) in the regression model.

Assume that $\mathbf{X}$ is the original matrix with the size of $N * M$, where N denotes the samples (rows), M denotes the variables, such as wavelength. Assume that y is the variable to be predicted. In general, the regression coefficients b need to be estimated by regression methods. This can be denoted by the equation

$$y = \mathbf{X}b,$$

In the Fourier regression, if $\mathbf{X}$ is transformed to the Fourier power spectra $\mathbf{P}$ we get $y = \mathbf{P}b$, which is solved generally by

$$\hat{b} = \mathbf{P}^{+}y,$$

where the generalized inverse $\mathbf{P}^{+}$ is from a regression method (e.g. PLS)

Similarly, $\mathbf{X}$ is transformed to the wavelet coefficients with respect to each sequential scale. The equation is obtained in general as

$$\hat{b} = \mathbf{W}^{+}y$$

where the generalized inverse $\mathbf{W}^{+}$ is from a regression method.

In analogy to the above regressions, AMT regression makes use of the AMT spectra, such as MA and MDY, which carry potential regression information at each corresponding scale [2]. An AMT regression model is established between the AMT complexity

spectra and a dependent variable. Assume that **A** is the AMT spectra that may be composed of MA and MDY or more indices. The analogous regression equation in general is given as

$$\hat{b} = \mathbf{A}^{+} y$$

where the generalized inverse $\mathbf{A}^{+}$ is from a regression method.

A schematic overview of AMT regression approach is shown in Fig. 1. This flow diagram generalizes the basic methodology of MAR. Any multivariate calibration methods can be applied to the specific problem in conjunction with AMT (MLR, PCR, PLS, etc.).

How much of the AMT spectra should be used in PLS analysis is problem-dependent. PLS offers a linear approach to analyze data with many noisy, collinear, and even incomplete variables in both *X* and *Y*. The precision of PLS method improves with the increasing number of *relevant X-variables* with regard to the observations. It is therefore recommended to use full spectra from as many AMT-scales as possible for the initial trials. However, use of full spectra may not always be necessary. One should perform *variable selection* in the scales to achieve an optimal number of scales for prediction according to some suitable prediction optimality criterion, of which many are available in chemometrics.

The multivariate AMT regression has brought a new approach to extract information for prediction from "measurement series", which in the present context are *unfolded* isotropic images (with no loss of information after unfolding). This approach offers a breakthrough in a major part of image analysis which converts *texturally isotropic* images into 1-D multivariate AMT-spectra completely without loss of fidelity. It views an image in a mathematically transformed way instead of by direct visualization. This work deals with isotropic *powder* images, but applies equally well in many other similar situations.

It is important to emphasize the definition of powder again [2]. A powder is an assembly of particles surrounded by fluids, whose behavior is influenced by the nature and interaction of the individual particles and of the fluid that surrounds them. Traditional image analysis on powder characterization focuses much on the *individual particles* using microscopic imaging and morphology descriptions [5]. In determination of particle sizes, for instance, intensive calculations are necessary because invariably image analytical techniques, morphological methods such as erosion and dilation, have to be used in order to be able to *segment* the particles. After segmentation and *individual* particle characterization, the desired powder parameters may now be pursued, often by histogram processing, or some other accumulative region-oriented techniques. This is therefore very often a long and troublesome procedure before even trying to translate this piecemeal information to characteristics of powders. This approach also necessarily involves a difficult and time-consuming *sample preparation* process, such as *dispersion* of the powders before microscopic imaging, etc. This makes it extremely difficult to carry out the on-line, at-line measurements in practical situations [6,7]. Instead of dealing with the individual particles, the present alternative approach acquires images directly from

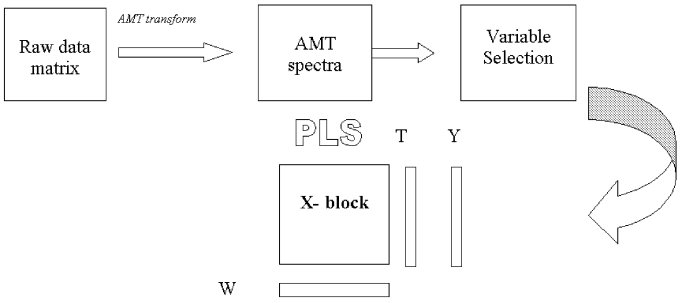

Fig. 1. A schematic overview of multivariate AMT regression using PLS, MAR.

powder with a minimum sampling preparation necessary, followed by MAR. Images taken on powders contain information not only about the individual particles, but also the *bulk powders*, which reflect interactive properties of the powder. The advantage of using AMT is that it characterizes the complexity of both local individual particles and global bulk powders simultaneously. For example, some local properties like individual particle size, shape, roughness, smoothness, and regularity can be represented, from which the related global properties like flowability, fluidization velocity, and wall friction angle can also be described by MAR. These important powder functional properties usually have to be measured by running large-scale experiments that demand much time and money. The AMT approach derives *predictions* of the relevant powder properties under one roof, however. The AMT image features—spectra—contain information necessary to predict a great many of these properties. The present work also aims to assess to what extent this is possible. This approach, based on simple and direct powder image analysis, coupled with chemometric data analysis, appears very practical and well suited for industrial use.

3. Experimental and results

3.1. Hardware and software

3.1.1. Camera and illumination

The camera used in all present experiments is named *Silvacam*, using red, green and near-infrared channels (R/G/NIR). See details in Ref. [2]. Oblique illumination sources are used in our unfolded AMT applications [2,8,9]. The unilateral illumination with optimized angles results in critically more detailed field-of-view imagery, including shadows created by the *individual particles*, or highlighted definitions of interstices and cavities *between* particles, etc. It is specifically held as a distinct advantage by this illumination set-up that, e.g. individual particle surface roughness, will also contribute to the complex light-shadow pattern created.

Average optimal settings for each series of powders to be characterised and compared need be obtained by experimental trial-and-error. Such *factors* need to be taken into account: number of light sources, angle of illumination, spatial resolution of camera, spectral characteristics of illumination sources, etc. It is important that all powder images to be compared be recorded under *exactly the same conditions.*

Image processing and AMT calculations in this work were implemented in a Dell computer with Pentium III processor and 128 MB RAM.

3.1.2. Software

The present 2nd generation of AMT program has been developed by the first author in MATLAB 5.3, with the central computation part written in Mex C for high speed. The software used for PLS modeling is the UNSCRAMBLER 7.5, from Camo ASA.

3.2. Prediction of powder functional properties

Throughout the experiments, all powders were imaged under identical conditions, where the optimized angle of illumination, focus distance, and image resolution were held constant, as were the scaling of axes, number of measurement scales in order for AMT transforms to be comparable.

To dampen the inaccuracies in sample preparation and measurement, each type of powder is imaged four times by rotating the sample container 90° clockwise. Consequently, four replicates for each type of powder are obtained for each powder type. Prediction models are then made both based on all replicates as well as on averaged spectra only in order to compare their differences. From this, one gains a visual impression of the reliability of the averaging procedure and the reproducibility of the ensuing PLS models, which are always based on the averaged results.

3.2.1. Prediction of particle size for different food powders

This group of powders includes a wide range of food samples such as spices, sugar, tea, etc. As shown in Fig. 16 in Ref. [2], some food powders display a variety of intrinsic complexities such as sizes, irregular shapes, roughness, color, and surface structure, while others, like salt and white sugar, appear relatively uniform due to identical color, size, and shape. Specific powder discrimination on these powders has been discussed in Ref. [2]. This work attempts to predict the particle sizes of these food samples from

the same AMT image features. Particle size ranges from less than 100 to about 5000 μm.

AMT spectra for all powders are shown in Fig. 2, where the spectra are composed of two parts, MA and MDY, the important AMT indices. See details in Ref. [2]. The spectra for salt lie at the bottom, and appear quite smooth without any characteristic angles/scales, which signify the simplicity of the salt image. The slightly higher curve with similar shape represents the spectrum for sugar, which visually appear very similar to salt. It may be the slightly larger size and brighter crystal surface that makes sugar spectra a bit more complex. There is a general trend that particle size is a very important factor to contribute to the complexity of powders; the larger the size of the powder, the more complexity there is. We deliberately also chose some rather irregular powders to put AMT to a tough test. They have different particle size distributions, color, and shape, etc. Intuitively, we consider that particle size is a geometrical parameter that must be related to the AMT scale domain. This should be the most direct/obvious variable that AMT can characterize. Therefore, we start off with the prediction of the mean, as well as the median particle size. The reference results for these two parameters were measured by a standard sieving method. The PLS modeling results are shown in Figs. 3 and 4. As expected, this AMT approach is capable of predicting particle sizes of different powders with no problems.

3.2.2. Prediction of powder behavioral properties

In today's powder industry, there is a serious need to know the relevance of the various characteristics, such as the roughness, size, surface structure, and shape, for prediction of e.g. behavior in silo filling/discharging and pneumatic transport. It is also the primary objective of this experimental work to determine to what extent the AMT approach can relate the basic static image characteristics to this type of bulk *behavioral properties*. Seven representative powders, which are widely used in the industry, are chosen for this purpose. Their raw images are shown in Fig. 7 in Ref. [2]. It should be mentioned that it is difficult to obtain more powders with all the following properties measured, which demands a very significant effort in large-scale experimental rigs.

The overview of their characteristics was described in Ref. [2].

The predicted parameters are listed below:

- Mean particle size, the average size of the sample (μm)

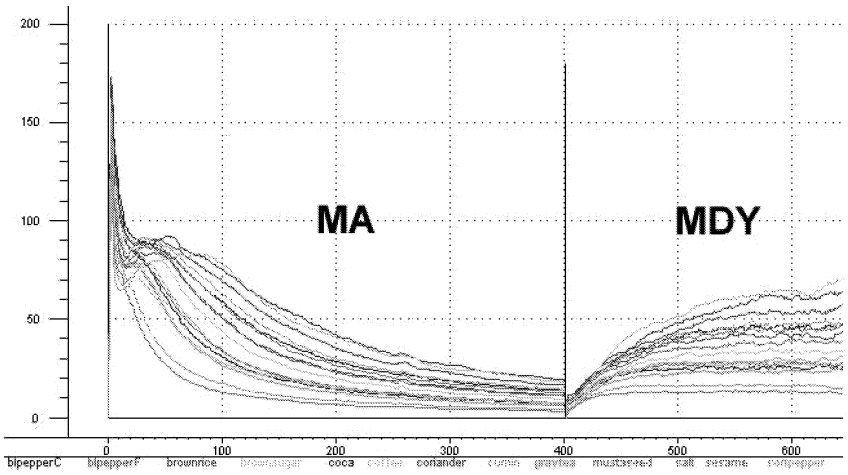

Fig. 2. Averaged AMT spectra of different food samples. There are some overlaps at smaller scales, but clear discrimination at all larger scales. Note that the AMT spectra are composed of two parts, MA and MDY (identical in all the following AMT spectra).

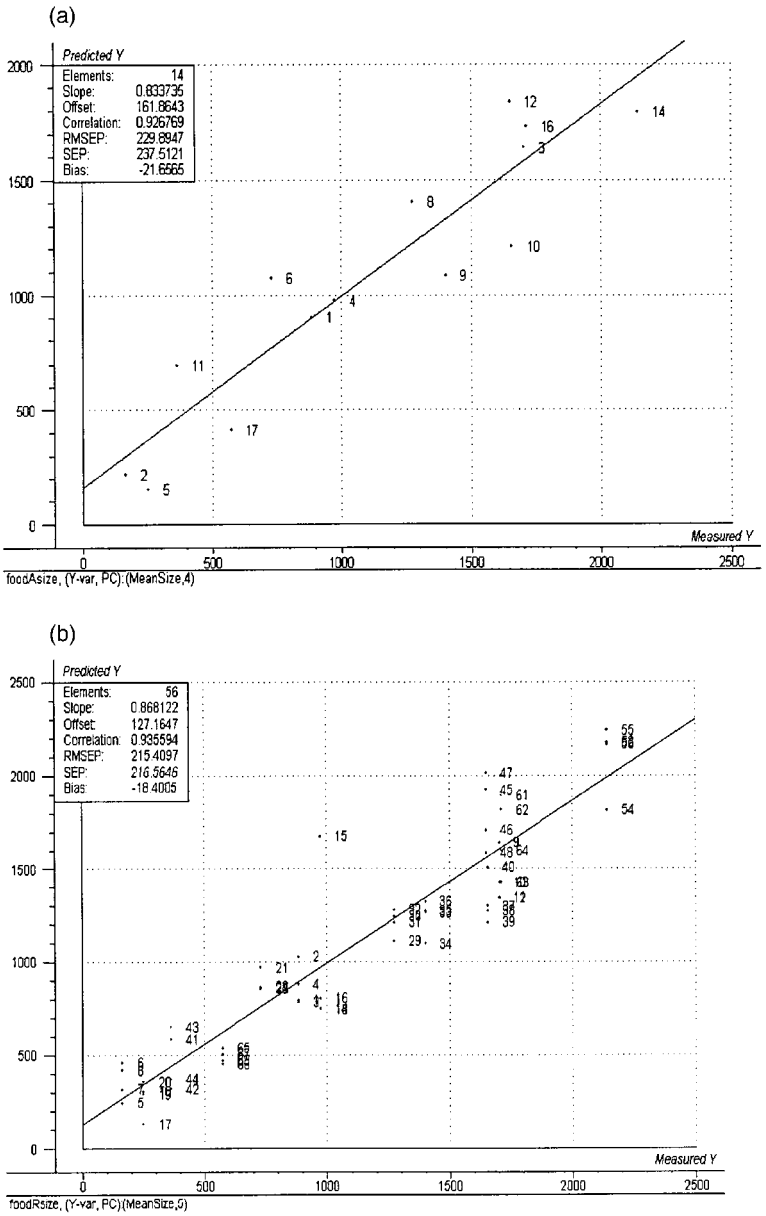

Fig. 3. Results for prediction of *mean size* of food powders. (a) Modeling results are based on averaged spectra. Correlation coefficient is 0.93; RMSEP is 229.8. (b) Modeling results are based on all sets of four replicates, which were put into the same segment when cross-validated. Correlation coefficient is 0.94; RMSEP is 215.4.

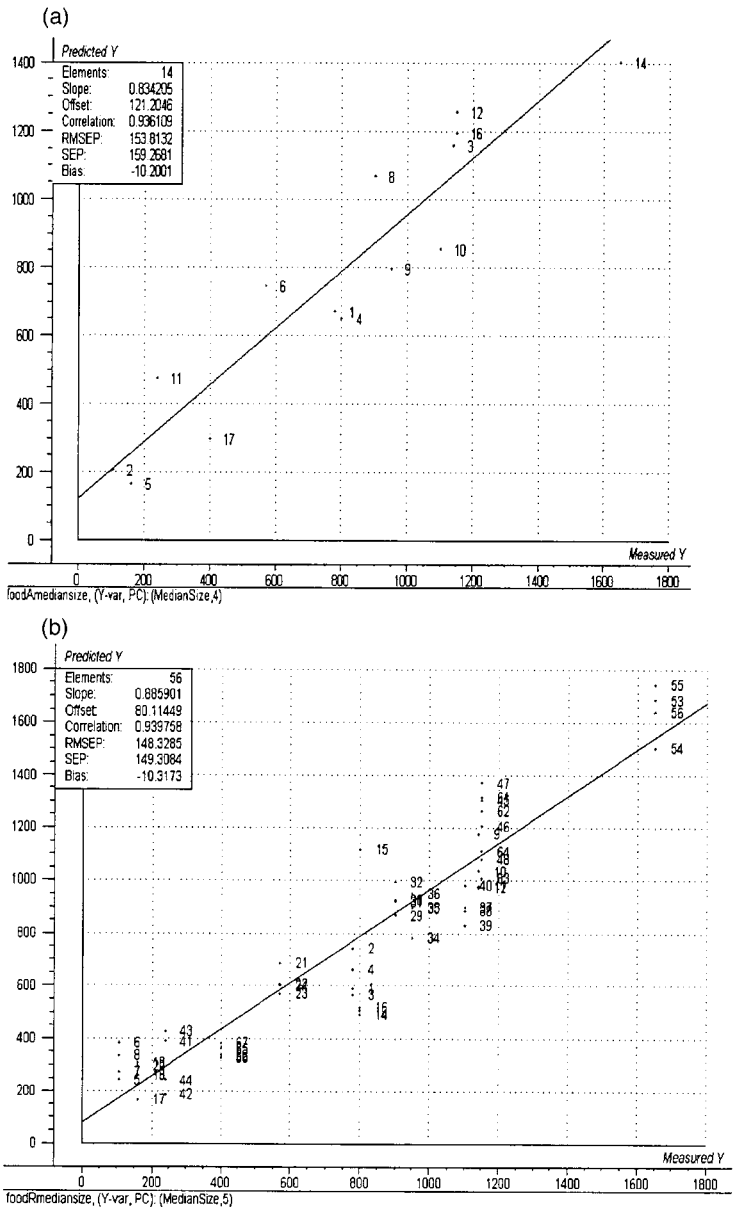

Fig. 4. Results for prediction of *median size* of food samples. (a) Modeling results are based on averaged spectra. Correlation coefficient is 0.94; RMSEP is 153.6. (b) Modeling results are based on all replicates, which were put into the same segment when cross-validated. Correlation coefficient is 0.94; RMSEP is 148.3.

- Particle density, characterizes the solid density of individual particles (kg/m^3)
- Bulk density, the density of the bulk, can vary depending on how it is measured, and on the condition of the powder (kg/m^3)
- Minimum fluidization velocity, is the minimum gas rate necessary to fluidize the powder (cm/s)
- Permeability prior to fluidization is the air velocity per specific pressure drop, which can be found from fluidization testers (m^2/Ps S)
- Wall friction angle against ST37 is the angle of a powder against the wall of steel type ST37 (grade)
- Static angle of repose, is the angle of the inclined surface of heap with the horizontal plane (grade)
- Dynamic angle of repose, gives the dynamic angle of repose, formed when the heap is being poured from the top (grade)

All these parameters constitute a minimum set of relevant powder material properties. Each demands specific tests for its material characteristics. We have attempted to predict as many of them as possible directly from the digital imaging of in-situ powders.

The AMT spectra give clear representations of the raw images. Fig. 9 in Ref. [2] shows that cement, alumina, and MD have smoother curves, which mean there are not much complexities in these images. It is easily understood that these three powders have simpler patterns to go along with their smoother individual grain surfaces. By contrast, the rest of the powders have higher complexities. The rape seed seems to have the largest complexity of all. This is probably because rape seeds have relatively larger particles and contain some irregular impurities like white petals. Pellets have the largest sizes but with a more regular surface, almost uniform color and shape. Therefore, the MA for pellets is located in the middle of all curves with a relatively smooth shape, showing just a little more complexity than the three fine powders. Spectra for sand and PVC are similar but still with a clear difference.

Table 1 shows physical and behavioral characteristics for these reference powders. It has been shown in many powder studies [6] that behavioral powder properties are more dominantly linked to the characteristics of the particles constituting the powder and to the nature of the size distribution(s) present. In the field of powder industry, it is regretted that knowledge cannot be extended to reliable and complete prediction of bulk powder behavior from an examination of these characteristics alone. Reference studies have shown that the fluidization behavior is very much related to the particle size and density. For instance, both Geldart's classification and Dixon's diagram show such relations that link these behavioral properties to basic characteristics. These two diagrams have been used very frequently in the powder industry. For more details, see Ref. [6].

A rough initial PLS2 modeling based on all reference variables (properties) show such relationships that are consistent with their study in the field of powder technology. As shown in Fig. 5a and b, minimum fluidization velocity is correlated to particle size, and density is negatively correlated to both. The figure also shows that some of the other relation-

Table 1
Physical and behavioral reference properties of seven representative powders
All reference values, courtesy of POSTEC, Porsgrunn (Powder Science and Technology Research Institute).

Powders	Particle density (kg/m^3)	Poured bulk density (kg/m^3)	Mean particle size (μm)	Minimum fluidization velocity (m/s)	Wall friction angle against ST37 (°)	Static angle of repose (°)	Dynamic angle of repose (°)
Pellets	913	555	3667	1.0×10^{0}	14.8	38	37
Rape	1164	687	1650	4.3×10^{-1}	18.7	30	30
Sand	2645	1590	687	2.5×10^{-1}	16.3	36	33
PVC	1414	518	472	8.1×10^{-2}	14.8	37	35
MD100	2865	1212	91	3.0×10^{-4}	26.1	63	39
Alumina	3399	939	87	3.1×10^{-3}	22.8	47	34
Cement	3095	734	15	3.2×10^{-4}	29.3	65	33

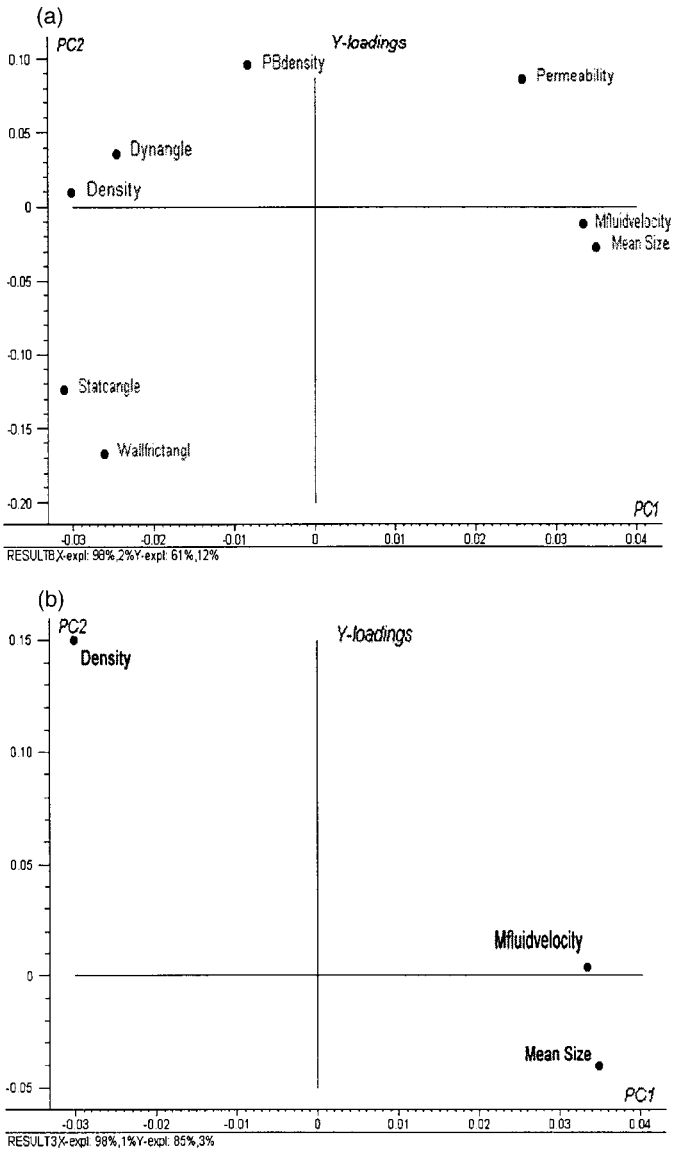

Fig. 5. (a) Loading plot from PLS2 modeling for all Y variables. (b) Loading plot from PLS2 modeling for three particular variables (density, mean size, minimum fluidization velocity).

ships, e.g. wall friction angle, are correlated to the static angle of repose. It is useful to see that a first PLS2 model gives initial results in predicting some of the important properties with apparent ease while

confirming well-known interrelationships among these basic static properties and the behavioral properties.

Final individual PLS1 models for each reference *Y*-variable were established for predictions. Comparative models based on all replicates and averaged spectra were made to test the reproducibility of the imaging method. Full cross validation was used for modeling based on the averaged spectra, due to a small number of certified reference samples (Table 1). As mentioned earlier, it usually takes a long time and great effort to measure parameters such as minimum fluidized velocity in powder industry. Segmented cross-validation was used for samples with replicates, in such a systematic way that all replicates went into the same segment in order to avoid overoptimistic results. Both full cross-validation and nonsystematic segmented cross-validation will give unrealistically good outcome when such replicates are present. Test set validation could not be adopted here since not enough reference samples can be obtained. For more details about validation, see Refs. [10,11]. Tables 2 and 3 show the statistical evaluations of these PLS1 models for all predicted properties. Most notably are the satisfactory results for density, minimum fluidization velocity, wall friction angle and static angle of repose, which strongly substantiate the capability of this new multivariate AMT approach. It does not work, however, with bulk density, permeability and dynamic angle of repose, as marked in gray color in these tables. Minimum fluidization velocity is a very important parameter in the field of fluidization. It is very encouraging that this parameter can be predicted and its relations with others can also be studied in our first modeling. Fig. 6 shows the predicted vs. measured evaluation plot for minimum fluidization velocity. Here four replicates and segmented cross-validation were used. One outlier, "pellets", was detected. The model manages to explain 88% *Y*-variance with 98% *X*-variance, as shown in *X*-loading weight plot in Fig. 6a. *X*-loading weights indicate that only the smallest scales *X*-variables are not used much for explaining *Y*. Full spectrum can be used for modeling without variable selection problems, or, alternatively, one may choose any convenient (interdependent) subset of scales if necessary. The *X*-loading weights plot can be used directly for variable selection in the present situation.

Note that for some properties, there may occur a smaller or larger clustering of the comparatively low number of reference powders, Fig. 6, while for others there is a more satisfactory spanning of the entire calibration range, Fig. 7.

Another modeling result, for the static angle of repose, is shown in Fig. 7. Reference studies [6,7] show that it has direct relations to particle shape, roughness, and irregularity, etc. It was also discussed earlier that the AMT is especially useful in characteriz-

Table 2
Comparative statistics (*fitted* regression models of "predicted vs. reference" values) pertaining to eight powder properties
Note that all results below are based on *averaged* AMT spectra. The parameters marked in gray color cannot be predicted.

	Slope	Offset	Correlation coefficient.	RMSEP	#PLS components
Mean size	0.95	21.5	0.97	135.3	2
Density	1.10	-363.3	0.93	286.9	2
Bulk Density					
Min.Fluid. Velocity	0.78	0.02	0.90	0.07	2
Permeability					
Wall friction angle against ST37	0.80	4.12	0.89	2.22	4
Static angle of repose	1.17	-9.74	0.95	5.55	3
Dynamic angle of repose					

Table 3
Comparative statistics (*fitted* regression models of "predicted vs. reference" values) of eight powder properties
Note that all results are based on *individual AMT spectra* (four replicates for each powder). All replicates were put into the same segment when the models were cross-validated. The parameters marked in gray color cannot be predicted.

	Slope	Offset	Correlation coefficient.	RMSEP	#PLS components
Mean size	0.95	17.4	0.97	135.3	1
Density	0.84	330.6	0.91	356.3	4
Bulk Density					
Min.Fluid. Velocity	0.86	0.02	0.91	0.07	3
Permeability					
Wall friction angle against ST37	0.92	-1.7	0.94	1.45	3
Static angle of repose	1.14	-7.8	0.94	5.72	3
Dynamic angle of repose					

ing complexity stemming from individual particle roughness, etc. Good prediction models were obtained as expected. Final predicted vs. measured evaluation plot for static angle of repose is shown in Fig. 7b. This model was based on averaged spectra. No outliers were found. The correlation coefficient is as high as 0.95. Again, X-loading weights plot shows that 97% X variance has been used to explain 76% Y variance. The w-spectra are particularly informative with respect to the relative scale influence. See Fig. 7a.

Good models for wall friction angle were also obtained. This parameter is, for instance, useful in describing powder behavior in silo systems. All final prediction results have been summarized in Tables 2 and 3, with and without replicate averaging, respectively.

The salient point made by the illustrations above is that it is fully possible to use the AMT-derived spectra *directly as is* for various prediction purposes —even though one is not necessarily able to fully interpret all the intricacies of the relative appearances of the AMT-spectra. These types of AMT spectra are now routinely used as a preprocessing facility at our laboratories, in addition to spectroscopy, FFT, and Wavelets for subsequent multivariate modeling.

The following example will show how multivariate AMT regression can also be used for powder mixing process analysis.

3.3. Prediction of mixing components

Mixing of particulate materials is widely used in the process and related industries. It is a deliberate act intended to increase the homogeneity of a mixture of different components or sizes [12]. The most important objective in mixing is usually the production of a homogeneous mixture of several components, i.e. an even distribution of concentrations throughout the mass. However, many present monitoring methods are either inapplicable, or too difficult, or too time-consuming, to be applied for on-line, or at-line monitoring and characterization. The difficulty of predicting the result of many independent or interdependent causes in mixing and segregation processes can become so great that the behavior of the system is unpredictable or chaotic for all practical purposes. An effective design procedure employing both heuristics and algorithms needs to be developed.

To meet these demands, image analysis is here used in combination with AMT and chemometrics. Although the mixtures are all close to chaotic, they

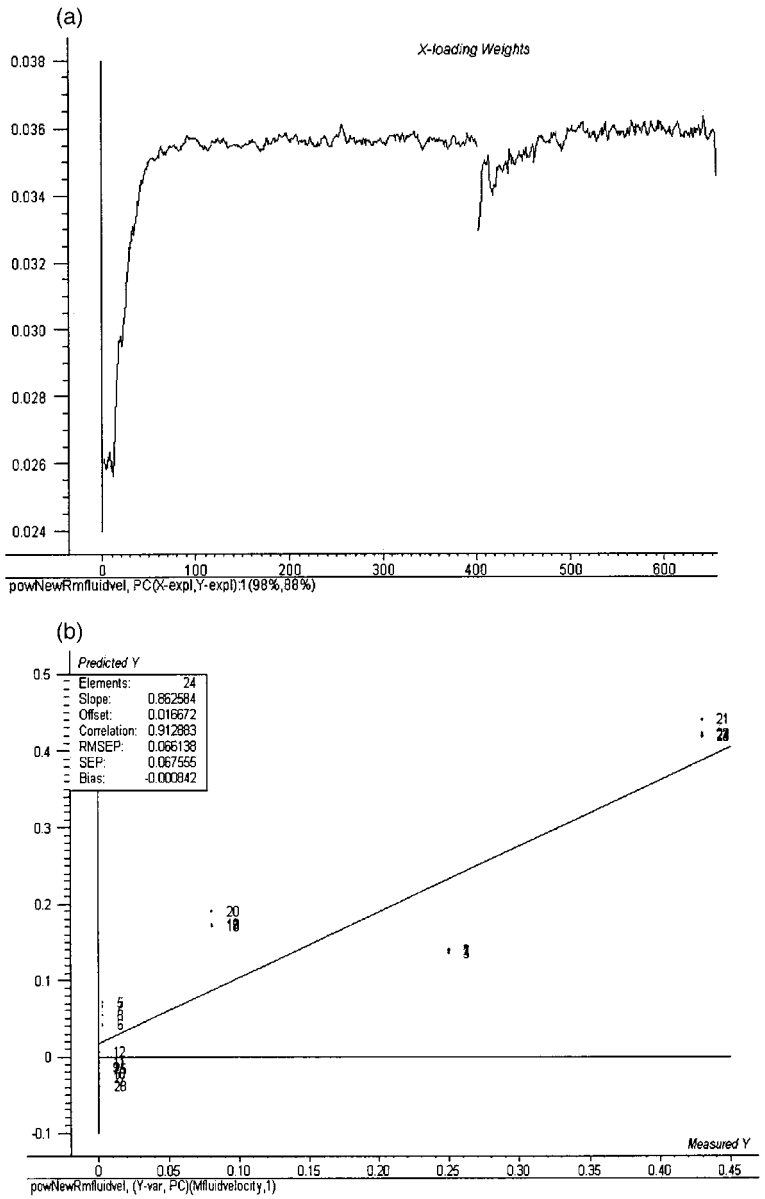

Fig. 6. (a) *X*-loading weights. 98% of *X* variance is used to account for 88% of *Y* variance. (b) Final predicted vs. measured evaluation plot for minimum fluidization velocity. Final modeling was carried out based on replicates which went into the same segment when cross-validated. Correlation coefficient is 0.91.

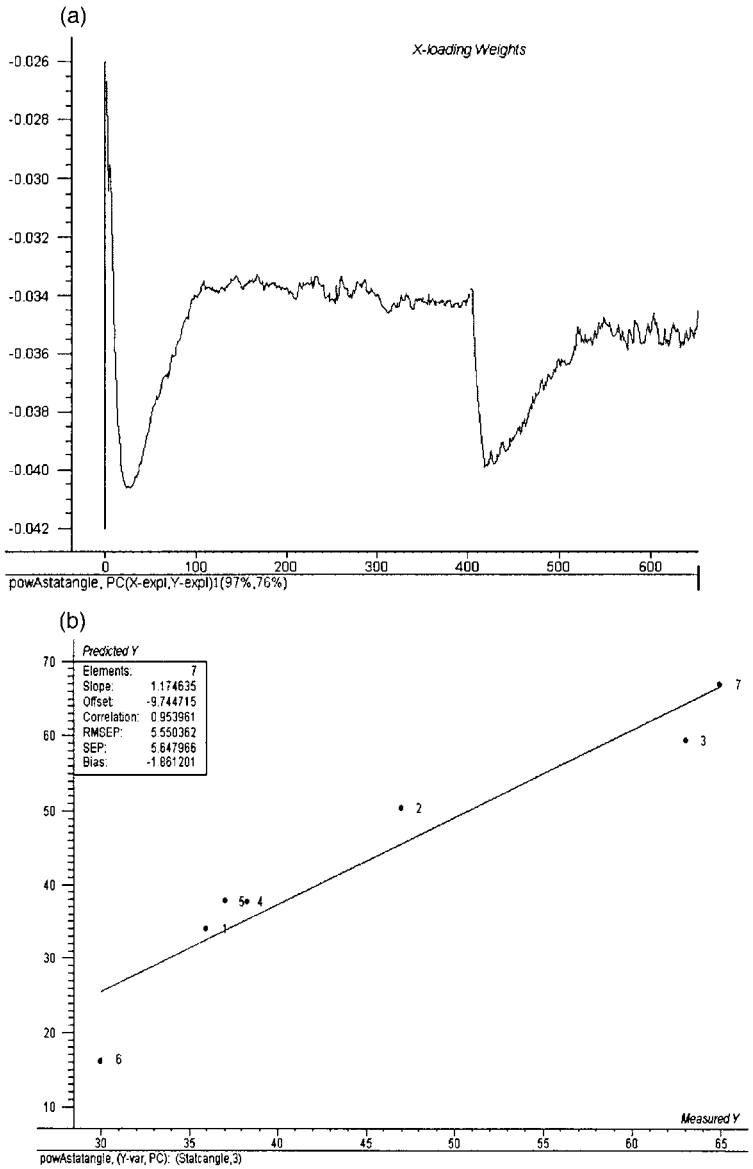

Fig. 7. (a) *X*-loading weights. 97% of *X* variance is used to account for 76% of *Y* variance. (b) Predicted vs. measured evaluation plot for static angle of repose. Final modeling was carried out based on averaged spectra using full cross-validation. Correlation coefficient is 0.95.

do have different characteristics, such as color, shape, size and density. It is exactly these characteristics that AMT can take advantage of to discriminate/distinguish between the fractions of components. With

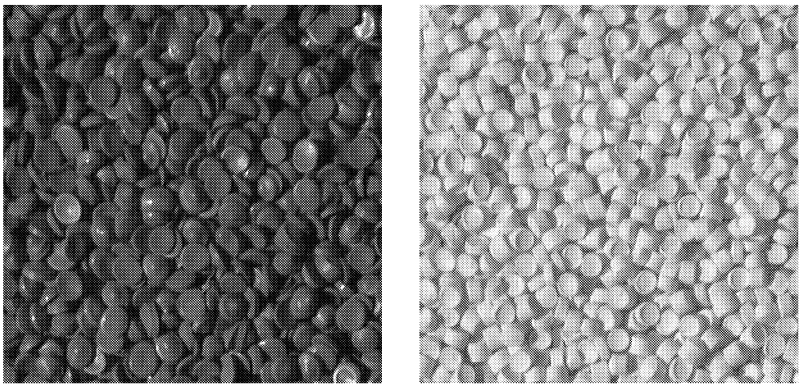

(a) (b)

Fig. 8. Images with one homogeneous component. (a) Black tablets (100%). (b) White tablets (100%).

this insight, we tried to establish multivariate models to predict the quantity of the selected mixtures with the aid of AMT image features, e.g. mixing fractions, homogeneity.

Several types of mixtures were prepared for mixing prediction modeling. First we deliberately chose two high-contrast types of tablets: one white and the other black. They have otherwise similar densities, sizes, and shapes, etc. Fig. 8a and b shows the images with one component before mixed. They are randomly mixed thoroughly and well distributed in the sample container.

Several mixture series were made with specific different proportions of components (10% increment), which is meant to *simulate* monitoring of a mixing process. Fig. 9 shows the mixture with 20%

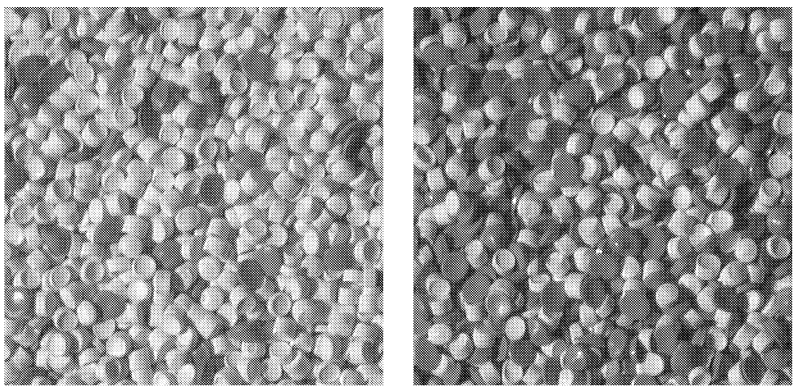

(a) (b)

Fig. 9. (a) Mixture with 80% white tablets and 20% black tablets. (b) Mixture with 50% white tablets and 50% black tablets. Note *random distribution* throughout the sample container.

black tablets and 80% white tablets, juxtaposed with the mixture with 50% white and 50% gray tablets. It would be of great interest to compare the AMT spectra derived from these two images for all mixtures.

Fig. 10 shows detailed comparison of some selected mixture AMT spectra with different proportions of components. The spectra for pure black tablets lie at the bottom because they are the "sim-

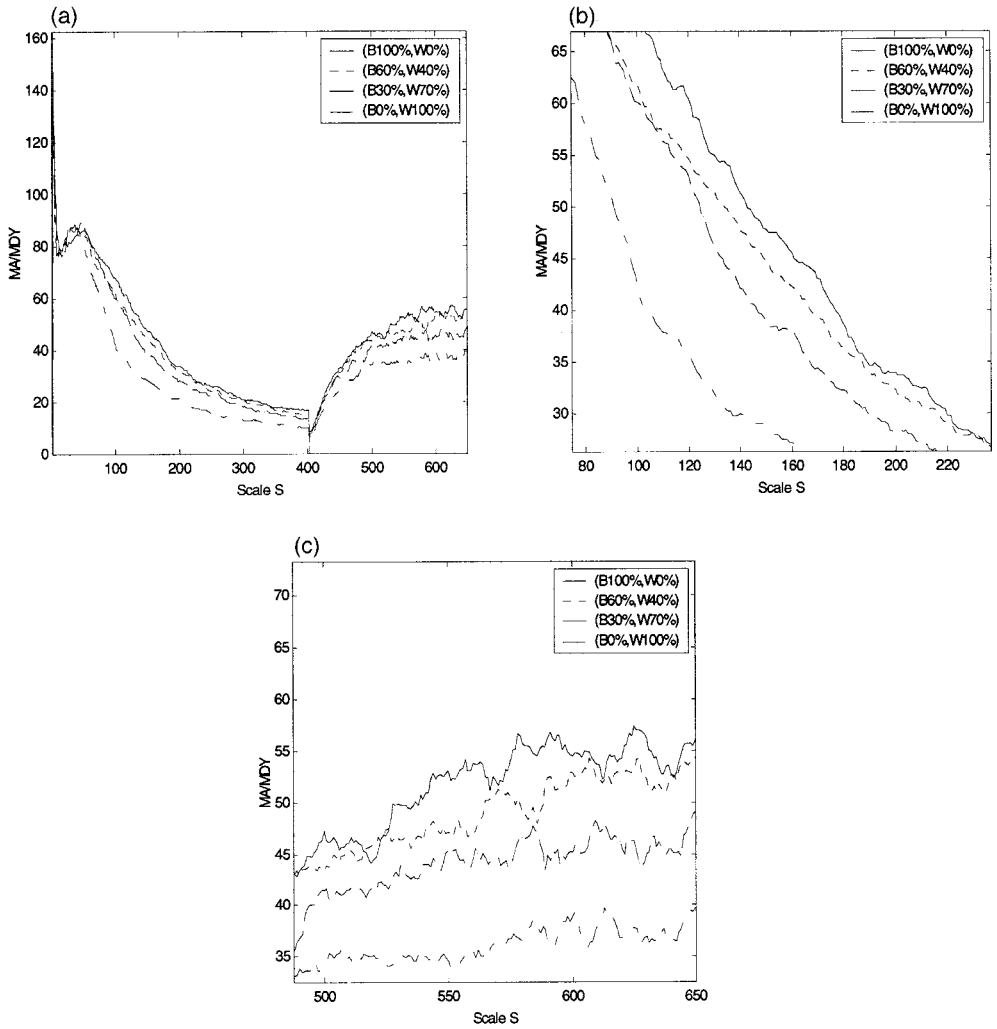

Fig. 10. (a) Comparison of selected AMT spectra. Mixtures of black and white tablets: (100%, 0%), (60%, 40%), (30%,70%), (0%,100%). (b) Blow-up of MA. (c) Blow-up of MDY. Note that spectra for pure black tablets and white tablets are *both* located at the bottom due to their simplicity and uniformity.

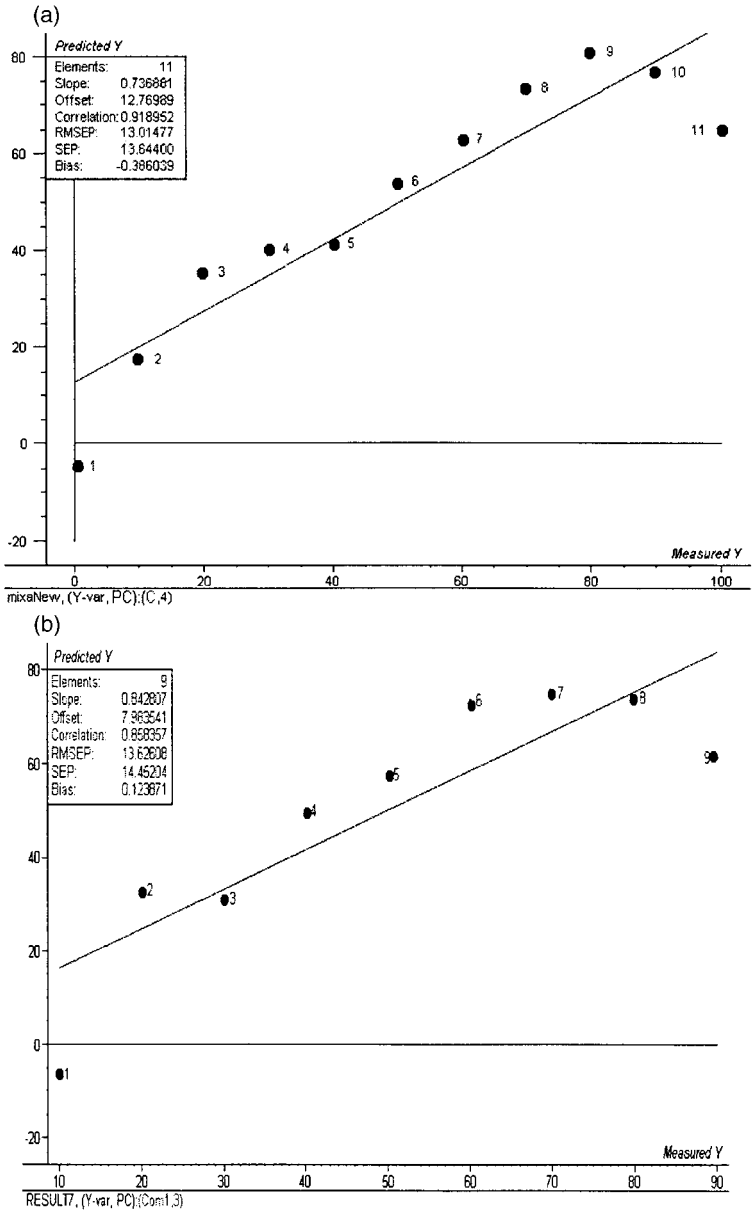

Fig. 11. Predicted vs. measured evaluation plots for mixing component prediction. Models based on averaged spectra. (a) Model with all 11 compositions of the mixture series. Nos. 1 and 11 represent the *pure end members*. Correlation coefficient is 0.86; RMSEP is 13.62. (b) Model *without* the pure black and white end members (Nos. 1 and 11 in (a)). Correlation coefficient is 0.92; RMSEP is 13.01.

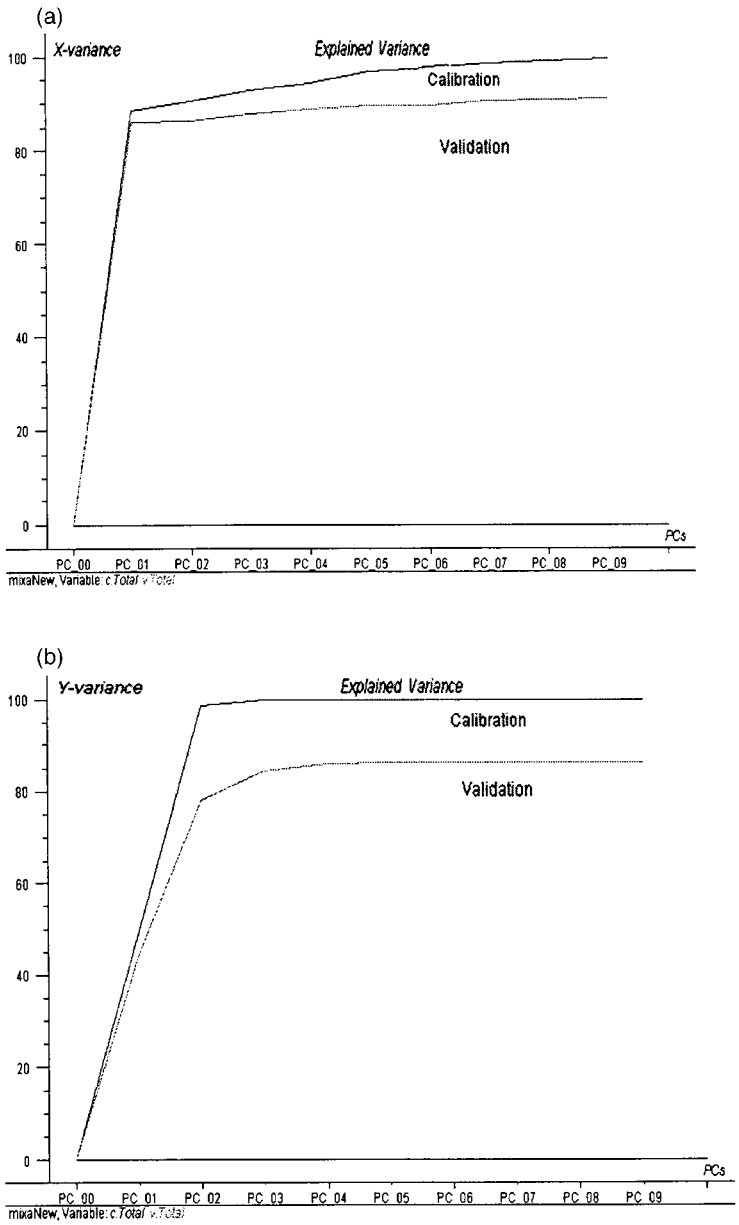

Fig. 12. (a) Explained X variance plot for both calibration and validation. (b) Explained Y variance plot for both calibration and validation for the mixing fraction prediction study.

plest" among these mixtures, as evidenced clearly by the raw images. Likewise, the spectra for pure white tablets are located just above the pure black tablets. It is easily understood that both are composed of one component alone, and therefore not of much complexity. Distinctly opposed to this, all the mixtures are more complicated so that their spectra are located higher than the components. This indicates principally different features for homogeneous media and mixtures. Clear systematic variations can be perceived from the enlarged MA and MDY spectra, Fig. 10b and c. There are some small *overlaps* between mixture spectra at smaller scales, which mean they have different degree of complexity at smaller scales.

These image features—AMT spectra—can now be used as *X*-block variables to predict the mixing components quantitatively (*Y* variables), by multivariate AMT regression. The results from this PLS modeling are illustrated below, in Fig. 11. The first attempts to predict mixing components are marginally successful, and the predicted vs. measured evaluation plot shows a reasonably promising result. It must be emphasized that subsequent optimization of e.g. illumination and imaging parameters leads to improved results for individual powder cases. We only show here the *potential* of this new approach; specific industrial application studies are under way.

The model based on *averaged spectra* is able to explain 90% of *X*-variance and 85% of *Y*-variance with two principal components. See Fig. 12. Regression coefficients from model using two PCs are shown in Fig. 13. Apparently, smaller scales of AMT spectra show higher importance in the modeling.

For on-line process monitoring, it would be interesting to study trajectory score plots that directly depict the simulated mixing process. As shown in Fig. 14, sample 1–11 represent the mixtures with different proportions of components. Number and its component proportions (%) are, 1 (B100, W0), 2 (B90, W10), 3 (B80, W20), 4 (B70, W30), 5 (B60, W40), 6 (B50, W50), 7 (B40, W60), 8 (B30, W70), 9 (B20, W80), 10 (B10, W90), and 11 (B0, W100). Fig. 14 shows that the sequence is exactly consistent with the proportional percentage of black and white tablets, indicating a progressive development of the mixing process. Numbers 1 and 11 correspond to pure black and white tablets, respectively. As can be seen, they are located at a comparatively large distance away from all others, because they are not actual mixtures. These two samples can thus also be considered *outliers* during the modeling, Fig. 11b. This type of trajectory plot can be used to represent the development of mixing components and evaluate the quality and performance of the mixing process. This type of plot

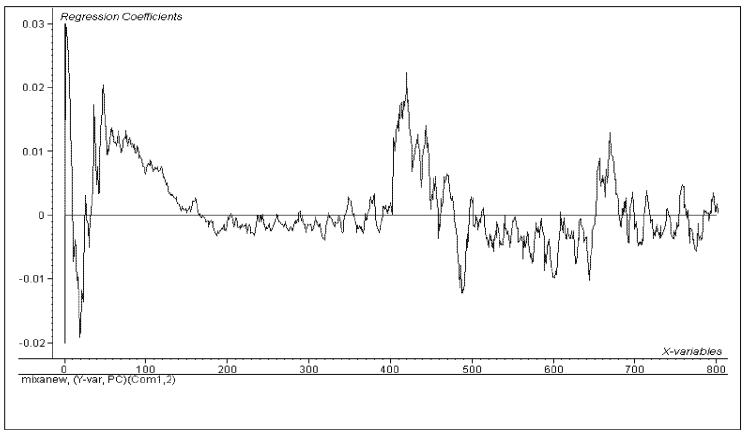

Fig. 13. Regression coefficients from the mixing model using two PLS components.

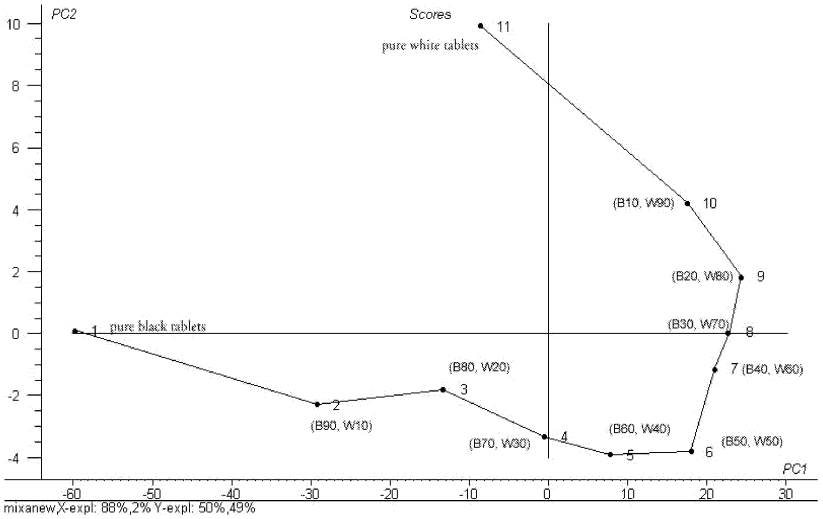

Fig. 14. Score plot from the mixing model. Note how the trajectory of samples represents the progressive development of mixing process. See details in text.

is thus suitable as a vehicle for on-line mixing process operator support.

It can be seen from the above results that this approach would appear promising with respect to more developed use in practice, e.g. image sampling from on-line, or at-line mixing processes.

4. Discussion and conclusions

As seen from all the above results, the models based on replicate and average spectra do not show much difference. This indicates that the measurements were basically conducted accurately and the method is reliable and reproducible, but studying models based on replicates is helpful in finding outliers and in dampening the unavoidable imaging inaccuracies. Therefore, we usually establish initial models based on all replicates to see if there exists outliers, and then average the remaining replicates to make the final models.

MAR provides a unified methodology of data analysis for a wide range of applications. The AMT image feature vectors enable the use of multivariate techniques for prediction of desired variables, which represent powder properties in this case. The attempts to predict functional powder properties and mixing components have been made based on very simple in-situ video powder images instead of microscopic images of individual particles. It is constructive that MAR is able to link the basic characteristics of powders to the behavioral properties from the AMT image features.

The general success of this new approach has proved that the present approach is a powerful new technique for prediction in powder science and industry, which lacks similar reliable, reproducible methods of characterization. The homogeneity of a mixture, an important homogenous powder characteristic, can be evaluated with the same technique no matter how complicated the mixture. Additionally, a mixing process may be simulated and observed from the process trajectory score plot. This latter pilot study indicates that some work remain before the intriguing mixing process monitoring will reach industrial applications standards, but these first results are certainly encouraging enough to continue our work.

Acknowledgements

The POSTEC research group, HiT/TF, Porsgrunn, is acknowledged for providing reference powders and generous support. We thank Sivert Ose, senior engineer at POSTEC, for very constructive discussions.

References

[1] R. Andrle, The angle measure technique: a new method for characterizing the complexity of geomorphic lines. Math. Geol. 26 (1994) 83–97.
[2] J. Huang, K.H. Esbensen, Applications of AMT(Angle Measure Technique) in image analysis: Part I. A new methodology for in-situ powder characterization. Chemom. Intell. Lab. Syst. 54 (2000) 1–19.
[3] K.H. Esbensen et al., Acoustic cheomoetrics—from noise to information. Chemom. Intell. Lab. Syst. 44 (1998) 61–76.
[4] B.K. Alsberg et al., An introduction to wavelet transforms for chemometricians: a time-frequency approach. Chemom. Intell. Lab. Syst. 37 (1997) 215–239.
[5] R.C. Gonzalez and, R.E. Woods, Digital Image Processing. Addison-Wesley, Reading, 1993.
[6] S.R. de Silva, Characterization of Particle Particulate Solids. Telemark Technological Center, POSTEC, Norway, 1995.
[7] S. Ose, Measuring Particle Size Distributions. Telemark Technological Center, POSTEC, Norway, 1995.
[8] K.H. Esbensen, K. Kvaal, K.H. Hjelmen, The AMT approach in chemometrics—first forays. J. Chemom. 10 (1996) 569–590.
[9] K.H. Hjelmen, AMT (Angle Measure Technique)—implementation at Telemark Institute of Technology and applications on time series and similar measurement series, MSc (Eng.) Thesis, Telemark Institute of Technology, Porsgrunn, Norway, 1995 (in Norwegian).
[10] K.H. Esbensen, Multivariate Data Analysis—In Practice. 4th edn., CAMO ASA, Oslo, 2000.
[11] K.H. Esbensen, J. Huang, Principles of Proper Validation, Submitted, 2001.
[12] S.R. de Silva, Mixing and Segregation in Industrial Processes. Telemark Technological Center, POSTEC, Norway, 1997.

PAPER III

Development of a new method for characterization of barley germination by automated image analysis and AMT (Angle Measure Technique)

Jun Huang[1*], Birthe Møller[2], Lars Munck[2], Kim Esbensen[1]

1: Applied Chemometrics Research Group, Department of Technology (TF)
Telemark University College (HiT), N-3914, Porsgrunn, Norway
2: Food Technology, Department of Dairy and Food Science,
The Royal Veterinary and Agricultural University (KVL),
Rolighedsvej 30, DK 1958 Frederiksberg C, Denmark

Abstract

Fast and even germination is an essential barley malting quality parameter. During the malting process the number of germinated kernels needs to be known in order to evaluate which variety of barley should be used in the malt house. Traditional manual germination tests are time-consuming and laborious so that it would be of great interest for the malting industry to have an automated, fast and objective instrumental method for assessing the contemporary level of germinated kernels.

The present unified approach allows for indirect quantitative germination assessment using fast imaging and AMT transform in combination with multivariate calibration. The validated PLS-prediction models constructed here are able to quantify the process of germination from a very early stage. This methodology development pilot study reports the initial levels of accuracy and precision obtainable.

Keywords: Barley Germination; AMT (Angle Measure Technique); PLS (Partial Least Square); Multivariate Modeling; Multivariate AMT Regression (MAR)

1. Introduction

Germination frequency - and speed of germination - play a key role for yield in agriculture and malting quality for the brewing industry. It is crucial for the malting industry to obtain a fast and reliable germination assessment in the malt house. Therefore it is of great importance to develop a fast and objective instrumental germination test to characterize the barley *before* malting it. A high percent germination and a vigorous growth means a good malting barley variety. Selecting an optimal variety is the first step in successful production - and marketing - of malting barley. Currently there is a lack of efficient methods available to measure the germination behavior of barley. The number of germinated barley kernels in a standard sample is usually counted *manually* in the laboratory. This is very laborious, time-consuming and at times partly subjective. There is a strong need from e.g. the brewery industry calling for fast,

* Corresponding author. E-mail: Jun.Huang@hit.no. Tel: +47 35 57 51 52. Fax: +47 35 57 52 50.

automatic methods instead. The new compound method presented here, the multivariate AMT approach in combination with image analysis, appears very promising for this industrial use due to its simple imaging requirements and fast PC-modeling. The present approach is able to characterize the germination process automatically and to conduct indirect instrumental measurements *on-line*.

Two varieties of barley grown at the KVL farm with rather different germination qualities due to weather, variety, fungal infection, and treatment were collected for the present germination test.

The Angle Measure Technique (AMT) was originally introduced by Andrle in 1994 for characterization of the complexity of geomorphic lines[1]. Later Esbensen and his group broadened the AMT concept and proposed the generic AMT approach for general signal complexity characterization, see details in the series related publications [2-6]. Applications now include image analysis, signal analysis, spectroscopy, quality control a.o.

We give full technical descriptions as an *appendix* for the interested reader.

3. Materials and Experimental

3.1. Materials

A standard number of kernels, e.g. 100, are placed on two layers of filter paper in a petri dish and 4 ml of water is added. The petri dish is placed at a controlled temperature of 20ºC and germinated for 72 hours. The number of germinated kernels is counted manually every 3 or 6 hours and then replaced in the controlled oven. Two rather different varieties of barley were chosen in the present screening experiment, A and B, in order to illuminate the inherent germination differences between barley varieties. For the present pilot study we are *only* interested in the principal behavior of these two different barley varieties; we need not even identify these. A systematic study is underway aimed at a proper survey of the entire barley field, Møller & Munck (*in prep*)[14].

3.2 Imaging

3.2.1 Measurement Setup

The schematic overview of measurement set-up is shown in Figure 4. Imaging was carried out with this optical system. The illumination system (*ReprostarII/Transilluminator,CAMAG*) can function in 6 modes of lighting with both direct and transmitted light. The CCD (Charge Coupled Device) camera system (*Photometrics*) played a major role in image acquisition [7]. A Nikon 105 mm UV photographic lens was connected to the CCD. An Apple Macintosh computer and image software IPLab Spectrum (*Signal Analytics Corporation*) were used to control CCD camera. The Apple Macintosh system was connected to the network and shared files with computers running Windows through the *TSStalk* [9]. Images can then be transferred to the other computers for further processing and analysis, as is important in the KVL chemometrics group.

During the entire experiment, the imaging room was darkened in order to avoid mixture of the artificial, controlled illumination light and daylight, which could otherwise perhaps lead to

wrong color reproductions a.o. It was also felt important that room temperature was controlled in the range of 16-20ºC. Unstable temperature may also have a negative influence on the imaging.

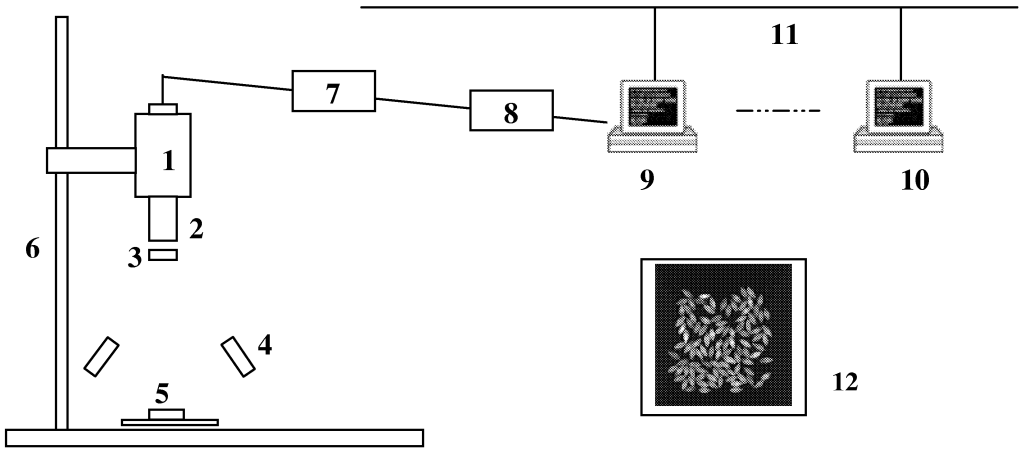

Figure 1. Schematics of the optical imaging system. 1. CCD camera; 2. Camera lens; 3. Optical (bandwidth) filter; 4. Illumination lights; 5. Sample holder (kernels); 6. Elevator; 7. Electronics controller; 8. Image frame grabber; 9. Computer (Macintosh); 10. Other computers; 11. LAN (Local Area Network); 12. Resulting images

3.2.2 Optimal Imaging Settings

Many imaging conditions were tried out before first generation optimized images were obtained. For the present purpose, we need to acquire images which will *distinguish* well between sprouts and the remaining parts of the kernels. It is easy to obtain high quality images under normal photographic lightening condition. Unfortunately images acquired in this way do not discriminate in this fashion at all. Optimal discrimination requires the use of various filters and specific illumination settings for a better solution. Quite a number of different filters in front of the lens and many different illumination lights were tried out to try to meet the requirements. UV and white light illumination, with a UV filter (397nm, 10nm bandwidth) were finally chosen. The UV illumination is used as excitation light to generate the necessary auto-fluorescence images, because the sprouts are particularly contrasted in the fluorescing images. Use of the UV filter enhanced the sprouts while reducing the light reflected from the kernel bodies. However, a severe price had to be paid for this increased discrimination, i.e. a significant weakening of the total intensity, which caused a certain unavoidable *blurring* of the images [10], but this was not a fatal consequence. Figure 2 shows a comparison of images taken with and without the UV-filter. Selection of the appropriate f-number and the exposure time

also became a trade-off, whether we wanted sharp images of low intensity or somewhat blurred images of high intensity. In our case, the signals were overall weak anyhow and the kernels should not be kept out of the controlled oven too long.

All these factors were taken into account before starting the formal imaging. With this in mind, a formal *experimental design* for obtaining the optimal imaging settings was instigated. Images were recorded with - and without - UV filter, using white and UV illumination alternatively, with different f-number and exposure times (four experimental factors). In the end the following optimal recording settings were chosen for the final imaging.

Illumination : white light
Filter: UV
f-number: 8
Exposure time:1sec.

As an example, Figure 2(a) shows corresponding images, recorded with white light illumination and without filter. Apparently, the image is of high quality, but it clearly doesn't emphasize the wanted part, the germination sprouts. Figure 2 (b), however, gives a much better discriminating *contrast* for distinguishing the sprouts from the rest of the kernel bodies.

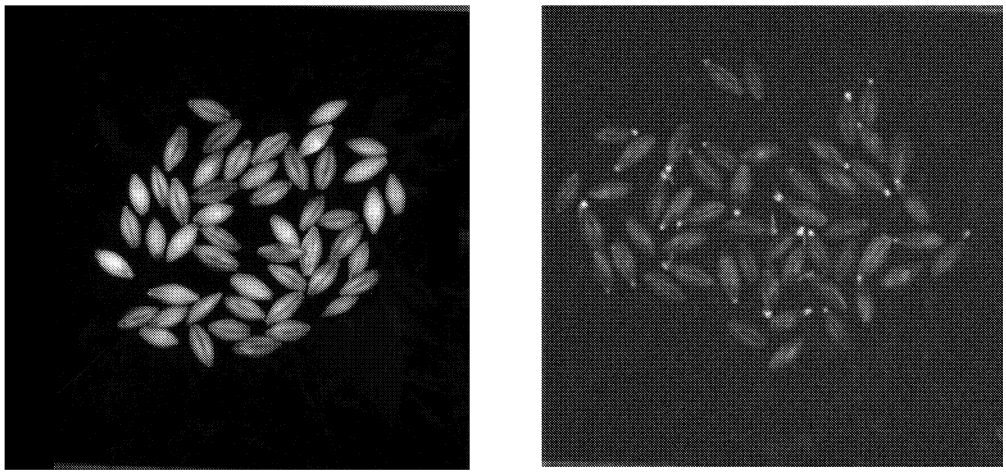

(a) **(b)**

Figure 2. A comparison of images taken under different illumination conditions. (a) white light illumination without UV-filter. (b) white light illumination with UV-filter.

3.2.3 Design of experiments

The entire measurement process lasted 72 hours as shown in Table 1. Two varieties of barley (100 kernels for each), samples A and B, were germinated under identical conditions

throughout. The kernels were randomly *spread* on the black sample holder during imaging; afterwards all kernels were replaced in the petri dishes for further germination. In this fashion the kernels were positioned as non-overlapping as possible for the present pilot development study. We have also already investigated the possibilities for *routine* imaging of samples not similarly manually prepared for camera presentations (samples are here *poured* directly into the sample holder without any further preparation etc); results from these studies will be reported in the systematic follow-up paper (in prep).

Every 3 or 6 hours, the kernels were imaged *four times* with random re-distribution of the kernels to investigate the repeatability of the present calibration method. We consequently obtained *four replicates* for each germination status. We subsequently employed *averaging* over all replicates in order to increase the basic image-sampling precision. Gray-scale images of size 1024*1024 were collected from a square sample area of 8cm*8cm. Figure 3 shows a set of *representative* images from different stages of the entire germination process. The number of germinated kernels clearly increases with time. At the end of the germination process the individual sprouts become quite long, and are now of no practical consequence for the characterization. It is important, indeed critical, only to know the early/earliest number of germination sprouts.

Table 1. Imaging during the germination process.

Day	Time	Germ. Hours	Sample A - Replicates				Sample B – Replicates			
			1	2	3	4	1	2	3	4
0	17	0	Start	Start	Start	Start	Start	Start	Start	Start
	20	3	x	x	x	x	x	x	x	X
	23	6	x	x	x	x	x	x	x	x
	2	9	-	-	-	-	-	-	-	-
	5	12	-	-	-	-	-	-	-	-
1	8	15	x	x	x	x	x	x	x	x
	11	18	x	x	x	x	x	x	x	x
	14	21	x	x	x	x	x	x	x	x
	17	24	x	x	x	x	x	x	x	x
	20	27	x	x	x	x	x	x	x	x
	23	30	x	x	x	x	x	x	x	x
	2	33	-	-	-	-	-	-	-	-
	5	36	-	-	-	-	-	-	-	-
2	8	39	x	x	x	x	x	x	x	x
	11	42	x	x	x	x	x	x	x	x
	14	45	x	x	x	x	x	x	x	x
	17	48	x	x	x	x	x	x	x	x
	20	51	x	x	x	x	x	x	x	x
	23	54	x	x	x	x	x	x	x	x
	2	57	-	-	-	-	-	-	-	-
	5	60	-	-	-	-	-	-	-	-
3	8	63	x	x	x	x	x	x	x	x
	11	66	x	x	x	x	x	x	x	x
	14	69	x	x	x	x	x	x	x	x
	17	72	x	x	x	x	x	x	x	x

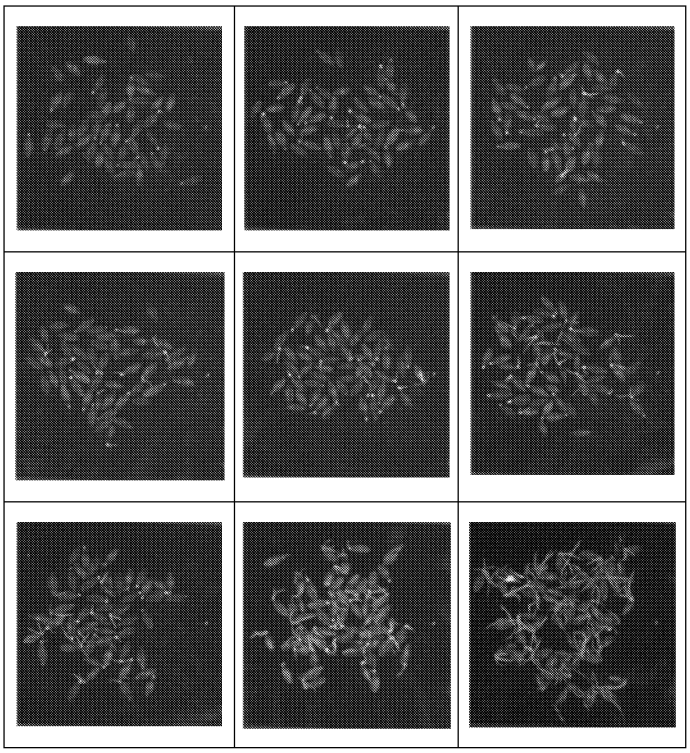

Figure 3. Representative images from different germination stages, arranged chronologically (left-right/top-bottom).

3.1. Image processing and data analysis

Images of size 1024*1024 were first collected in 16-bit IPLab format, then converted into 8-bit tiff format and resized into 512*512 pixels (to reduce computation time). All images were *median filtered* to enhance the desired sprout/kernel contrasts and sharpen the edges while the other parts were smoothed [10]. The images were all *unfolded* into vectors of length 512*512 pixels row-wise[11]. The AMT transforms on the vectorized images were carried out in Matlab 5.3 with the core computation part written in Mex C code for higher speed [12]. A Pentium III computer was used for processing and analysis. The AMT spectra composed of MA (Mean Angle) and MDY (Mean Difference Y) were calculated with scales ranging from 1 to 200. The AMT spectra, in Matlab formats, were finally imported into the *Unscrambler 7.5* software system for multivariate calibration.

4. Results and Discussion

4.1. AMT spectra of the images

Three selected images from the germination process are shown in Figure 7. (a) shows only a few kernels sprouting at a very early stage. (b) shows how more kernels have sprouted at this intermediate stage, as the number of visually recognizable brighter dots increase. Most kernels have germinated at the end of process as shown in Figure (c). Some of these latter sprouts are distinctly elongated.

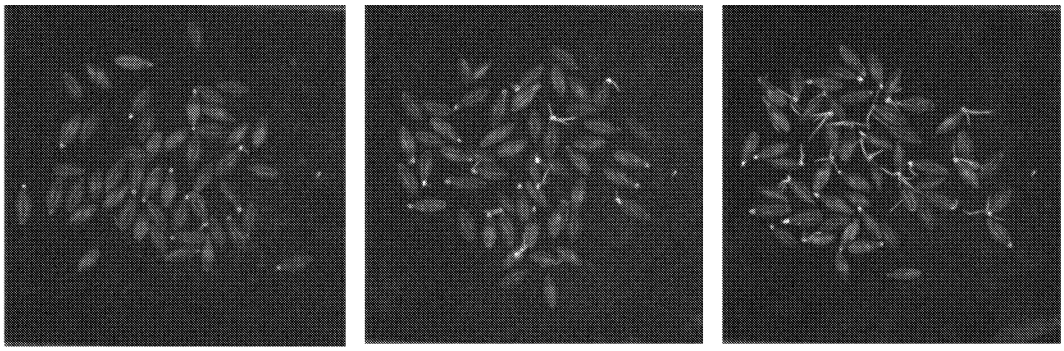

(a) **(b)** **(c)**

Figure 4. Selected images illustrating the image manifestation of the germination process. (a) beginning of germination, sample GA106; (b) intermediate stage of germination, sample GA110; (c) end of germination, sample GA114.

Figure 5 and 6 show how even small differences between images are well reflected in the AMT spectra, i.e. after the AMT transform. For both the MA and MDY spectra, sample GA114 (representing the end of process) lies on the top, while that of GA106 (beginning of germination) is located at the bottom. In general, the higher the specific values of MA and MDY are, the more complex are the original signals. The individual spectrum irregularity also indicate higher original signal complexities. In Figure 4 (a) to (c), the images become more intricate and irregular as the sprouts get longer. The corresponding MA and MDY spectra both show the same trend, in that the AMT spectra values increase as the images become more complex. This is especially clear in the zoomed-in, close-up comparisons of these spectra in Figures 5 and 6. It is apparent that there is indeed no overlap among the spectra, but MDY is getting quite irregular as more sprouts appear in the image. These few illustrations are meant to demonstrate the inherent AMT-sensitive to even minute changes of complexity in the original signals/images. It is exactly these systematic variations in the AMT spectra which can be utilized for multivariate modeling. It should therefore be entirely possible to model, and subsequently predict the number of germinated kernels (Y) based upon these AMT spectra (X) through a standard multivariate calibration modeling, using e.g. PLS, PCR.

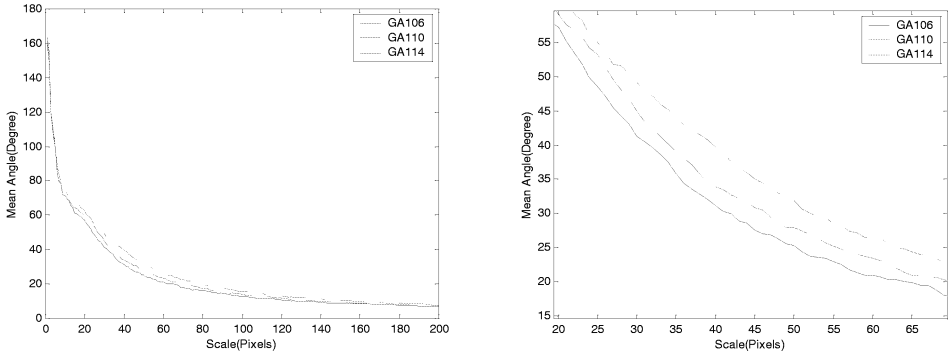

(a) (b)

Figure 5. Illustration of corresponding AMT spectra, Mean Angle (MA), corresponding to the images in Fig. 4. (a) MA for scales 1-200; (b) Close-up of MA. GA114 lies on top, GA106 at the bottom. Notice the highly systematic variation completely without overlap.

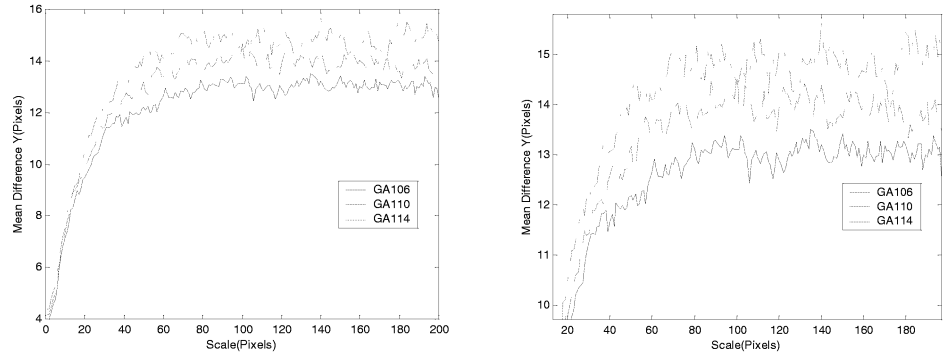

(a) (b)

Figure 6. Illustration of corresponding AMT spectra, Mean Difference Y (MDY), again pertaining to Fig. 4. (a) MDY for scales 1-200; (b) Close-up of MDY. GA114 lies on top, GA106 at the bottom. Notice the almost equally systematic variation again without overlap in spite of considerable more noise. MDY-variance gets larger as the image gets more complex.

4.2. Multivariate data analysis: PCA model diagnostics

Representative images taken at certain germination stages were chosen for analysis. There are four replicates for each time point. Each image (512×512) is *unfolded* to a 1-D measurement series with length of 512×512. A aggregate matrix is assembled, composed of one such vector for each image to be subjected to multivariate data analysis e.g. PCA, PLS.

It is practically unavoidable to obtain some abnormal recordings, e.g. either due to accidentally faulty experimental operations, or to uncertain imaging conditions etc. Several hundreds of images were recorded from the beginning to the end of germination process. It is not practical to inspect each image one by one. However, with PCA on the image AMT spectra, this became

very easy. Each row of the aggregate X-matrix is composed of the compound AMT spectra (MA+MDY), which represent the essential features of one image. In the PCA models presented below, there are different diagnostics available to reveal such *outliers* such as the PCA score plot itself, various contribution plots, Hotelling T^2, residuals etc. We here used score plots, Hotelling T^2, and residuals to detect and remove such outliers, see e.g. Figure 7. Two extreme samples (numbers 4, 12) are clearly located far away from the pertinent Hotelling Ellipse. A check on the corresponding images turned out to reveal both an over-exposed as well as an under-exposed image; both resulted in but almost identically blurred, and quite useless, images however. During several iterative stages all outliers were quickly removed in this way until all samples were well within the control limits.

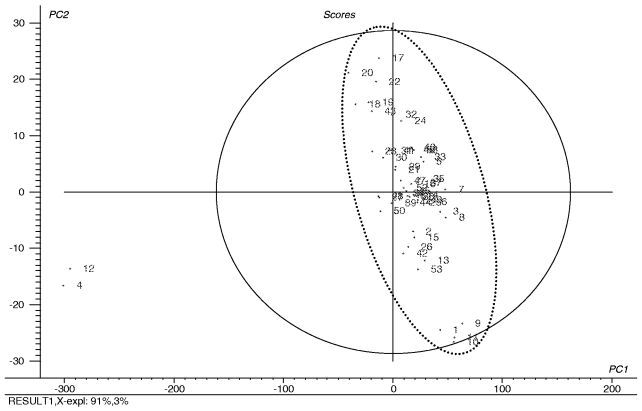

(a)

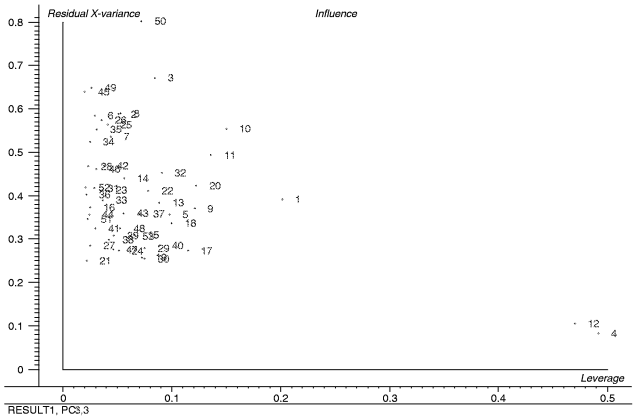

(b)

Figure 7. (a) Score plot with Hotelling T^2 ellipses. The solid and dashed ellipses represent the control limits before and after the two outliers (No. 4,12) were removed. (b) Residual X-variance vs. leverage plot. Also here No. 4 and 12 are clearly distinguished, but they were removed primarily because of their score-plot relationships in (a).

4.3. Prediction models

In this methodological pilot study it is our primary objective to model whatever relationships present between the AMT spectra (X) and the germination process stages, as expressed by the number of manually counted sprouted kernels (Y). Multivariate AMT Regression (MAR), see Appendix A, was used to predict Y. 9x4 images at 9 representative germination stages, Table 1, were chosen for the decisive multivariate regression modeling, in which the replicate spectra were *averaged*. Subsequently, a X-matrix with 9 samples and 400 variables (two AMT scales) was formed. For the present modeling, full cross validation had to be employed, since we only have at our disposition 9 objects for each model [13].

Table 2 shows comparative PLS modeling results for prediction of the number of germinated kernels with these AMT image features. The objective of the comparison is to express the relative usefulness of this approach for the two barley varieties. The results shown are not much different. The correlation coefficient for variety A is 0.91, and 0.93 for variety B. Both RMSEPs are around 10.0. An average standard prediction uncertainty of +/- 10 *kernels* can of course not yet be considered within a satisfactory optimized range, but method optimization and parameter fine-tuning has not even begun properly yet.

Table 2 also shows that 89.80% of the X-variance and 99.41% of Y-variance can be explained in the model for variety A, with 86% of X-variance and 94% of Y-variance for variety B, both using 3 PLS-components. These cross-validated modeling fractions would appear satisfactory for both models. The only particularly *distinguishing* feature between these two models would be the slope of the *fitted* prediction statistics. The slope for variety A is distinctly more acceptable, 0.86, than what would appear to be the case for variety B, which displays a rather less satisfactory slope of 0.73 only, see Figure 8, 9.

Table 2. Comparative statistics (*fitted* regression statistics) pertaining to the two barley varieties. Results are based on the *averaged* AMT spectra at each of the nine selected germination stages.

	Explained X variance (%)	Explained Y variance (%)	Correlation coefficient.	RMSEP	#PLS components
Variety A	89.80	99.41	0.91	10.0	3
Variety B	89.28	99.13	0.93	10.5	3

4.4 Discussion

An overview of PLS modeling results for variety A and B are shown in Figure 8 and 9. *Process trajectory* plots shows clear, progressive development of the germination process in Figure 8, where the first PLS component alone explains 79% Y-variance (77% X variance). The plot of X-loading weights, w_1, shows the relative role of the various AMT-scales for the model. Notice, for instance, the very marked difference in the pertinent loading weight spectra in Figure 8 and 9. In Figure 8, AMT-scales of approx. 30-200 pixels for both MA and MDY show equal

importance for the model, while a very different case with the model for variety B is shown in Figure 9. It is here obvious that the MA spectra at scales of approx.20-80 play the absolutely most important role for the model, while the MDY spectra show no significant contribution to model at all. The validation Y-variance plots are indicative of our selection of the proper number of PLS-components. Both these Predicted vs. Measured plots show moderately encouraging validation statistics for both varieties A and B.

The above results show that this new multivariate AMT approach is basically successful in characterizing barley germination process stages but that it predicts the quantified percentage of germination with accuracies and precisions commensurate with a very first pilot study only.

There will have to be conducted a large amount of follow-up studies, based on the basics of the approach which has been worked out here, before the true potential of this method can be said to have been put to a satisfactory test. These necessary studies are well under way already[14]. In all likelihood they will also have to include further imaging optimizations a.o.

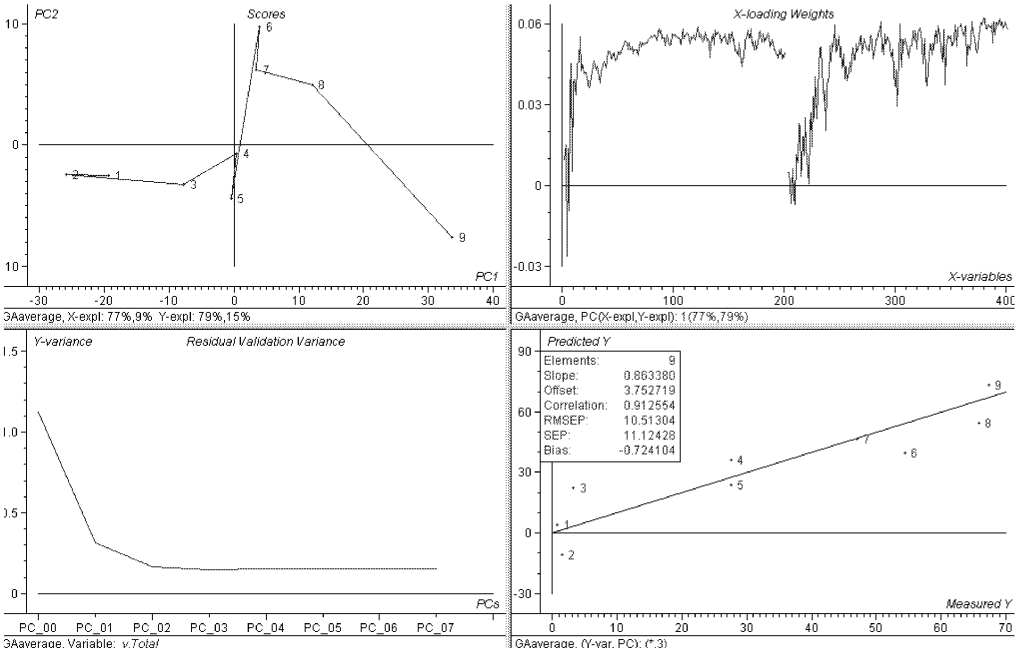

Figure 8. PLS modeling results pertaining to Barley variety A. *Upper left:* Score plot (process *trajectory plot*); *Upper right:* X-loading weights; *Lower left:* Validation Y-variance plot; *Lower right:* Predicted vs. Measured plot. Corr. Coeff . =0.91; RMSEP=10.5; slope=0.87.

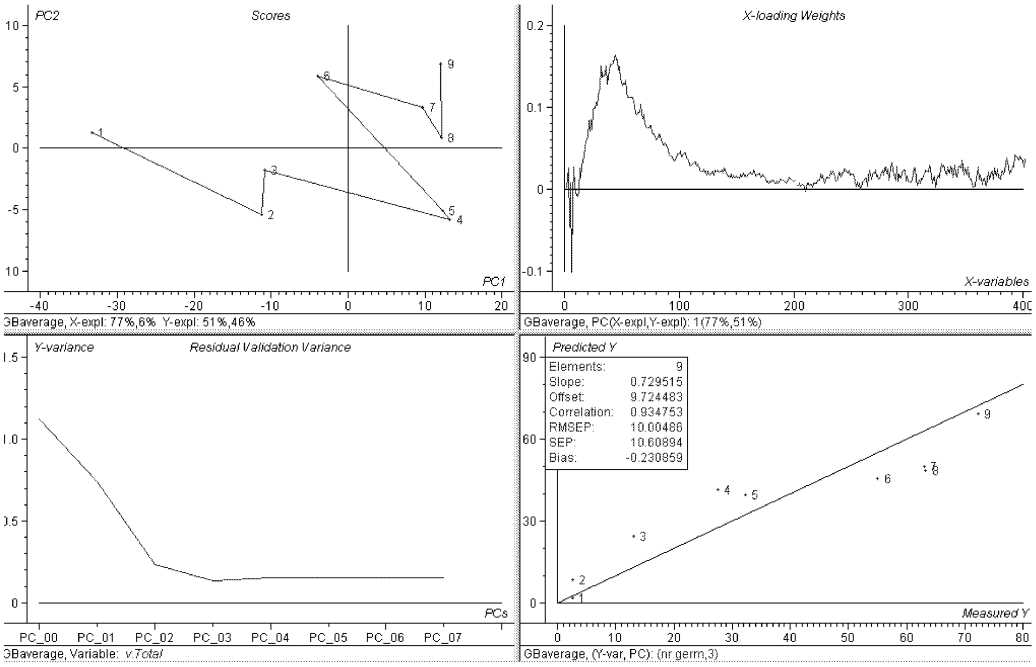

Figure 9. PLS modeling results pertaining to Barley variety B. *Upper left:* Score plot (process *trajectory plot*); *Upper right:* X-loading weights; *Lower left:* Validation Y-variance plot; *Lower right:* Predicted vs. Measured plot. Corr. Coeff . =0.93; RMSEP=10.0; slope=0.73.

5. Conclusions

The AMT transform is a powerful new method for characterizing the complexity of measurement series in general, of textured images in particular. It creates a new domain, the scale domain, which often captures and preserves quantitative texture information from the original domain.

The combination of AMT pre-processing with chemometric PLS-regression has been used here for a first investigation of the potential for quantitative barley germination assessment. The pilot study results presented allow for optimism w.r.t. further development, but significant further methodology optimizations are most likely needed, as is an extensive survey over the entire malting barley field. These studies are ongoing [14].

Appendix A. Methods

A.1 Angle Measure Technique (AMT)

A.1.1 Basic concept

The AMT (Angle Measure Technique) is a new signal description method developed for characterizing the *complexity* of contiguous data such as time series, spatial data series, indeed any *measurement series*. The AMT transform produces so-called *complexity spectra* by calculating the geometric angles which characterize the *directional change*, or the corresponding X/Y difference, when tracing the measurement series outward from a set of randomly chosen sample points along the 1-D (or 2-D) series for a set of increasing measurement *scales*, Fig. A1. The AMT spectrum is consequently to be viewed as a function of these scales, from the local to global, characterizing the complexities (intricacies, sinuosity, roughness, etc.) of the measurement series. At a more fundamental level, a new domain is created, the scale-domain. The AMT is applied to unfolded image data series in this work. Further details on AMT theory are given in our earlier expositions [1-4].

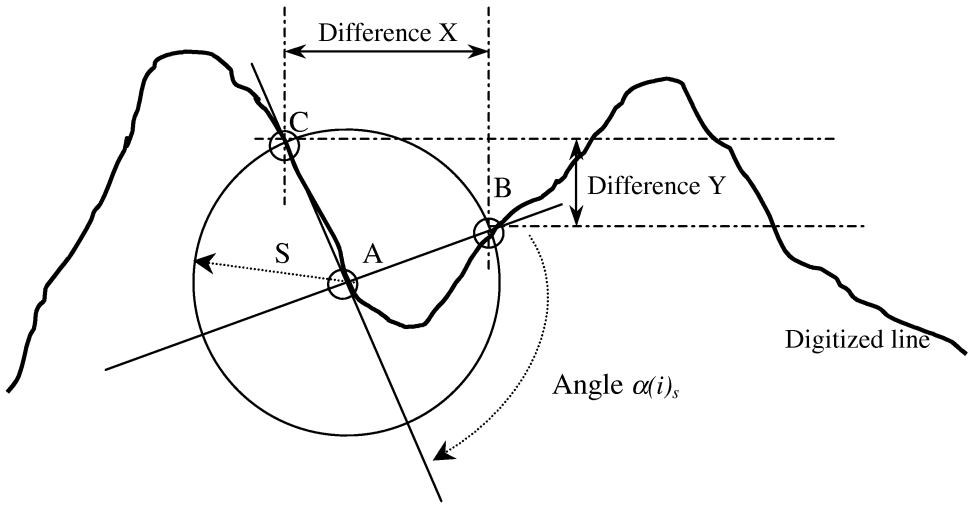

Figure A1. Explanation of AMT. A number of points "A" are chosen randomly along the entire measurement series (usually 500). A circle with contemporary radius, S, will intersect the measurement series in two points B and C, which in turn defines the complexity-related angle CAB. The solid line represents the 1-D measurement series (*unfolded* from a 2-D gray-level image in this case). The individual "Angle $\alpha(i)$" is measured (for each of the random points A along the entire measurement series) as the supplement to angle CAB. This produces a statistically robust "mean angle" measure, **MA,** of the local complexity corresponding to the scale "S". Additional AMT-indices are also calculated: Mean Difference Y (**MDY**) is the *vertical* distance between point C and B. By letting S=S + 1, the (**MA**, **MDY**) AMT-measures will *simultaneously* characterize the complexity *at all scales*.

A pseudo-code illustration for AMT calculations (Mean Angle) is shown below. Other indices such as MDX/Y can be obtained in the same way.

For S=1:M

$$A(s) = \frac{1}{N} \sum_{i=1}^{N} \alpha(i)_s$$

end

where $\alpha(i)_s$ denotes the individual angle at the corresponding scale
$A(s)$ denotes the Mean Angle (MA) as a function of scale
M denotes the number of measurement scales (maximum S)
N number of randomly chosen points along the entire measurement series (500)

Figure A2 shows AMT spectra derived from an unfolded image. Observe how MA and MDY capture different, but complementary aspects of the intricacies of the scale-complexity interrelationships. The horizontal axis represents "log S". MA displays a complexity "peak" corresponding to a scale of approx. 25-30 (pixels). This illustration pertains to one AMT-derivation for one image. When a number of AMT-spectra derived from a set of images are collected into a common X-matrix, the (log S) scale is now used as the joint variable dimension. Such an aggregated X-matrix can now be used for e.g. multivariate calibration a.o.

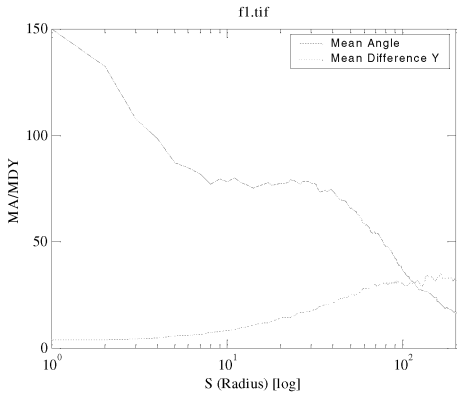

Figure A2. Illustrative (MA, MDY) complexity-spectra (upper: MA; lower: MDY).

A.1.2. Features of AMT

The most useful aspect of the AMT transform is that the compound (**MA**, **MDY**) spectra can be used as 1-D object vectors for multivariate data modelling (e.g. PCA, PCR or PLS). For 2-D image objects it is the *local texture* of the field-of-view which is transformed into a corresponding 1-D *complexity spectrum*. These complexity spectra, Figure A2, implicitly carry are very high information richness related to all scale(s). This is the principal feature of AMT

which performs as a useful pre-processing in very many of applications. Some major characteristics of AMT in image analysis are:

- Digital images are often (very) large 2-way data. AMT transforms a 2-D image into a 1-D complexity spectrum, *without* losing textural information.
- AMT can thus (partly) be considered as a data compression method due to the fact that the image data can alternatively be represented by AMT spectra at a fixed number of scales which are often significantly less than that of original signal.

AMT has a high sensitivity with respect to even (very) small complexity-scale changes, see Huang & Esbensen [3 - 5].

A.2 Multivariate AMT Regression (MAR)

MAR was proposed in a previous study [4]. In multivariate AMT regression, the AMT spectra such as MA and MDY, which carry information at each corresponding scale, work as feature extractors for further multivariate calibration. AMT regression models are established between these AMT complexity spectra (X) and a dependent variable (Y). Assume that A is the AMT spectra which may be composed of MA and/or MDY. The regression equation in general is given as

$$\hat{b} = A^{+}y$$

where the generalized inverse A^{+} from a regression method such as PCR, PLS etc.

A schematic overview of AMT regression approach is shown in Figure A3. This flow diagram generalizes the basic methodology of Multivariate AMT Regression (MAR). Other multivariate calibration methods can be applied to the specific problem in conjunction with AMT.

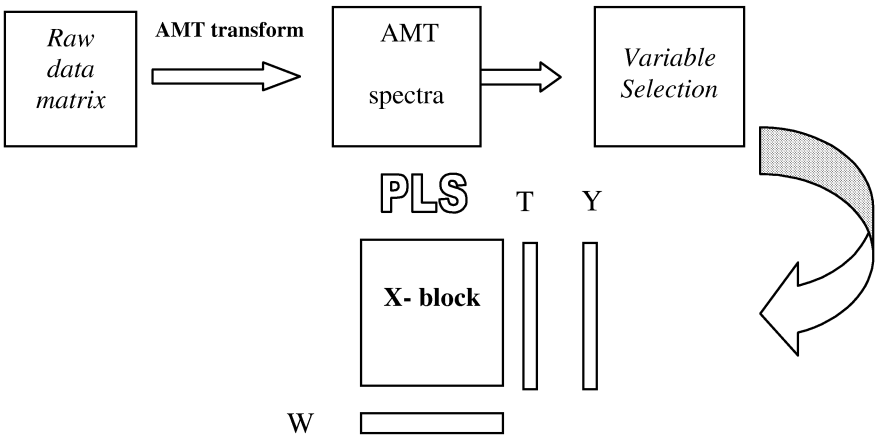

Figure A3. A schematic overview of multivariate AMT regression, using PLS [4]

REFERENCES

1. Andrle R, The Angle Measure Technique: A New Method for Characterizing the Complexity of Geomorphic Lines. *Mathematical Geology*, 26, 83-97. 1994.
2. Esbensen KH, Kvaal K and Hjelmen KH, The AMT Approach in Chemometrics—First Forays. *Journal of Chemometrics*, 10, 569-590. 1996.
3. Huang J and Esbensen KH, Applications of AMT (Angle Measure Technique) in Image Analysis Part I. A New Methodology for *in-situ* Powder Characterization. *Chemometrics and Intelligent Laboratory Systems. 54/1*. (2000) pp 1-19
4. Huang J and Esbensen KH, Applications of AMT (Angle Measure Technique) in Image Analysis Part II. Prediction of Powder Functional Properties and Mixing Components using Multivariate AMT Regression (MAR). *Chemometrics and Intelligent Laboratory Systems. In print*. 2000
5. Hjelmen KH, 'AMT (Angle Measure Technique) – implementation at Telemark Institute of Technology and applications on time series and similar measurement series', M.Sc.(Eng.) Thesis, Telemark Institute of Technology, Porsgrunn, Norway, 1995 (in Norwegian)
6. Photometrics CCD camera system User's Manual. *Photometrics Inc.,* Arizona, 1991.
7. IPLab Spectrum V3.1 User's Guide for the Macintosh. *Signal Analytics Corporation*. USA. 1995.
8. Thursby Software Systems, Inc. http://www.thursby.com/.
9. Wold JP, Rapid quality assessment of meat and fish by using near-infrared spectroscopy autofluorescence spectroscopy and image analysis. Ph.D thesis. Agricultural University of Norway. 2000.
10. Gonzalez RC and Woods RE, Digital Image Processing, Addison-Wesley, Reading, 1993.
11. Geladi P and Grahn H, Multivariate Image Analysis, *John Wiley & Sons Ltd*, 1996.
12. Hanselman D and Littlefield B, Mastering Matlab 5 – A comprehensive Tutorial and Reference, Prentice Hall, Upper Saddle River, New Jersey, 1998.
13. Esbensen KH, Multivariate Data Analysis—in practice 4th , CAMO ASA, Oslo, 2000
14. Møller B & Munck L, Barley germination studies, 2001 (*in prep*).

PAPER IV

Applications of Angle Measure Technique (AMT) in image analysis – Part III: High-sensitivity particulate impurity detection and quality control

Kim H. Esbensen* and Jun Huang

Applied Chemometrics Research Group, Department of Technology (TF)
Telemark University College (HiT), N-3914, Porsgrunn, Norway

ABSTRACT

Image AMT (Angle Measure Technique) is developed for particulate matter impurity detection and quality control. Images of *in-situ* powders are used to illustrate this new technique for high-sensitivity applications, in which *unfolded* video imagery is converted by the AMT transform to multivariate data for quantitative prediction of pollutants. This approach reaches sensitivity levels essentially into the *per mil* range (v/v), which was quite unsuspected. This AMT sensitivity is shown to be a direct consequence of the *unfolding* employed. We demonstrate technological and industrial applications with laboratory as well as industrial types of contaminant quantifications. This new image AMT approach can be applied on-line for product/process control with low cost due to its simple imaging and fast data analytical modeling.

Key Words: Image analysis; AMT (Angle Measure Technique); impurity detection; quality control; PLS (Partial Least Squares); Multivariate AMT Regression; unfolding

1. INTRODUCTION

The existence of non-neglectable quantities of *impurities* (pollutants) in virtually any mass produced product is unavoidable in many industry sectors because of competitive economic and production technology pressures a. o. Sectors like food, feed and beverage production are prime examples, but the problem of a non-zero impurity level is almost universal in the *particulate industries*. The purity of final products is one of the critical criteria for many quality evaluations. Sugar manufacturer, for instance, need strict control and very high-sensitivity detection of the impurity levels in their process and products. Wheat/rice producing companies have to check very thoroughly for impurities of foreign grains, e.g. sand and small stones in their products. Currently used standard image analysis techniques are typically either too laborious (sample preparation), too expensive, or too slow to be applied for effective on-line, precise manufacturing control. Current processes rather demand fast, inexpensive and time-saving methods for higher profits. We aim to show how the present technique rises to all these demands with but very modest image technology - and calculation requirements.

* Corresponding author. E-mail: Kim.Esbensen@hit.no. Tel: +47 35 57 5150. Fax: +47 35 57 52 50.

The new approach is comprised by the AMT image feature extraction technique with subsequent multivariate calibration (PLS) [1]. We earlier described the basic technology in detail in our previous papers in this present series [2-3], in which extensive applications of AMT on image analysis have also been given, to which the reader is referred for full expositions if needed [1-5].

Fast digital imaging of *in-situ* powders with a calibration range of trace amounts of various pollutants, coupled with Multivariate AMT Regression (MAR) [3], provides an effective approach for many multivariate calibration purposes, e.g. as for quantitative impurity characterization in this work. We earlier focused on *porosity characterization* [1] and *powder functional properties* [3]. We are currently also developing this methodology for describing complex *mixing processes and mixing product characterization*. Below we shall focus on the extreme one end of a mixing series characterization, i.e. the situation in which one end-member is allowed to gradually reduced in concentration literally to the vanishing point. We are going to investigate to what extent the MAR approach can deal with characterizing a mixing system in which progressively smaller *trace levels* of the one component ultimately becomes an *impurity* in an otherwise pure matrix. We shall exclusively be working in the *sub-%* area of pollutant concentrations, indeed sometimes even below the *per mil* range.

At the outset of our image AMT mixing and trace concentration characterization studies we had no idea that the presently presented levels of accuracy and precision would be obtainable – indeed the results presented below initially came as a complete surprise. Intensive rationalization has since revealed that the success below is nothing but a direct (hitherto unrecognized) consequence of the use of the *unfolding* operator on otherwise standard digital video imagery.

The experiments reported here aim directly to simulate industrial situations. We present this work as part of our continuing efforts to develop industrial image analytical process/product sampling -, monitoring - and process control systems.

2. EXPERIMENTAL AND MATERIALS

2.1 Experimental design and imaging

Three different types of mixed particulate matters have been experimentally studied here. The first two sets are used to illustrate the characteristics of this new variant of the image AMT approach. We here make use of plastic pellets with different textures and colors are to function as *pseudo-products* and *impurities* respectively in our image laboratory. The third set represents a real-world example from the food manufacturing industry: five different types of grain products polluted by small stone impurities.

Video imaging, illumination conditions, data capture and all other experimental contexts were described extensively in reference 2, 3 and will not be iterated here. We used a standard R/G/B digital camera (SONY) for some of our studies, and a modified JVC camera with the blue channel substituted with a NIR-channel, “SilvaCam”, for others, *ibid.* In the present studies we always use the channel which delivered the *largest contrast* between impurity and

background as the basis for AMT, see also further below. Other than this the image analysis examples below are virtually self-explanatory.

The field-of-view areas of impurities addressed here are strictly controlled so as always to make up under 1% of the whole imaged area of the pure matrix (termed "background"). The imaging was conducted in such a way that the impurity materials (pellets or stones) were placed individually and randomly on the background "pure products". The number of impurities added was in a random order so as to eliminate any possible differential thermal effects on the imaged objects. To counteract the unavoidable inaccuracies involved in repeated sample preparation and image recording of the granular surfaces presented to the camera, each *polluted product* was replicated four times by rotating the sample container 90° clockwise [2,3]. Consequently four replicates for each degree of polluted powder are obtained for the modeling. Prediction models based on both replicates as well as their averaged spectra are compared below in order to assess the reproducibility of these two imaging modes. Not surprisingly there are very significant precision advantages related to this averaging scheme.

Optimal settings for imaging each pollution series of powders to be characterised and compared need to be obtained by experimental trial-and-error. Such *factors* need to be taken into account as the number of light sources, angle of illumination, spatial resolution of camera, spectral characteristics of illumination sources etc. It is particularly emphasized that symmetric, high angle illumination is used in the present case. This is opposite from the low-angle oblique illumination required for other AMT powder characterizations, as described in detail in reference [2]. It is important that all mixing and pollution powder series to be compared be recorded under the same conditions of course. Throughout the experiments each of the eight powder *series* reported below were thus imaged under the exactly same internal conditions, where the illumination, focus distance, and image resolution etc. were held constant, while there were smaller or larger differences *between* the different settings for local series optimizations. Likewise w.r.t. scaling of Y-axes (the quantitative gray-levels in the individual camera channels), number of AMT-scales [1-5] (resulting in the same number of X-variables), which were also kept constant in order for the AMT transforms to be comparable.

2.2 Multivariate calibration

Following our established routines for image AMT, each video image is *unfolded* into 1-D vectors, followed by the AMT transform [1-4]. AMT transforms and characterizes each raw image by its corresponding *complexity-spectrum*, ibid, all with an identical scale range (X). This scale-array represent a new, *derived* variable-mode for the original images, which themselves make up the corresponding objects. Thus AMT transforms a series of 2-D images into a series of 1-D complexity spectra with a common variable way. Subsequently, the AMT spectra obtained (MA, MDY) are concatenated into an X- block for multivariate regression modeling.

Specifically, the percentages, or *per mil* of impurities can be used as reference Y-values; alternatively the actual *number* of impurity grains may be used. PLS is chosen as regression method and test set validation is used throughout [9]. The AMT transform is implemented in

the Matlab 5.3 [8] which takes less than two seconds for a 512x512 image, and the subsequent modeling is done in the Unscrambler 7.5 software package. Technically it is therefore easy to envisage how to implement a virtually real-time, on-line impurity detection facility to any industrial production line in which the necessary image recording can be carried out.

3. RESULTS

3.1. AMT feature extraction

Figure 1 shows two original images of polluted products, which are made by placing black pellets randomly on a white pellets background. In these experiments typically some 40 x 40 (1600) grains are contained within the image field-of-view. All our experiments reported here used only the extreme trace levels of impurities in the interval (0,15) *individual* grains. This corresponds to a range from 0 to 1% (v/v). We actually use the *number* of pollutants grains directly in the resulting models below, so that the calibration ranges for all models established are all identical in this 0-1% (v/v) interval; these alternative quantification options are trivial.

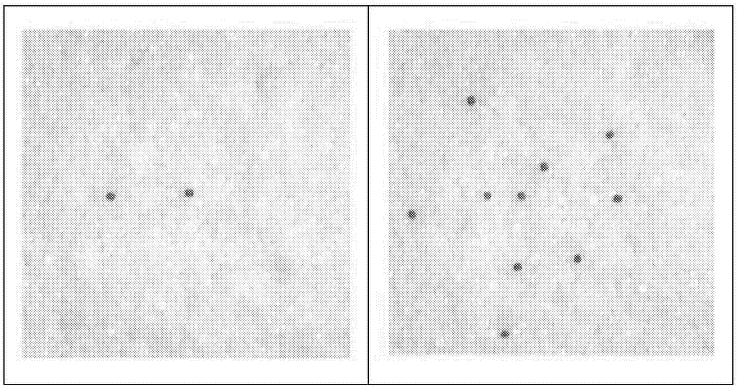

Figure 1. Original images of *polluted products* with different numbers of pollutant grains. Black impurity pellets are randomly placed on a white pellets background. Each field-of-view contains at least 1600 individual grains. This is a particular high-contrast case, *cmp.* Fig.s 5-7.

Representative AMT spectra for a number of images with different amounts of impurity are shown in Figure 2. Clearly there is a systematic variation in the spectra, which indicates that the AMT spectra are capable of detecting even very subtle differences between the images, indeed it would appear that the *entire* AMT spectrum (both MA and MDY) carries information directly correlated to the individual number of pollutant grains even in the extreme trace level of 1-15 grains (in approx. 1600 grains), i.e. well into the *per mil* levels. This is by any standards a remarkably high sensitivity. The enlarged detailed view of AMT spectra (MA, MDY) shows a uniform trend of increasing spectral values as more pollutants are added. This is a powerful reflection of AMT's capability of very accurately quantifying the complexity of granular and powder surface morphologies [1-3]. The higher the number of

impurities grains in an image, the more complex they are, and the higher their AMT spectra are positioned in the salient spectra comparison plot of Figure 2. As discussed above the AMT transform works on *all image scales simultaneously*, increasing from the local to global. This consistent and systematic variation in the AMT spectra is a good sign for the possibilities for further multivariate calibration.

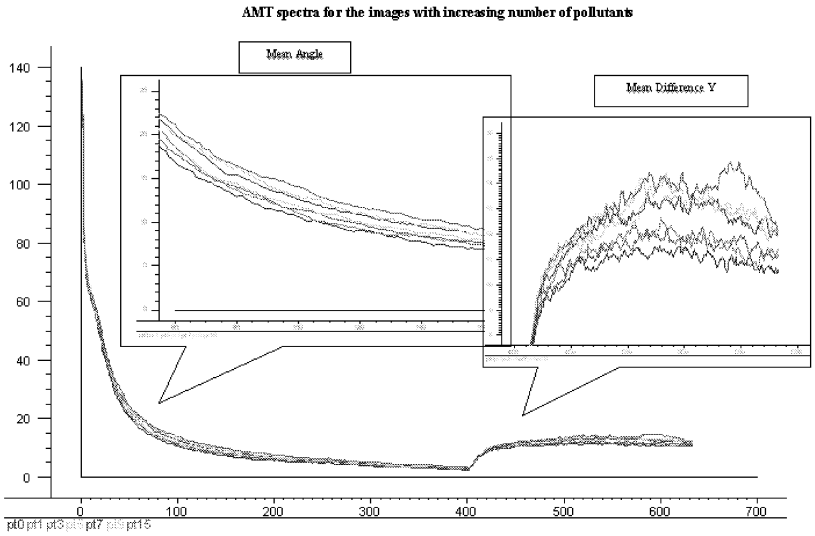

Figure 2. Selected AMT-spectra for an impurity series, corresponding to 0 to 15 pollutant grains. Note blow-up of MA and MDY for details. The MA and MDY values rise systematically, *without crossings* of the respective spectra over the entire scale range, as the number of impurity grains grow, i.e. the complexity of the AMT-spectra is directly correlated with the number of impurity pellets added. Note that even though there are considerable local noise levels especially in the (right hand) MDY-spectra, this is of no consequence as it will be completely cancelled out by the subsequent PLS-regression [9].

Below we shall show that the predictive PLS-models developed in some cases are able to predict with an accuracy of some 1-2 particles essentially all the way down to zero number of grains. How is this possible?

3.2 Rationale for high-sensitivity AMT

Figure 3 is designed to show how this comes about. Figure 3 shows that the contemporary scale, the radius of the AMT-circle, always *must* meet with the parts of the unfolded measurement series which correspond to the pollutant grain(s) at some scale in the interval (0,M). In the AMT computation, each circle with radius, s, grows outward from the randomly selected data points A, only one of which are shown here. The set of continuously increasing circles per force *must* all intersect with the parts of the measurement series which corresponds to the contrasting pollutant particles, even if only one (sic). Thus *all* impurity grains will *all*

be reflected at some scale by all circles, which is the reason that the entire AMT-spectrum carries systematic information on the number of impurity grains. It is the *unfolding* operation which creates this very high amplification of the impurity signal/noise ratio. Due to this unfolding the entire "background" area of the image field-of-view is also drawn into the pertinent signal detection basis, with an immensely increased sensitivity of the effective detection level(s).

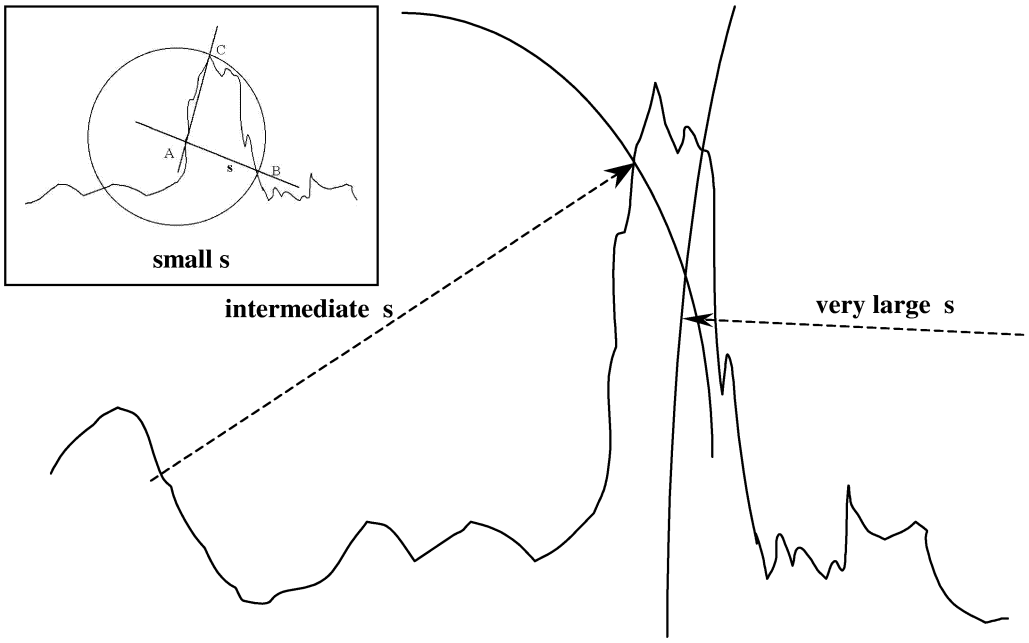

Figure 3. Sketch rationalizing how the intrinsic AMT analysis mode [1-5] will detect *all* impurity-related contrasting peaks/valleys along the otherwise much more "flat" measurement series (reflecting the background areas of the image). Any number of "impurity peaks" (or valleys, in the case of reversed contrast) will be intersected by *all* incrementing scale circles with radius s. Shown here is the case in which a single polluting particle (one single light pollutant particle, on dark background) is detected both by small, intermediate as well as large and very large circle radius s. This feature will be repeated in direct proportion to the number of such individual particles present, hence the greatly amplified sensitivity w.r.t. even both *per mil* pollutant concentrations and even fractions hereof.

In Figure 1 *only* the few camera lines (pixel lines) directly portraying the pollutant particle(s) are affected and can thus be said to carry a signal reflecting the impurity. When the same image is *unfolded* however, the entire image field is now used in the AMT-characterizations of the pollutant particle(s), as is depicted in Figure 3. The 500 "A" points spanning the measurement series (i.e. distributed over the *entire* image field-of-view) will now *all* serve as centers for the growing AMT-circles, which consequently all will intersect the pertinent segment(s) of the measurement series, at some high(er) scale or other, thus all contributing to

an enormous *amplification* of the sensitivity with which the resulting AMT-complexity spectrum carries *enfolded* quantitative information of the number of pollutant grains.

The fact that the AMT spectra are able to reveal such exceedingly small changes in the original (unfolded) images makes it possible to establish multivariate prediction models for quantification of the fraction (or number) of pollutant particles (Y) based on the derived AMT spectra alone. The AMT transform here works as an effective image domain-transform pre-processing for the ultimate PLS- multivariate calibration.

3.3. Multivariate regression analysis - validations and results

Partial Least Squares Regression (PLS-R) is employed for all multivariate AMT regressions (MAR) below. Test set validation is adopted throughout in order to obtain proper validation of the predictive power of the calibrated models [9,11]. It is explicitly mentioned that all test set measurements were all obtained at later dates - with the general experimental settings reproduced from scratch. This is in order that the *complete* sample preparation, sample presentation and image recording variances were all included in the validations, ibid.

3.3.1 Black and White particles of high contrast

Figure 1 has already shown raw images with black impurities on a simple white pellets background. Validation results based on both replicate and averaged AMT feature spectra are shown in Figure 4. Modeling based on averaged spectra gives much better precision, signifying a considerable stabilizing effect. The first two PLS components explain more than (87,2) % X-variance and (92,6) % Y-variance respectively. This scenario (black particles on white background) probably represent an *optimal contrast situation*; below we shall immediately test several examples of much less contrasting configurations between impurities and background in order to get a first idea of the possible *limits* to the present approach. The best model shown in

Table 1 below gives excellent prediction ability with correlation coefficient as high as 0.99, and a relative RMSEP as low as 2.2%, corresponding to a precision of +/- 2 particles. These prediction statistics must be compared with the extreme trace concentration levels modeled, 0-15 particles in 1600 (*sic*).

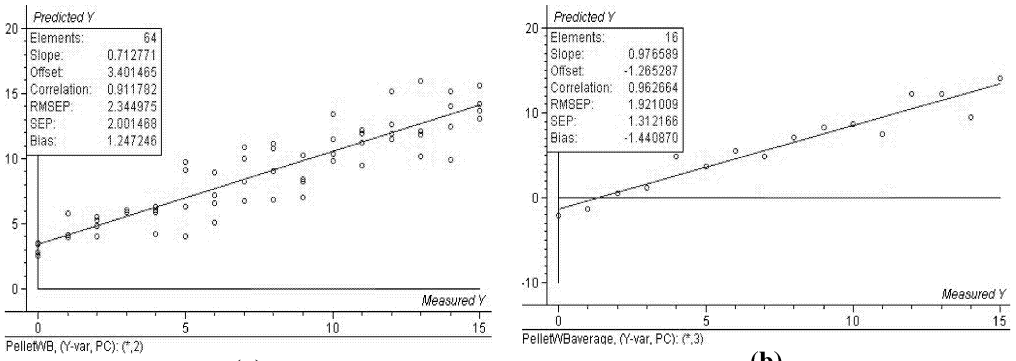

Figure 4. Test set validation (Predicted vs. Measured) plots. White impurity pellets on black pellets background. (a) Model based on all replicates. Corr.coeff.=0.91, RMSEP=2.34, slope=0.72 (b) Model based on *averaged* spectra. Corr.coeff.=0.96, RMSEP=1.79, slope= 0.98.

3.3.2 Colored particles of low contrast

Red and yellow pellets (otherwise morphologically identical to the white/black pair used above) are used as a system with considerably less contrast in the image field-of-view, as seen in Figure 5. Red tablets and yellow pellets are both used as impurities and background respectively. As seen from the evaluation results summarized in Table 1 this approach works well as long as there is a reasonable imaging contrast between impurity and background products. Fig. 7 shows that this contrast need not necessarily be reflected in dramatic visual contrast.

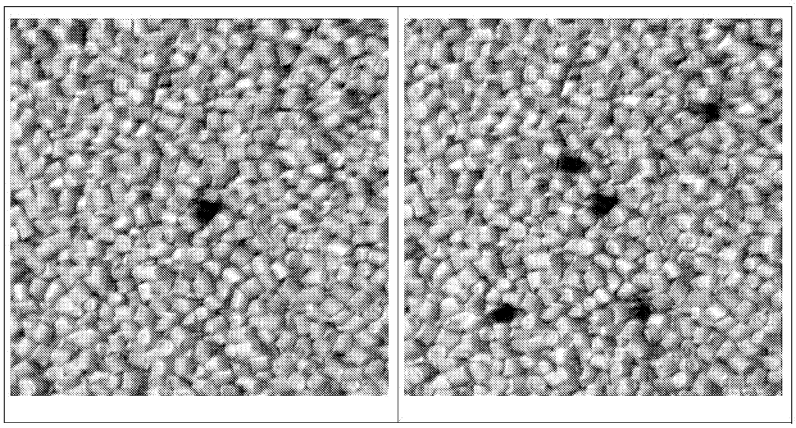

Figure 5. Original images of red pollutant pellets on yellow background particles, displaying a significantly reduced contrast compared to Figure 1. The results show that this is still well within the contrast range which can be quantified without problems however.

Table 1 summarizes comparative PLS modeling results for a systematic impurity detection study where pollutants and background products are black-white powders of high contrast, and red-yellow powders of lower contrast. Illumination and/or inherent contrast features of the systems to be characterized play a very important role. Contrasts can be significantly improved, or destroyed, by the specific choices of illuminating conditions; these results are based on further contrast improvement during our later, more fully developed work. These four scenarios are all satisfactory first results for the present new technique.

Table 1. Comparative PLS results for impurity detection; all results based on test set validation

PLS models	Corr.Coeff.	Slope	RMSEP	No. of factors
White pellets background, Black pellets pollution	0.97	1.1	0.72	3
Black pellets background, white pellets pollution	0.99	0.99	0.33	2
Red tablets pollution and yellow tablets background	0.98	0.92	0.87	2
Yellow tablets pollution and red tablets background	0.97	0.91	0.66	2

3.3.3 Grain-stone systems

For the ultimate test we here employ a set of real-world examples: five types of grains (products) with small stones (of similar dimensions) as impurities were chosen because they make up a very difficult, but realistic contrast situation. This system represents a *bona fide* industrial situation of a real need for product purity monitoring of great practical and commercial interest. This particular situation was in fact the specific problem which promoted our efforts towards developing effective image analytical impurity detection systems (thanks to TECATOR and FOSS NIR Systems for this motivation).

From an extensive series of pilot studies the grain/stone system is known to exhibit the by far lowest contrasts investigated. The polluting stones are placed randomly embedded in the surface of the different grain product samples, Figures 6 and 7. From Figure 6 it is apparent that the red channel is of optimal contrast among all three (R,G,B) channels, and thus chosen for the AMT transforms. Some modeling based on the other two, Green, Blue - or even NIR channels - were of course also tried out, but unsurprisingly with less unsatisfactory results.

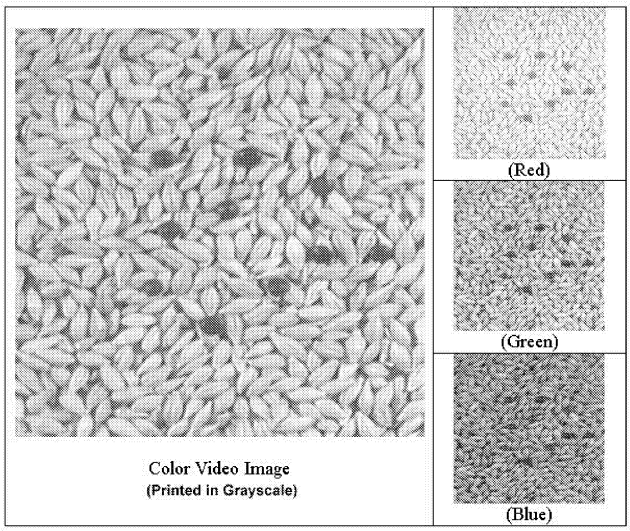

Figure 6. Real-world example: stone impurities in grain. Left panel: color video image (printed here in gray-scale). The impurities are not as clearly discernable as for the introductory laboratory plastic pellet systems treated above. Right panel: Split Red, Green and Blue channels. Note that the red channel is of *optimal contrast*, and thus used for AMT-modeling.

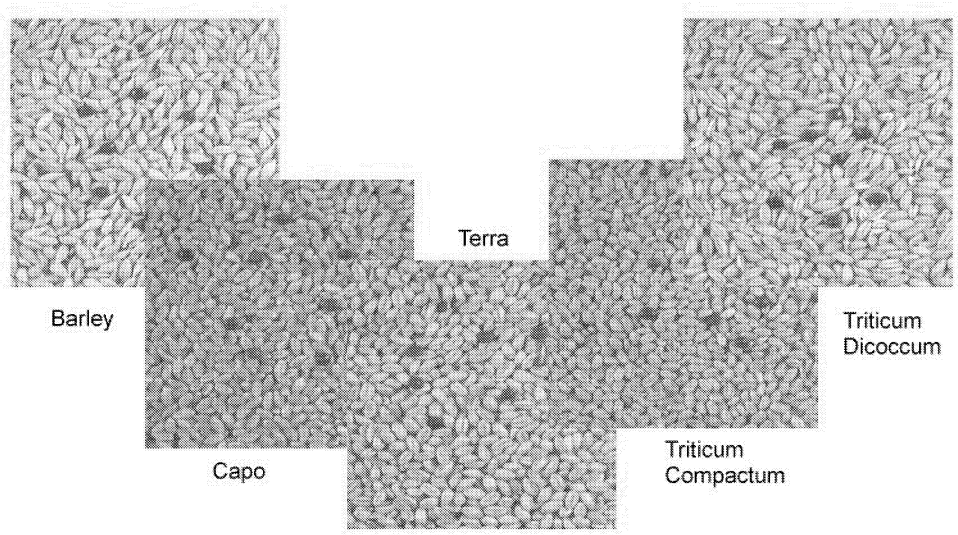

Figure 7. Five selected types of grain polluted by stones (identical pollutants used for all). Note considerable different expressions of *contrast*, which is caused by *both* the color differences (impurity/product) *as well as* expressions of the different morphological grain forms.

During these grain systems experiments the 1 - 15 impurity stones are again added to background grain surface in a random fashion to avoid possible thermal effects that perhaps could be generated by differential heating of the impurities/products. No such effects were observed however.

Test validation results from all five types of grains are listed in Table 2 below. The prediction ability of the salient PLS-models are generally satisfactory, although the reduced contrast is manifested in both larger prediction errors and by a reduction in the overall statistical accuracy (slopes of fitted predicted vs. measured regression lines). One observes how the general morphological expression of the background product also plays an important role in delineating the "contrast" w.r.t. the pollutants. Among all five grains, the best model is obtained with the grain variety '*Triticum Dicoccum'* (Corr. Coef. 0.98, RMSEP 0.77, slope 0.94), and the worst 'Capo' (Corr. Coeff 0.89, RMSEP 1.97, slope 0.72).

Table 2. Comparative test set validation results for selected types of grain with stone impurities.

Type of grain	Corr.Coeff.	Slope	RMSEP	No. of factors
Barley	0.96	0.89	1.18	1
Capo	0.89	0.72	1.97	3
Terra	0.97	0.91	1.00	1
Triticum Compactum	0.91	0.78	1.77	2
Triticum Dicoccum	0.98	0.94	0.77	2

An overview of PLS modeling results for '*Triticum Dicoccum'* is shown in Figure 8. The first PLS component explain 97% Y-variance. The predicted vs. measured plot shows very encouraging validation statistics, e.g. Corr. Coeff .= 0.98, RMSEP=0.77 (i.e. +/- one particle), slope=0.94. It is noted that "only" some 70% of the X-variance (AMT-spectral variances) are correlated with the quantitative Y-pollutant levels; 30% of the image information is effectively filtered out by the PLS-model.

Figure 8(b) shows the X-loading weights w_1, which delineate the relative role of the various AMT-scales for this excellent model. The dominant "peak" for the scale corresponding to 10-12 pixels (in both the left hand MA- spectrum as well as in the right hand MDY-spectrum) of course corresponds to the *average grain size* in the image field-of-view. There are only but (very) subtle contributions from the higher scale(s) in these relatively simple two-component systems.

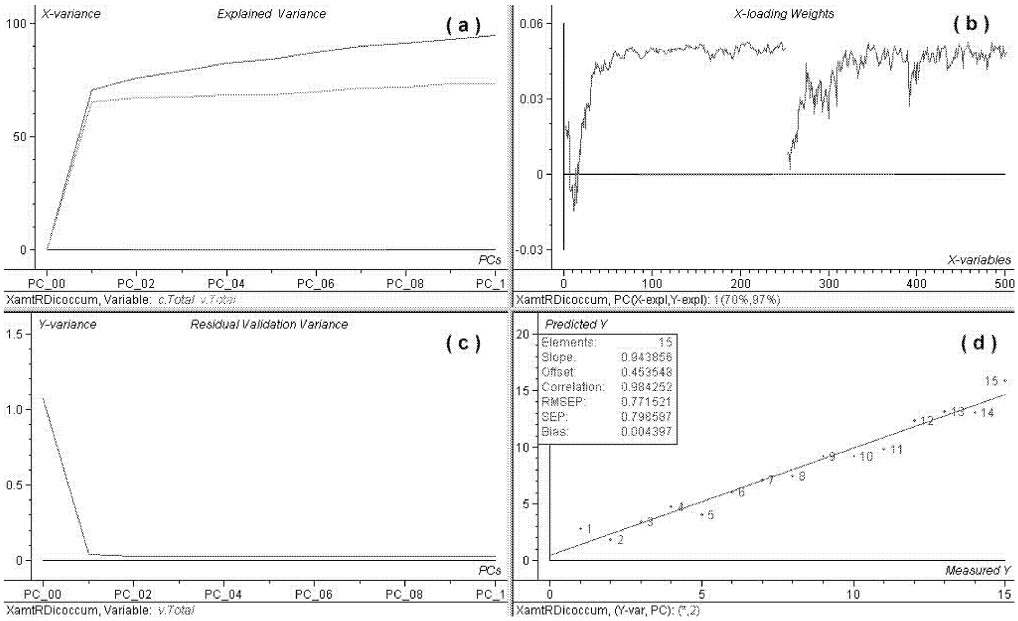

Figure 8. PLS modeling results pertaining to grain variety *'Triticum Dicoccum'*. (a) Explained X-variance (both calibration and validation) (b) X-loading weights (c) Y-validation variation (d) Predicted vs. Measured plot. Corr. Coeff . =0.98; RMSEP=0.77; slope=0.94.

4. DISCUSSION

It is mentioned that along the way we have considered in detail some factors which could be considered so as perhaps also influencing the modeling, i.e. a possible differential thermal effect. Initially it was somewhat unbelievable that the technique developed could detect impurities at such extremely low trace levels. For this reason, for example, we suspected that the powerful illuminations used perhaps would heat up the two different types of materials differentially so that successive images of the background would be brighter as the sample temperature increased chronologically. Such a hypothesis could be excluded however after it was found that absolutely no model could be established based on an alternative Y-variable representing the *time* elapsed since the start of the experiments when adding the pollutants etc. To completely eliminate this possible thermal effect we still even resolved to adding the number of impurity particles in a *random order* onto the background products (adding and/or removing particles according to a random design).

The success of this new AMT approach is critically dependent on achieving an *optimal contrast* between impurity and product background. Oblique illumination may e.g. cause unwanted *shadow effect* which is certain to bring additional uncertainty to the modelling. Black pollutants on white background may e.g. generate dark shadow accentuations which in fact would - falsely - appear to *increase* the area of black pollutant etc. Therefore, systematic,

bilateral high-angle illumination should be applied for the present image AMT impurity detection purposes. We emphasize that this is in direct opposition to the other AMT approaches treated in the previous two studies of this series[2,3]. Naturally there will always be a strong problem-dependent illumination dependency for any specific application context

In this work we have only used ordinary R/G/B or R/G/NIR video images as long as there is sufficient contrast between the impurity and background product. The present approach can easily be extended also to other types of illumination and cameras etc. In some specific situations, low-light sensitive CCD-cameras can be used. This would be especially useful for on-line manufacturing/mixing processes under adverse light conditions a.o. Other situations may call for UV illumination (fluorescence). Many biological materials are especially sensitive in NIR or UV etc.

It is conceivable that the present approach will also work for e.g. microscopic imagery - as indeed also for remote sensing (satellite platform) as well as for astronomical imagery a.o.

Additionally there is an uncharted aspect involving what could be called *textural contrast*, Figure 9. From traditional image analysis there exist a plethora of texture filtering facilities, which may be used in order to enhance the contrasting aspects of the *morphological forms* of the individual particles a.o [6, 7, 10]]. In such applications one would use both the raw image(s) as well as the texture derived counterparts for compound AMT complexity spectra. The ensuing multivariate calibration modeling will pass judgment on which type of spectra are most strongly correlated with the impurity quantifications. This area, still completely unexplored in our work, may even turn out to have interacting relationships with the complex illumination conditions etc [1-3]. We shall have to address these aspects elsewhere.

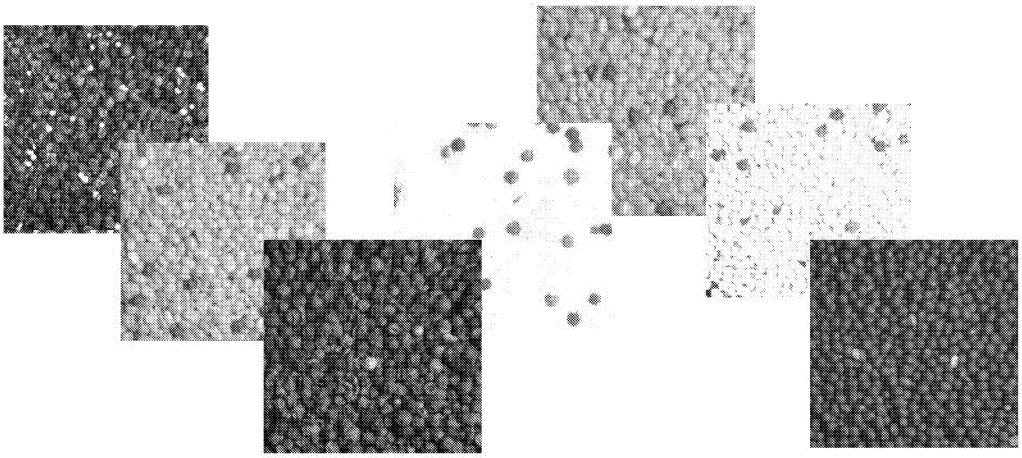

Figure 9. Examples of concurrent *color* - as well as *morphological* contrasts. The latter will probably benefit from specific image texture derivations *before* application of the AMT approach. Note that *form contrast* is often correlated with color contrasts pointing to the need for both color (illumination) enhancement as well as form enhancement (texture filtering) a.o.

5. RELATIONSHIPS TO IMAGE ANALYSIS

Undoubtedly it *may* also be possible e.g. to identify pollutant particles by conventional image analytical means. This would necessitate tracing the perimeters of all particles in the field-of-view (segmentation), followed by an identification step, discriminating pollutant particles from the "inert" background counterparts (classification) - after which a similar regression modeling could have been set up. It is highly significant that this sequence of image analytical operations is orders-of-magnitude computationally more demanding however, involving considerably more complex image analysis software facilities a.o.

In contrast to this we here presented the AMT-transform, a much simpler and more efficient approach, which has been implemented as but a few hundred lines of MATLAB code only. The otherwise needed image capturing hw/sw is identical for both alternatives. Add to this only standard chemometric software encompassing PLS-regression/validation facility - *et voila!*

6. CONCLUSIONS

As proven by the above test set validation statistics for all nine investigated systems of pollutants/background particulate matters, the new image AMT approach for impurity detection is highly satisfactory. As but the first *feasibility study* the present results call for much optimism, as well as for further refinement work. There are likely further improvement possibilities concerning the imaging, illumination and textural morphological features.

The ultimately obtained levels of precision and accuracy are simply astounding. In the interval 0-15 particles (in 1600), corresponding to volume concentrations in the interval 0-1 %, the derived AMT spectrum (both MA and MDY) carries information directly correlated to the individual number of pollutant grains even in the extreme trace levels well into the *per mil* levels. This is by any standards a remarkable sensitivity for a technique which only uses of-the-shelf, inexpensive standard digital video cameras and chemometric data analysis (AMT, PLS).

The reason for these surprising results was analyzed and shown to result from be a significant sensitivity *amplification* gain due to the *unfolding* operation used, whereby the *entire* image field-of-view could be made useful as a basis for the AMT quantification, Figure 3.

There are very many potential technical and industrial on-line implementation - and application scenarios for this new technique. These will most certainly not be confined to the general area of particulate matters, which was chosen here as but a didactically expedient exposition vehicle only. Surface characterization (microscopic, microscopic) is one prominent possibility - there are undoubtedly many others. Viewed in this much broader context the interesting potential for *process control* specifically and for *quality control* in general also springs to mind immediately.

The present contribution forms part of a larger strategic development program currently undertaken by the Applied Chemometrics Research Group, in which also quantitative image analytical mixing fraction assessments plays an important role. We have elsewhere presented

the corresponding first systematic results from this related area [12]. These current research areas also impinge upon the area of "sampling" (sampling of heterogeneous materials), an area of fundamental neglect within chemometrics to which much interest shall be directed in the future.

REFERENCES

[1] K.H. Esbensen, K. Kvaal and K.H. Hjelmen, The AMT Approach in Chemometrics—First Forays. Journal of Chemometrics, 10, 569-590. 1996.

[2] J. Huang and K.H. Esbensen, Applications of AMT (Angle Measure Technique) in Image Analysis Part I. A New Methodology for *in-situ* Powder Characterization. Chemometrics and Intelligent Laboratory Systems. *54/1*. (2000) pp 1-19

[3] J. Huang and K.H. Esbensen, Applications of AMT (Angle Measure Technique) in Image Analysis Part II. Prediction of Powder Functional Properties and Mixing Components using Multivariate AMT Regression (MAR). Chemometrics and Intelligent Laboratory Systems. *In print*. 2000

[4] K.H. Hjelmen, 'AMT (Angle Measure Technique) – implementation at Telemark Institute of Technology and applications on time series and similar measurement series', M.Sc.(Eng.) Thesis, Telemark Institute of Technology, Porsgrunn, Norway, 1995 (in Norwegian)

[5] R. Andrle, The Angle Measure Technique: A New Method for Characterizing the Complexity of Geomorphic Lines. Mathematical Geology, 26, 83-97. 1994.

[6] R.C. Gonzalez and R.E. Woods, Digital Image Processing, Addison-Wesley, Reading, 1993.

[7] P. Geladi and H. Grahn, Multivariate Image Analysis, John Wiley & Sons Ltd, 1996.

[8] D. Hanselman and B. Littlefield, Mastering Matlab 5 – A comprehensive Tutorial and Reference, Prentice Hall, Upper Saddle River, New Jersey, 1998.

[9] K.H. Esbensen, Multivariate Data Analysis—in practice 4th , CAMO ASA, Oslo, 2000

[10] S. de Silva, ' Characterization of Particle Particulate Solids', Telemark Technological Center, POSTEC, Norway, 1995

[11] K.H. Esbensen, Principles of Proper Validation, *Submitted*, (2001).

[12] T. T. Lied, I. H. Matveyev, D.F. Karlsrud, J. Huang and K.H. Esbensen, Image-Analytical Quantitative Monitoring of Heterogeneous Mixture Processes: Comparing and Combining Angle Measure Technique (AMT) and Multivariate Image Regression (MIR). *Submitted*.2000

PAPER V

Multi-way Methods in Image Analysis--- Relationships and Applications

Jun Huang* and Kim H. Esbensen

Applied Chemometrics Research Group, Department of Technology (TF)
Telemark University College (HiT), N-3914, Porsgrunn, Norway

SUMMARY

Multivariate data analysis on images focuses on "weak" multi-way models such as unfolded PCA/PLS. Multivariate Image Analysis (MIA) and Multivariate Image Regression (MIR) are typical examples. Some "strong" multi-way methods such as PARAFAC, Tucker3, Multi-linear PLS are introduced and tentatively also applied to image analysis in this work. Which method should be used is problem dependent. Based upon macro satellite images, virtual fluorescence images and microscopic functional property image examples, the performance of each alternative method is presented, as well as comparisons between weak and strong multi-way models. It is demonstrated that efficient handling of multiple images requires a clear overview of the relationship between problem formulation and data array configurations, which should be given more attention in dealing with image modeling. Appropriate preprocessing techniques, such as 2-D FFT and Wavelet transform, may also be needed in order to transform and configure image data to forms suited for further multi-way modeling.

Application I shows the possibility for application of strong multi-way methods on multi-spectral images, otherwise conventionally analyzed by MIA. By contrast, application II attempts to investigate the feasibility of applying MIA models on typical three-way data, normally handled by the strong multi-way methods and provides a new perspective of dealing with fluorescence spectra as images. In application III, microscopic images were taken on a set of different cheeses, which were made from a factorial experiment by varying coagulation temperature and the amount of rennet enzyme at a number of levels. The objective here ultimately is to derive functional properties prediction models. Reference rheological properties for these cheeses were tested by uniaxial compression techniques. Attempts have earlier been made to discriminate different cheeses and predict rheological parameters from these cheese images by multi-way methods.

The present exposition allows to draw some tentative first conclusions as to the proper relationships between strong and weak multi-way data decompositions, their pro's and con's and their relative merits.

KEY WORDS: Multivariate image analysis; MIA; Multi-way analysis; Unfold-PCA/PLS; PARAFAC; Tucker3; N- PLS; 2-D FFT;

---

* Correspondence to: Jun Huang, ACRG, Telemark University College, N-3914, Porsgrunn, Norway.
Email: Jun.Huang@hit.no. Tel: +47 35 57 51 52. Fax: +47 35 57 52 50.

1. INTRODUCTION

There exists a plethora of univariate digitized image analysis/processing across a wide range of fields in science and technology. A huge literature can be found on color imaging/analysis[1, 2]. Many numerical, mathematical, or statistical techniques have been applied to image data in the vast area of image analysis. Some multivariate techniques have also be introduced to image analysis, dealing with data modeling of relatively complex images. Multivariate Image Analysis (MIA) also including Multivariate Image Regression (MIR)/Multivariate teXture analysis (MIX) are typical methods[3 - 8]. The basic concept of MIA was first proposed by Geladi and Esbensen at the end of 1980's[3]. Applications have since been found in many fields such as microscopy, satellite remote sensing, medical imaging, radiology, chemistry, spectroscopy and astronomy, etc[1 – 11,29,30].

However, the true potential of multivariate data analysis on images has not at all been explored fully. In this work, attempts have been made to apply multi-way methods to image analysis, defined as 3-way (N-way) image analysis. One unique aspect of N-way image analysis is the possibility of modeling of *multiple* images simultaneously combining both spatial and spectral information, as opposed to just of *one single* multivariate image. MIA is thus one particular approach to N-way image analysis. Principles and applications of MIA have been given in full detail in the past decade. Typical examples are related to well-known multi-spectral images such as satellite images, microscopic images etc[1, 3-11]. There is no need to repeat much of this development here.

Below we have also tried to apply strong multi-way methods on multi-spectral images which are otherwise conventionally analyzed by the MIA approach as well as to apply MIA on 3-way (fluorescence) data usually handled by strong multi-way methods. Another focus of this work is concerned with more easily obtainable images, which possess common properties and interrelationships. The microscopic cheese images to be introduced in application III are of quite similar properties such as appearance and rheological characteristics etc, but they do not fit any of the se two conventional 3-way array formats. They can nevertheless be juxtaposed, transformed and reorganized so as also to form a three-way data array for multivariate data modeling using alternative multi-way methods. Illustration examples given attempt to discriminate different cheeses and predict the rheological properties from images by N-way image analysis

The objective of this survey is to review the gamut of multi-way methods from the perspective of proper (i.e. problem-dependent) data array organization and the many multi-way methodological methods presented in the literature. Within 3-way/multivariate image analysis chemometrics there has been a rather bewildering *ad hoc* modus operandi concerning how to organize the pertinent object-way(s), variable way(s), time way etc. and what particular method to use. We here focus on the systematic correspondence between the specific 3-way (N-way) problem formulation(s) and their *matching* data array setups, from which follows which methods are at all possible - or not. We want to show that exploitation of multi-way methods is not a free optional matter, but rather that it is in many ways more logically restricted by the problem/data array prerequisites. Therefore our survey is also composed of "cross-over" methodological experiments, for example using typical (**OOV**)-methods on decidedly (**OVV**)-data arrays and *vice versa*, in order to present a fairly complete catalogue of representative usages of the many multi-way methods.

2. TERMINOLOGY AND NOMENCLATURE IN N-WAY IMAGE ANALYSIS

2.1. Terminology

Some confusion and misunderstandings may arise when dealing with multivariate analysis on images and other types of 3-way arrays. It is therefore necessary to give a clear explanation of terminology and nomenclature to be used in the following. An intensity/gray-level image can be 2-D, 3-D or N-D. The images discussed in the present context are in 2-D form. As mentioned above, the term N-way image analysis is characterized by multivariate analysis of a stack of images in general. N-way image data consist of a stack of images which usually have similar properties, i.e. chemical, biological characteristics or inherent correlations, or intrinsic variations, etc. A multivariate image is a stack of *congruent images* on the same field-of-view measured for a series of different 'variables', e.g. wavelength, frequency, etc[1]. Multi-way methods can be categorized into weak and strong multi-way methods[12]. Unfold-PCA/PLS are considered weak multi-way methods because they actually unfold 3-way data array into 2-way, followed by ordinary 2-way analysis, instead of utilizing the entire multi-way structure during the modeling. It should be noted that the term multi-way PCA (MPCA)[27] has been used in chemometrics for unfolding and doing ordinary PCA (hence Tucker1) modeling. Bro pointed out that it is improper to use this term since it is easily confused with multi-mode PCA, which is the term accepted for the Tucker models in general[13]. Thus we use here the term unfold-PCA/PLS instead of multi-way PCA/PLS to avoid further confusion. Strong multi-way methods usually refer to the trilinear PARAFAC model, Tucker3 model, and the more advanced PARAFAC2 and PARATUCK models, which distinguish themselves from unfold-PCA by using the multi-mode structure in the data in general, and they also offer different attractive features. Multi-linear calibration is a strong multi-way regression approach, together with which PARAFAC and Tucker3 models will be used in our first forays at N-way image analysis below.

2.2. Nomenclature

In the following, digitized images are denoted by bold capitals, and 3-way (image) array by underlined bold capitals. Lower-case italics are used for scalars, and bold lower-case characters for vectors. The letters, *I, J and K* are reserved for indicating the dimension of different modes. The *ijk*th element of $\underline{\mathbf{X}}$ is called x_{ijk} and is the element in the *i*th row, *j*th column and *k*th tube of $\underline{\mathbf{X}}$. The name *way* is defined as geometrical dimension, and the name *order* indicates number of ways. Object modes are denoted by bold capital letter **O**, and variable modes by **V,** following Esbensen et al[14].

3. DATA CONFIGURATION IN MULTIVARIATE DATA ANALYSIS ON IMAGES

3.1. Data arrangement in N-way image analysis

Choosing an optimal data analytical methodology requires an appropriate data configuration pertaining to specific problem formulations in multivariate data analysis[14]. N-way image analysis is no exception. The proper arrangement of a large amount of image data is intimately connected with the scientific goal or the pertinent problem formulation.

Arrays of three-way data can be characterized by a categorical object/variable (**O/V**) mode convention[9, 14]. The entire class of all possible four different three-way configurations are represented by the codes (**OOO**), (**OOV**), (**OVV**) and (**VVV**), of which the two extremes are usually of no practical consequence for multivariate data analysis. A three-way data array composed of a multivariate image, for instance, may be characterized as **OOV**, which is perhaps the most familiar three-way data array in N-way image analysis. Data configuration may become more complicated when a third categorical direction (mode) is introduced, *time*. It is sometimes argued that time should be treated as a **V**-direction or its own direction, as *time* would appear to be equivalent to V-direction in some process chemometric applications. Multitemporal multivariate images are a stack of images of the same object by using time intervals[1]. This type of image data array can be represented as **OOT**. We will not go into details here. There is a need for classification of these O/V/T-issues.

3.2. Analytical Problem Formulation

A significant part of multivariate data analysis can be covered by the following three types of problem formulation[14]:

1) data description (exploratory data analysis);
2) inter-class classification and discrimination;
3) intra-class correlation and regression.

This partitioning is not possibly complete, but can serve as a systematic basis also for carrying out higher-order data analysis, see more detail in reference 14. This strategic overview should be kept in mind when doing N-way image analysis of all kinds.

3.3. Relationship between data configuration and problem formulation in 3-way image analysis

Major types of data modeling in N-way image analysis are described in the following with focus on the dominant **OOV** and **OVV** data arrays.

3.3.1. Data description

A multivariate image is a two-way array (**OO**) with a third way as the variable mode (**OOV**). The standard MIA way of doing multivariate image analysis is to reorganize/unfold the three-way data array to two-way first, and then to perform ordinary two-way analysis on unfolded 2D array. The approach is usually termed unfold-PCA/PLS if used in conjunction with PCA/PLS. Due to its original three-way arrangement and inherent unfolding, unfold-PCA/PLS can be categorized as a weak multi-way method. See the graphical presentation in Figure 1. The term multi-way PCA may be confused with three-way modeling[13], and therefore not used here.

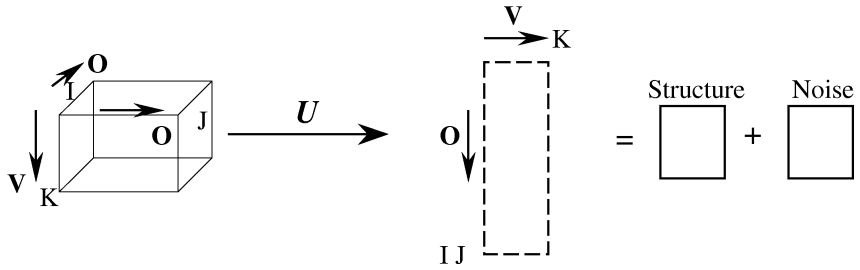

Figure 1. A three-way array is unfolded to a two-way array, on which the PCA is then performed. ***U*** denotes the unfolding operator.

For an image array with **OOO** structure, domain transformations may occasionally be implemented to obtain an **OVV** or **OOV** array which is trilinear and thus suited for strong multi-way analysis. We give one such example in application III below.

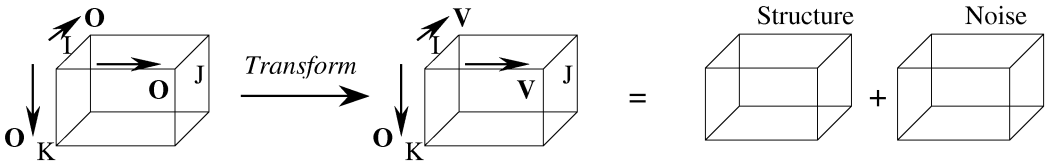

Figure 2. An **OOO** three-way data array may be transformed to an **OVV** (or **OOV**) data array suited for subsequent multi-way modeling.

3.3.2. Classification and discrimination

One of most important demands on image analysis is to extract information pertaining to classification or discrimination of pixels in one or more classes, or of one or more entire images, depending on the specific problem to be solved. There are two principal types of classifications in terms of **OOV** and **OVV** data array configurations, see Figure 3.

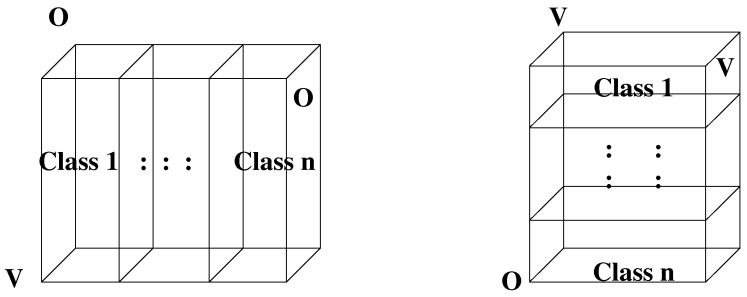

(a) (b)

Figure 3. Classifications/discriminations pertaining to different data configuration and problem formulation. (a) **OOV** data array. Classification is performed simultaneously on each **OO** plane which represents IJ objects. (b) **OVV** data array. Classification is performed along the object mode. One single plane here represents one object only.

3.3.3. Regression

When regression modeling is applied to 3-way image data, it is called 3-way image regression. There are three basic types of regression in 3-way image regression. See graphical representation in Figure 4. Image regression can be established not only between images, but also between image data and physical or chemical properties of what's been imaged. The latter will be focused in application III, which is concerned with regression between microscopic images and rheological properties of cheeses. The possible data configuration problems may be described by Figure 4.

Multivariate Image Regression (MIR) based on unfold-PLS has recently be reformulated with details to be found in Lied and Esbensen[9,30]. MIR deals with **OOV** data arrays exclusively.

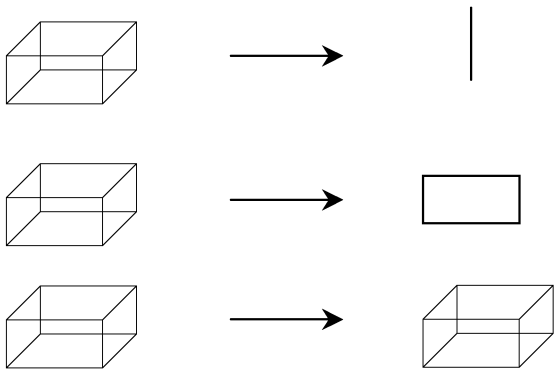

Figure 4. A graphical representation of three types of image regression, classified according to the pertinent order of the Y-array.

4. THEORY ON MULTI-WAY DECOMPOSTION METHODS

4.1. Weak multi-way methods

As discussed in section 3, unfold PCA/PLS is categorized into the family of weak multi-way methods. Unfolding breaks the correlations in either (**OO**) or (**VV**) modes.

4.1.1. OOV three-way image data array

The typical **OOV** three-way image data array consists of K images of size I×J measured e.g. at K wavelengths in Figure 5. For **OOV** type of data, the three-way matrix **X** (I×J×K) is *unfolded* into a two-way array so that each image pixel work as an object while each wavelength (or frequency, energy etc.) is maintained as a variable. Then PCA is performed on the two-way data set (IJ×K). With unfold-PCA, in each component the data are decomposed into a long score vector (IJ) which can be rearranged to a two-way score image (I×J). The loading vectors $\mathbf{p}_f$ (K×1) describe the variations in variable space for each component. See below a graphical presentation of MIA modeling (**OOV**) in Figure 5. The model can be written

$$\underline{X} = \sum_{f=1}^{F} T_f p_f + \underline{E}$$

The index ***f*** denotes a component, and **E** residual images from unfold-PCA. The components are orthogonal and can be calculated sequentially.

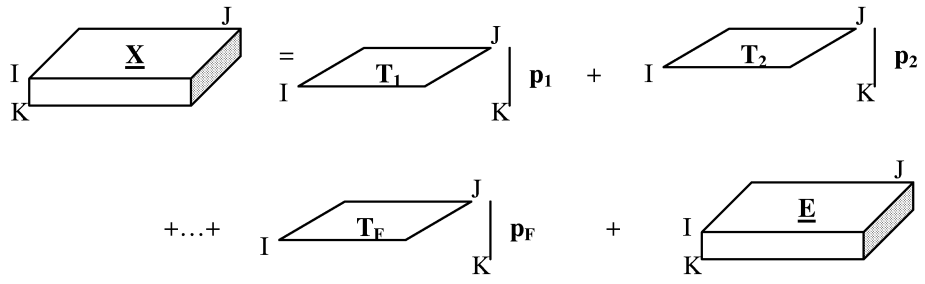

Figure 5. A graphical presentation of MIA modeling (**OOV**). The matrix **X** contains K images measured at a variable direction. **E** is the matrix of residual images. The indices I, J denote the objects, and K variables.

4.1.2. OVV three-way image data array

Decomposition of the **OVV** three-way image array is different from **OOV**. The distinction is that unfolding is now performed on the two-way variable mode instead of object mode. As compared to **OOV** (e.g. MIA) data decomposition, the three-way **OVV** array matrix **X** (I×J×K)

is *unfolded* into a two-way array (K×IJ) where the object direction of the images is maintained (the sample mode). Likewise, in each component the data are decomposed into a score vector (K×1) in sample image mode, $\mathbf{t}_f$, and a long loading vector (IJ) which can be *backfolded* to a two-way loading matrix $\mathbf{P}_f$ (I×J) (or loading image) as shown in Figure 6. $\mathbf{P}_f$ describes the variation in the 2-D variable domain space for each component. The structure model with residuals is

$$\underline{X} = \sum_{f=1}^{F} t_f P_f + \underline{E}$$

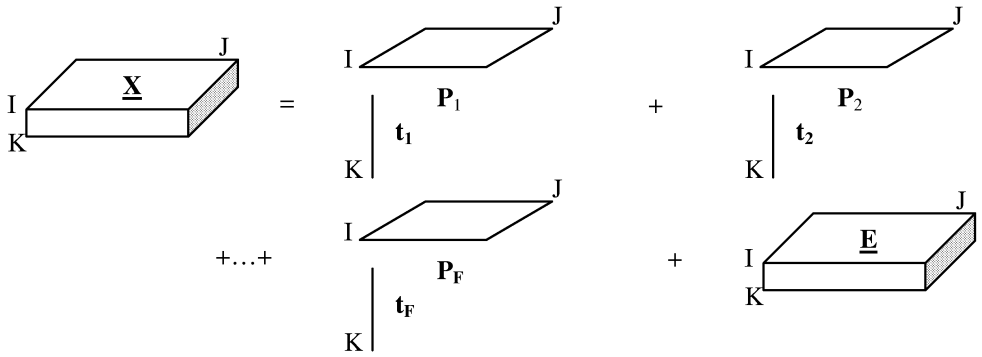

Figure 6. Decomposition of **X** by unfold-PCA to F principal components. The matrix **X** contains K **OVV** image data array. **E** is the residual images. The indices I, J denote the variables, and K the samples. Note the opposed symmetry difference with respect to Figure 5.

4.2. Strong multi-way methods in N-way image analysis

Some strong multi-way methods such as PARAFAC and Tucker3 can be adapted to image analysis. PARAFAC is a *de facto* trilinear decomposition method, conceptually comparable to bilinear PCA, while the Tucker3 decomposition is another generalization of PCA to higher orders[13]. A detailed tutorial on PARAFAC is given by Bro[15]. A PARAFAC model of a three-way array is expressed by *three loading matrices*, **A**, **B** and **C** with elements a_{if}, b_{jf}, c_{kf}, and the residuals as shown in Figure 7. It can be written

$$x_{ijk} = \sum_{f=1}^{F} a_{ij} b_{jf} c_{kf} + e_{ijk}$$

where ***F*** is the number of components, e_{ijk} denotes the residual elements.

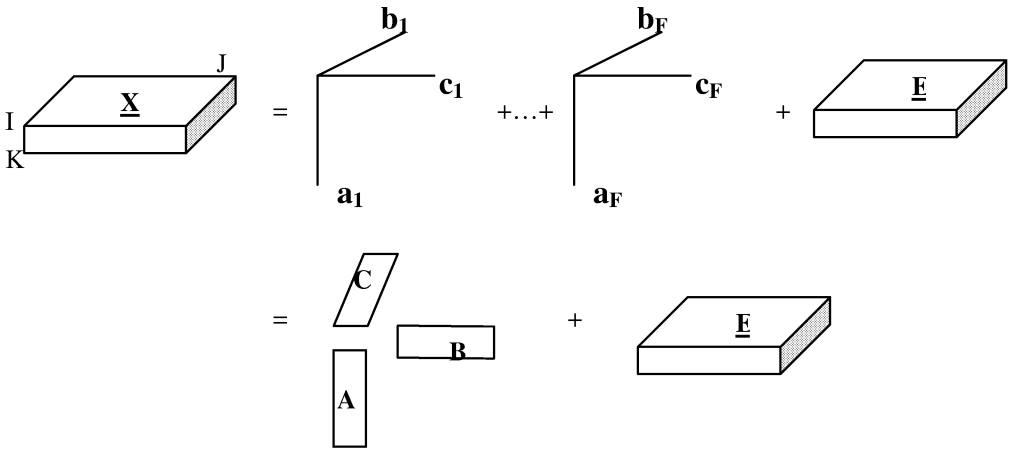

Figure 7. An F-component trilinear PARAFAC model of the 3-way data array **X** .

One of most attractive features of the trilinear PARAFAC model is the solution uniqueness. The Tucker3 model, also known as 3-way PCA, is another basic strong multi-way method used in chemometrics. As compared to PARAFAC model, a Tucker3 model allows for extraction of different number of factors in each of modes, and thus offer more flexibility, but is usually also more difficult to interpret. It has been used for decomposition, compression, and interpretation in many three-way applications, with the coverage of PARAFAC model as a special case under such constraints[19 - 22]. However, both PARAFAC and Tucker3 are simpler than the alternative approach, unfold-PCA, due to fewer parameters in the models. A tucker3 model is a weighted sum of all possible outer products between the factors stored as columns in **A**, **B** and **C** with the weight of the outer products determined by a core array **G** (w_1, w_2, w_3). It can be written in a same manner to PARAFAC

$$x_{ijk} = \sum_{d=1}^{D} \sum_{e=1}^{E} \sum_{f=1}^{F} a_{id} b_{je} c_{kf} g_{def} + e_{ijk}$$

where the index ***D, E, F*** denotes the number of components in each mode, and g_{def} the elements of core array **G**.

A graphical representation of Tucker3 model is given by Figure 8, in which **X** is a I×J×K matrix, **G** is a D×E×F, **A** is I×D, **B** is J×E, and **C** is K×F. When one mode in **X** is not compressed (e.g. D=I, F=K or E=J), the Tucker3 model becomes a Tucker2 model. If two dimensions are equal (e.g. F=K and E=J), then the model is called a Tucker1 model, which is simply equivalent to unfold-PCA *without* utilizing three-way structure of data. Another special Tucker3 model is PARAFAC model under the specific constraints that the number of factors in each direction is the same, D=E=F, and the core array **G** is a superdiagonal identity matrix. More detailed descriptions on the Tucker3 model can be found in literatures[19-22].

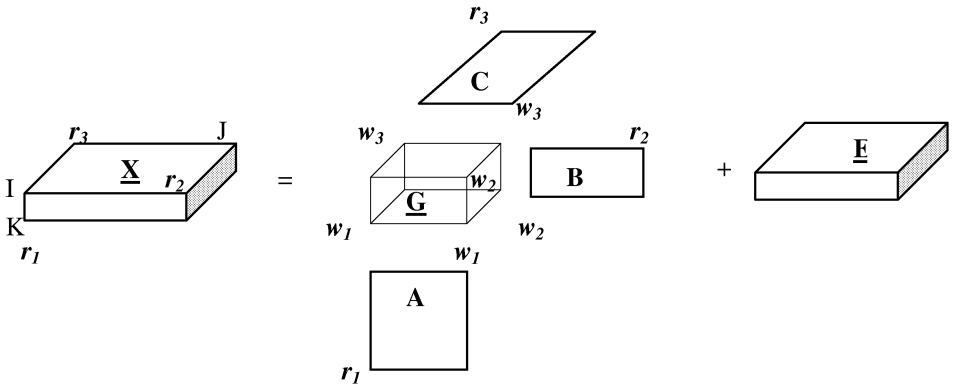

Figure 8. A graphical representation of the Tucker3 model.

4.3. Multi-way Calibration

There are many possible multi-way calibration methods, among which unfold-PLS and N-PLS associated with a trilinear (PARAFAC-like) model are introduced here. Unfold-PLS is characterized by performing ordinary PLS on a two-way array unfolded from a three-way array and **y** variable(s), while keeping the object mode of **X** in common with the dependent y intact. N-PLS based on PARAFAC model can be represented graphically in Figure 9 (with one **y** variable illustrated). As described earlier, the Y-block can be a vector, a two-way matrix, or a three-way (N-way) matrix.

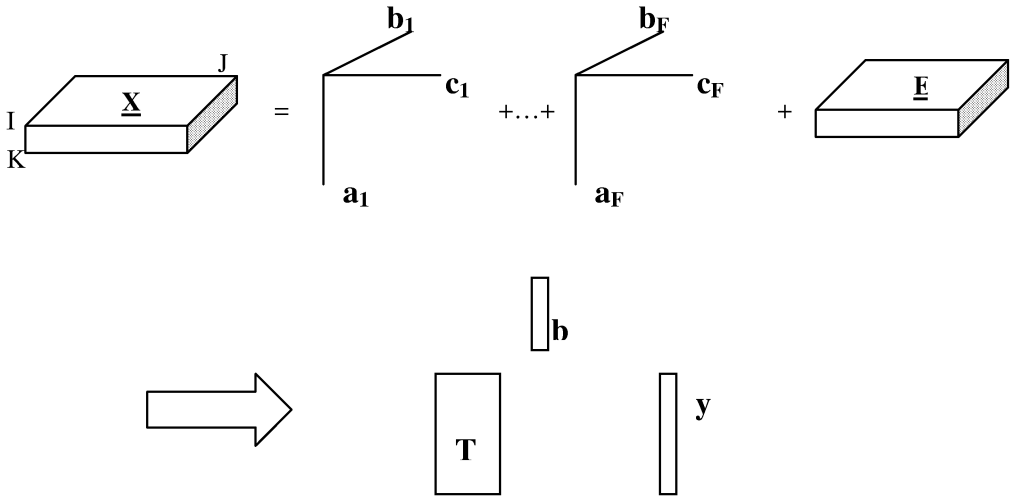

Figure 9. N-PLS model based on two steps: PARAFAC decomposition of **X**, followed by PLS on scores from **X** and **y**.

Details on multi-linear calibration are given by Bro and Smilde[17, 18]. Bro pointed out that the advantages of N-PLS (including tri-PLS) over unfold-PLS can be highlighted by the following two points: 1) The trilinear model is more parsimonious, simpler and thus easier to interpret; 2) Less prone to noise due to decomposition across all modes[17].However, there is no general rule in choosing which method to use. The knowledge of data sets under investigation and a priori knowledge of calibration methods, proper problem formulation, is always an important guideline. For instance, we have often found that unfold-PLS works very well in multivariate image regression (MIR)[30], by virtue of inherent weak correlations in one way etc. There might also be a possibility of applying N-PLS in multivariate image regression, i.e. finding regions of interest.

In the following three sections, three application examples on multispectral images, virtual fluorescence images and microscopic image-functional property correlation using above methods will be given.

Both weak and strong multi-way methods are applied in order to decompose and characterize image data, and obtain some insight into their abilities to capture data structure. Application I and II apply both MIA and strong multi-way methods on typically MIA data and strong 3-way data in order to evaluate their scientific playgrounds. Application III in addition attempts to investigate the relationships between transformations of original images and their corresponding functional properties. Comparisons of the ability of these methods are given. The goal of comparison is not to verify one method over another, but rather to explore more alternative approaches to N-way image analysis.

5. APPLICATION I: MULTI-WAY ANALYSIS OF OOV IMAGE ARRAY
MULTI-SPECTRAL IMAGE EXAMPLE

5.1. Data

This data set, Figure 10, is a multi-spectral satellite image of Mobile Bay, Alabama, which has been described in the chemometric literature (Geladi & Esbensen, 1991). The image size is 512*512 pixels of Mobile Bay and the city of Mobile, Alabama, USA (coordinates 30.6°N, 88°W). It is made up of four variables (“channels”), the wavelength bands 500-600nm (yellow-green), 600-700nm (orange-red),700-800nm (red-deep red) and 800-1100 nm (near-infrared). In each wavelength band, the reflected intensities of the earth surface are digitized in the range 0-127. One pixel is about 80*80 m.

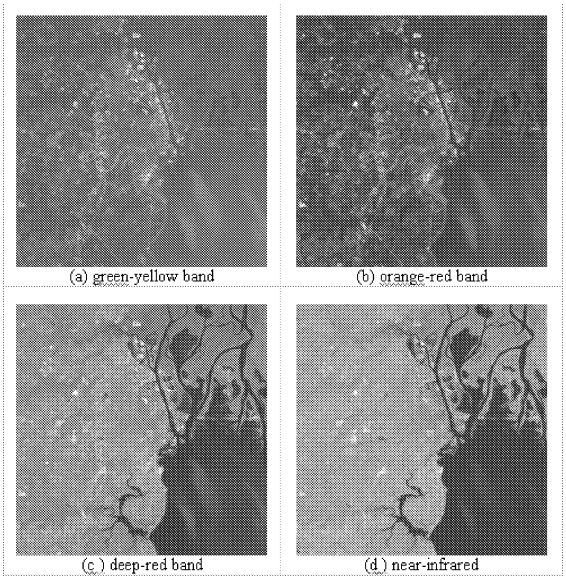

Figure 10. The 4×512×512 satellite image measured at different wavelength bands

This is a typical **OOV** image array (4 wavelengths × 512pixels × 512 pixels) since two spatial directions form object modes and the wavelengths form a variable mode, see Figure 11. In the following, both weak (unfold-PCA/Tucker1) and strong methods (PARAFAC and Tucker3) are applied to this **OOV** image array.

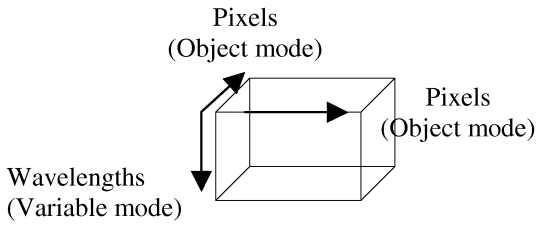

Figure 11. Data configuration of the 4×512×512 satellite image (**OOV** image array), Mobile Bay.

5.2. Multi-way analysis of multi-spectral images

5.2.1 Unfold-PCA model (Tucker1 model)

This type of multi-spectral image is an archetype for MIA. MIA's objective is to conduct unfold-PCA analysis on the multivariate image, i.e. to conduct an interactive study of scene (raw images/score images) and feature space (score and loading plots). The score images are obtained after the PCA calculations on these four raw images (four variables). The displays in Figure 12 are scaled optimally in the standard gray-scale range of 0-255. The visual image results of MIA calculations on this multivariate image are shown in Figure 12 and 13. Score images are in maximum contrast to each other due to orthogonality of the PC scores. Residual images from a model with 3 components show mostly the noise, e.g. closer look shows some horizontal lines etc. These result largely from optic-electro instrument artifacts. Still it can be advantageous to be able to assess even this mini-scale noise fraction in its proper spatial context.

We will not go to detail since the detailed MIA analysis of this example has been given elsewhere[1, 3].

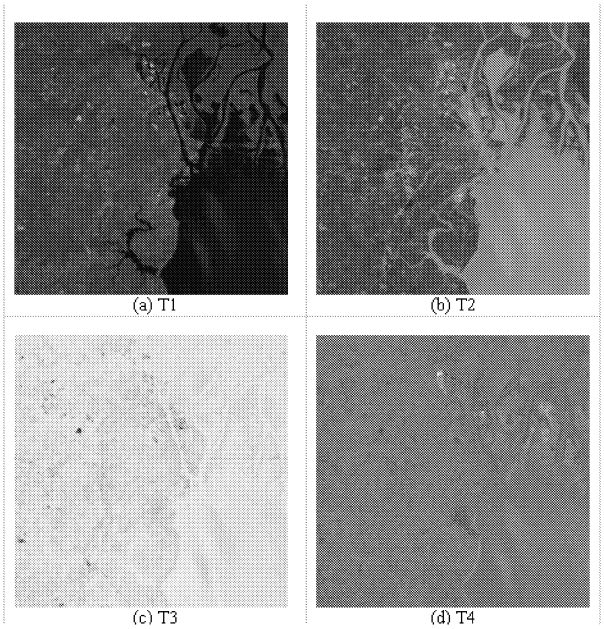

Figure 12. The four score images of the 4×512×512 satellite image: T1,T2,T3,T4. The first three contain most information, while the last image contains very nearly only residual noise. The score images are in maximum contrast with each other as a result of orthogonality of scores.

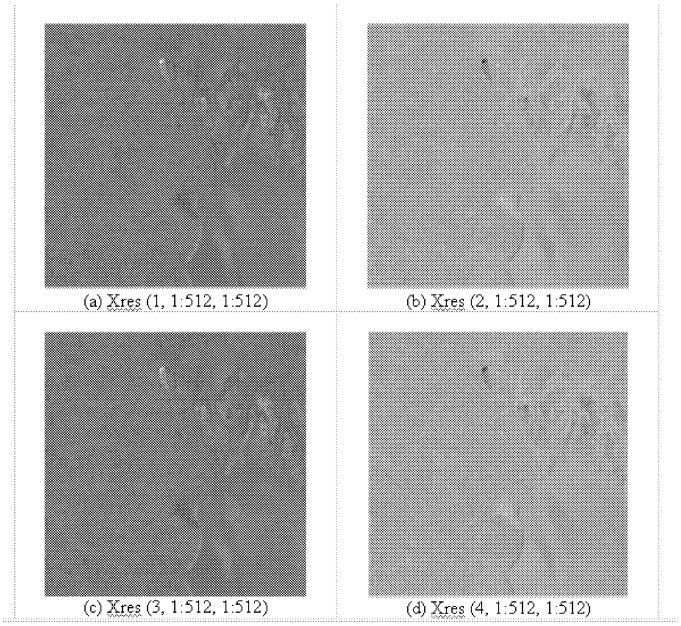

Figure 13. Noisy residual images from unfold-PCA model with 3 components. Note that while these residual images carry only the most minute fraction of variance, there is a distinct advantage in being able to view (even) this in its proper spatial context.

5.2.2. PARAFAC model

A three-component PARAFAC model is now fitted to the same image array for direct comparison. Figure 14 shows a set of four reconstructed images from the structure model, which has the same size as raw image array. These four images appear extremely blurred (but the profiles of bay in image (b), (c), (d) are perhaps faintly discernable). It is quite apparent that PARAFAC failed in modeling the multivariate image variance efficiently in this case. The reason is clearly that three components are not enough to account for the most variation as PARAFAC modeling requires equal components in all modes. There are only 4 wavelengths in variable mode, and as many as 512 pixels in two object modes. Few variables make it impossible to choose enough components for a well-fitted model. As clearly seen from modeling results, three components are not capable of explaining major variations along three modes.

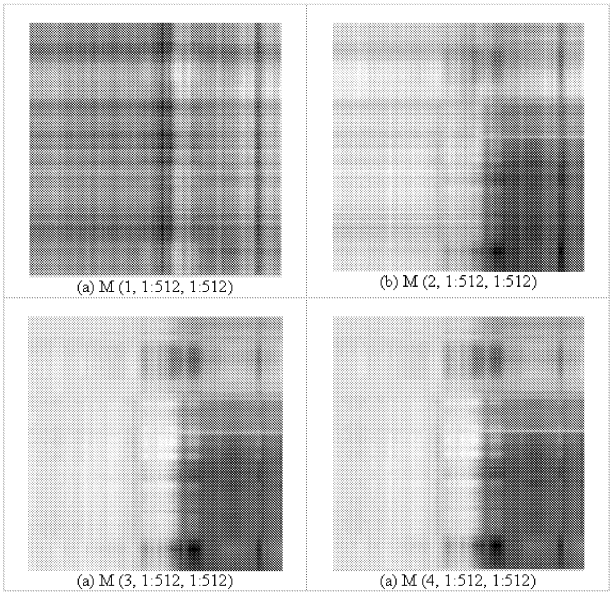

Figure 14. Reconstructed structure parts from a three-component PARAFAC model. Notice the extreme difference with respect to Figure 12.

5.2.3. Tucker3 model

A Tucker3 model offers more flexibility than PARAFAC in that it allows for a choice of different number of components in the different modes. Therefore, we can choose more components precisely in the two object modes unlike for the PARAFAC model. Different component options have been tried out. After trial and error, 3 components are chosen in variable mode, and 64 components in each object mode, as this model captures 98.93% of the total variance. The reconstructed images from structure part are shown in Figure 15. This structural model is calculated from $\underline{\mathbf{X\_structure}} = \mathbf{AG}\ (\mathbf{C}^T \otimes \mathbf{B}^T)$, where **A**, **B**, **C** are loading arrays, and **G** core array, and the symbol $\otimes$ denotes Kronecker multiplication, see Ref. 22.

The reconstructed images (by proper image analysis scaling in the structural model) appear quite clear and optimally contrasted. They are complementary to each other, but it should be noted that reconstructed images here are not exactly orthogonal to each other, which is different from score images derived from unfold-PCA model. Clearly, a Tucker3 modeling provides a different approach to describe the image data from a new perspective. Tucker3 modeling of multi-spectral images may be useful for e.g. de-noising, data compression, visualization etc. Also shown here are residual images in Figure 16. They are mostly random noise due to possible illumination, non-linear optical behavior etc. The Tucker3 model successfully captures most of the image variance with this (3,64,64) setup of components, as is also very clearly evidenced by the corresponding residual images in Figure 16.

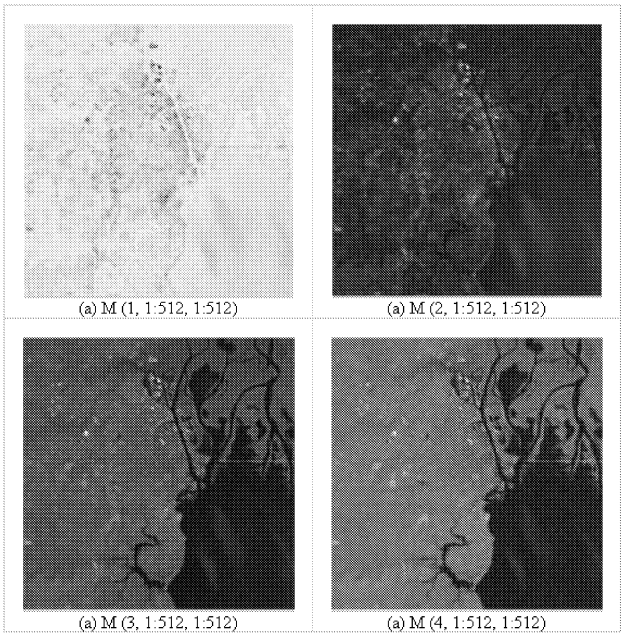

Figure 15. Reconstructed structure parts from a Tucker3 model with (3,64,64) components in each of the three mode (**VOO**). Notice the differences with respect to Figure 12.

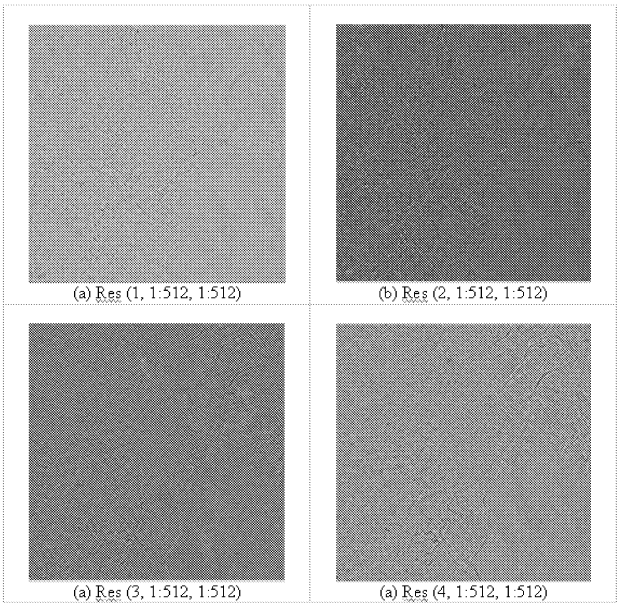

Figure 16. Reconstructed noisy residual images from a Tucker3 model with (3,64,64) components in each of the three modes (**VOO**).

Table 1. Cumulative variations captured by unfold-PCA, Tucker3 and PARAFAC models. For Tucker3 model, 64 components are chosen in each object direction, while the components in the variable mode vary from 1-3.

Number of components/factors	Unfold-PCA (%)	Tucker3 (%)	PARAFAC (%)
1	86.55	91.41 (1,64,64)	89.57
2	99.13	97.86 (2,64,64)	94.28
3	99.66	98.93 (3,64,64)	94.76

It is interesting to compare these three different methods on this type of **OOV** image data array. Table 1 gives the percentage of variations explained after 1,2,3 components (in first mode for Tucker3). With three components, unfold-PCA explains the largest variation, 99.66%, followed by Tucker3, 98.93% and PARAFAC, 94.76%. This is understandable since PARAFAC is most parsimonious. Furthermore, both unfold-PCA and strong 3-way models maximize the fit of model to the data in the bilinear and trilinear sense respectively. It is not difficult to see that unfold-PCA is nothing but Tucker1 in the specific sense that the model is fitted. Therefore, MIA and other three-way/N-way modeling of images form different cases of N-way image analysis. In the above unfold-PCA/Tucker1 model, two object modes are left uncompressed, and only variable mode is compressed. The object modes and variable mode are compressed with different components in Tucker3 model, whereas the PARAFAC model compresses all modes with an equal number of components. It is also of interest to compare the respective loading plots from the three models as shown in Figure 17. Loadings from the unfold-PCA and Tucker3 models show very small differences only, but differ somewhat from the PARAFAC model. The reason is that the Tucker model compresses three modes separately, and establish a relationship between factors in the three modes spanned by the core array. Here both Tucker1 and Tucker3 use 3 factors in the variable mode. As compared to Tucker models, PARAFAC does not have a core array to allow this flexibility in choosing different factors. The three factors here are directly interrelated to each other. However, on the general level all three models show almost the same interrelationships in this particular example..

Which model to use depends on the problem to be solved. The MIA approach is based on unfold-PCA, for instance, which offers the tools for data decomposition and interactive study of scene and feature space for segmentation and classification etc. The latter is largely due to the fact that pixels in two object modes are kept uncompressed, and thus pixels in the score plot correspond to those in score images backfolded from scores after unfold-PCA. For more information, see Ref. 1.

Therefore, MIA is probably better suited for explorative data analysis and classification purpose etc, while the Tucker3 model could be used for image data compression, exploration of 3-way structure, de-noising etc. The PARAFAC model may only be considered when there are approximately as many variables as comparable to objects present.

A significant amount of practical work still needs to be done in this area before a more satisfactory body of experience is at hand.

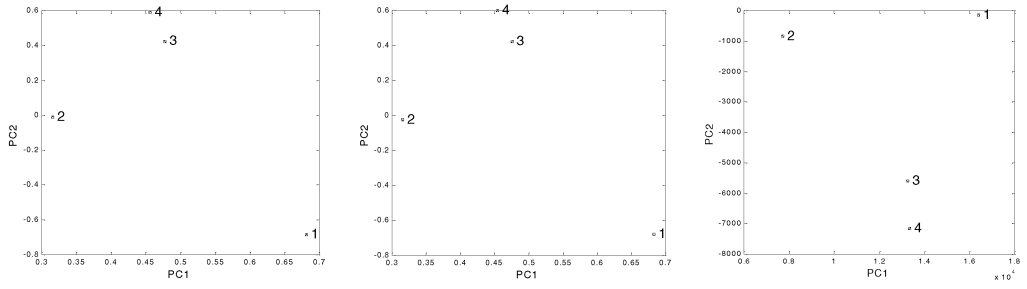

(a) (b) (c)

Figure 17. Loading plots (**p**1vs.**p**2) in the variable mode from different models. (a) Unfold-PCA/Tucker1 model; (b) Tucker3 model; (c) PARAFAC model.

6. APPLICATION II. DECOMPOSITION OF FLUORESCENCE DATA WITH MIA
VIRTUAL SPECTROSCOPIC IMAGE EXAMPLE

6.1. Data set

This well-known data set was obtained from Dr. Rasmus Bro at the Royal Veterinary and Agricultural University, Copenhagen. It has been used in many 3-way data decomposition expositions. Five samples were measured on a PE LS50B spectrofluorometer with excitation 250-300nm, emission 250-450nm in 1nm intervals. Two samples contain different amounts of tyrosine, tryptophane and phenylalanine[15], see Figure 18 (a) and (b). Three other samples are pure components of these 3 analytes, respectively, see Figure 19 (a), (b) and (c). This is an archetype trilinear three-way data (**OVV**). It has been demonstrated that the 3 pure spectra can be estimated almost perfectly by the unique PARAFAC decomposition of the fluorescence spectra of two samples containing different amounts of Try, Trp, and Phe, see details in Ref. 15.

In the present context it is not our intention to seriously pit the MIA approach against the strong three-way methods (PARAFAC), but rather to analyze such spectroscopic data from an imaging point of view only -- in order to investigate the possibilities (if any) and limitations (many expected) of applying MIA on 3-way (**OVV**) spectroscopic data. The reason is that virtually every spectroscopic technique can be used to generate chemical images. Fluorescence data is a very good example of this since each sample is a "landscape" composed of the excitation and emission spectra. Intuitively, such a landscape can well also be considered as an image with appropriate conversion/scaling, see Figure 18 (c), (d) and Figure 19 (d), (e) and (f).

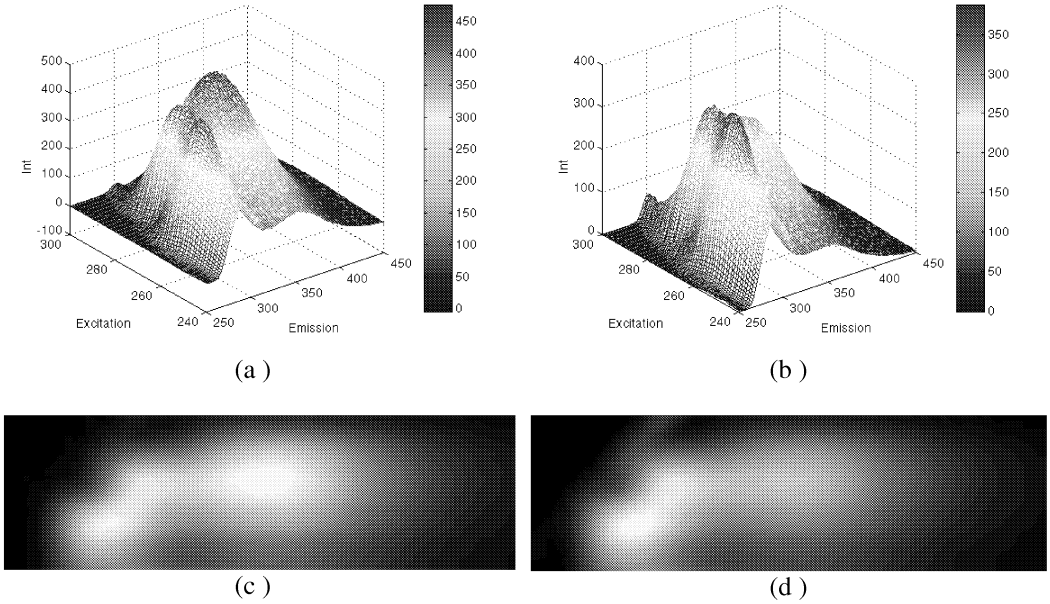

Figure 18. (a) Fluorescence spectra of a sample containing different amounts of Trp, Tyr and Phe; (b) Fluorescence spectra of another sample containing different amounts of Trp, Tyr and Phe; (c) Image converted from the spectra corresponding to (a); (d) Image converted from the spectra corresponding to (b);

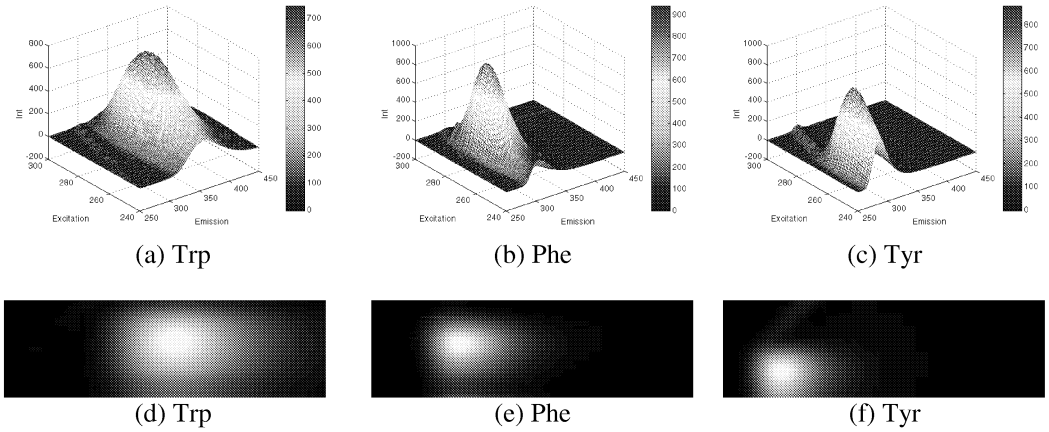

Figure 19. (a) The pure fluorescence spectra of a sample containing only Trp; (b) Pure fluorescence spectra of a sample containing only Phe; (c) Pure fluorescence spectra of a sample containing only Tyr; (d) Converted image representing Trp; (e) Converted image representing Phe; (f) Converted image representing Tyr

6.2. Results and discussion

Fluorescence spectra of the two samples with a mixture of three analytes were first converted into appropriately scaled images, and then put into a MIA model. This conversion necessitates a "transformation" of the original data configuration from **OVV** data into a virtual **OOV** data set as shown in Figure 20. The otherwise standard MIA is now performed on this **OOV** data array, which results in "transposed" object–variable relationships, which should be kept firmly in mind below.

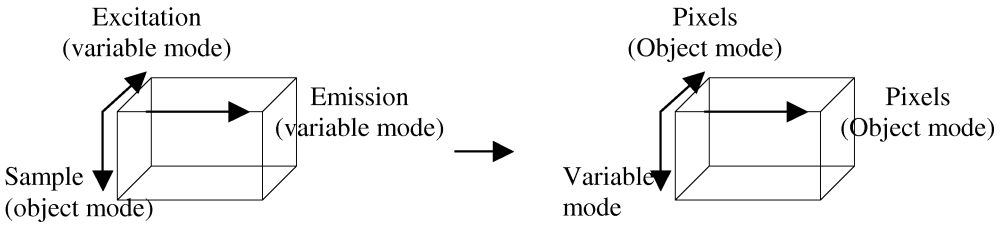

Figure 20. Original data configuration type is converted from **OVV** to *virtual* **OOV**. This is necessary in order to be able to apply the MIA approach. Note that OVV is "transposed" into **OOV**.

The score image (printed in grayscale) shown in Figure 21 is in reality a pseudo-color composite formed by assigning score image 1, 2, 2 into R, G, B channel for a visualization purpose. As seen in Figure 21, the three analytes can be seen clearly with different colors (shown by approximately enclosing markings). Notice the *Rayleigh scatter* (the triangular part in the upper left corner), which is easily distinguished in the image. This is, however, very obscure in the original images shown in Figure 18. The shape of each analyte is similar to the corresponding pure component image in Figure 19 (d), (e) and (f).

An interactive study of score plots (feature space) and score image (scene space) is conducted in a conventional MIA fashion shown in Figure 22 and 23. Four groups, which correspond to three analytes and the *Releigh scatter* effect respectively, can be classified easily by mapping typical MIA masks in score plots (**t**1-**t**2). These selected areas are then projected so as to be compared to the corresponding chemical analytes in scene space (score image), Figure 23. See details about MIA operations in Ref.1, 3-9.

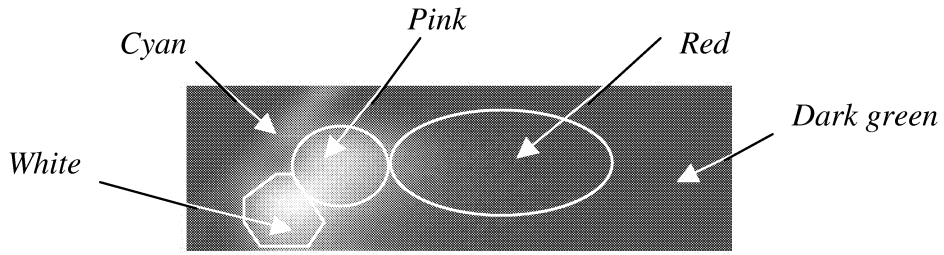

Figure 21. Pseudo-color composite (printed in grayscale) obtained by assigning score image 1,2,2 into R, G, B channel. Note the regions of interest are represented by different colors: Red (Trp); Pink (Phe); White (Tyr). Cyan (Releigh scatter).

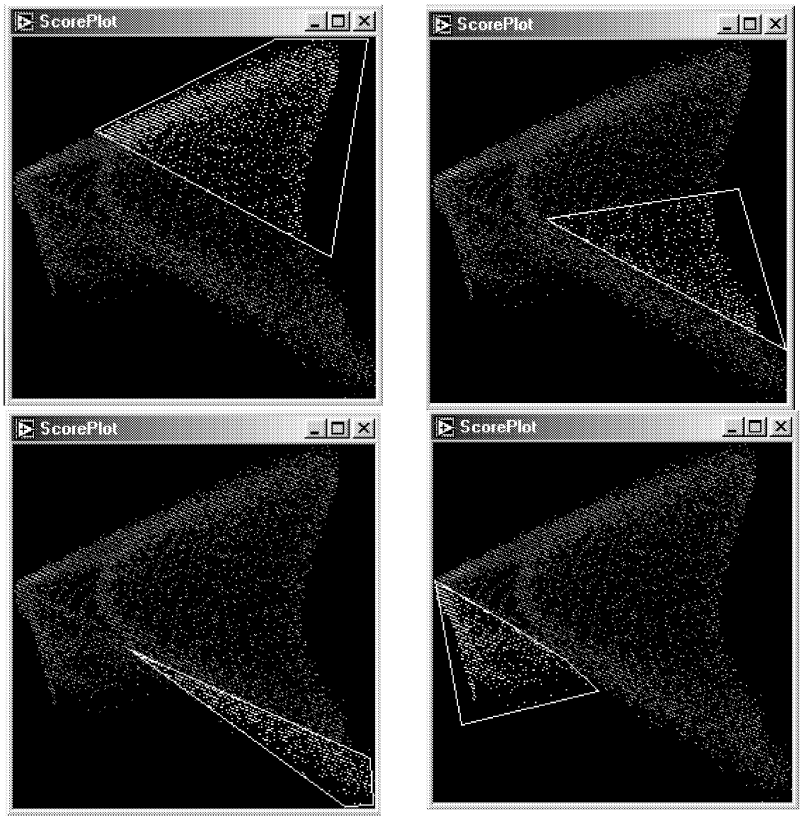

Figure 22. Score plots (t1-t2) by plotting two score images against each other. Clusters indicated by different MIA polygon masks represent different groups in the image plane, Figure 23.

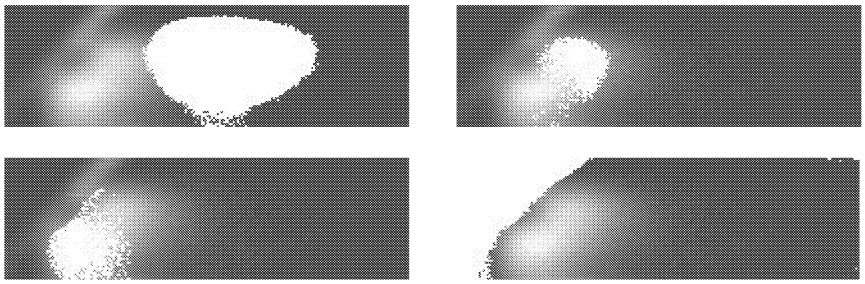

Figure 23. Regions of interest marked in white color in the image plane are the corresponding pixel groupings from mapping in score plots in Figure 22.

As is easily seen, MIA does not provide precise results quantitatively as compared to the PARAFAC model, and neither is MIA aimed at such an objective. However, it does offer a simple way of direct visualization of spectroscopic/image data which may be useful in more complex situations, e.g. forensic analysis etc. It may be helpful to look at the data visually and study the spatial chemical data interactively in appropriate situations.

In conclusion, applying a MIA model on the fluorescence 3-way data (**OVV**) of course does not seem to be a natural idea for the purpose of quantitative decomposition of the data. The reason is of course that the MIA approach is specially designed for **OOV** multivariate image data. However, our objective here only is to propose imaging as a complementary way of doing spectroscopy, which may change one's perspective to recognize some spectroscopic problems in a possibly fruitful new light.

7. APPLICATION III—MULTI-WAY ANALYSIS OF OVV IMAGE ARRAYS
MICROSCOPIC IMAGE EXAMPLE

7.1. Data set and problem formulation—"incongruent multiple images"

Images in many areas such as biochemistry have largely been analyzed by traditional image analysis. These methods tend to be restricted for use in one single image at a time. There is a lack of good methods which can be used to characterize series of images efficiently. With multivariate data analysis on images, many serial images can potentially be analyzed simultaneously.

14 types of cheeses were made from a factorial experiment where coagulation temperature with rennet enzyme, the amount of rennet enzyme and the length of time at coagulation temperature before cooling were varied, i.e. a three-factor experiment. For each of these cheeses four transmission electron micrographs were recorded on four different parts of the cheeses. Each set of four images therefore constitutes four replicates of the same cheese.

As seen from selected images shown in Figure 24, such cheese images appear relatively homogenous and very similar at first glance. It should be stated that we are interested in classifying each image *in toto* instead of regions of interest inside each image e.g. MIA. Global features hidden in each image should receive more attention in this case. The objectives were to characterize/discriminate different types of cheeses based on this type of microscopic images and investigate the closeness of replicates, and especially to relate these global images to selected functional properties to the cheeses by N-way image analysis.

Uniaxial compression, a rheological testing method, has been used to obtain the rheological properties of these cheeses, such as fracture-stress, -strain, -work and modulus. From a biotechnological point of view it would obviously be of interest to look for the relations between the 'image' results and the 'rheological' results. Therefore unfold-PLS and N-PLS have been tried to reach this goal.

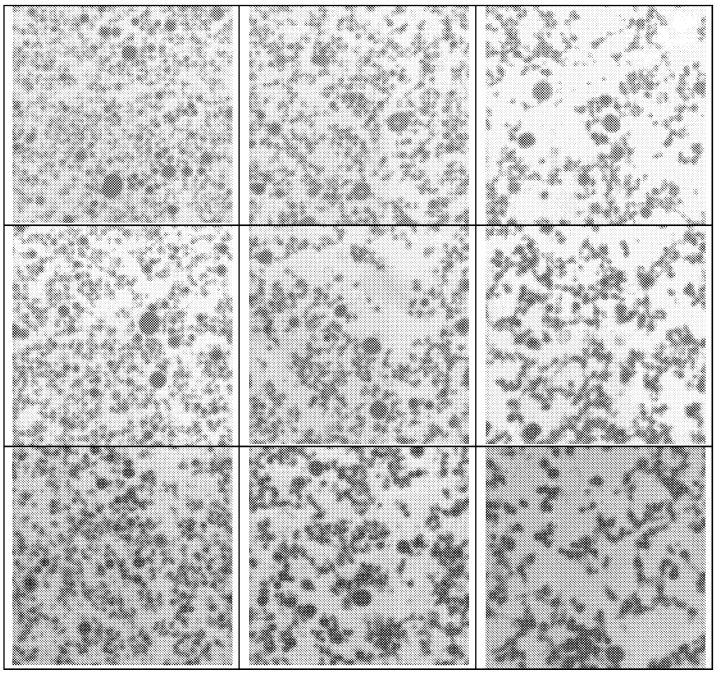

Figure 24. Microscopic images of cheeses (1-9), made from a factorial experiment by varying coagulation temperature and the amount of rennet enzyme, each on 3 levels.

7.1.1. Necessary transformations

As inspected from the raw cheese images in Figure 24, at a certain scale they appear relatively homogeneous and quite "similar". There is currently a lack of efficient methods to characterize and discriminate such multiple images in traditional image analysis. Some image analysis combined with chemometric methods have been initiated on this problem especially concerning

the interesting new AMT-transformation, but this is deferred to a later occasion[25, 26]. Here we focus on the well-known FFT transformation.

The 14×4 serial images of size 512×512 are stacked on top of each other to form a 3-way array, which will be of the **OOO** category. This type of data array is obviously not trilinear, and thus cannot be used for multi-way analysis directly. Different transformation techniques such as FFT, Wavelet Transform (WT), have been applied to this **OOO** data array in order to obtain a trilinear **OVV** data array. Such a transform is necessary to bridge the gap between each image through the new domain[25,26]. FFT-transformed data (power spectra) are used for illustration here since these give the most illustrative models, see Figure 25.

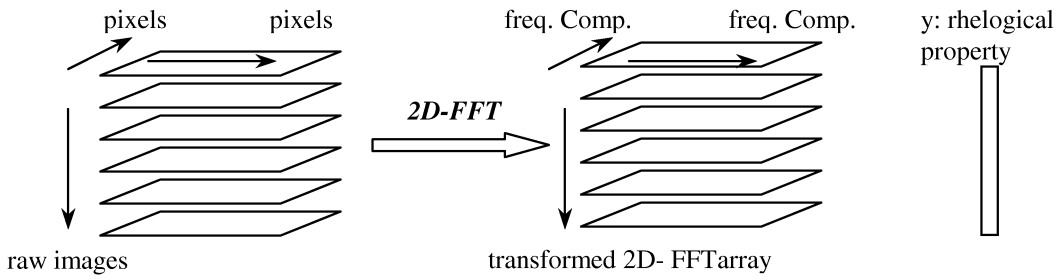

Figure 25. Data configuration of cheese image data for subsequent modeling. Raw images are organized as a 3-way **OOO** data array, and subsequently transformed by 2D FFT to a three-way **OVV** array, in which the 2-D frequency domain forms the two new variable modes (**VV**). Vector **y** represents a rheological property which corresponds to the individual original images in the **O**-direction.

As is appreciated, these 14×4 images of size 512×512 comprise a large amount of data, and will cause a long calculation time when applying 3-way methods. All 64 images were therefore resized to 64×128×128 and transformed to 2-D FFT array of size 64×128×128 so that the time spent on actual modeling could be decreased significantly. All modeling was carried out with *the N-way toolbox for Matlab* by Andersson and Bro[23]. Image processing and transform were conducted with the signal processing and image processing toolbox in Matlab 5.3.

7.2. *Structural models and cheese discrimination*

The cheese image data were explored by both weak and strong multi-way methods, unfold-PCA, PARAFAC, Tucker3 and Tucker2. Models were calculated based on the derived 64×128×128 2-D FFT array. The pertinent data arrays are centered across the first mode. No scaling was used since all frequency components in the second and third mode are in same units and ranges.

Table 2 shows the modeling results of all image decompositions using the above methods. All methods are able to explain over 99% variance fractions with three components, among which unfold-PCA explains the highest percent of cumulative variation, followed by Tucker2,

Tucker3 and PARAFAC. All models fit data almost equally well with but very marginal difference only. This is as expected, since it has been pointed out that theoretically a Tucker 1 model (unfold PCA) always fits data better than a Tucker3 model, which will fit better than a Tucker2 followed by the PARAFAC model[15, 24].

Table 2. Cumulative variance fractions explained by alternative multi-way methods: unfold-PCA, Tucker3, Tucker2, PARAFAC models. The numbers of factors in three modes for Tucker3 and Tucker2 model are given in parentheses. For the Tucker2 model, -1 represents no compression in the first mode, the image mode.

Number of components/factors	Unfold-PCA (Tucker1) (%)	Tucker3 (%)	Tucker2 (%)	PARAFAC (%)
1	98.97	98.90 (1,2,2)	95.99 (-1,1,1)	95.99
2	99.07	98.97 (2,2,2)	98.97 (-1,2,2)	98.96
3	99.11	99.05 (3,3,3)	99.06 (-1,3,3)	99.04

It will be useful and interesting to compare in more detail the four N-way decompositions summarized above. Their score plots (**t**1-**t**2) are compared from unfold-PCA, Tucker3 and PARAFAC models in Figure 26-28. It is observed that cheeses 1-9 span most of empirical variation found, while cheeses 10-14 lie in between cheeses 1-9. This is as expected: from the factorial experiment background it is known that cheeses 1-9 were from an experiment involving varying coagulation temperature and amount of rennet enzyme, each on 3 levels. They were all left at the coagulation temperature for 22 hours before being cooled. Cheeses 10-14 were, by way of contrast, all coagulated with an intermediate amount of enzyme only at the middle temperature, but here the length of time at the coagulation temperature before cooling varied from 1-22 hours. It is apparent that this can easily be perceived from score plots. Cheeses 1-9 span the whole range of variation, while cheese 10-14 are somewhat clumpy in the middle ranges only. The replicate groups are, by and large, close to each other with a little overlap. Notice that replicates lie closer (e.g. sample 9, etc.) in the PARAFAC model than unfold-PCA. This is because PARAFAC model is more parsimonious and less influenced by the noise. The strong multi-way models account for more structure than the weak unfold-PCA model, and hence remove more noise from the final structural model.

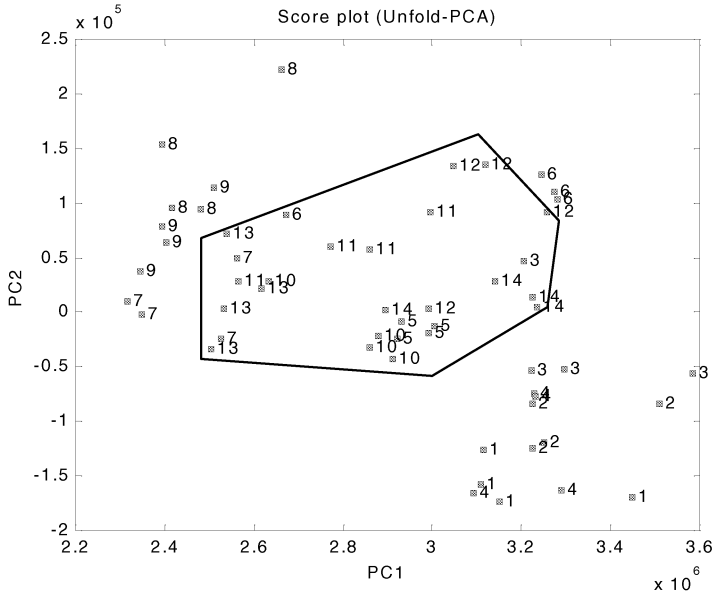

Figure 26. Score plot (**t**1-**t**2) from *unfold-PCA*. Notice the trend that cheeses 1-9 span the complete variation from SE to NW. Cheeses 10-14 are located in between (shown by a special marking).

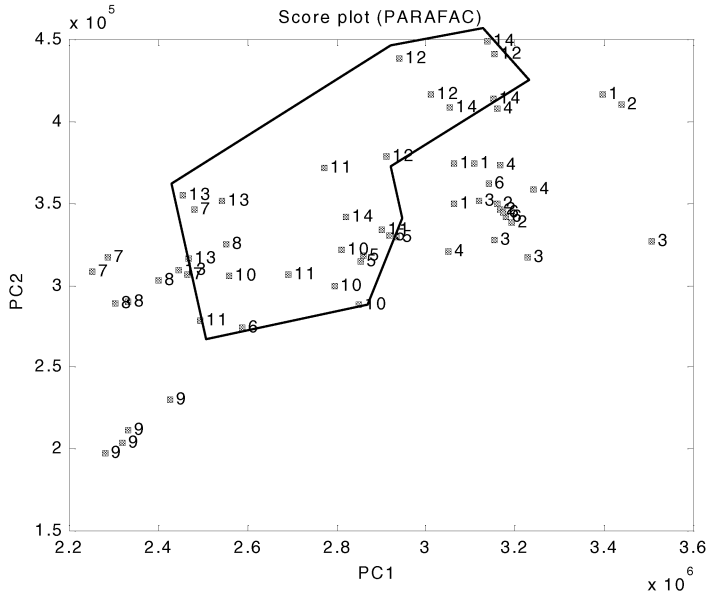

Figure 27. Score plot (**t**1-**t**2) from *PARAFAC*. Cheeses 1-9 span the total variation from NE to SW. Cheeses 10-14 lie in between (shown by a special marking). Note that replicate samples generally lie closer than those in unfold-PCA; four Sample 9 replicates especially clustered together.

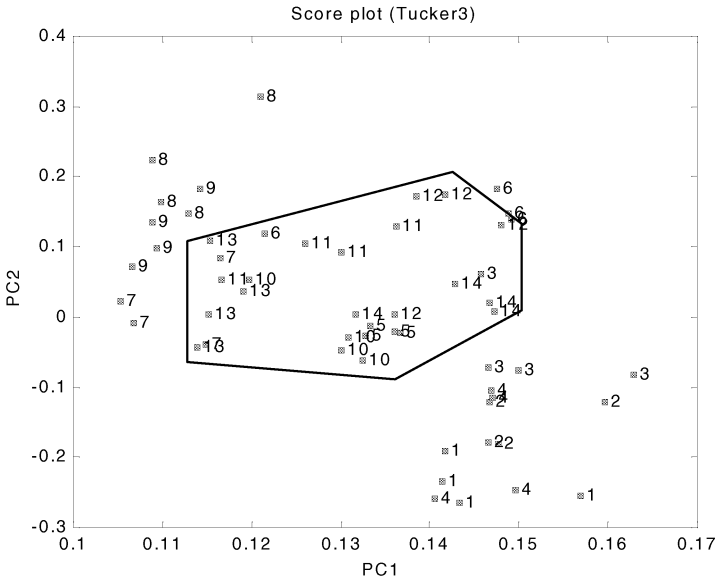

Figure 28. Score plot (**t**1-**t**2) from *Tucker3*. Notice the similar distribution of samples to unfold-PCA (Tucker1).Cheeses 10-14 shown by a special marking.

7.3. Predictions of rheological properties of cheeses

For each cheese a rheological testing was applied independently, and thus the rheological properties are known, e.g. fracture stress, strain, work and modulus. These are used as reference values in the following regression models. Prior to modeling all four replicates are averaged across the sample/object mode, and thus the 64×128×128 FFT data array is reduced to a 14×128×128 array. It is obvious to look at relations between FFT-feature arrays derived from these images and the corresponding rheological properties. To predict these properties two kinds of calibration models are tried out: strong N-PLS on the 14×128×128 three-way array, and weak unfold-PLS on the appropriate 14×16384 two-way array.

Calibration results using unfold-PLS and N-PLS are shown in Table 3. It is gratifying that the rheological properties can be well related to the microscopic images by means of multi-way modeling. Both unfold-PLS and N-PLS models can be established for predicting *fracture stress, strain, work and modulus*. Unfortunately, *Facture strain* seems difficult to predict in this way. As can be seen from the comparative modeling results, N-PLS models are distinctly superior to unfold-PLS in predictions of all these rheological properties. For instance, unfold-PLS gives a model in predicting *fracture stress* with Corr.Coeff.=0.78, RMSEP=13921, while N-PLS provides a clearly better model with Corr.Coeff.=0.91, RMSEP=8321.

Table 3. Comparative modeling results for rheological properties, using unfold-PLS and N-PLS. *Fracture strain* can not be predicted. All samples are kept in modeling with no outliers. Modeling parameters: Correlation Coefficient (Corr.Coeff.), Root Mean Square Error of Prediction (RMSEP) and number of factors are shown.

Calibration methods	Rheological properties	Corr.Coeff.	RMSEP	No. of factors
Unfold-PLS	Fracture Stress	0.7750	13921	2
	Fracture Strain	×	×	×
	Fracture Work	0.8149	4783	2
	Modulus	0.6916	47499	2
N-PLS	Fracture Stress	0.9125	8321	4
	Fracture Strain	×	×	×
	Fracture Work	0.9141	3036	2
	Modulus	0.9138	21584	3

We now try to delve into the interpretation of these N-PLS and unfold-PLS models by illustrating the calibration and full cross-validation process in prediction of one of rheological parameters. Table 4 shows percentages of variation explained in both X and Y during the calibration and full cross-validation in prediction of the property *–fracture work*. Both N-PLS and unfold-PLS give reasonably good models, but with distinctly different efforts. N-PLS fits 29.05% X-calibration variance, and explains 16.45% X-validation variance, 91.06% Y-calibration variance and 84.75% Y-validation variance with RMSEP=3036 using 2 PLS-components. By contrast, unfold-PLS fits 37.37% X-calibration variance, and explains 18.47% X-validation variance, and 99.06% Y-calibration variance and 67.38% Y-validation variance with RMSEP=4783, also by using 2 PLS-components. Clearly, unfold-PLS gives lower predictability and tends to overfit the models in both X and Y. For instance, it fits 37.37% X variation but explains only 18.47% in terms of full cross validation. The same phenomenon occurs for y variation, e.g. it fits 99.06% y variation but explains only 67.38% in terms of full cross validation. Such overfits most likely give rise to misleading model parameters and hence to an overly optimistic interpretation of the model. On the contrary, the N-PLS model appears more parsimonious and sensible though it also displays a minor degree of overfit of X and y. It describes a little less X variation but more y variation than unfold-PLS as shown in Table 4, and gives lower RMSEP indicating higher predictability.

Table 4. Comparative percent variance captured in both X and Y by using both N-PLS and unfold- PLS in predicting the rheological property---*Fracture Work*. Both calibration and validation variations are shown in terms of full cross-validation. LV denotes the number of latent variables, number of factors. Also shown are RMSEP values. Two components are found to be optimal in both cases.

Calibration methods	-----X-Block-----			-----Y-Block-----	
	LV #	Fitted	Xval	Fitted	Yval	RMSEP
N-PLS	1	27.28	14.63	67.02	57.65	5060
	2	29.05	16.45	91.06	84.75	3036
	3	29.33	16.54	98.93	83.59	3149
	4	29.61	16.56	99.90	83.46	3161
	5	29.84	16.58	99.99	83.21	3186
	6	30.08	16.61	100.00	83.15	3191
Unfold-PLS	1	29.98	18.11	79.60	64.53	4987
	2	37.37	18.47	99.06	67.38	4783
	3	44.24	18.52	99.98	67.05	4807
	4	50.19	18.55	99.99	67.09	4804
	5	56.97	18.65	100.00	67.10	4803
	6	62.76	18.79	100.00	67.10	4803

7.4. Evaluation

In this application (domain transformed "multiple imagery"), the strong multi-way methods show several distinct advantages over the weak multi-way methods–unfolding methods. This is essentially because strong multi-way methods are more parsimonious, with specific use of the three-way structure in the modeling. The trilinear models underlying PARAFAC and N-PLS are more restricted than unfolding models[22]. This leads to the fact that the fit of a trilinear model is lower than the fit of a corresponding bilinear model. Conversely, unfolding may risk taking away some three-way information and fitting more noise to the structural model. For instance, the stronger coherence of replicates in PARAFAC model allows for stronger discriminability than unfold-PCA etc. Furthermore, N-PLS gives better prediction results of rheological properties than unfold-PLS.

8. DISCUSSION AND CONCLUSIONS

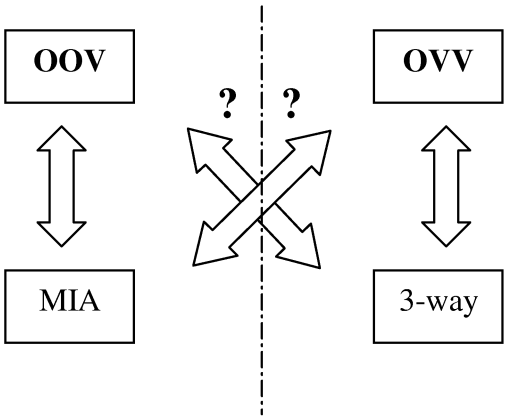

Figure 29. Relationships between data array configurations and corresponding proper 3-way data analysis methods, i.e. relations between MIA, 3-way methods, **OOV** data arrays and **OVV** data arrays. Dashed line represents a demarcation between **OOV**/MIA and **OVV**/3-way routine. Question marks indicate whether or not one can advantageously cross this boundary for new development.

It should be underlined that *a priori* knowledge of the data problem (and the data background) and the appropriate problem formulation is imperative. Strong multi-way methods have many advantages over unfold methods in many senses. But it does not mean that they will work better than unfold methods on any and all three-way data arrays. For instance, MIA based on unfold-PCA is very well suited for exploration and classification purposes as shown in application I. Applying different multi-way methods is intimately connected with proper data configuration and pertinent problem formulation. We have particularly focused on applying strong multi-way methods on both conventional **OOV** and transformed **OVV** image data array, since MIA/MIR has proven successful on **OOV** three-way image array. We have also tried to apply multi-way methods directly on raw **OOO** image arrays. As expected, no models could be obtained. It is certainly possible that for some purposes strong multi-way methods (e.g. PARAFAC) might not work well on **OOV** three-way image array, i.e. multi-spectral images in our application I. Lied and Esbensen have pointed out that there is a demarcation between strong three-way data analysis and multivariate image analysis using unfold methods[9]. At the moment, it may be stated very generally that strong multi-way methods are more suitable for **OVV** data array, and unfold methods (e.g. MIA) better suited for **OOV** data array in image analysis, see Figure 29.

In applications I, II and III we have deliberately crossed over this demarcation, that is to say, both unfold-PCA and strong 3-way methods have been applied to **OOV/OVV** image arrays. Whether and when to apply MIA or strong three-way analysis on **OOV/OVV** image data array varies from example to example. Many points remain debatable. Follow-up expositions and synthesizing discussions on this issue will be presented in a sequel paper.

This paper has given a first overview of the potential for multi-way methods in image analysis, termed N-way image analysis. Care must always be taken when applying different multi-way methods on image data. It is emphasized that data configuration and problem formulation has direct impacts on the proper choice of pertinent multi-way methods.

ACKNOWLEDGEMENTS

The authors gratefully acknowledge Prof. Rasmus Bro, at Royal Veterinary and Agriculture University, Denmark, for his helpful comments and suggestions. The authors would like to thank Prof. Karsten Qvist, at the same university, for providing the interesting cheese images. ERDAS, Inc. supplied the original Mobile Bay multivariate image (K.H.E), greatly appreciated.

REFERENCES

1. P. Geladi and H. Grahn, Multivariate Image Analysis, John Wiley & Sons Ltd, 1996
2. R.C. Gonzalez and R.E. Woods, Digital Image Processing, Addison-Wesley Publishing Company, 1993
3. K.H. Esbensen and P. Geladi, Strategy of Multivariate Image Analysis (MIA), Chemometrics and Intelligent Laboratory Systems, 1989, 7 pp 67-86
4. K.H. Esbensen, P. Geladi and H. Grahn, Strategies for multivariate image regression, Chemometrics and Intelligent Laboratory Systems, 14 (1992) 357-374
5. P. Geladi et.al, Principal Component Analysis of Multivariate Images, Chemometrics and Intelligent Laboratory Systems, 1989,5 pp 209-220
6. P. Geladi, and K.H. Esbensen, Regression on multivariate images: Principal component regression for modeling, prediction and visual diagnostical tools. Journal of Chemometrics, Vol.5, 97-111 (1991)
7. P. Geladi and K H. Esbensen, Multivariate Image Analysis in chemistry: an overview, Applied Multivariate Analysis in SAR and Enviromental Studies, Kluwer, Dordrecht, pp.415-445
8. K. Esbensen, et.al, Image analysis in chemistry I. Properties of images, gray-level operation, the multivariate image. TrAc, Trends in Analytical Chemistry, 1992.11(1) 41-53
9. T.T. Lied and K.H. Esbensen, Principles of MIR, Multivariate Image Regression – I: regression typology and representative application studies. Chemometrics and Intelligent Laboratory Systems, 2001. In press.
10. J.P. Wold, K. Kvaal and B. Egelandsdal, Quantification of intramuscular fat content in beef by combining autofluorescence spectra and autofluorescence images, Applied spectroscopy, Vol.53, No.4, 1999
11. J.P. Wold, Rapid quality assessment of meat and fish by using near-infrared spectroscopy autofluorescence spectroscopy and image analysis. Ph.D thesis. Agricultural University of Norway. 2000.
12. Eigenvector Research, Inc & R. Bro, Lecturing notes on course 'applied multi-way analysis', SSC6, Porsgrunn, Norway, 1999
13. R. Bro, Multi-way analysis in the food industry. Doctoral thesis. Royal Veterinary and Agricultural University, Denmark. 1998

14. K.H. Esbensen, S. Wold, and P. Geladi, Relationships between higher-order data array configurations and problem formulations in multivariate data analysis. Journal of Chemometrics, Vol. 3, pp.33-48. 1988
15. R. Bro, PARAFAC. Tutorial and applications, Chemom. Intell. Lab. Syst.38, 149-171 (1997)
16. R. Henrion, N-way principal component analysis. Theory, algorithms and applications, Chem. Intell. Lab. Syst. 25, 1-23 (1994)
17. R. Bro, Multi-way calibration. Multilear PLS. Journal of Chemometrics, vol 10, 47-61 (1996)
18. A.K. Smilde, Comments on multilinear PLS. Journal of Chemometrics, vol 11, 367-377 (1997)
19. C. A. Andersson, Exploratory multivariate data analysis with applications in food technology. Ph.D dissertation. Royal Veterinary and Agricultural University, Denmark. 2000
20. C. A. Andersson and R. Bro, Improving the speed of multi-way algorithms. Part I:Tucker3, Chemom. Intell. Lab. Syst.42, 93-103 (1998)
21. R Bro and C.A. Andersson, Improving the speed of multi-way algorithms. Part II: Compression, Chemom. Intell. Lab. Syst.42, 105-113 (1998)
22. C.A. Andersson and R. Bro, Interactive course for N-way analysis, Royal Veterinary and Agricultural University, Denmark. URL: http://www.models.kvl.dk/
23. C.A. Andersson and R. Bro, The N-way toolbox for Matlab, Royal Veterinary and Agricultural University, Denmark. URL: http://www.models.kvl.dk/source/
24. J. A. Westerhuis, T. Kourti and J.F. Macgregor, Comparing alternative approaches for multivariate statistical analysis of batch process data. Journal of Chemometrics, **13**, 397-413 (1999)
25. J. Huang and K.H. Esbensen, Applications of AMT (Angle Measure Technique) in Image Analysis Part I. A New Methodology for *in-situ* Powder Characterization. Chemometrics and Intelligent Laboratory Systems. 54/1(2000)
26. J. Huang and K.H. Esbensen, Applications of AMT (Angle Measure Technique) in Image Analysis Part II. Prediction of Powder Functional Properties and Mixing Components using Multivariate AMT Regression(MAR). Chemometrics and Intelligent Laboratory Systems. Submitted. 2000
27. B. Wise et.al., A comparison of principal component analysis, multiway principal component analysis, trilinear decomposition and parallel factor analysis for fault detection in a semiconductor etch process, Journal of Chemometrics, **13**, 379-396 (1999)
28. P. Geladi, Analysis of Multi-way (Multi-Mode) Data, Chemometrics and Intelligent Laboratory Systems, 7(1989) pp 11-30
29. P. Geladi, H. Bergner, L.Ringqvist, From experimental design to images to particle size histograms to multiway analyiss. An example of peat dewatering. Journal of Chemometrics, 14 (2000) 197-211.
30. T. T. Lied, P. Geladi and K. H. Esbensen, Multivariate image regression (MIR): implementation of image PLSR – first forays. Journal of Chemometrics, 14 (2000) 585-598.

PAPER VI

Non-invasive Monitoring of Powder Breakage during Pneumatic Transportation using Acoustic Chemometrics

Jun Huang[*1], Sivert Ose[2], Sunil de Silva[1,2] and Kim H. Esbensen[1]

1) Department of Technology (TF)
Telemark University College (HiT), N-3914, Porsgrunn, Norway
2) Tel-Tek, dept Powder Science and Technology (POSTEC) N-3914 Porsgrunn, Norway

Abstract

Six types of alumina with different particle size distributions and different production histories have been tested for breakage in a plant-scale transport rig. Acoustic chemometrics is used to monitor the powder breakage during pneumatic transport. This is a non-invasive on-line monitoring technique. The correlation between the acoustic signals and the degree of powder comminution is investigated. By relating the acoustic information to dust fractions from the process, we assess the possibility of predicting powder breakage during transport, based on acoustic sensor technology and multivariate data modeling.

Keywords: Acoustic chemometrics; Powder Breakage; Pneumatic Transport; Monitoring;

1. Introduction

Particulate materials ("powders") are some of the most versatile goods used in industry. They include extremely valuable pharmaceuticals and chemicals, as well as lower value minerals, polymers and foodstuffs. The quality of these materials is important for the correct operation of many industrial processes. We have here investigated the breakage of particles during pneumatic transport, and the applicability of acoustic chemometrics as a tool for discovering quality variations (i.e. varying particle size).

It is understandable that particles transported in a pipeline can break due to the collisions with the inner walls, and especially as they are transported around bends. As a result, the dust fraction/particle size distribution of the powder changes, possibly with a corresponding change in the acoustic output from the particle flow. Acoustic signals generated from pneumatic transport lines contain abundant information about the process; earlier investigations have shown that information about flow rate [1-3] and particle size distribution [4] can be extracted from such signals.

Acoustic chemometrics is an emerging discipline, encompassing diverse fields such as electronics, applied engineering and chemometrics [1-3]. It combines acoustic sensor technology with multivariate data analysis. In this work, we use easy "clamp-on" acoustic

[*] Corresponding author. E-mail: Jun.Huang@hit.no. Tel: +47 35 57 51 52. Fax: +47 35 57 52 50.

sensors followed by integrated signal analysis and multivariate chemometric data modeling to extract information from the acoustic energy outputs.

2. Theory

2.1. Data path of Acoustic chemometrics

The working of acoustic chemometrics principally consists of four main elements:

Sensor technology: Selection of types/number of sensors, positioning, mounting etc;
Data acquisition: cabling, signal conditioning (amplification, filtering), signal processing (A/D conversion etc.);
Signal analysis: Transformations including FFT, Wavelets, AMT (Angle Measure Technique) [5], autocorrelation, etc;
Multivariate modeling/calibration: PLS regression for multivariate calibration and prediction of quality parameters of interest from acoustic data.

Figure 1 shows a general data path from the initial acoustic phenomenon to the final multivariate modeling including future prediction ability.

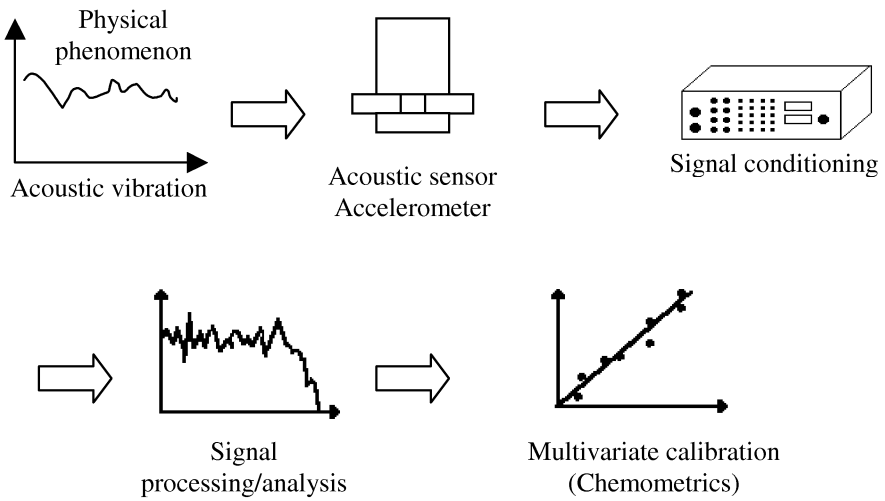

Figure 1. Schematic data flow sheet in acoustic chemometrics

Chemometrics originated in analytical chemistry, but it also serves as a generic data analytical technology. The multivariate nature of many sophisticated instruments demands the use of chemometrics to analyze the complex data generated. It is indispensable as an integral part of many new measurement techniques. Acoustic chemometrics combines applied engineering,

instrumentation, electronics, signal analysis and chemometrics to form a new interdisciplinary approach for the monitoring and control of industry, laboratory and scientific processes [1-4].

2.2. Acoustic Sensors (acoustic mechanism)

The fundamental idea of this approach is that emission of "noise" is an inherent characteristic of many production, manufacturing and transportation processes. "Noise" here means acoustic energy output not only in the audible range (5-20KHz), but also denotes the forms of vibrational energy in contiguous frequencies outside audible range, i.e.0-5, 20-250KHz.

It should be emphasized that the acoustic sensor used in this study is a "passive" sensor that can only "listen" to the acoustic energy output, in contrast to an ultrasound approach where both the acoustic impulse input and output is controlled. Ultrasound sensors are "active sensors".

The main types of sensors in acoustic chemometrics include generic accelerometers as well as specialized units. In this work, we use a sensor type shown in Figure 2 (b): Brüel & Kjær 4396. Data I/O links can be used with both portable and desktop PC. A measurement kit can be composed of a PC, powder supplies, universal connector array, amplifier/filtering unit, cabling and accelerometer(s), see e.g. Figure 2 (a).

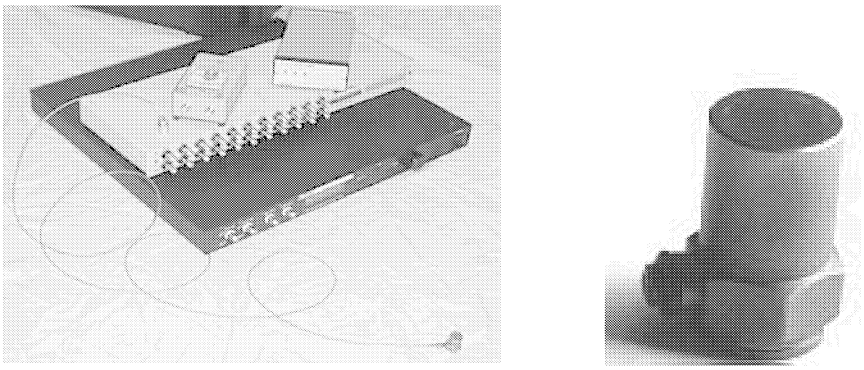

(a) (b)

Figure 2. (a) Measurement kit including (top to bottom) power supplies, universal connector array, amplifier/filter, cabling, and accelerometer. (b) A close view of an accelerometer. Model type: Bruel & Kjær 4396

2.3. PLS Regression method (PLSR)

The PLS (Partial Least Squares) regression method is a widely used method for multivariate calibration and has been used with great success in very many chemometric and other applications. PLS is a projection method that models the relationship between the Y values of interest and X predictors, which is the workhorse of the data analysis part of acoustic chemometrics. PLS interactively decomposes two blocks of variables, the matrices X and Y,

which in this work contain acoustic signals (X) and quality parameters (dust fractions) (Y) of the transported powder, respectively. PLS has been thoroughly described in the literature [6,7].

The blocks can be simultaneously decomposed as follows:

$$\mathbf{X=TP'+E}$$
$$\mathbf{Y=UQ'+F}$$

where **T** and **U** are *score matrices* and **P** and **Q** are the *loading matrices*; **E** and **F** are residual (error) matrices. The inner relations of **X** and **Y** are mutually related by **T** and **U**, for each factor (PLS-component):

$$\mathbf{u}_a = b\mathbf{t}_a$$

where *b* is the regression coefficient for each factor (a),

Y is calculated from $\mathbf{u_a}$ as

$$\mathbf{Y=TBQ'+F}$$

The algorithm and more details are given in reference [6,7].

A good model fit does not necessarily mean that the model will be optimal for the future prediction. We have to validate/test the model on new data and choose the model that gives the minimum prediction error, *ibid*. "Full cross" validation is used to evaluate the prediction ability of the proposed models when there are only a (very) small number of observations available for modeling as is indeed the case for the present study (15 objects). Full cross validation means that one builds up as many sub-models as there are objects, each time leaving out one of the objects and only use this one for the testing successively. This procedure is iterated, gradually building up the prediction evaluation, e.g. Figure 9 below. Details can be found in [6,7].

An important evaluative validation parameter is the Root Mean Square Error of Prediction (RMSEP), given by

$$\text{RMSEP}=\sqrt{\frac{\sum_{i=1}^{N}(\hat{y}-y_{i,ref})^2}{N}}$$

where $\hat{y}$ is the predicted value by the proposed model and $y_{i,ref}$ the reference value by other methods.

Both calibration and validation variance are calculated at each step of modeling after each factor, called PLS components. The model complexity is directly related to the number of components involved. RMSEP tells about the model prediction ability when the optimal number of PLS components have been included in the model. A plot of the RMSEP as a function of number of components is a very useful guide to determine how many components to

use, see Figure 9. The minimum value of this RMSEP plot corresponds to the optimal number of components.

2.4. Data Modeling

PLS-based acoustic data modeling can be described by the following schematic overview shown in Figure 3.

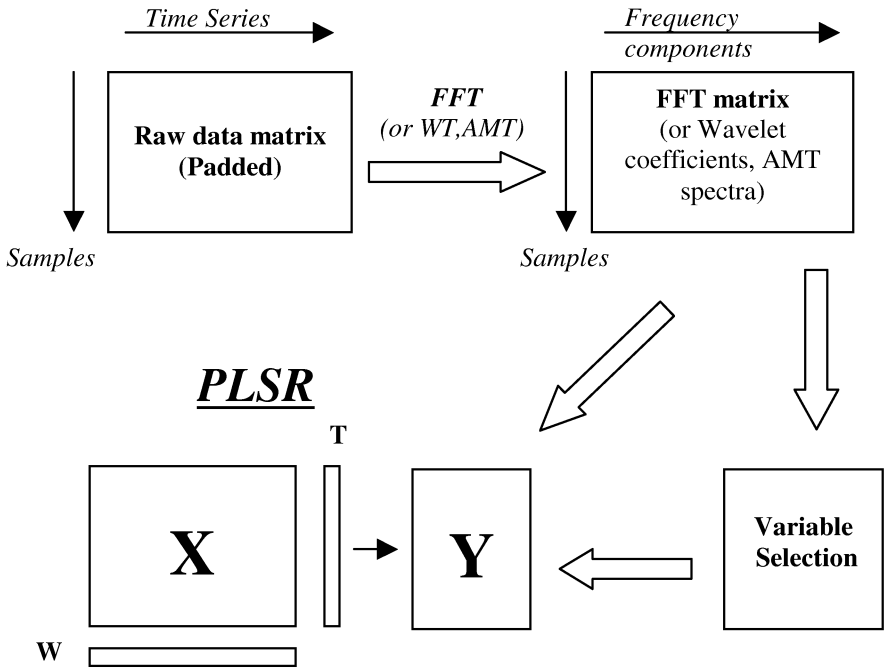

Figure 3. Overview of general steps taken in acoustic data transformation and multivariate regression analysis.

The steps in data processing and regression analysis can be described:

1) Record raw time series from the process, and if necessary, pad each to the nearest length 2^n, n=integer.
2) Choose a proper transformation technique(s), i.e. FFT, WT, AMT. In this work, these three techniques have been tried as preprocessing for regression modeling. FFT was found best suited for extracting information from the acoustic signals, and for the further PLS regression modeling.
3) If necessary, variable selection can be conducted for the purpose of reducing computation time a.o. In this work, the full FFT spectra are used for maximum information since modeling time is not an issue here.

4) Perform PLS modeling based on the proper X and Y-matrices, Figure 3. Any other alternative multivariate regression methods may also be applied in this approach, e.g. PCR (Principal Component Regression). In this work, the X-block variables are composed of PSD (Power Spectral Density) spectra derived from the acoustic signals, while the reference quality parameters construct the Y-block variables.

3. Experimental

3.1. Pneumatic transport test rig and sensor positioning

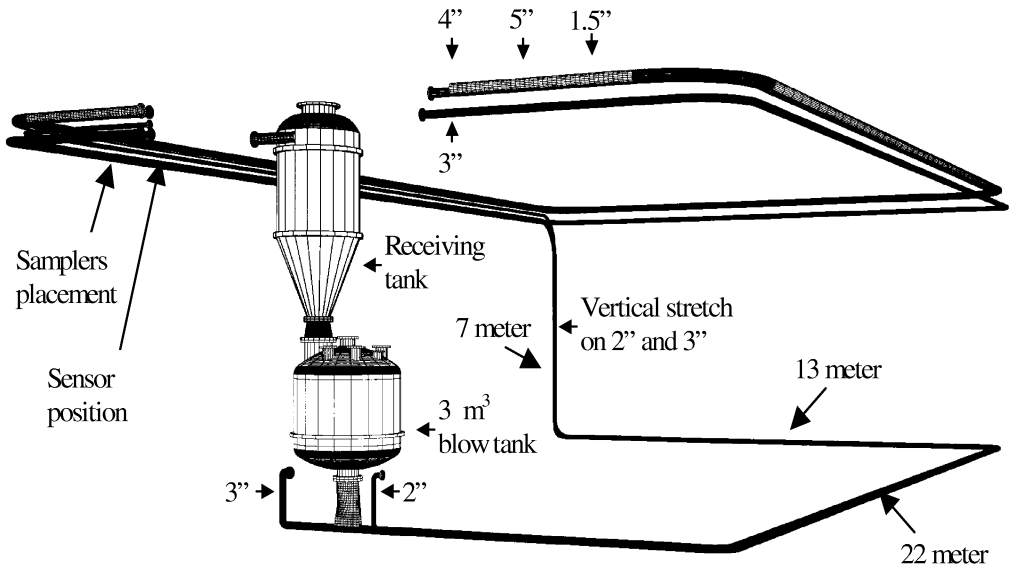

Figure 4. Pneumatic transport test rig. Note the acoustic sensor and samplers are positioned on the upper left.

The pneumatic transport test rig used in the experiments is shown in Figure 4. It is an industrial scale unit, and can be changed to resemble various modes of transport. Various powder feed configurations are available into pipes of varying diameter and lengths (maximum transport length is approx. 500 m). In these experiments, the powder was transported 140m (2 loops x 70m each) through pipes with an inner diameter of 3” (ca. 7.5 cm). One sampler was placed in each loop taking physical samples of the powder as it was transported. The samplers were Gustafsson type PR. The accelerometer was placed on the outer wall of the pipeline, approx. 3m before the samplers, see Figure 4. Earlier investigations [1,2] on pneumatic transport have shown that the optimal sensor positioning is to mount the accelerometer at the bottom of a straight pipeline section. A close look of the bottom-mounted accelerometer is shown in Figure 5.

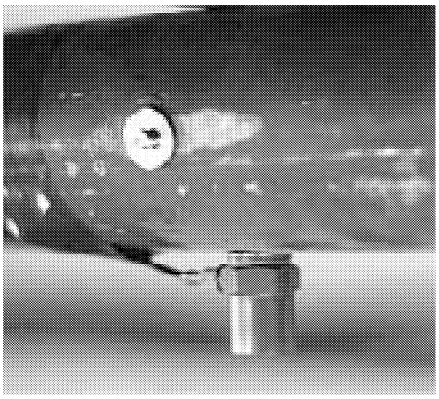

Figure 5. An accelerometer mounted at the bottom of pipe.

3.2. Samples/material

Six types of alumina (aluminum oxide, Al_2O_3) were tested for breakage during pneumatic transport. They have different intrinsic particle size distributions and otherwise span a wide range of qualities, as they represent a rather wide range of production histories. These six powders are expected to show rather varying breakage behaviors (details of production are confidential). For each type of alumina powder, we ran 15 loops and took 5 replicates at each run. 15x5 samples were obtained for each type of powder. For some calculations all replicates were used individually, while for others averages were derived.

3.3. Implementation

Signal conditioning was carried out by a programmable differential amplifier and a low-pass filter board (Alligator Technologies). The signal-to-noise ratio was enhanced, and suitably amplified, and band-limited analogue signals from this board were then converted to digital representation, using a data acquisition board with a sampling rate of 50 KHz (National Instruments Inc). The software part with GUI is based on Labview 5.0 [9]. It controls the data acquisition, signal processing, and store the time series and frequency data.

The time-domain signals acquired from the accelerometer appear quite irregular at first sight. Our assumption is that the information of interest is hidden beneath the cover of “noise”, and can be revealed only by data analysis. The power spectral density (PSD) derived from acoustics by the FFT transform is an advantageous signal representation, which enables easy comparison of the signal frequency components from one record to another. PSD spectra were used in the final modeling.

The six types of alumina powders used in the experiments are coded as AL-A, B, C, D, E and F. For each type of aluminum, 15 loops were run and 5 replicated time series were obtained at each loop run. Each time series was divided into 100 parts and FFT was conducted on each part. The 100 PSD spectra derived were then averaged to generate a vector containing 512 FFT

frequency components. Consequently an X-block is composed of 15x5 objects and 512 variables (frequencies). Replicates were then typically averaged for the final modeling; the size of the X-block was then reduced to 15x512. The X-PSD spectra comprising 512 frequencies corresponding to the range of 0-24.7 KHz for AL-B is shown in Figure 6. The models below are all based on similar complete X-variable sets.

The reference values for the Y-block were obtained from particle size analysis using a laser diffraction instrument (Sympatec). They represent the dust fractions in the powder (particles smaller than 42 µm or smaller than 21 µm). Figure 7 shows the reference values of Alumina type B, and shows the content of dust as a function of the number of loop runs. The Y-block contain reference values of powder samples from both the samplers, A and B.

For many reasons it is likely that outliers may occur in both the X-block and Y-block [1-3,6,7]. An example is the reference value for Alumina C, run 12 and sampler B as shown in Figure 8. Outliers like these were removed in the data modeling.

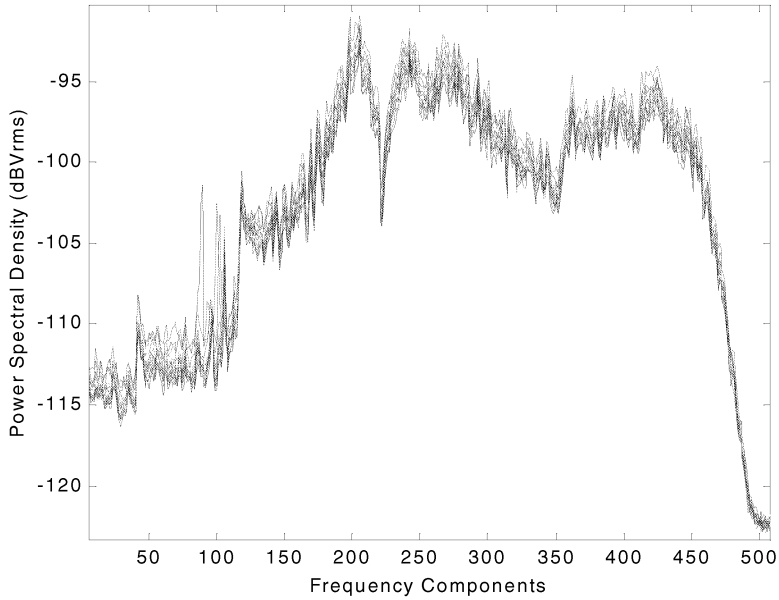

Figure 6. FFT Power Spectral Density (PSD) spectra of 15 runs of AL-B comprising 512 frequency components distributed over the range of 0-24.7 KHz.

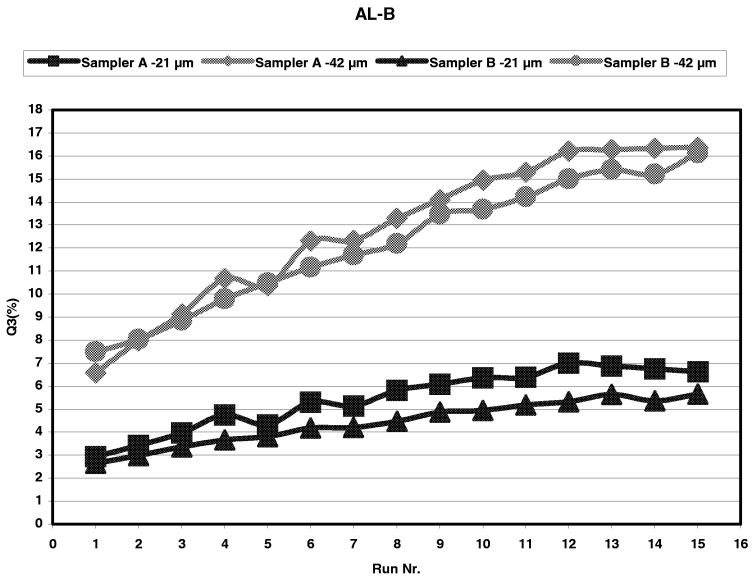

Figure 7. Reference values of AL-B: Fractions 21um and 42um from Sampler A and B at each run measured by laboratory particle size analysis

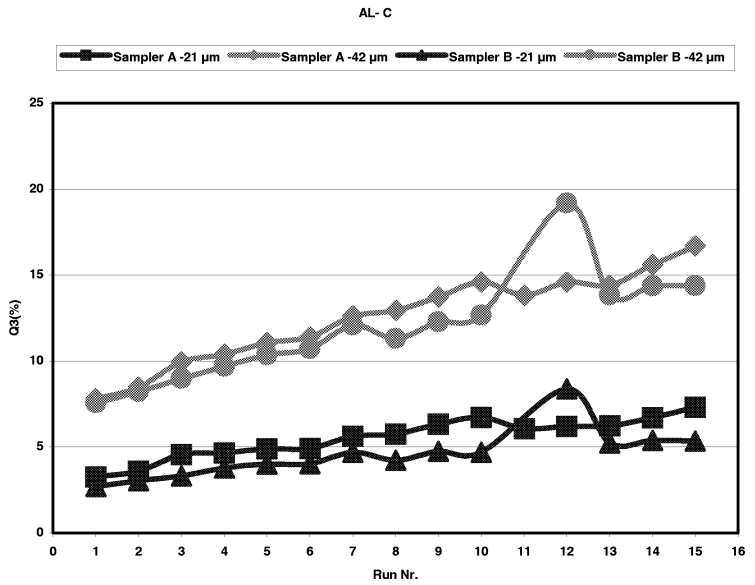

Figure 8. Reference values of AL-C: Fractions 21 and 42 from Sampler A and B respectively, at each run measured by laboratory particle size analysis. Note the Run 12 is an outlier which was removed in the data modeling.

4. Results and Discussion

Regression models, through multivariate PLS-calibration, were established to describe the relationship between the acoustics (X) and dust fractions as measured by particle size analysis (Y). The regression models for all six types of powders, 24 models altogether, have been established between the acoustics and references from both samplers A and B. All modeling results are summarized in Table 1. Correlation coefficients (for "Predicted vs. Reference" values, as determined by validation) for all models except AL-A are higher than 0.80, indicating that this acoustic approach has proven itself successful in discovering modelable connections. All models are validated by full cross validation as discussed earlier (small sample case: 15 objects). The validation results for AL-B, AL-C, AL-D are generally satisfactory, indicating a fair predictability. Evaluative statistics in Table 1 show that models for AL-A are worst. (lowest correlation coefficients, slopes, large offset, highest minimum RMSEP values, more outliers, and highest number of PLS-components, i.e. higher model complexity). However, this was the first powder tested, and there were a number of experimental difficulties in collecting reference values for AL-A. This shows this technique also depends on acquiring a good set of correct reference values.

Models for AL-E, AL-F have fairly good correlations but the slopes are less than 0.7, which falls below the requirements. These models need to be improved. The different types and quality of the selected pilot study set of alumina powders have clearly managed to span a relevant "breakage" range, as was expected.

By comparison, we found that models based on Sampler B were slightly better than those on Sampler A as evidenced by the marginally higher correlation coefficients. This is reasonable since Sampler B is located on the same loop as the acoustic sensor. Again, this means that precise reference values impact directly on the validity of prediction models.

Table 1. Summary of PLS modeling results for all types of powders. The code "21" denotes dust fraction –21um and "42" dust fraction –42 µm. The letter "A" means sampler A, and "B" sampler B.

Type of Aluminum	Sampler/ Dust fraction	Corr.Coeff	Slope	Offset	RMSEP	Objects/ Outliers	#PLS-components
AL-A	A 21	0.72	0.52	5.38	0.78	15/2	5
	A 42	0.71	0.52	5.39	0.78	15/2	5
	B 21	0.80	0.48	2.07	0.60	15/3	5
	B 42	0.73	0.57	5.78	1.97	15/3	5
AL-B	A 21	0.94	0.84	0.86	0.43	15/0	3
	A 42	0.95	0.86	1.80	0.98	15/0	3
	B 21	0.95	0.85	0.66	0.31	15/0	3
	B 42	0.96	0.88	1.45	0.81	15/0	3
AL-C	A 21	0.83	0.70	1.63	0.66	15/2	3
	A 42	0.84	0.71	3.53	1.44	15/2	3
	B 21	0.80	0.66	1.45	0.52	15/2	3
	B 42	0.82	0.70	3.41	1.28	15/2	3
AL-D	A 21	0.95	0.73	1.95	0.80	15/0	3
	A 42	0.96	0.74	0.74	1.89	15/0	3
	B 21	0.94	0.73	1.52	0.62	15/0	3
	B 42	0.95	0.75	4.06	1.63	15/0	3
AL-E	A 21	0.85	0.62	2.72	0.73	15/1	3
	A 42	0.86	0.57	7.08	1.54	15/2	3
	B 21	0.91	0.66	1.93	0.48	15/1	3
	B 42	0.91	0.66	5.09	1.37	15/1	3
AL-F	A 21	0.84	0.60	2.60	0.70	15/3	4
	A 42	0.79	0.43	9.20	2.53	15/1	4
	B 21	0.89	0.54	2.47	0.62	15/1	4
	B 42	0.87	0.52	7.39	2.06	15/1	4

In the following we shall explain the modeling results in detail using the AL-B powder based on dust fraction -42 µm and Sampler B since this model is significantly better than all others. This model has highest correlation coefficient, 0.96, largest slope, 0.88, smallest offset, 1.45, and lowest minimum RMSEP (for –42um), 0.81, shown in Table 1. Figure 9 shows the visual graphical PLS modeling results with fraction -42um from Sampler B as reference values. The model manages to account for 76%+7% X-variance and 71%+26% Y-explained variance respectively, with the first and second PLS-components, see Figure 9 (a) and (c). Figure 9 (b) depicts the X-loading weights from which one can see the importance of the individual X-variables (frequencies) on the model. Lower frequency components have slightly larger

absolute weights than higher frequencies, but overall all frequencies 0-24.7 KHz carry important information.

The most important evaluative validation statistics, Predicted vs. Measured plot, is given in Figure 9 (d). The correlation coefficient is as high as 0.96, the slope 0.88, and RMSEP 0.81. No outliers were found in the modeling, indicating good experiment procedures. As can be seen in Figure 10, the minimum RMSEP value is found at the third component. Also seen from Figure 9 (a) and (c), three PLS components are able to explain up to 85.4% X-variance and 99.8% Y-variance. Therefore, most of the variance in the X- and Y-block can be represented by a 3-component PLS-model. It is encouraging that more than 85% X-information hidden in acoustic signals can be related to Y quality parameters –particle size distribution by the PLS regression modeling. This is very good as acoustic chemometrics for powder systems go [2,3,4].

The results for the other five alumina powders obtained in the same way are shown in Table 1. Since this technique works well for some of the tested powders, further development would appear promising. Naturally a larger range of powder types needs to be investigated than what could be accommodated by the present pilot study.

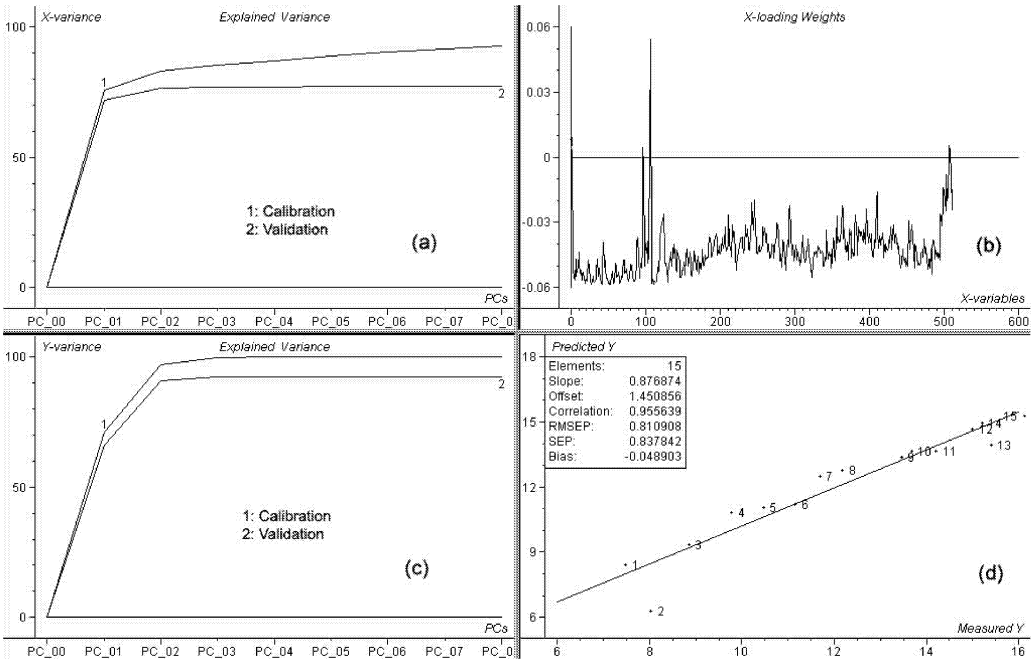

Figure 9. Visual graphical PLS modeling results for AL-B pertaining to fraction -42um and Sampler B. (a) Explained X-variance (both calibration and validation) (b) Explained Y-variance (both calibration and variation (c) X-loading weights (d) Predicted vs. Measured plot. Corr.Coeff.= 0. 96; Slope=0.88; RMSEP= 0.81. It may well be discussed whether object No.2 should rather be designated as an outlier, but this will increase the modeling/prediction strength.

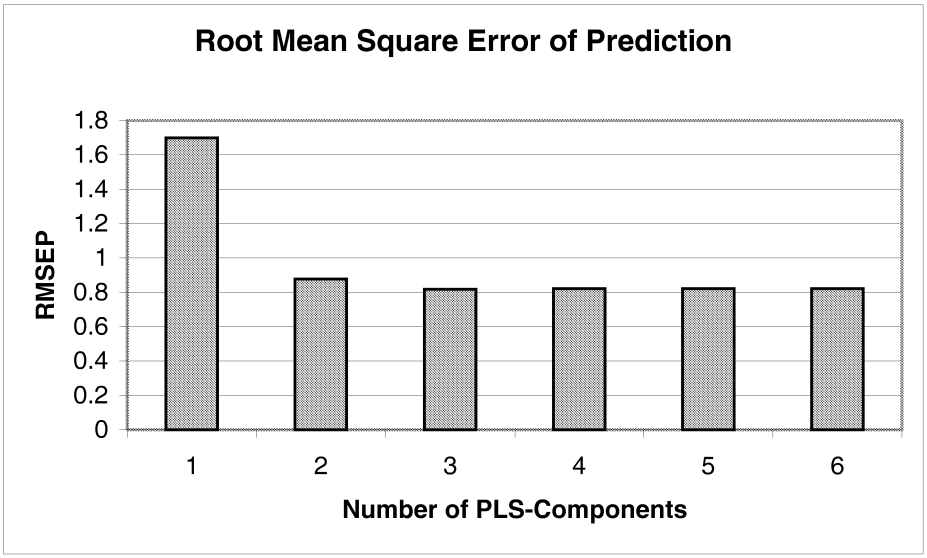

Figure 10. RMSEP vs. number of principal components from the AL-B model. Three PLS components are optimal.

We have also evaluated two other alternative domain transformation techniques: Wavelet Transform (WT) [8] and the Angle Measure Technique (AMT) [5]. It was originally believed that wavelet coefficients and AMT spectra derived from acoustic signals could also be utilized in combination with chemometric modeling. Having compared results from the three transformation techniques, we found FFT transform works best –with a large margin–in this case however. We therefore do not show any of those inferior results here.

5. Conclusions

This paper has presented the technique of acoustic chemometrics to monitor powder breakage during pneumatic transportation. This is a relatively inexpensive, non-invasive monitoring method. By transforming the acoustic data series to FFT PSD-spectra, we show that good models for predicting the degree of breakage can be established for half of the set of pilot powders selected. Overall six tested aluminum powder types exhibited a general correlation coefficient in the range of 0.8-0.96 between the acoustic signals and the particle size, but three out of six powders could not be modeled satisfactorily by the present first attempts. Further development of this technique is ongoing.

Knowing the particle size distribution is important for the correct operation of many industrial processes. Our results indicate that acoustic chemometrics may successfully be used to monitor the particle size distribution of a transported powder. There are several obvious improvement and options to be explored [1-4], which are likely to lead to further prediction enhancements.

Acknowledgements

The authors gratefully acknowledge M. Halstensen, at ACRG, Telemark University College, for his great help in setting up the acoustic experiment system.

References

1. K.H. Esbensen, et al, Acoustic chemometrics—from noise to information, Chemometrics and intelligent laboratory systems 44 (1998) 61-76.
2. K.H. Esbensen, et al, Acoustic chemometrics for fluid flow quantifications –II: A small constriction will go a long way, Journal of Chemometrics 13, 209-236 (1999)
3. M. Halstensen, S. de Silva, and K.H. Esbensen, Acoustic Monitoring of Pneumatic Transport Lines: From noise to information. KONA, Powder and Particles No.16 (1998)
4. M. Halstensen and K.H. Esbensen, New developments in acoustic chemometric prediction of particle size distribution -- ' the problem is the solution'. Journal of Chemometrics 14, 463-481 (2000)
5. J. Huang and K.H. Esbensen, Applications of AMT (Angle Measure Technique) in Image Analysis Part II. Prediction of Powder Functional Properties and Mixing Components using Multivariate AMT Regression (MAR). Chemometrics and Intelligent Laboratory Systems. *In print*. 2000
6. H. Martens and T. Næs, Multivariate Calibration, Wiley, UK, 1989
7. K.H. Esbensen, Multivariate Data Analysis –in practice, 4th, CAMO ASA, 2000
8. J. Trygg and S. Wold, PLS regression on wavelet compressed NIR spectra. Chemometrics and intelligent laboratory systems 42 (1998) 209-220.
9. LabVIEW user manual, National Instruments Inc., 1998

Appendix

The AMT toolbox for Matlab™

The AMT toolbox for Matlab has been developed by Jun Huang for general signal analysis, image analysis, and other possible application areas. For those who are interested, please contact the author or Kim H. Esbensen for copyright details. Our current email addresses are: Jun.Huang@hit.no, and Kim.Esbensen@hit.no.

The toolbox highlights include:

- Graphical User Interface (GUI) of the major AMT operations, which makes it easier to choose raw file, conduct AMT calculations, save results;
- AMT parameter settings for different types of signals;
- Interface for image preprocessing; i.e. removal of background/foreground pixels, and juxtapose the pixels;
- Interface for selection of image channels;
- Batch AMT calculations for many signals/images;
- Calculates AMT landscapes (two-way complexity spectra);
- Visualization features, i.e. display of 1-D signal, 2-D image, AMT complexity spectra;
- Major AMT calculation part written in MEX C, providing high speed for on-line applications.

The major files are described briefly in the following:

AMT_dll.c: Matlab EXcutable C (MEX C). Calculates AMT complexity spectra

AMT_dll.dll: Complied DLL file. Can be called directly by Matlab M-file

AMTN: GUI for AMT analysis of a 1-D signal; Opens a data file, conducts calculation, displays and saves results

AMTI: GUI for AMT analysis of a 2-D image; Opens an image file, conducts calculation, displays and saves results

NWAYAMT: Calculates two-way AMT landscape.

SELECTCHANNEL: Interface for selecting a desired image channel for a color image/multi-spectral image

PLOTAMT: Plots all results, AMT complexity spectra

AMTB: Batch AMT for processing many images/signals in one go

IMGPREP: Interface for image preprocessing, i.e. choosing cut-off level, removing background, etc.

CALIMG.c: Matlab EXcutable C (MEX C) file. Preprocess an image, i.e. remove background

CALIMG.dll: Complied DLL file. Called directly by IMGPREP

IMG_DAT: Unfold an image, i.e. row-wise, or column-wise

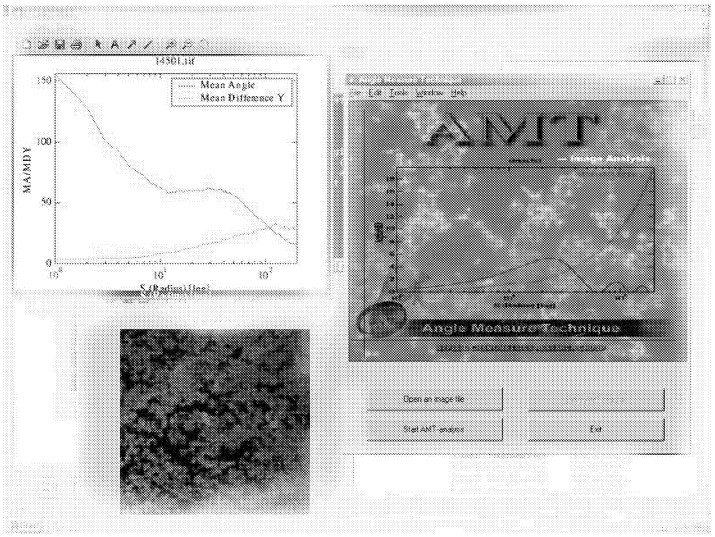

This program will soon appear as a new module in the "PLS Toolbox", Eigenvector Research Inc, USA